Norwegian University of Life Sciences
Faculty of Environmental Sciences
and Natural Resource Management

Philosophiae Doctor (PhD)
Thesis 2021:95

Characterization of Radioactive Particle Exposure Using Micro and Nano-Focused X-ray Techniques

Karakterisering av radioaktiv partikkel eksponering ved hjelp av mikro- og nanofokuserte røntgenteknikker

Ian Thomas Behnke Byrnes

Characterization of Radioactive Particle Exposure Using Micro and Nano-Focused X-ray Techniques

Karakterisering av radioaktiv partikkel eksponering ved hjelp av mikro- og nanofokuserte røntgenteknikker

Philosophiae Doctor (PhD) Thesis

Ian Thomas Behnke Byrnes

Norwegian University of Life Sciences
Faculty of Environmental Sciences and Natural Resource Management

Ås (2021)

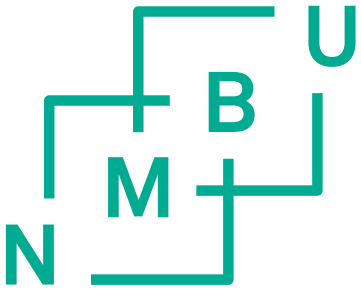

Thesis number 2021:95
ISSN 1894-6402
ISBN 978-82-575-1872-1

Supervisors

Professor Ole Christian Lind

Centre for Environmental Radioactivity (CERAD) CoE

Faculty of Environmental Sciences and Natural Resource Management (MINA)

Norwegian University of Life Sciences (NMBU)

Email: ole-christian.lind@nmbu.no

Professor Dag Anders Brede

Centre for Environmental Radioactivity (CERAD) CoE

Faculty of Environmental Sciences and Natural Resource Management (MINA)

Norwegian University of Life Sciences (NMBU)

Email: dag.anders.brede@nmbu.no

Professor Deborah Oughton

Centre for Environmental Radioactivity (CERAD) CoE

Faculty of Environmental Sciences and Natural Resource Management (MINA)

Norwegian University of Life Sciences (NMBU)

Email: deborah.oughton@nmbu.no

Professor Brit Salbu

Centre for Environmental Radioactivity (CERAD) CoE

Faculty of Environmental Sciences and Natural Resource Management (MINA)

Norwegian University of Life Sciences (NMBU)

Email: brit.salbu@nmbu.no

Professor Koen Janssens

Antwerp X-ray Imaging and Spectroscopy Laboratory (AXIS)

Department of Physics

University of Antwerp

Email: koen.janssens@uantwerpen.be

Evaluation Committee

Doctor Rodolphe Gilbin

Institute for Radiological Protection and Nuclear Safety (IRSN)

IRSN – PSE-ENV/SRTE

BP 4

F-13115 Saint-Paul-Lez-Durance

France

Phone: +33 (0)4 42 19 95 37

E-mail: rodolphe.gilbin@irsn.fr

Professor Gareth Law

University of Helsinki

Radiochemistry Unit, Department of Chemistry, Kumpula Campus,

00014 University of Helsinki

Finland

Phone: +358 (0) 5055 60920

E-mail: gareth.law@helsinki.fi

Professor Lindis Skipperud

Norwegian University of Life Sciences

Faculty of Environmental Sciences and Natural Resource Management (MINA)

Ås, Norway

Phone: +47 67231891

E-mail: lindis.skipperud@nmbu.no

Acknowledgements

This PhD project was financially supported by the Norwegian University of Life Sciences (NMBU) and the Research Council of Norway through its Center of Excellence (CoE) "Center for Environmental Radioactivity" funding scheme (Project No. 223268/F50). The research work was primarily carried out at the Isotope Laboratory at NMBU.

I want to start by thanking my main supervisor, Professor Ole Christian Lind (NMBU) who chose me for this deeply rewarding PhD project. I am incredibly grateful for his guidance and mentorship, teaching me the intricate details of using X-ray techniques to study radioactive particles. I could not have finished this work without his experience, patience, and encouragement.

To help guide me through this four-year endeavor, I was extremely lucky to have an exceptional supervisor group. Professor Dag Anders Brede (NMBU) has been a constant source of much appreciated, inciteful discussion on all topics but especially toxicology and biology (and not just because he was trapped in the office with me!). I owe a big thank you to Professor Deborah Oughton (NMBU) for guidance on nanoparticle characterization and exposure studies. For her wisdom and advice on the details of radioecology and radioactive particles, I am deeply grateful to Professor Brit Salbu (NMBU). Finally, I must thank Professor Koen Janssens (UA) who gave his support and advise on our work using X-ray techniques.

To all my co-authors for their tremendous amount of support and without whom I could not have completed this work, I would like to express my gratitude. I am incredibly thankful for the support from beamline scientists, Dr. Miguel Gomez Gonzalez (Diamond), Dr. Daniel Grolimund (SLS), and Dr. Dario Ferreira Sanchez (SLS) who received our samples, handled them with care, and ensured we got the measurements we needed to be successful in this work. The synchrotron measurements were also supported by Gert Nuyts (UA), who was pivotal to the data analysis, and Dr. Estela Reinoso-Maset (NMBU), for all her help and assistance. The *Daphnia magna* studies in this project could not have occurred without Shane Scheibener (NMBU) who set-up the culture and taught and helped me with the maintenance and upkeep. Also, I could not have completed the nanoparticle exposures without the expertise of Dr. Lisa Rossbach (NMBU), who also provided a steady hand in carefully sectioning our samples. I would like to thank

Dr. Jakub Jaroszewicz (WP) who expertly scanned countless daphnia for us and provided his expertise on tomographic analysis. Finally, I am very appreciative to Professor Hans-Christian Teien (NMBU) for insightful discussion on aquatic uranium toxicology, to Dr. Elisabeth Hansen (DSA) who helped with the radiation dosimetry of Dounreay particles, and to Dr. Václav Čuba (CTU) for providing the uranium nanoparticles for this research.

This work could not have been done without my wonderful friends and colleagues at the Isotope Laboratory, the Faculty of Environmental Sciences and Natural Resource Management (MINA), and the NMBU Imaging Center. You all were immeasurably welcoming and supportive and the atmosphere you created helped me be successful in this PhD project.

I will close by thanking my parents who raised me to be scientifically curious, to care about the environment, and have a passion for travel. I am a reflection of their best virtues.

Finally, none of this could have been done without Lisa, who has my heart, and kept me calm and level-headed through the finish line.

Ian

Ås, November 5, 2021

Contents

Summary

Radionuclides may be introduced into the environment from a variety of sources both naturally occurring, such as weathering from ore deposits, and anthropogenic, such as releases associated with the nuclear weapons and fuel cycle. The environmental transport, ecosystem transfer, external and internal exposure, and biological effects of released radionuclides is dependent on the distribution of physico-chemical species (i.e., the speciation). In most events involving the release of refractory radionuclides to the environment, particles are expected to comprise an important fraction of the source term. The characteristics of these released aggregates of radioactive atoms are dependent on the source and release scenario. While relatively large particles can carry a substantial amount of radioactivity and act as point sources of radiological risk, submicron and nanometer sized particles may exhibit a greater environmental mobility and bioavailability. These colloids and nanoparticles are continuously generated by biogeochemical processes inducing weathering of larger particles as well as nucleation, particle growth, and aggregation mechanisms.

The present PhD project aimed to reduce uncertainties in environmental impact and risk assessments of particle contaminated sites by characterizing the exposure to radioactive particles (nm to mm). To this end, physico-chemical properties of spent nuclear fuel particles (> 0.45 μm), released during reprocessing activities at the Dounreay facility (Thurso, Scotland), were investigated to link the source term and release scenario to the environmental behavior and potential exposure to man and the environment. Furthermore, engineered uranium nanoparticles (UNPs) were used to study the uptake and retention of colloidal species (3 kDa < x < 0.45 μm) in aquatic model organism *Daphnia magna*. This research was carried out using a range of laboratory and synchrotron, micro and nano-focused analytical X-ray techniques including X-ray fluorescence (XRF), X-ray absorption near edge structure (XANES) analysis, and X-ray absorption computed tomography (CT), to complement the exposure characterization of Dounreay particles and standardized toxicity assessments according to OECD guidelines.

Focusing on the importance of linking physico-chemical characteristics to particle source term and release scenario, the spatial distributions of matrix elements including uranium were assessed in two different types of Dounreay spent fuel particles, Materials Test Reactor (MTR) and Dounreay Fast Reactor (DFR) particles (Paper I). Using laboratory-

based micro-X-ray fluorescence analysis (μ-XRF), MTR particles were shown to contain a heterogenous distribution of U and Al indicative of the UAl_4 dispersion fuel in the MTR reactor. In contrast, U and Nb were spatially correlated in DFR particles with stochiometric considerations indicative of a U-Nb alloy that formed as a result of the high temperature release scenario. These characteristics are important with respect to biogeochemical processes in the environment that could lead to weathering of particles and remobilization of radionuclides. The particle characterization was somewhat different from the existing contact dose risk assessment model, which only assessed MTR type particles and assumed a homogeneous distribution of radionuclides. Therefore, a revised dose assessment was conducted for each MTR and DFR particle characterized in this work. The results were consistent with the previous assessment and thus validated the existing model put forward by the Scottish Environmental Protection Agency (SEPA).

The potential uptake and retention of UNPs was studied in experiments by exposing freshwater invertebrate *D. magna* to well characterized UNP suspensions in moderately hard reconstituted water (MHRW, pH 6.8) (Paper II – III). Size fractionation results revealed U present in the LMM (< 3kDa, 0 – 53 %), the colloidal (3 kDa < x < 0.45 μm, 27 – 71 %), and the particulate fractions (> 0.45 μm, 5 – 44 %) suggesting both dissolution of the UNPs and aggregation. For comparison, D. magna were also exposed to similar concentrations of a U reference solution (U_{Ref}) which featured a similar size distribution indicating colloidal species were formed. Acute toxicity tests showed that 48 h UNP exposures caused mortality in adult *D. magna* (LC_{50} = 402 μ L^{-1} [336 - 484]) but were slightly less toxic compared to the U_{Ref} solution (LC_{50} = 268 μg L^{-1} [229 - 315]). Measurement of U body burden identified a 3- to 5-fold greater concentration in daphnia exposed to the UNPs (~ 20 – 60 ng $daphnid^{-1}$). Furthermore, assessment of survival as a function of body burden indicated that uptake in UNP exposures, compared to the U_{Ref}, was mainly comprised of species of lower specific toxicity despite the similar size distributions. Based on this assessment, daphnia specimens exposed at 320 ± 30.6 μg L^{-1} UNP and 159 ± 13.7 μg L^{-1} U_{Ref} were prepared for a range of X-ray imaging analyses to assess U localization and histological effects.

The elemental biodistribution of the whole body (5 μm resolution) was determined by using synchrotron μ-XRF (μ-SRXRF) of intact, chemically dried *D. magna* samples (Paper II). Areas of significant U accumulation revealed heterogeneous U distributions

throughout the daphnia and regions of interest (ROI) were chosen for 2 μm resolution scanning. Based on the high-resolution mapping, several organs were identified as targets of U exposure in both the UNP and the U_{Ref} treatments including the gills (epipodites), the digestive tract, the heart, the maxillary gland, and the embryos. Biodistribution results identified potential uptake pathways via the epipodites and the intestine. Furthermore, U was highly accumulated in the nephridium, part of the maxillary gland that may represent a previously undescribed U detoxification route. Maternal transfer was confirmed by U present in the embryos of the UNP exposed organism. High U intensity in remains of egg chorion was also observed in the brood chamber. However, daphnia derived from sublethal (< LC_{50}) exposures (UNP and U_{Ref}) were able to reproduce despite maternal transfer. The F1 generation did exhibit, however, altered reproductive behavior, including earlier reproduction and increased fecundity compared to controls. Both μ-SRXRF and CT indicated the UNPs had aggregated in the digestive tract where they represented high local concentrations of U. However, given the toxicity test results, these aggregates appeared to be less bioaccessible than other species. Nano-focused synchrotron XRF analysis (nano-SRXRF, 75 nm step size) of histological sections of *D. magna* midgut from the U_{Ref} exposure revealed U bound to ingested algae cells. This shows that the presence of residual feed even after evacuation of the intestine prior to exposure can influence the retention of U (Paper III).

Nano-SRXRF and μ-SRXRF with histological and anatomical analyses, were used to assess whether biological effects at the organ and tissue levels were co-localized with U. The results showed that the hepatic ceca, an organ associated with the production of digestive fluids, was a major target of exposure in both treatments (Paper III). Computed tomographic renderings revealed shrunken, straightened ceca following the 48 h exposure that was correlated with U entering the region via the midgut as shown by μ-SRXRF scans. Histological sections revealed that significantly damaged and destroyed epithelial cells were the underlying driver of morphological changes to the hepatic ceca. High resolution nano-SRXRF scans of the tissue sections showed U particulates (< 500 nm) throughout the damaged tissues and cells indicating a relationship between relatively high local U exposure and histological changes. The midgut was also severely affected following both exposures (UNP and U_{Ref}) with evident tissues stress and deformities, although U could only be detected in a detached cell, and not in the epithelium, possibly due to concentrations below the limit of detection for the method.

In the presented work, analytical X-ray techniques were employed to characterize facets of the exposure to radionuclide bearing particles and nanoparticles. The characterization of Dounreay fuel particles provides novel inputs on physico-chemical properties critical for ecosystem transport and radiological dosimetry models, thus improving predictive environmental impact and risk assessments. The studies in this project also present the first detailed assessments of UNP uptake and retention, which revealed aggregation within the midgut and migration into the hepatic ceca of *D. magna*. By identifying target organs, including the epipodites and the maxillary gland, the results of this work have provided important contributions to our overall understanding of U toxicokinetics in cladocerans. Furthermore, combining micro and nano-focused XRF analysis with histological and anatomical analyses linked U distribution with adverse effects in organs, tissues, and cells to improve interpretation of toxicological consequences to the organism. Finally, the techniques demonstrated here provide an advanced platform to characterize the exposure of other types of toxicants to a variety of test organisms and should prove useful for future development of an aggregate exposure pathway framework (AEP).

Sammendrag

Radionuklider slippes ut i miljøet fra en rekke naturlige og antropogene kilder som for eksempel vitring av malmmineraler og utslipp forbundet med kjernebrensel- og kjernevåpensyklusene. Transport i miljøet, overføring i økosystem, ekstern og intern eksponering, samt biologiske effekter av radionuklidene i miljøet vil avhenge av fordelingen av fysisk-kjemiske tilstandsformer (det vil si spesieringen). I de fleste hendelser som innebærer utslipp av ikke-flyktige radionuklider til miljøet vil det forventes at partikler utgjør en viktig andel av kildetermen. Egenskapene til disse aggregatene av radioaktive atomer som slippes ut er avhengige av utslippskilde og utslippsforløp. Mens relativt store partikler kan inneholde en vesentlig mengde radioaktivitet og fungere som punktkilder med tilhørende risiko, vil nanometer-mikrometer store partikler med potensielt større mobilitet og biotilgjengelighet kontinuerlig dannes gjennom biogeokjemiske prosesser som vitring av større partikler, partikkelvekst og aggregeringsmekanismer.

Målsetningen for dette PhD-prosjektet har vært å redusere usikkerhetene i miljø- og konsekvensutredninger for partikkelkontaminerte områder ved å karakterisere eksponeringen som knyttes til nanometer til millimeter store radioaktive partikler. Til dette formålet har brukt brensel partikler (> 0.45 μm) som ble sluppet ut i miljøet i forbindelse med reprosesseringsaktiviteter ved Dounreay-anlegget (Thurso, Scotland) blitt karakterisert med hensyn til partikkelegenskaper for å knytte kildeterm og utslippsforløp til potensielle effekter ved eksponering av mennesker og miljø. Videre har fremstilte uran nanopartikler (UNP, < 0.45 μm) blitt brukt i eksponeringsforsøk for å studere opptak og retensjon av uran i den akvatiske modellorganismen *Daphnia magna*. En rekke laboratorie- og synkrotronbaserte mikro- og nanofokuserte analytiske røntgenteknikker (XRF, XANES og CT) ble brukt for å komplementere eksponeringskarakteriseringen av Dounreay-partikler og standardiserte OECD toksisitetstester.

Med tanke på å knytte fysisk-kjemiske egenskaper til utslippskilde og utslippsforløp, ble romlig fordeling av matrikselementer inkludert uran undersøkt i to forskjellige typer Dounreay brukt brensel partikler, Materials Test Reactor (MTR) og Dounreay Fast Reactor (DFR) (Artikkel I). Ved bruk av laboratoriebasert μ-XRF, ble det vist at MTR partiklene er karakterisert ved en heterogen fordeling av U og Al som reflekterer UAl_4

brenselet i MTR-reaktoren. I DFR partiklene var derimot den romlige fordelingen av U og Nb korrelert og støkiometriske betraktninger tydet på at en U-Nb legering ble dannet som resultat av de høye temperaturene under utslippsforløpet. Disse egenskapene er viktige for å vurdere vitring av partikler og remobilisering av radionuklider som følge av biogeokjemiske prosesser i miljøet. Partikkelegenskapene var ikke helt i samsvar med de som ble brukt i tidligere risikovurderinger av doser forbundet med kontakt med partikler, som var basert på kun MTR partikkelkarakteristika og antok homogen fordelinger av radionuklider. I dette arbeidet ble det derfor utført en revidert risikovurdering av kontaktdosimetri for både MTR og DFR partiklene som var tilgjengelig i dette arbeidet. Resultatene viste at den eksisterende dosemodellen som brukes av Scottish Environmental Protection Agency (SEPA) gir gode resultater for begge typer partikler.

Potensielt opptak og retensjon av UNP i ferskvanns- og invertebratorganismen *Daphnia magna* ble undersøkt ved eksponering til karakteriserte suspensjoner av nanopartiklene i 'moderately hard reconstituted water' (MHRW, pH 6.8) (Artikkel II – III). Størrelsefraksjonering viste U fordelt i lavmolekylære former (< 3kDa, 0 – 53 %), kolloider (3 kDa < x < 0.45 µm, 27 – 71 %) og partikler (> 0.45 µm, 5 – 44 %), hvilket tyder på oppløsning av U fra UNP samt aggregeringsprosesser i suspensjonene. *D. magna* ble også eksponert for sammenliknbare konsentrasjoner av en U referanseløsning (U_{Ref}) med tilsvarende størrelsesfordelinger inkludert dannelser av kolloider. Akutt toksisitetstester viste at 48 timers UNP eksponeringer forårsaket noe lavere dødelighet i voksne *D. magna* (LC_{50} = 402 µg L^{-1} [336 - 484]) enn U_{Ref} løsningene (LC_{50} = 268 µg L^{-1} [229 - 315]). Total opptak av uran målt ved ICP-MS analyse viste 3-5 ganger høyere nivå pr daphnia fra UNP (~ 20 – 60 ng $daphnid^{-1}$) som for U_{Ref} (~ 10 – 20 ng daphnid-1) eksponeringer. Analyse av overlevelse av total opptak av UNP var dominert av tilstandsformer med lavere spesifikk toksisitet sammenlignet med U_{Ref} eksponeringen selv om fraksjoneringen viste lik størrelsesfordeling. Basert på resultatene fra toksisitetstestene, ble daphnia eksponert for 320 µg L^{-1} UNP og 159 µg L^{-1} U_{Ref} preparert for en rekke analyser med ulike røntgenteknikker for å undersøke U biodistribusjon og histologiske effekter.

Helkropps elementfordelinger (5 µm romlig oppløsning) ble analysert ved hjelp av synkrotronbasert µ-XRF (µ-SRXRF) på intakte, kjemisk dehydrerte *D. magna* (Artikkel II). Heterogene fordelinger på ulike deler av daphnia viste seg som områder med særlig høy

akkumulering av U. På grunnlag av disse fordelingene ble områder av særlig interesse (ROI) valgt ut for elementfordelingsanalyse ved høyere oppløsning (2 μm). Disse analysene identifiserte høy akkumulering av U i flere organer inkludert gjeller (epipoditter), fordøyelseskanalen, hjertet, nephridium og 'maxillary gland' (nyre) og embryoer, fra både UNP og U_{Ref} eksponeringer. Biodistribusjonsresultatene identifiserte en sannsynlig opptaksvei for U via gjeller (epipodite) og fordøyelsessystemet. I tillegg sannsynliggjør de høye U verdiene i «nyre» (nephridium og maxillarykjertelen) at dette organet utgjør et hittil ubeskrevet ekskresjons-/detoksifiseringssystem. Deteksjon av U i embryo i yngelkammeret bekrefter overføring fra mor til avkom. Det ble også påvist høye U nivåer i rester av eggekapsel (chorion). Til tross for overføring av U fra mor til avkom var daphnia eksponert for subletale konsentrasjoner (< LC_{50}) av UNP og U_{Ref} i stand til å produsere levedyktige avkom. F1 generasjonen viste likevel endringer i reproduktiv adferd, inkludert tidligere reproduksjon og økt kullstørrelse. Resultater fra både μ-SRXRF og CT viste at UNP aggregerte og ble oppkonsentrert i fordøyelseskanalen slik at de representerte høye lokale konsentrasjoner av U, men basert på de høyere LC_{50} verdiene for UNP ser det ut til at aggregatene var mindre biotilgjengelige enn andre tilstandsformer av uran. Nano-XRF (75 nm oppløsning) elementfordelingsanalyse utført på histologiske snitt av tarmen på *D. magna* etter U_{Ref} eksponering viste at U var bundet til delvis nedbrutte algeceller. Dette viser at det er rester av fôr i tarmen selv når daphnia ikke mates siste døgnet før eksponering, og at dette kan påvirke retensjon av uran (Paper III).

Ved å kombinere nano-SRXRF og μ-SRXRF med analyser av histologi og anatomiske endringer for å vurdere om biologiske effekter var samlokalisert med høy akkumulering av uran, ble det etter begge typer eksponering påvist at hepatic ceca, et organ som er knyttet til produksjon av fordøyelsesvæsker, er et viktig målorgan (Paper III). Etter 48 timers eksponering viste CT-analyser i kombinasjon med μ-SRXRF elementfordelinger at innskrumpne og forlengede hepatic ceca var korrelert med translokasjon av uran fra mellomtarmen til de skadede organene. Histologi av mikrotomsnitt viste at betydelig skadde og ødelagte epitelceller var en underliggende årsak til de morfologiske endringene i hepatic ceca. Ved hjelp av høyoppløste nano-SRXRF elementfordelingsanalyser av mikrotomsnitt ble det gjennomgående påvist U partikler (< 500 nm) i skadde celler som indikerer at det er en sammenheng mellom høy lokal uraneksponering og histologiske endringer. Epitelceller i mellomtarmen på daphnia ble

også betydelig stressede og deformerte som følge av begge typer uran eksponering (UNP og U_{Ref}), men i disse cellene ble uran ikke detektert, enten på grunn av begrensninger knyttet til prøvepreparereringen eller metodens deteksjonsgrense.

I dette arbeidet har analytiske røntgenteknikker blitt benyttet til å karakterisere eksponering av nanometer-millimeter store radioaktive partikler. Karakteriseringen av Dounreay brenselspartikler har gitt ny informasjon om fysisk-kjemiske egenskaper med betydning for transport i miljøet og radiologiske dosimetrimodeller og som vil bidra til forbedrede miljø og risikokonsekvensvurderinger. Dette arbeidet omfatter også de første detaljerte undersøkelser av UNP opptak og retensjon i biota og viste at nanopartiklene aggregerer i tarmen til daphnia og translokeres til hepatic ceca. Gjennom å identifisere målorganer for uran, inkludert epipodittene og maxillarykjertelen, har dette arbeidet gitt viktige bidrag til forståelsen av urans toksikokinetikk hos akvatiske cladocera organismer. Videre har det å kombinere mikro- og nanofokuserte XRF elementfordelingsanalyser med analyser av histologiske og anatomiske endringer gjort det mulig å knytte akkumulering av uran med skadelige effekter på organ-, vev- og cellefunksjoner og på den måten forbedre grunnlaget for tolkningen av toksikologiske konsekvenser for organismen.

Metodene som er presentert i dette arbeidet representerer en avansert plattform som kan brukes til å karakterisere eksponering av en rekke testorganismer, også overfor en rekke andre kontaminanter inkludert partikulære og kolloidale former, slik at de kan integreres i fremtidige aggregerte eksponeringsforløp (AEP)-rammeverk.

Abbreviations and Acronyms

U	Uranium
NP	Nanoparticle
UNP	Uranium Nanoparticle
U_{Ref}	Uranium Reference Solution
NORM	Naturally Occurring Radioactive Material
TENORM	Technically Enhanced Naturally Occurring Radioactive Materials
IAEA	International Atomic Energy Agency
UKAEA	United Kingdom Atomic Energy Agency
SEPA	Scottish Environmental Protection Agency
US EPA	United States Environmental Protection Agency
NCRP	National Council on Radiation Protection and Measurements (USA)
NRPB	National Radiological Protection Board (UK)
OECD	Organization for Economic Cooperation and Development
MTR	Dounreay Materials Test Reactor
DFR	Dounreay Fast Reactor
LMM	Low Molecular Mass
HMM	High Molecular Mass
FIAM	Free Ion Activity Model
MHRW	Moderately Hard Reconstituted Water
DLS	Dynamic Light Scattering
LC_{50}	Lethal Concentration in 50 % of the Population
LC10	Lethal Concentration in 10 % of the Population
AEP	Aggregate Exposure Pathway

AOP	Adverse Outcome Pathway
XRF	X-ray Fluorescence
XAS	X-ray Absorption Spectroscopy
XANES	X-ray Absorption Near Edge Structure
CT	X-ray Absorption Computed Tomography
ROI	Region of Interest
SEM-XRMA	Scanning Electron Microscopy X-ray Micro Analysis
TEM	Transmission Electron Microscopy
STEM	Scanning Transmission Electron Microscopy
EDS	Energy Dispersive Spectroscopy
ICP-MS	Inductively Coupled Plasma Mass Spectroscopy

List of Papers

Paper I

Byrnes, I., Lind, O.C., Hansen, E.L., Janssens, K., Salbu, B. (2020) *Characterization of Radioactive Particles from the Dounreay Nuclear Reprocessing Facility*, Science of the Total Environment, 727, 138488 doi: https://doi.org/10.1016/j.scitotenv.2020.138488

Paper II

Byrnes, I., Rossbach, L.M., Brede, D.A., Grolimund, D., Sanchez, D.F., Nuyts, G., Cuba, V., Reinoso-Maset, E., Salbu, B., Janssens, K., Oughton, D., Scheibener, S., Teien, H.C., Lind, O.C. *Synchrotron-based X-ray Fluorescence Imaging Provides New Insights on Uranium Toxicokinetics in Daphnia magna following Exposure to Uranium Nanoparticles* (Manuscript)

Paper III

Byrnes, I., Rossbach, L.M., Jaroszewicz, J., Grolimund, D., Sanchez, D.F., Gomez-Gonzalez, M., Nuyts, G., Reinoso-Maset, E., Janssens, K., Salbu, B., Brede, D.A., Lind, O.C. *Combined Structural and Nanoscopic Elemental Imaging Identifies Damage to Digestive Tract of Daphnia magna associated with Uranium Nanoparticle Acute Toxicity* (Manuscript)

1 Introduction

Sources of environmental radionuclides include naturally occurring radioactive materials (NORM), and those released as byproducts of anthropogenic activities. Over time, biogeochemical processes will influence the distribution of physico-chemical species (i.e., radionuclide speciation), which, in turn, impacts ecosystem mobility and interactions with biota where retention and elimination mechanisms play a role in the resulting exposure. Uncertainties related to the source term, environmental behavior, and uptake in biota lead to challenges in assessing the overall risks to radionuclide contaminated ecosystems. Therefore, effective environmental impact and risk assessments, whose outcomes guide decisions about radionuclide contaminated ecosystems, require good evaluation of the physico-chemical properties, the environmental behavior, and the potential uptake in biota.

1.1 Radionuclide Speciation

Environmental impact assessments of radionuclides are often based on the assumption of a homogeneous distribution of simple ions and molecules using bulk measurements of contaminated soil or water (Salbu et al. 2004). However, a significant fraction of radionuclides, such as those released from a nuclear accident, are present as radioactive particles, often with actinide (U, Pu, Th) matrix elements (IAEA-CRP, 2011). Today, sites of radioactive contamination are recognized as containing a broad array of physico-chemical forms (i.e., species), including a range of the low molecular mass (LMM) species to the larger particles and fragments (> 2 mm). Analysis of the distribution of radionuclide species in ecosystem components, also called radionuclide speciation, is the cornerstone to understanding the subsequent environmental behavior and potential impact to biota (Fig. 1) (Salbu 2009).

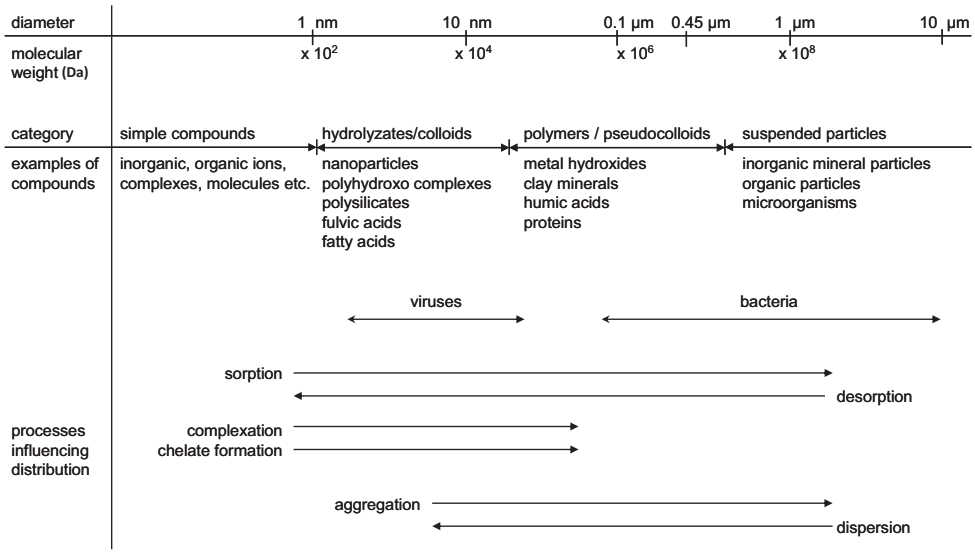

Figure 1: The speciation of radionuclides in aquatic systems includes a range of sizes and physico-chemical forms (modified from Salbu 2009).

Low molecular mass species (< 3 kDa) are widely considered more mobile in the environment and more bioavailable compared with colloids (1 nm – 0.45 µm) or particles (> 0.45 µm), the latter of which are subject to gravitational settling in aquatic systems (Markich 2002). However, colloids and particles can impact the environment through direct uptake by organisms or dissolution and release of LMM species (Salbu et al. 2018). Colloids and nanoparticles (NPs) have unique characteristics and behavior that should be assessed as a separate phase rather than grouped with simple ions and molecules as "dissolved" fractions (anything < 0.45 µm) (Geckeis et al. 2011). Furthermore, the remediation of radionuclide contaminated sites is often designed for ionic species which can lead to uncertainties associated with environmental transport predictions and radiological dose assessments. By moving towards an acknowledgement of the speciation of environmental radionuclides, including colloids and particles, consequences such as analytical inconsistencies, irreproducible results, and erratic conclusions may be avoided (Salbu et al. 2004).

1.1.1 Radioactive Particles

When accounted for in field studies, radioactive particles have been identified at nearly all sites contaminated by releases of radioactive materials (Salbu et al. 2015). In 2011,

the International Atomic Energy Agency (IAEA) issued a technical report (IAEA-TECDOC-1663) outlining the sources, identification, characterization methods, and mitigation of radioactive particles (IAEA-CRP, 2011) and defined them as:

> *"A localized aggregation of radioactive atoms that give rise to an inhomogeneous distribution of radionuclides significantly different from that of the matrix background"*.

The majority of anthropogenically released radioactive particles are derived from either nuclear weapons tests or the nuclear fuel cycle (e.g., U mining, spent fuel storage, and spent fuel reprocessing) (Salbu et al. 2015). As a result, the refractory radionuclides include actinides, mainly U, Pu, Th, and their decay products. Other anthropogenic sources of radioactive particles in the environment involve nuclear powered satellite sources, conventional detonation of nuclear weapons, and depleted uranium (DU) uses (civilian and military) (Salbu et al. 2015). Radioactive particles have also been associated with NORM and technically enhanced NORM (TENORM) (Cagno et al. 2020; Lind et al. 2013). Actinides typically constitute a major mass fraction of radioactive particle matrices, although there are exceptions such as the "cesium beads" found at the Fukushima accident site (Furuki et al. 2017) and orphaned ^{60}Co sources (IAEA 2004).

According to Salbu et al. (2015), radioactive particle characteristics depend on the source term and corresponding release scenario. The *source term* is a qualitative, semi-qualitative, or quantitative description of radionuclides released from a source and includes the composition of radionuclides, physico-chemical forms, and release rates. The *release scenario* refers to the conditions under which particles were formed and entered the environment. Proper characterization requires the assessment of parameters such as particle size distributions, structure and morphology, the elemental and isotopic compositions as well as radionuclide oxidation states (Salbu & Lind 2020). These characteristics directly impact the environmental behavior of particles and the subsequent chemical interactions which may remobilize radionuclides contained in the particle matrix. Once a particle is released into the environment, local conditions, such as pH, oxidation-reduction potential, and climate, drive dissolution and weathering processes, often over long periods of time. These factors both influence the particle characteristics leading to complex behaviors that determine ecosystem transfer and radionuclide bioavailability. In many cases, such as in aquatic systems, a particle may

become sequestered in soils and sediments where chemical interactions over time (often years to decades) can lead to localized release of LMM species as well as NPs and other types of colloids that may influence the long-term environmental impact (Skipperud & Salbu 2015).

1.1.2 Colloids and Nanoparticles

Colloids range between 1 nm to 1 μm in size and refer to a variety of naturally occurring species and those formed from anthropogenic substances that are capable of staying in suspension when dispersed in a medium (Christian et al. 2008). Nanoparticles are defined more specifically as:

> *"A natural, incremental, or manufactured material containing particles, in an unbound state or as an aggregate or as an agglomerate and where, for 50% or more of the particle in the number size distribution, one or more dimensions is in the size range of 1 to 100 nm."* (2011/696/EU)

Radionuclide bearing colloids and nanoparticles may be released into the environment from anthropogenic sources (such as discharges from nuclear sources), through formation in aquatic systems, or through the reaction with dissolved organic substances and clays to form larger pseudo-colloids (Salbu et al. 2001). Furthermore, colloids and NPs can be formed through the mechanical breakdown and weathering of larger particles or by direct precipitation from LMM species (Salbu et al. 2018). Colloids and NPs have a large surface-to-volume ratio, meaning a larger proportion of atoms are on the surface compared with the bulk material (Handy et al. 2008). Consequently, these species tend to have unique reaction chemistry, especially in aqueous systems where dispersion, aggregation, and agglomeration forces are all acting on the particles simultaneously. Nanoparticle sources are classified as either natural, incidental (i.e., via direct or indirect human influence), or engineered (Hochella et al. 2019). Unless taken into account, colloids and NPs bring uncertainty to environmental risk assessments as they have different mobility and bioavailability compared to ions, molecules, and larger particles.

Natural sources of radioactive colloids and NPs often include actinides within their matrix, such as those derived from rich ore deposits (Schindler et al. 2017). Naturally occurring actinide nano-minerals have also been observed in association with the fossil and mineral fuel sectors (Silva et al. 2021). More recently, engineered, actinide bearing

NPs have been used in the catalyst industry (Hasan & Ghosh 2013; Wang et al. 2008) and for nuclear fuel production (Čubová & Čuba 2019), although releases to the environment are not yet documented. There is a range of different types of incidentally formed radionuclide containing colloids including eigen-colloids, pseudo-colloids, and bio-colloids (Geckeis et al. 2011). Eigen-colloids refers to species formed through polymerization, such as Pu(IV) polymers (Neck et al. 2007). In contrast, pseudo-colloids are mineral fragments of crystalline or amorphous solids that have bound radionuclides within the structure. Actinide (Pu, U, Am, Cm) incorporation into pseudo-colloids structures have been observed in ground water mixing zones around deep geological storage for nuclear waste (Kim 2006; Kunze et al. 2008). Uranium colloids have been observed from uranium ore and associated with mining sites (Cagno et al. 2020; Wang et al. 2013; Wang et al. 2014). Corrosion products from nuclear waste storage are also a well-studied source of uranium colloids (Bots et al. 2014; Kaminski et al. 2005; Neill et al. 2019; Shoesmith 2000). Finally, a broad range of organic colloids, including humic or fulvic acids (Kim 1991) exist, which have an affinity for binding radionuclides, and are sometimes termed bio-colloids. The microbial bioreduction of environmental U(VI) to U(IV) has been shown to produce uranium nanoparticles (UNPs). This microbial induced bioreduction of uranium to an insoluble state has been proposed as a remediation method useful for actinide contaminated sites.

1.2 Radioactive Particle Impacts on Biota

Radionuclide bearing particles often have a high specific activity and represent point sources of radiological exposure (IAEA-CRP, 2011). Furthermore, many radioactive particles frequently bear other elements of toxicological concern within their matrix (Salbu et al. 2019). Therefore, impacts to biota are complex and influenced by the physico-chemical characteristics of the particle. Radioactive particles may interact with biota via several pathways including inhalation, surface adsorption, transfer across gill membranes, and ingestion (Salbu et al. 2018). At contaminated sites, such as Maralinga (Australia), Palomares (Spain), and Thule (Greenland), particle uptake in biota has been documented and appears to be facilitating the ongoing transfer of radionuclides in the ecosystem, and in some cases, human consumables (Aragón et al. 2008; Eriksson et al. 2008; Johansen et al. 2014). In addition, laboratory studies have shown that particles can

be retained in filter feeders and induce acute ulcerations as a result of relatively high contact dose rates (Jaeschke et al. 2015).

As many radioactive particles contain actinides, the contact radiological exposure results in a combined gamma, beta, and alpha dose that leads to a complex energy deposition that is correlated to the particle size and specific activity (Aydarous et al. 2008; Gesell et al. 1999). The dosimetry of hot particles has been studied and summarized by both the U.S. National Council on Radiation Protection and Measurements (NCRP) and the U.K. National Radiological Protection Board (NRPB) (Gesell 1999; NRPB 1997). The skin contact threshold for ulceration is 2 Gy according to the NRPB. These reports are focused on human health risks which have been shown to be insufficient for protecting wildlife (Clement et al. 2009). Recently, models for treating exposure to plants and animals separately, mainly through the use of computational phantoms have been developed (Caffrey & Higley 2014; Caffrey et al. 2016; Higley et al. 2015; Martinez et al. 2016).

Radioactive colloids and NPs represent potential environmental impact and risks associated with uptake and retention in biota. As the particle size reduces, the radiological risk to the organism is also diminished. Micro-dosimetry is a field of study concerned with acutely measuring radiation doses at a tissue, cell, and subcellular level (Cruz 2016) and may have applications to the radioecotoxicology of radioactive NPs in the future. However, the main risk from uptake of colloids and NPs, such as those containing U, is their chemical toxicity and propensity to transit biological membranes and assimilate into organs and tissues. Nanoparticle reaction chemistry results in different properties from those of ions, molecules, and larger micro and millimeter particles. The surface charge and reactivity of NPs may result in further aggregation or dissolution following uptake in an organism (Handy et al. 2008). The dissolution of NPs after ingestion may lead to the localized release of bioavailable ionic species of toxicological concern.

1.3 Uranium Aquatic Toxicology

Natural U is ubiquitous, found in surface waters and soils (Choppin et al. 2002). In aquatic ecosystems, U can appear in a large variety of physico-chemical species including ions (UO_2^{2+}), complexes with inorganic ligands (uranyl carbonate and uranyl phosphate), and humic substances in dissolved, colloidal, and particulate forms (Markich 2002). Uranium has two primary oxidation states U(IV) and U(VI) with different solubilities in water, and

different ecosystem mobility (Markich & Brown 2019). Chemical parameters, such as pH or the presence of competing ions, influence U aqueous toxicity by altering the relative abundance of bioavailable fractions; mainly U(VI) ions such as UO_2^{2+} and UO_2OH^+ (Goulet et al. 2015; Lofts et al. 2015). In oxidizing conditions, U particles may undergo a change in oxidation state from U(IV) to U(V) or U(VI), releasing potentially bioavailable LMM species in the process (Salbu et al. 2005). Although radioactive, the chemical toxicity of natural U is generally predominant, because of the long half-life of ^{238}U, and drinking water thresholds have been set to 30 μg L^{-1} by the World Health Organization (WHO, 2001; Sheppard et al. 2005). Therefore, when evaluating impact and risk of U contaminated sites, physico-chemical species including particles and NPs, their associated environmental behavior, and exposure to biota must be considered.

1.3.1 Daphnia magna Studies

Ecotoxicological studies take advantage of model organisms, which are well characterized species of flora and fauna that are broadly representative and critical to their ecosystem. For freshwater studies, *Daphnia magna*, a 2 – 5 mm crustacean, are a typical example as they are highly sensitive to trace metals and serve a key ecological function in nutrient cycling (Ebert 2005; Stollewerk 2010). Daphnia have been used to study U toxicity in aquatic systems for several decades and show a sensitivity that ranges from μg to mg U L^{-1} depending on water chemistry parameters (Poston et al. 1984; Sheppard et al. 2005). More recent works have implicated energy allocation and reduced food assimilation as drivers of toxicity (Massarin et al. 2010; Zeman et al. 2008). Toxicokinetic studies suggest that U is not retained for long in *D. magna* and mainly depurated through molting (Scheibener et al. 2021). Although studies using U colloids or NPs are scarce, small (< 500 nm) uranium precipitates have been identified in exposed daphnia intestinal epithelia pointing towards colloidal species in the exposure or formed in the gut or the cells (Massarin et al. 2011). Biodistribution studies have been limited to indirect observation of tissue damage in histological assessments (Massarin et al. 2011) or through toxicokinetic studies showing distribution between carapace, the eggs, and total body U concentration (Scheibener et al. 2021). However recent work using synchrotron based X-ray micro techniques to observe Zn distributions in *D. magna* indicated that metals accumulate in target organs such as the gills (epipodites) (De Samber et al. 2013).

1.4 X-ray Techniques to Characterize Radioactive Particle Exposure

X-ray techniques are well suited for characterizing radioactive particles (Salbu & Lind 2020) and the biodistribution in exposed organisms (Wang 2021). Taking advantage of the emission of characteristic X-rays, X-ray fluorescence analysis (XRF) is a well-established, non-destructive technique to assess the elemental distribution in a sample. Using various types of focusing optics, XRF analysis can be spatially resolved, and often quantified, on a micro and nanoscale (Janssens et al. 2010). These analyses are typically conducted at a synchrotron which provides a highly tunable, coherent source of X-rays. A synchrotron beam energy can also be varied allowing for several types of X-ray absorption spectroscopies (XAS). By alternating the beam energy around the absorption edge of the target element, X-ray absorption near edge structure (XANES) analysis can provide localized information of the oxidation state of the sample (Salbu, B. et al. 2001; Salbu & Lind 2020). X-ray absorption computed tomography (CT) is a complementary technique that provides contrast information about the internal structure of the sample based on the linear attenuation coefficient of the sample constituents. Rendered tomographic sections provide a three-dimensional model of the sample, such as a radioactive particle, useful for structural and morphological assessments (Cagno et al. 2020). Recent technological advances have brought many of these techniques into the laboratory setting where safety conditions are ideal for measurement of radioactive particles (Haschke 2014; Ritman 2011). However, for assessments at a tissue and cell level, the finely tuned, high flux beam at a synchrotron facility is required for the improved sensitivity and spatial resolution.

1.5 Research Hypotheses

Radionuclide associated particles, colloids, and NPs introduce significant uncertainty to the environmental risk assessment through their unique physico-chemical properties, ecological mobility, and impact to biota. The overall aim of the current PhD project was to reduce these uncertainties by characterizing aspects of exposure to particles ranging in size from nm to mm. Therefore, the following research hypotheses were put forth:

Hypothesis 1

Detailed knowledge on the compositional and morphological variations between different types of environmental Dounreay particles will improve existing impact and risk assessment models

Characterization of particle structure and morphology, elemental and isotopic compositions, and radionuclide oxidation state, which are source and release scenario dependent, will contribute to reducing uncertainties in radiation dosimetry models and environmental impact assessment.

Hypothesis 2

Uranium nanoparticles will be incorporated in tissues and organs giving rise to micro and nanoscale hotspots resulting in a heterogeneous biodistribution

In aqueous exposure studies, suspended uranium nanoparticles will enter the food chain via uptake into filter feeding organisms where retention can be identified at an organ and tissue level using synchrotron based analytical X-ray techniques.

Hypothesis 3

Uranium nanoparticles will exert local tissue or organ stress leading to adverse effects in exposed organisms

Tissue and organ stress, as shown by 2D and 3D histological and anatomical assessment, can be co-localized with the uranium nanoparticle distribution, and thereby providing insights into the adverse effects to the organism following exposure.

1.6 Research Objectives

To test these hypotheses, the research objectives for the project were:

Objective 1:

To investigate the compositional and morphological characteristics of Dounreay fuel fragments recovered from the marine environment using micro-X-ray fluorescence analysis, scanning electron microscopy, and synchrotron-based X-ray absorption near edge structure analysis, and to perform a dose assessment of the beta/gamma exposure to test current dose models

Objective 2:

To determine the uranium biodistribution (from whole organism to tissue level) in model organism *Daphnia magna* after exposure to uranium nanoparticles by means of laboratory and synchrotron-based analytical X-ray techniques and to identify potential target organs and tissues

Objective 3:

To compare histological and anatomical assessments (2D and 3D) of uranium nanoparticle exposed *Daphnia magna* with micro and nanoscale synchrotron based X-ray fluorescence analysis to identify relationships between adverse effects and the uranium spatial distribution in tissues and cells

2 Experimental Methods

To test the hypotheses of this work, a series of experiments using radioactive particles in sizes from nm to mm were conducted using micro and nano-focused X-ray techniques (Fig. 2). Compositional and morphological characteristics in two types of Dounreay fuel fragments were studied and the existing radiation dosimetry model was tested (Paper 1). To study the potential biological effects of radionuclide bearing colloids and NPs, *D. magna* exposure experiments using engineered uranium nanoparticles (UNP) were conducted, and samples were analyzed using synchrotron-based X-ray methods (Paper II - III).

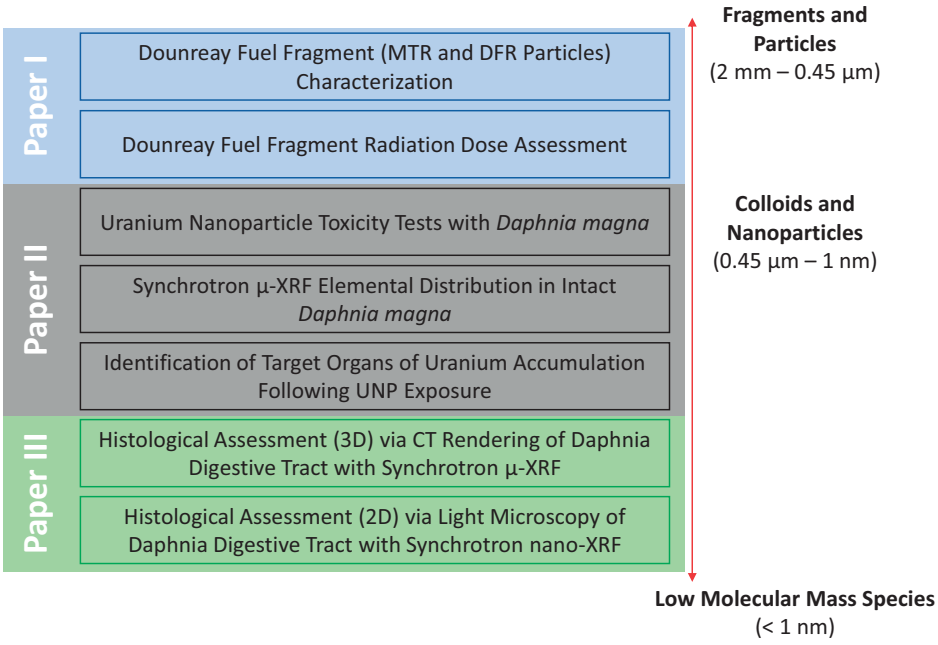

Figure 2: The experimental design for studying key properties related to the exposure to particles (2 mm – 0.45 µm) and colloids and nanoparticles (0.45 µm – 1 nm).

The following two subsections will discuss the materials investigated (2.1) and the analytical techniques (2.2) used in this study.

2.1 Materials Investigated

2.1.1 Dounreay Fuel Fragments

Dounreay fuel fragments, studied in Paper I, were chosen to investigate the characteristics of μm and mm particles. Released from the Dounreay Nuclear Fuel Reprocessing facility in Thurso, Scotland during routine operations in the 1950s, 1960s, and 1970s, the first Dounreay fuel fragment was found on the facility foreshore in 1986 (DPAG 2008). Since that time, particles have been recovered from surrounding beaches, including those that were open to the public, and offshore at a rate of 5 – 10 per month (PRAG 2012). Dounreay particles have a diverse range of characteristics, however, they all contain irradiated fuel, were created during fuel reprocessing activities, and escaped containment via the liquid effluent system and entered the local marine environment. Further background on the Dounreay Facility can be found in Paper I.

The two most common varieties of Dounreay fuel fragments are Materials Test Reactor (MTR) and Dounreay Fast Reactor (DFR) particles. Both MTR and DFR particles are derived from the reprocessing of spent U-based fuels. Three particles of each type (MTR and DFR) were provided by the Scottish Environmental Protection Agency (SEPA) to the Norwegian University of Life Sciences (NMBU) for analysis. These particles were used prior to this PhD project in a blue mussel study that resulted in some degradation of MTR2 and MTR3 and the DFR particles (Jaeschke et al. 2015). For the analysis presented in Paper I, all particles were mounted on black carbon tape secured to a mylar film (6 μm) stretched over an x-cell (31 mm Double Open-Ended X-CELL ®).

2.1.2 Uranium Nanoparticles

Environmental U colloids or NPs were not obtainable for this PhD project and engineered UNPs were used as representative samples for studying uptake and retention mechanisms in biota. The UNPs were synthesized for this experiment at the Czech Technical University (Pavelkova et al. 2013; Pavelková et al. 2016). The NPs were chosen due to their uniform size (3 – 5 nm) and natural U source. Stock suspensions (1.0 g U L^{-1}) were prepared in 10 mL N_2-purged (3 h) ddH_2O (15 MΩ cm) with a dispersant agent, 1 % polyoxyethylene glycerol trioleate (Kleiven et al. 2018). A Branson Sonifier S-450D (Branson Ultrasonics) equipped with a standard 13 mm disruptor tip (model 101-147-037) was used to disperse the UNPs which was completed in an ice bath for temperature control. All stocks were characterized and used immediately following sonication.

To obtain meaningful and reproducible results, characterization of the UNPs throughout the exposure period was of great importance. X-ray diffraction (XRD), provided by the supplier, was used to determine crystalline structure. At the microXAS beamline (SLS), μ-XANES of dry particles was completed (Paper II). For each exposure experiment, a separate stock suspension was prepared and characterized (Papers II – III). Measurements of hydrodynamic diameter and zeta potential, a measure of aggregation state and surface charge respectively, were completed using a Malvern Zetasizer ZS (Malvern Instruments Ltd., Worcestershire, UK) equipped with a 633 nm laser. Measurements were conducted in triplicate, 5 runs each, with autocorrection functions of 10 s. Additionally, electrophoretic mobility was measured, and zeta potentials for stock solutions were determined by Smoluchowski approximations. Individual particle sizes and shape were examined using transmission electron microscopy (TEM), and energy dispersive X-ray spectroscopy (EDS) for elemental compositions, on a JEOL JEM-2100F equipped with a Gatan Porius 200D CCD camera (JEOL Ltd., Tokyo, Japan) at the Faculty of Mathematics and Natural Sciences at the University of Oslo.

During the exposure, size fractionation was used to assess the distribution of U species in the *particulate* (> 0.45 μm), *colloidal* (0.45 μm > x > 3 kDa), and *LMM* (< 3 kDa) fractions with filtration and centrifugation methods (Fig. 3). In brief, the colloidal fraction was determined by drawing 1 mL of exposure media through a 0.45 μm syringe filter (VWR, Radnor, Pennsylvania, United States) and sampling 100 μL from the filtrate. Next, 400 μL of the remaining filtrate (< 0.45 μm solution) was removed into a pre-conditioned 3 kDa Amicon cellulose membrane filter (Amicon Millipore, Billerica, MA) and centrifuged at 14,000 g for 30 min. From the remaining filtrate, 100 μL was sampled to determine the < 3 kDa fraction. All samples were measured using triple quadrupole inductively coupled plasma mass spectrometry (QQQ-ICP-MS, Agilent 8900, Hachiōji, Japan).

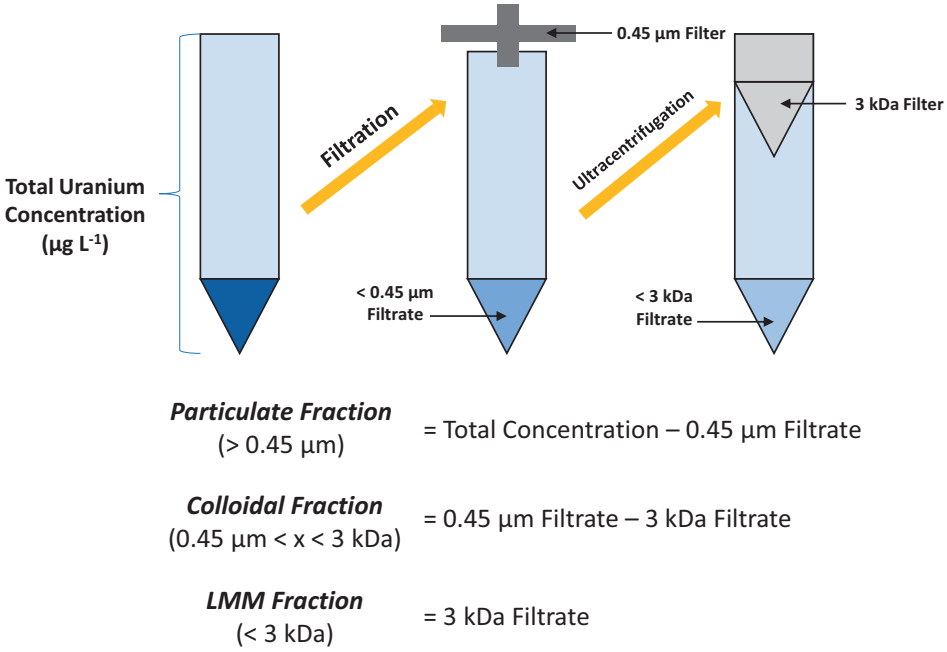

Figure 3: Size Fractionation Measurements

2.1.3 *Daphnia magna* Experiments

Daphnia magna were chosen as a model organism for UNP uptake and retention experiments (Fig. 4). Daphnia species are ubiquitous in freshwater bodies where they consume primary producers such as planktonic algae and bacteria and are themselves consumed by fish species (Ebert 2005). As a result, daphnia are an important member of the freshwater food chain and serve an important role in nutrient cycling (Stollewerk 2010).

All daphnia species (cladocerans) are classed as branchiopoda; a group of crustaceans that are identified by the presence of gills placed at the ends of their appendages. *Daphnia magna* are among the larger species, attaining lengths of 2 – 5 mm, and are often called water fleas due to their "hopping" swimming style, achieved with a pair of large antennae at the top of the body. Like all cladocerans, the body of the daphnia is covered in a chitinous carapace that encloses the whole abdomen. The head, which contains a larger compound eye that can be moved, is surrounded by a helmet of similar structure to the carapace. Below the swim antennae, daphnia possess five pairs of appendages that end

in a gill sac called the epipodite. With the heart located behind the intestine and above the brood chamber, daphnia have open haemolymph circulation.

Daphnia magna are filter feeders, consuming primarily microalgae of a size range 1 – 50 μm. Food is drawn into the food groove and foregut by a water current generated by the five thoracic appendages. The intestine runs vertically through the whole animal and is broken up into three main sections: the foregut, midgut, and hindgut. The midgut, made up of cuboidal epithelial cells containing microvilli, comprises the majority of the intestine. Digestive enzymes are produced by a pair of hepatic ceca, or diverticula, located at the top of the midgut. The hepatic ceca and all epithelia surrounding the midgut, are protected by a peritrophic membrane, secreted onto the food as it exits the foregut. Overall, daphnia digestion is a rather ineffective process, and food is only partially digested and eventually egested via the hindgut.

In good environmental conditions, *Daphnia magna* reproduce parthenogenically where females produce offspring with little genetic variation. Ovaries are located along the midgut and deploy fertile embryos via a small oviduct into the brood chamber located below the anterior carapace. Daphnia embryos develop directly in the brood chamber over approximately 48 h at which point they are released as fully-developed, miniature daphnia called neonates.

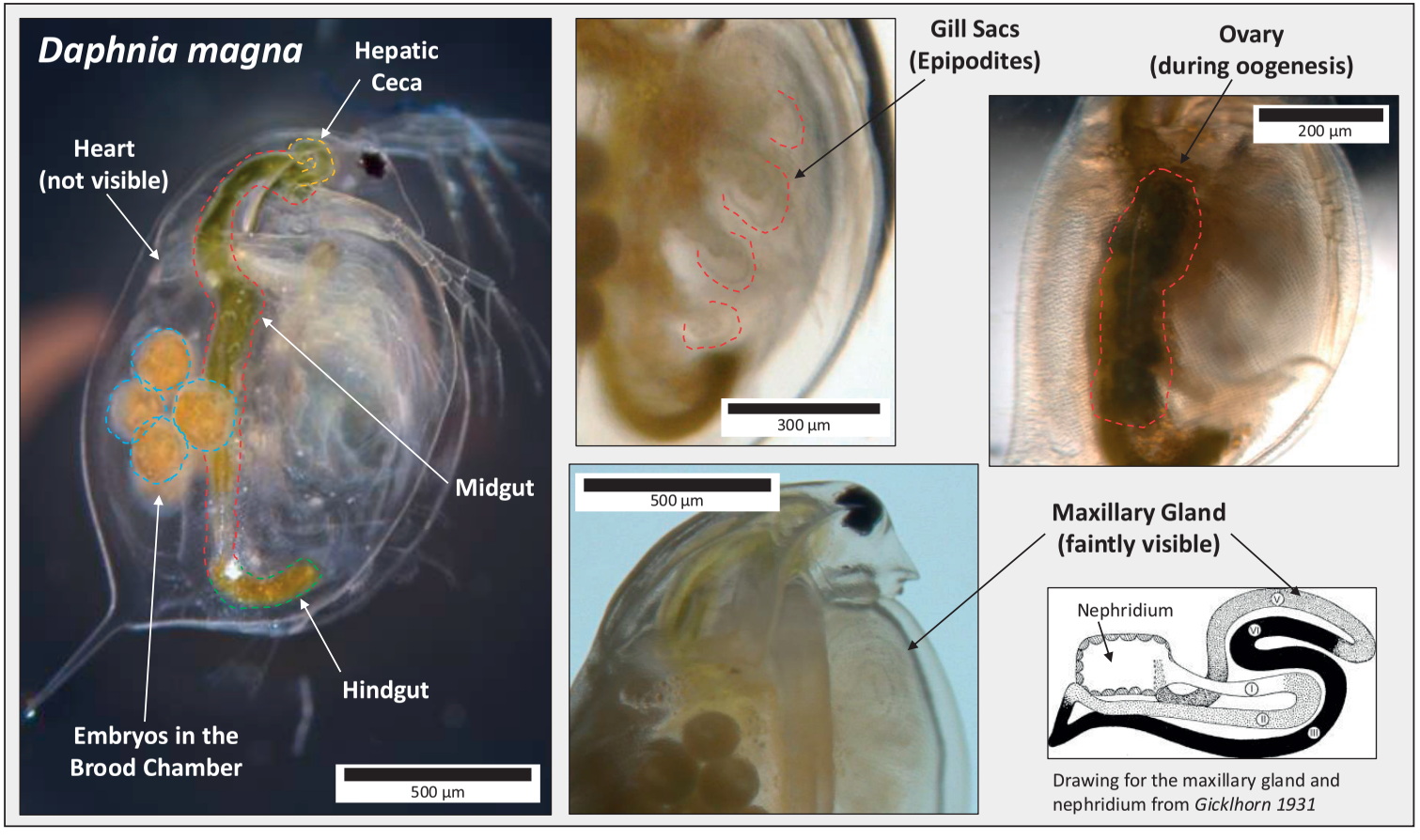

Figure 4: *Daphnia magna* physiology

Daphnia magna are also well-suited for the imaging objectives presented in this work. Daphnia cultures are easy to maintain under laboratory conditions, (described in more detail in Paper II – III) and reproduce parthenogenically every 3 to 4 days. Their mostly translucent bodies allow for easy microscope analysis. Finally, *D. magna* are sensitive to waterborne U species at concentrations that are relevant to anthropogenic releases (Sheppard et al. 2005).

Uranium Nanoparticle Exposures

The aquatic toxicity of U to *D. magna* has previously been assessed (Barata et al. 1998; Sheppard et al. 2005; Zeman et al. 2008), however no tests using UNPs are available in literature. Therefore, acute toxicity tests (48 h) using a standardized OECD protocol (OECD 2004) were conducted to establish toxic effect levels (LC_{50} and LC_{10}) (Paper II). Nanoparticle toxicity test protocols typically use an ionic control exposure to assess particle-specific effects (NANoREG 2017). For this study a natural U reference (U_{Ref}) solution (1.0 g L^{-1} in 2 % HNO_3, CRM-129A, United States Department of Energy, Argonne, Illinois) was used. The U_{Ref} exposures were conducted by adding an aliquot of the desired exposure from a 10x diluted stock (100 mg U L^{-1}) into an empty 50 mL exposure cup and gently evaporating to remove acids that would affect the pH of the exposure media. After evaporation, exposure media was added to each cup 24 h prior to the start of the toxicity test for U dissolution and equilibration. For comparison purposes, size fractionation, as described for the UNP exposures, was also performed on the U_{Ref} solutions (Paper II and III).

All exposures were conducted in moderately hard reconstituted water (MHRW) adjusted to a pH of 6.8 prior to the addition of UNPs or the U_{Ref} and all pH values were confirmed throughout the experiment to 6.8 ± 0.1 (USEPA 2002). This exposure media was chosen for its low ionic strength, to minimize the agglomeration and aggregation of the UNPs, and lack of phosphates which effectively would bind simple uranyl ions and reduce bioavailability (Markich & Brown 2019), and has been previously used in a series of nanoparticle ecotoxicology studies in our laboratory (Kleiven et al. 2018; Rossbach et al. 2020). Similarly, pH 6.8 was chosen to maximize bioavailable U species while remaining within the tolerable range of *D. magna* (Ebert 2005). Finally, to assess the maternal transfer effects of U and UNP exposures, adult (< 7 d old) daphnia were used for the exposure and imaging studies. The exposure experimental design is shown in Figure 5.

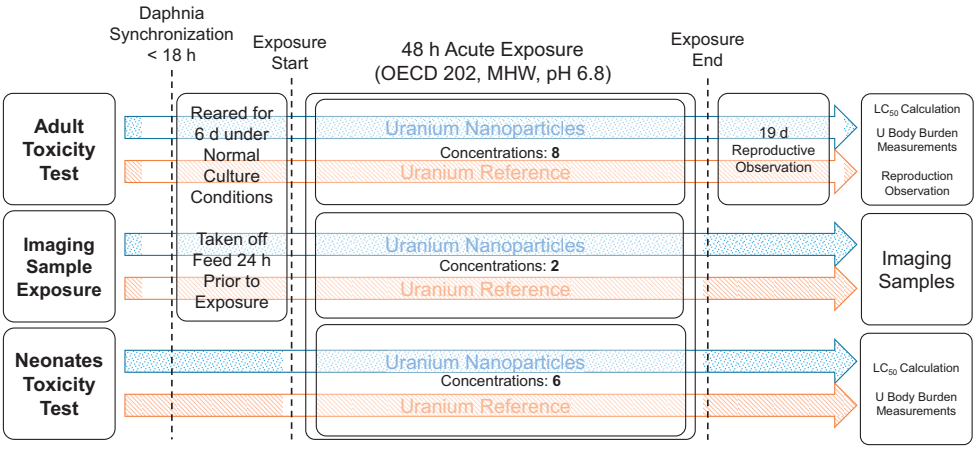

Figure 5: *Daphnia magna* Exposure Experiment Design

Synchronized neonates, born within 18 h of each other, derived from the second clutch or later were used for all exposure experiments. Daphnia were reared for 6 d at which point they were removed from feed (green algae) into clean MHRW to acclimate prior to the experiment. After 24 h, when the first stages of embryonic development were observable in the ovaries, daphnia were moved into exposure solutions at 5 mL per daphnid. For both the UNP and the U_{Ref}, concentrations from 0 – 1000 µg L^{-1} were tested. All exposure waters were sampled for total U concentration at 0 h and 48 h. Toxic effect levels were derived from the measured U concentrations.

Surviving individuals in each cup were documented at 24 and 48 h. Daphnia with no visible movement after 15 s of light agitation were considered immobilized as per OECD 202 protocol. After 48 h exposure, three individuals were collected for measurement of U total body burden (n = 3, ng U $daphnid^{-1}$) using QQQ-ICP-MS. To determine a 48 h LC_{50} and LC_{10}, the survival results were modeled using the MOSAIC web interface for statistical analyses in ecotoxicology (Charles et al. 2018). The computations in MOSAIC utilize the R package 'morse' (Delignette-Muller et al. 2016). Further statistical analyses of the survival and body burden results was completed using Minitab® (Minitab Inc. 2010). Using a significance level of 0.05, the difference between exposures and the control were analyzed using an ANOVA test followed by a Tukey's range test. When the residuals of the ANOVA test were not normally distributed, a Kruskal-Wallis test was conducted.

To interpret effects on reproduction, three daphnia from sub <LC_{50} concentrations were transferred to clean MHRW with algae feed following the 48 h acute exposure. These individuals (F0 generation) reproduced overnight (18 h later) and the neonates (F1 generation) were counted and moved into growth media with feed and reared under normal practices. The age of the F1 daphnia at first spawning and clutch size were documented.

As the OECD 202 guidelines for LC_{50} determination normally suggest using < 24 h *D. magna* neonates, the previously described process was repeated, to obtain direct comparisons with previously published toxicity data.

Based on the determined toxic effect levels (LC_{50} and LC_{10}) associated with UNPs and the U_{Ref} for *D. magna*, exposures were repeated at two concentrations (UNP: 320 ± 30.6 and 64.6 ± 3.53 µg L^{-1} / U_{Ref}: 159 ± 13.7 and 36.3 ± 6.05 µg L^{-1}) to produce samples dedicated for analytical X-ray measurements. Exposures were conducted by the same method as previously described. After 48 h, daphnia were rinsed three times (2x MHRW, 1x Deionized Water) and prepared for sample preparation.

2.1.4 Sample Preparation

Research objectives 2 and 3 required elemental imaging of the U biodistribution in *D. magna* from the whole organism to the tissue and cell levels, and often at a date much later than the exposure time. Furthermore, the measurement conditions for the X-ray techniques used in this project called for measurement times that precluded the imaging of a live organism. Therefore, *D. magna* samples were prepared for whole body measurements and sectioned for histological examinations. The overall goal of all sample preparation techniques was to maintain the original biological integrity as much as possible. Thus, the following sample preparations were chosen:

Preparation of Whole Body, Intact Organisms

A method developed for electron microscopy imaging was used to preserve intact *D. magna* (Laforsch & Tollrian 2000). Following the exposure experiment and rinsing step described previously, the daphnid was pre-fixed in 2 mL of 5 % methanol solution for 10 min (Tan et al. 2016). Next, samples were dehydrated in a graded acetone series (70 %, 80 %, 90 %, 2 x 98 %, and 2 x 100 %) for 10 min each and then immersed in 1 mL 1,1,1,3,3,3-hexamethyldisilazane (HMDS, Sigma-Aldrich, St. Louis, USA). Next, ~90 % of

HMDS was removed and samples were left overnight in a desiccator at 200 mbar vacuum for dehydration. The dried specimens maintained internal and external organ structural integrity. Samples were stored at room temperature in plastic dishes until mounted for X-ray analysis (Fig. 6).

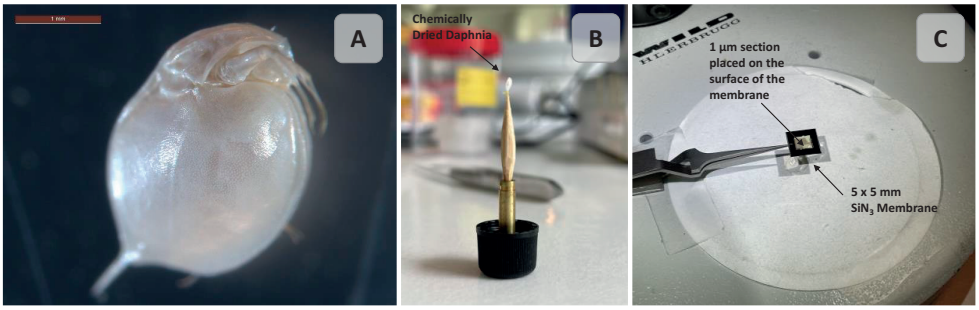

Figure 6: (A) Chemically dried *D. magna* (B) µ-SRXRF Mounting to toothpick (C) nano-SRXRF mounting on SiN_3 membrane

Daphnia were also prepared in an ethanol (100 %) suspension for tomographic measurements. In this case, individuals were placed in a fixative solution of 2.5 % glutaraldehyde and 3 % paraformaldehyde in a Na cacodylate buffer at 0.1 M overnight in cold storage at 4°C. Next, the samples were rinsed in fresh 0.1 M Na cacodylate buffer and dehydrated through a graded ethanol series (30 %, 50 %, 70 %, 90 %, 95 % 1 x 60 min, 100 % 2 x 30 min). Dehydrated, suspended samples were stored at 4°C until measurement.

To address potential U loss during each sample preparation step, exposed daphnia from a pilot study were used. In this test, an aliquot (100 µL) from each sample preparation stage, from the two above techniques, was taken for QQQ-ICP-MS measurement and measured for total U concentration. At the end of the sample preparation, the daphnia was digested for total U measurement (Paper II).

Preparation of Tissue Sections

Histological sections of *D. magna* were required to study the U biodistribution on a tissue and cell level. Whole *D. magna* were fixed overnight using a solution of 2.5 % glutaraldehyde and 3 % paraformaldehyde in a Na Cacodylate buffer (pH 7.2) at 0.1 M at 4°C. Next, samples were washed in fresh buffer and decalcified in 10% HCl for 30 min followed by a 1% osmium tetroxide (OsO_4) buffer step for 1 h in the dark under constant

shaking. Samples were washed in fresh buffer (Na Cacodylate) again and dehydrated in a graded ethanol series (30 %, 50 %, 70 %, 90 % 1 x 1 h, 100 % 3 x 1 h) before embedding in EPON resin (Agar Scientific Ltd., Essex, United Kingdom).

Thin sections (1 – 5 µm for histology, 1 µm for nano-SRXRF), were cut via ultramicrotome equipped with a diamond knife (Diatome Ltd. Nidau, Switzerland). Histological sections were dried on a glass slide and stained with Stevenell Blue dye. Sections were imaged at 10x, 20x, 40x, and 100x magnifications on a Leica DM6B light microscope using the LAS X analysis software (Leica Microsystems, Wetzlar, Germany).

2.2 Analytical Measurement Techniques

X-ray techniques were chosen to characterize the radioactive particles (the Dounreay fuel fragments) and the biodistribution of U bearing nanoparticles (the UNPs) within a biological matrix (*D. magna*) (Fig. 7). These techniques are ideal for their elemental specificity, high spatial resolution, and non-invasive nature that leaves the sample in original, or near-original condition. In the following sections, the specific techniques are explained along with the laboratory instruments and synchrotron facilities where samples were measured. Finally, a few supporting methods are discussed at the end.

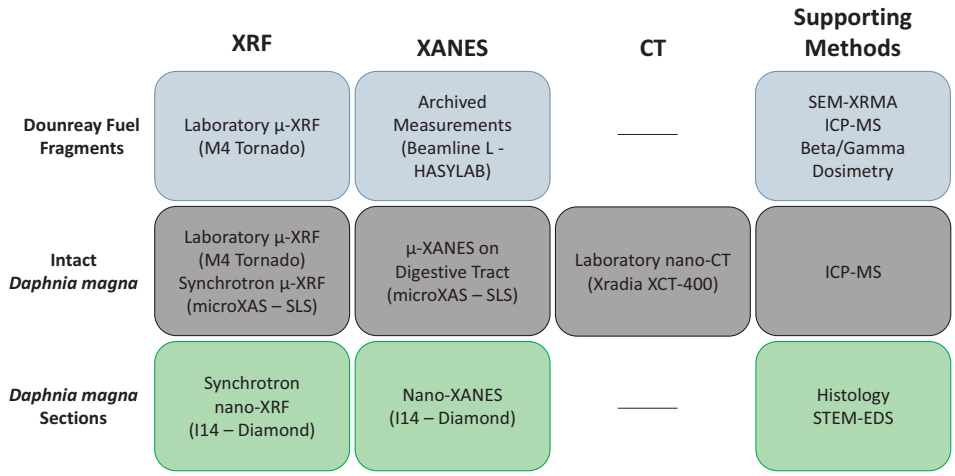

Figure 7: Analytical techniques used to study Dounreay Fuel Fragments and *D. magna* following exposure to UNPs

2.2.1 X-ray Nano and Micro Techniques

X-ray analysis techniques are one of the major scientific advances of the twentieth century and are not restricted to research in physics, being applicable to biological and chemical studies as well. X-rays were traditionally defined by their energies, which range from 120 eV to 120 keV. However, the modern definition differentiates X-rays as photons that originate from processes related to the electrons orbiting the atomic nucleus in contrast to gamma rays which are emitted from the nucleus, fundamental particle decays, and annihilation events (Willmott 2019). By measuring the interactions between X-rays and a sample, various properties can be determined such as elemental composition and spatial distribution, internal structures, and oxidation states of matrix radionuclides. These attributes are critical to the characterization of the Dounreay fuel fragments and UNPs present in this work. More specifically, X-ray fluorescence analysis (XRF), X-ray absorption near edge structure (XANES), and X-ray absorption computed tomography (CT) were used extensively to accomplish the research objectives.

X-ray Fluorescence

Atoms in a sample matrix enter an excited state after an incident X-ray interacts and its energy is transferred to a bound electron. As a result, the excited atom ejects a photoelectron with an energy equal to the difference between the energy of the incident photon and the binding energy of the electron. The atom now has a vacancy in the orbital that emitted the photoelectron which is, in turn, immediately filled by a less strongly bound electron, producing a cascade of shell transitions that emit fluorescent X-rays being characteristic of the absorbing atom. X-ray fluorescence analysis leverages the "fingerprint" nature of these characteristic X-rays emitted by photoelectric absorption to determine the elemental composition of a sample (Haschke 2014). By focusing the X-ray beam into a fine point, a sample can be studied, non-destructively, with a very high spatial resolution (Janssens et al. 2010). X-ray fluorescence was critical to identifying elemental distributions in this work and was employed in every experiment.

X-ray Absorption Near Edge Structure Analysis

As the X-ray beam passes through a target, some fractions of the X-rays interact with the atoms in the sample matrix and are either absorbed or scattered from the beam. The

intensity, I, of an X-ray beam after passing through a sample is described by the Lambert-Beer Law for linear absorption (Willmott 2019):

$$I(x) = I_0 e^{-\mu_L x}$$

where I_0 is the initial intensity of the beam, μ_L is the linear attenuation coefficient (cm^{-1}), and *x* (cm) is the sample thickness. Steep increases in attenuation occur when the X-ray energy matches the ionization potential of a bound core electron. This is called the *absorption edge* and the associated features are reflective of the chemical speciation of the absorbing element. Examining the fluctuations in intensity around the absorption edge in X-ray absorption spectroscopy (XAS) is called X-ray absorption near edge structure (XANES) analysis and was used in this work to interpret the oxidation state of U in Dounreay fuel fragments and in *D. magna* samples following exposure to UNPs and the U_{Ref}. For U, key factors that influence the XANES profile are the valence state and the presence of uranyl species (Denecke 2006). Therefore, XANES analysis of U often requires a well-defined standard to compare against (Salbu, B. et al. 2001; Salbu & Lind 2020).

X-ray Absorption Computed Tomography

Tomography is a method to study the inner structure of a sample by measuring the absorption of X-rays attenuated through a target matrix. These measurements result in a radiograph with contrast that is proportional to the density of the sample matrix, indicative of the relative attenuation coefficient (μ_L) of the material (Kastner & Heinzl 2018). By rotating the sample on its central axis, a series of radiographs can be taken and rendered into "virtual slices", called tomograms, that are stacked into a three-dimensional model of the sample. This method is called computed tomography (CT) and is particularly useful for studying the structural and morphological integrity of soft tissue structures such as those in *D. magna*.

2.2.1.1 Laboratory Techniques

Laboratory instruments take advantage of conventional X-ray tubes to produce a beam suitable for the techniques explained previously. Although laboratory machines do not have the same flux and thereby sensitivity or beam coherence as a synchrotron X-ray source, they have the advantage of accessibility which is particularly helpful when handling materials that require strict controls such as radioactive particles. In this work,

a Bruker M4 Tornado (Bruker Nano GmbH, Berlin, Germany) was used to conduct μ-XRF elemental mapping of Dounreay fuel fragments and daphnia samples and a Zeiss XRadia Micro XCT-400 (Carl Zeiss, Oberkochen, Germany) was used to conduct tomography of *D. magna*.

Bruker M4 Tornado μ-XRF

The M4 Tornado is a commercially available benchtop μ-XRF equipped with a Rh-target X-ray tube with a 0.1 beryllium side window that was operated at 50 kV and 600 μA for measurements made in this work. The X-rays are focused into a "pencil tip" beam using polycapillary optics. In brief, hollow, glass capillaries collect X-rays emerging from the Rh tube and redirects them, by total reflection within the capillary, to form a focused tip similar to a sharpened pencil (Haschke 2014). The resulting focal spot size is excitation energy and working distance dependent. Per the manufacturer's settings, the focal spot size was ~ 25 μm in this work. The detection of fluorescent X-rays was facilitated by two XFlash® silicon drift detectors (type SDD VH50P) at 45° angles to the X-ray beam and feature an active area of 30 mm^2 each. The samples are mounted on a stage that can move in the x-y-z with an x-y step control down to 5 μm allowing for oversampling.

In the present work, the M4 Tornado μ-XRF was mainly used to scan and determine the elemental distributions in Dounreay fuel fragments. The 25 μm beam and 5 μm pixel size (through oversampling) were just sufficient to investigate the larger MTR particles, which were 1 – 2 mm in size, and the smaller DFR particles (< 500 μm). Details of the specific measurements taken can be found in Paper I. Daphnia samples were also measured on the M4 Tornado. Ease of access to the instrument allowed for measurement of anesthetized daphnia immediately following exposure. Individuals were secured between two pieces of ultralene (6 μm) and measured at atmospheric pressure for 3 cycles. Measurement settings were chosen such that the total measurement time did not exceed 1 h to avoid distortion from evaporation of water. Preserved samples from the chemical drying preparation were also measured under vacuum conditions (20 mbar) to improve signal quality. Elemental mapping for these samples was made at 5 μm step size and repeated 10 times to improve the signal-to-noise ratio.

The M4 Tornado includes on-board software, ESPIRIT (Bruker Nano GmbH, Berlin, Germany), for visualization and analysis during and after scanning. Further analyses

were made possible by exporting the elemental mapping data to the DataMuncher software which converted the raw data into edf line scan files, sum spectra, and maximum pixel spectra (Alfeld & Janssens 2015). These files were, in turn, read into the software package PyMCA to perform fitting of the sum and maximum pixel spectra (Solé et al. 2007). ImageJ was used to color and restack final images (Schindelin et al. 2015).

XRadia Micro XCT-400

The XRadia Micro XCT-400 is a laboratory CT scanner at the Faculty of Materials Science and Engineering at the Warsaw University of Technology used to render full body reconstructions of *D. magna* prepared by both chemical drying and in the ethanol suspension. This instrument is equipped with a Hamamatsu 150 keV X-ray source and a 2K Andor CCD camera. The XCT-400 innovates on conventional projection CT by pairing a micro-focused X-ray source with a series of focusing optical lens (0.5x, 4x, 10x, 20x, and 40x). Each objective first contains a scintillator that converts the X-ray projection into visible light which is, in turn, magnified through the lens improving the resolution of the image. This system has two critical advantages for studying the *D. magna* samples as it improves the contrast and resolution of small structures, down to submicron, within the sample and it provides improved phase contrast for low Z elements. As a result, no staining was necessary to visualize the soft tissue structures in *D. magna* for this work.

Daphnia magna exposed to UNPs (320 μg L^{-1}), the U_{Ref} (159 μg L^{-1}), and controls were scanned at a 2 μm resolution with 1000 projections taken over the 180° rotation. The reconstructed output contained a stack of tomograms (virtual slices), visualized using DataViewer (Bruker Nano GmbH, Berlin, Germany), that revealed the inner morphology of the measured organisms in a greyscale that was correlated with X-ray attenuation in the sample. The tomograms were mainly visualized in the X-Z plane to match the dorsal histological sections such that internal structures such as the hepatic ceca and midgut of the daphnia could be easily identified. Further data handling, analysis, and volumetric reconstruction was completed using Bruker visualization software solutions (CTVOX, CTVOL, CTAN, Bruker Nano GmbH, Berlin, Germany). In brief, CTVOX and CTVOL handled the rendering of tomographic data and sample coloring and transparency, while CTAN provided density examination, size and structure measurements, and region-of-interest analyses (Paper III).

2.2.1.2 Synchrotron Techniques

Synchrotron radiation is produced through the energy loss from charged particles, usually electrons, that are accelerated radially (i.e., perpendicular to the direction of travel). A *synchrotron* is a source of X-rays that consists of an evacuated storage ring (on the order of hundreds of meters to kilometers in diameter) inside which highly energetic electrons are circulated at relativistic velocities to produce synchrotron radiation (Willmott 2019). A synchrotron facility provides a high intensity source of X-rays that is also highly coherent and tunable; the resulting beams have dimensions on the scale of a micrometer down to a few tens of nanometers. The energy of the monochromatic beams produced in coherent undulator sources can be tuned to take advantage of the energy dependence of photoelectric absorption providing key advantages to element-specific sensitivity and speciation analysis (via XANES as previously discussed). In comparison to the previously discussed laboratory techniques, synchrotron beamlines offer unparalleled fluxes and resolution with better sensitivity for excitation of matrix elements and improved signal-to-noise ratios resulting from the incident monochromatic beam. Furthermore, a range of analysis techniques are possible at the same beamline end station.

In the presented study, experimental measurements to assess the biodistribution of U in *D. magna* on an organism level and within tissues and cells were conducted at the microXAS beamline (X05LA) at the Swiss Light Source (SLS), Switzerland and the i14 beamline at the Diamond Light Source, United Kingdom. Archived μ-XANES measurements of Dounreay fuel fragments were used in this work, however; these measurements were conducted prior to the PhD project at beamline L, HASYLAB, Hamburg. The parameters of the two facilities and beamlines used in this work are summarized in Table 1.

Table 1: Synchrotron Facilities Used in this Work

Facility, Country	Storage Ring Circumference (m)	Storage Ring Energy (GeV)	Brilliance (ph/s/mm²/mrad²/0.1% BW)	Beamline	Beam Diameter (nm)	Photon Energy Range (keV)	Methods Used	Samples Examined
Diamond Light Source, United Kingdom	562	3.0	3×10^{20}	i14	65	5 - 23	Nano-XRF Nano-XANES	*Daphnia magna* Sections
Swiss Light Source, Switzerland	288	2.4	4×10^{19}	microXAS	1000	3 - 23	μ-XRF μ-Tomography μ-XANES	*Daphnia magna* Whole Organisms

Swiss Light Source microXAS Beamline

Analyses of whole body, intact daphnia were performed at the microXAS (X05LA) beamline at the Swiss Light Source. The instrument facilitates microscale multimodal chemical imaging using XRF, XAS, and XRD techniques. The microXAS beamline was chosen due to the improved beam intensity, detector sensitivity, and 10-fold improvement of XRF mapping resolution over the laboratory μ-XRF. These improvements facilitated the identification of organ and tissue specific elemental distributions in UNP and U_{Ref} exposed *D. magna*. Chemical speciation measurements via XANES analysis were also conducted in support of the elemental distribution measurements.

Daphnia samples, following chemical drying, were mounted by gluing the sharpened point of a toothpick to the bottom of the carapace at the tail spike (Fig. 6B). Replicates were also mounted to Kapton tape inside a film cassette in case the toothpick mounted samples were damaged in transit to the beamline. At microXAS, the incident photon energy was set to 17.2 keV, just above the U L_{III} absorption peak, and each daphnia sample was first subjected to rapid scans at 20 μm resolution with a 200 ms dwell time. Next, a 5 μm resolution whole body scan was performed. Using the resulting U distribution map, ROIs were selected for 2 μm resolution elemental mapping and sections were chosen for tomographic slices. These scans were performed on a UNP (320 μg L^{-1}), a U_{Ref} (159 μg L^{-1}), and a control daphnia sample (Paper II). To complement the CT anatomical assessments, a ROI (2 μm resolution) around the midgut and hepatic ceca was scanned for the UNP and the U_{Ref} daphnia samples. Hotspots of U identified in the UNP exposed organism were chosen for XANES analysis (Paper III). Additionally, dry UNP powders

were thinly spread onto Kapton tape and sealed by folding it over. This sample was used for characterization of the dry, pristine UNPs by XANES analysis (Paper II).

Diamond Light Source i14 Beamline

A nanoscale beam was needed to identify the distribution of U in tissues and cells from histological sections and beamtime was granted at the hard X-ray nanoprobe (i14) at the Diamond Light Source (Oxfordshire, UK) (Quinn et al. 2021). Thin (1 µm) sections of daphnia cut dorsally through (1) the hepatic ceca and (2) the midgut were mounted on 5 x 5 mm SiN_3 frames (Silson Ltd., Warwickshire, UK) (Fig. 6C). For each sample, the resultant microtomy section was stained for conventional histological assessment by light microscopy where ROIs were pre-identified prior to the beamtime. At i14, the sample frames were placed inside the holder and secured in the beamline for nano-SRXRF elemental mapping using an incident beam energy of 17.3 keV (Paper III). Each sample was first investigated with coarse 50 x 50 µm scanning with a 225 nm step size and a 200 ms dwell time. For fine resolution ROI maps, a 75 nm step size was used and the dwell time was increased to 400 ms. The hepatic ceca sections of a UNP (320 µg L^{-1}) and a U_{Ref} (159 µg L^{-1}) exposed daphnia were measured. Only the midgut of the U_{Ref} exposed organism was measured due to complications installing the UNP exposed sample at the beamline. Areas of high U intensity were selected for XANES analysis, however, the concentration was below the detection limit for this technique.

Raw Data Analysis

Measurements at the synchrotron beamlines produce a large volume of data that requires reduction. Therefore, several methods are needed to extract useful results from the beamline experiment. PyMCA is an open source toolkit developed by the Software Group at the European Synchrotron Radiation Facility (ESRF) for treating X-ray fluorescence spectral data (Solé et al. 2007) and was used to fit all sum spectra and produce imaging results (TIFF files). Image files for each element were then imported to ImageJ (Schindelin et al. 2015) where the contrast could be adjusted, Look-Up Tables (LUTs) applied, and multiple images stacked to produce multicolor images. X-ray absorption raw data, for XANES analysis, was treated using the ATHENA software (Ravel and Newville 2005).

2.2.2 Supporting Measurements

Although the X-ray based analyses in this work were critical to accomplishing the research objectives, supporting measurements were still needed to properly interpret results. In the following sections, the supporting methods will be briefly described.

Electron Microscopy

The resolution of the M4 Tornado μ-XRF was too low to properly assess structural and morphological features of the Dounreay fuel fragments. However, scanning electron microscopy (SEM) is an extensively used method to characterize such particles and properties (Salbu & Lind 2020). Additionally, X-ray micro-analysis (XRMA) can provide point elemental identification that compliments the XRF scanning. Each of the Dounreay fuel fragments in this work were analyzed using a JEOL JSM 840 with an ISIS 300 XRMA system (Oxford Instruments, Oxford, UK) (Paper I). Secondary electron imaging (SEI) mode was utilized to view surface structures of the particles, while backscatter electron imaging (BEI) mode highlighted areas of high density (i.e., indicative of high atomic number elements such as U). All SEM-XRMA measurements were completed prior to this PhD project and before the blue mussel study conducted by Jaeschke et al. (2015).

Scanning transmission electron microscopy (STEM) is a high magnification, subcellular resolution analysis technique employed to assess ultrathin (< 100 nm) sections of *D. magna* midgut from UNP and U_{Ref} exposures. When coupled with Energy Dispersive X-ray Spectroscopy (EDS), features such as the UNPs around and inside gut epithelial cells can be identified. This technique is complimentary to the nano-SRXRF conducted at Diamond i14 but has the advantage of higher magnification which facilitates viewing U spatial distributions in and around the gut microvilli, a critical region of potential uptake, and inside intestinal cells. However, due to the limited field of view, STEM-EDS analyses were difficult to interpret and spatially correlate to histological effects in the way that was accomplished with nano-SRXRF.

Inductively Coupled Plasma Mass Spectrometry

A review of literature indicated the Dounreay fuel fragments were highly enriched with respect to ^{235}U for nuclear fuels, which are normally < 20 % ^{235}U (Choppin et al. 2002; Dennis et al. 2007). However, the X-ray techniques used to study the particles cannot provide information on the isotopic composition of U in the particles. Therefore, small

fragments of MTR2 and DFR3 were sacrificed, digested, and measured using QQQ-ICP-MS (Agilent 8900, Hachiōji, Japan) to determine $^{235}U/^{238}U$ isotope ratios. The method is described in detail in Paper I.

Quantitative analysis of elemental concentrations in UNP stock suspensions, exposure experiment media and size distribution fractions, as well as U body burden in *D. magna* were all conducted using QQQ-ICP-MS and those specific methods are explained in Papers II – III.

Radiation Dosimetry

Harrison et al. (2005) provided a detailed assessment of the health risks from encountering a Dounreay fuel fragment. The proposed model has been generalized to fit all Dounreay fuel fragments for the purposes of public safety. On contact with the radioactive fuel particle, the beta and gamma emissions are of primary concern, as alpha radiation would not penetrate the dead layer of skin. Harris et al. determined that a $^{90}Sr/^{137}Cs$ ratio of 0.9 could be used to estimate the ^{90}Sr (and ^{90}Y) activity and associated beta emissions after non-destructive measurement of ^{137}Cs via conventional gamma spectrometry. To test this ratio, a SPAB-15 alpha/beta probe containing a Passivated Implanted Planar Silicon (PIPS) detector connected to a Radiagem 2000 Portable Dose Rate and Survey Meter (Mirion Technologies, Lamanon, France) was used to measure beta emissions and to estimate the $^{90}Sr/^{90}Y$ activity in each particle (Paper I). Next, each particle was examined using gamma spectrometry (Liquid Nitrogen Cooled Low Energy Germanium detector, Canberra Instruments, relative efficiency 25 %, resolution 1.8 keV) to determine the ^{137}Cs activity. Finally, VARSKIN 6 was used to calculate the contact dose based on the ^{90}Sr and ^{137}Cs activities. VARSKIN6 is a skin dosimetry calculator developed by the United States Nuclear Regulatory Agency (USNRC) out of the information published in NCRP 130 (Gesell 1999) and utilizes a different mathematical model (Anspach & Hamby 2018) that, to the knowledge of the authors of Paper I, has not yet been used to assess Dounreay fuel fragments. The results, $^{90}Sr/^{90}Y$ activity and skin dose per particle were compared with the model presented by Harrison et al., 2005.

3 Summary of Papers

3.1 Paper I

Characterization of Radioactive Particles from the Dounreay Nuclear Reprocessing Facility

Ian Byrnes, Ole Christian Lind, Elisabeth Lindbo Hansen, Koen Janssens, and Brit Salbu

https://doi.org/10.1016/j.scitotenv.2020.138488

In Paper I, the physico-chemical properties of two varieties of Dounreay fuel fragment, MTR and DFR particles, were studied and compared, and the existing radiation dosimetry model was tested (Fig. 8). The results showed MTR and DFR particle characteristics differed considerably. Particles derived from the MTR were larger (740 – 2000 μm) and metallic, showing characteristics that were indicative of the UAl_x type source fuels. Using laboratory μ-XRF analysis, MTR particles exhibited U and Al heterogeneously distributed on the surface of the particle with Nd colocalized with U at 1 – 2 % mass concentration. The elemental mapping complimented SEM-XRMA analysis and point XRF spectra showed a 25 – 45 mass % U variation on the surface. Analysis of the oxidation state of the MTR particle indicated U(IV) was present and could be associated with oxidation of U on the surface, as may be expected for UAl_x type fuels. In contrast, DFR particles were smaller (100 – 300 μm) and contained spatially correlated U and Nb, part of the original fuel cladding, with an atomic ratio of ~2. Analysis by μ-XANES also pointed to U(IV) which, along with stoichiometric considerations, suggested DFR particles may be a UNb_2O_7 alloy that formed during high temperature reprocessing accidents. Analysis of $^{235}U/^{238}U$ isotope ratios in both types of particles indicated the presence of highly enriched uranium (> 70 % ^{235}U) in agreement with literature values. Based on this characterization, a dose assessment was performed for each Dounreay fuel fragment to test an existing model that assumes an MTR particle of homogeneously distributed U (15 % by mass) with a $^{90}Sr/^{137}Cs$ ratio of 0.9. Measured beta/gamma emissions were proportional for all particles investigated ($^{90}Sr/^{137}Cs$ activity ratio ≈ 0.8) and correlated to the particle size. Contact dose rate for the largest MTR particle was 74 mGy h^{-1}. Although the particle characterization differed from the existing model, dose assessments were in agreement.

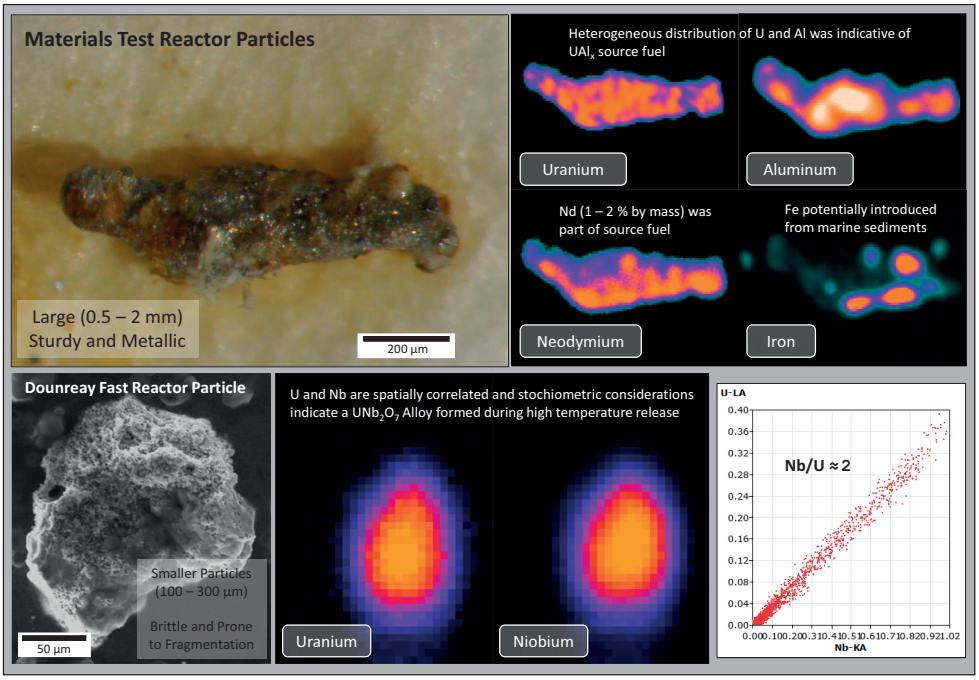

Figure 8: Graphical summary of the main findings of Paper I

3.2 Paper II

Synchrotron-based X-ray Fluorescence Imaging Provides New Insights on Uranium Toxicokinetics in Daphnia magna following Exposure to Uranium Nanoparticles

Ian Byrnes, Lisa Magdalena Rossbach, Dag Anders Brede, Daniel Grolimund, Dario Ferreira Sanchez, Gert Nuyts, Vaclav Cuba, Estela Reinoso-Maset, Brit Salbu, Koen Janssens, Deborah Oughton, Shane Scheibener, Hans-Christian Teien, Ole Christian Lind

In Paper II, the biodistribution and adverse effects in *D. magna* following exposure to UNPs and U_{Ref} solutions were investigated using a combination of synchrotron based XRF analysis and acute toxicity tests (Fig. 9). Speciation analysis of the exposure solutions revealed U was present in the LMM, colloidal, and particulate fractions in both treatments indicating dissolution of the UNPs and colloid formation in the U_{Ref} solution. Despite similarities of the U speciation, acute toxicity tests (48 h) indicated minor differences in lethal concentration (LC_{50}) of the UNP suspension (LC_{50} = 402 μg L^{-1} [336 - 484]) and the U_{Ref} solution (LC_{50} = 268 μg L^{-1} [229 - 315]). The neonate exposure (< 18 h) yielded comparable LC_{50} values (UNP LC_{50}: 127 μg L^{-1} [102 - 163], U_{Ref} LC_{50}: 112 μg L^{-1} [89.5 - 136]). However, despite a 3- to 5-fold greater uptake of the UNPs, results indicated lower toxicity from the NPs, compared with the U_{Ref}.

The μ-SRXRF results revealed U distributed throughout most organs and tissues of *D. magna* following both the UNP and the U_{Ref} exposures with similar target areas of accumulation. On the external surfaces, U bound to the gills (epipodites) suggested a potential site of systemic uptake. In both treatments, U was significantly concentrated within the digestive tract where U was measured in association with the luminal contents and the soft tissues, which indicated a potential uptake route through the epithelial cells. In the UNP exposed organism, high intensity U hotspots were observed in the midgut, not seen in the U_{ref} exposed daphnia. Accumulations in the heart and the maxillary gland, an organ associated with the excretory system, suggested systemic uptake of U into the haemolymph of *D. magna*. Moreover, U identified in the nephridium, a kidney-like organ associated with the maxillary gland, may be a possible removal mechanism. The age of the daphnia was chosen such that maternal transfer could be investigated and the studied daphnia exposed to the UNPs exhibited U in the embryos. Additionally, U bearing structures, possibly remains of the chorion, were observed in the brood chamber. Despite U accumulations by the embryos, a reproduction follow-up study showed successful

spawning of the subsequent generation (F1). Nevertheless, the F1 generation exhibited developmental effects including early reproduction and increased fecundity compared to control.

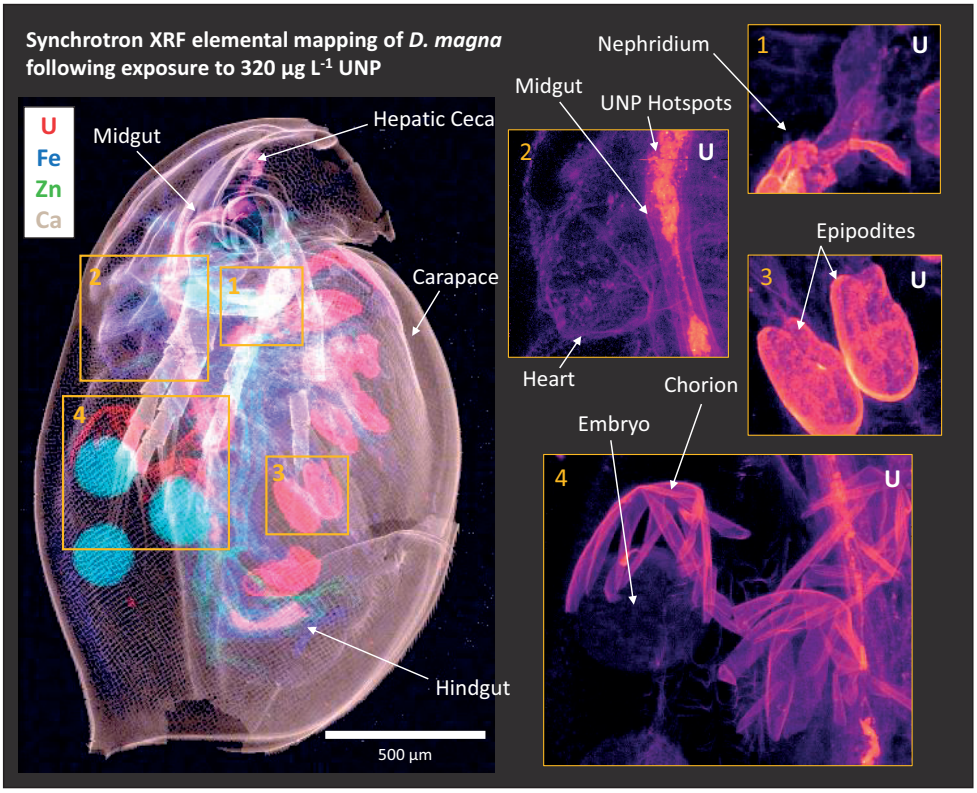

Figure 9: Graphical summary of the µ-SRXRF results from Paper II

3.3 Paper III

Combined Structural and Nanoscopic Elemental Imaging Identifies Damage to Digestive Tract of Daphnia magna associated with Uranium Nanoparticle Acute Toxicity

Ian Byrnes, Lisa Magdalena Rossbach, Jakub Jaroszewicz, Daniel Grolimund, Dario Ferreira Sanchez, Miguel Gomez-Gonzalez, Gert Nuyts, Estela Reinoso-Maset, Koen Janssens, Brit Salbu, Dag Anders Brede, Ole Christian Lind

In Paper III, organ, tissue, and cell histological effects in the digestive tract of *D. magna* following sublethal exposure to UNPs (320 μg L^{-1}) and a U_{Ref} solution (159 μg L^{-1}) were compared with U distributions determined by μ-SRXRF and nano-SRXRF (Fig. 10). Adverse morphological changes to the hepatic ceca and midgut regions of the digestive tract were visualized using laboratory-based CT at a voxel size of 2 μm. The resulting analysis identified damaged, shrunken hepatic ceca in exposed daphnia from both treatments with at least a 2-fold reduction in volume compared with unexposed organisms. Elemental mapping (2 μm step size) using μ-SRXRF showed U had migrated out of the midgut and into the ceca. Furthermore, U appeared predominantly associated with the contents of the lumen in both exposures (UNP and U_{Ref}). Intestinal epithelial tissues also exhibited U signal suggesting uptake in the cells and, potentially, further into the body systems. Nano-SRXRF (75 μm step size) was used to assess histological sections (1 μm) of hepatic ceca and midgut tissues. Damages to cells and tissues were identified with traditional light microscopy and regions of interest were scanned at the hard X-ray nanoprobe (I14) at the Diamond Light Source. Using the Os signal, introduced as part of the sample preparation, elemental maps were overlaid on histological images to show the correlation between the U distribution and the tissue and cell damages. Small U particulates (380 – 970 nm) were identified throughout the damaged tissues of the hepatic ceca in both the UNP and the U_{Ref} exposure. Analysis of the midgut contents found additional U particulates throughout the lumen as well as localized within a detached epithelial cell. Partially digested algae content in the lumen contained a substantial U signal indicating possible sequestration within the digestive tract following exposure.

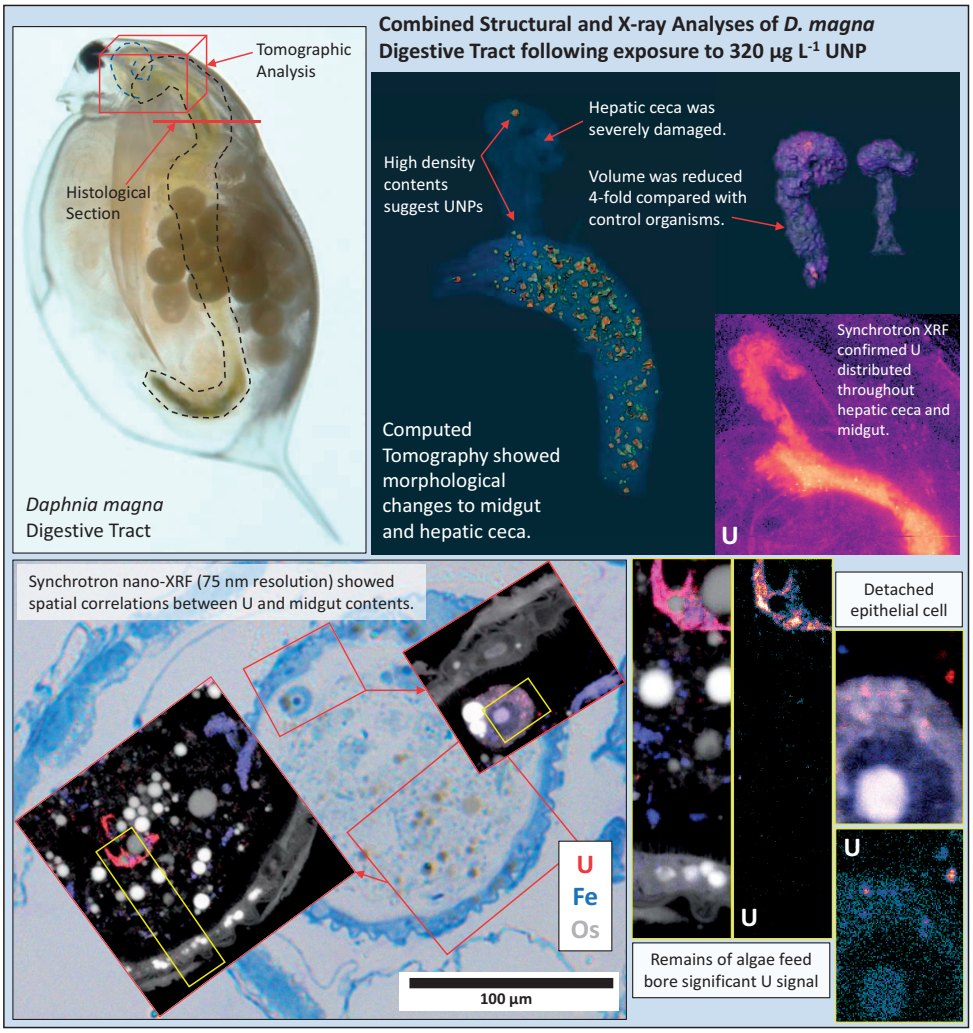

Figure 10: Graphical summary of the results from Paper III

4 Discussion

The main objective of the presented research was to reduce uncertainties in environmental impact and risk assessments brought about by a lack of scientific understanding related to the behavior and impact of nm to mm sized radioactive particles. Previous studies have shown that radioactive particles feature physico-chemical properties that are source term and release scenario dependent (Salbu et al. 2015). However, a remaining challenge is to link those characteristics to environmental behavior and uptake in biota, in order to develop a more holistic view of the exposure characterization (Salbu et al. 2018). Doing so represents several challenges that were interrogated in this work. Ecosystem mobility and exposure risk to biota are influenced by biogeochemical processes between the particle associated elements and the environmental media in the immediate vicinity of the particle. At smaller sizes (< 0.45 μm), colloids and NPs may be retained inside organisms resulting in retention in organs and tissues, and may be of consequence to toxicity. Furthermore, linking the internal localization of contaminants to adverse effects is critical for determining the hazard to biota.

The research performed during this PhD project addressed these uncertainties by characterizing the compositional and morphological properties of Dounreay fuel fragments and the biodistribution following exposure to UNPs in the model organism *D. magna*. For this purpose, analytical X-ray techniques were employed for nondestructive analyses of elemental distributions, oxidation states, and morphology. The approaches used for characterizing environmental Dounreay particles were adapted from mature, existing methodologies (Salbu & Lind 2020) (Paper I).

By combining rigorous NP characterization (Kleiven et al. 2018), synchrotron techniques for *D. magna* biodistribution assessment (De Samber et al. 2013), and histological evaluation of biological effects, this work represents the development of a robust experimental platform for studying consequences of colloid and NP exposure (Paper II – III).

4.1 Characterization of Dounreay Fuel Fragments

An estimated total activity of 10 PBq was discharged to the marine environment during operations at the Dounreay facility until decommissioning in 1994 (DPAG 2008). As a

result, a fishing exclusion zone (2 km) around the facility and routine monitoring programs of local beaches have been implemented due to potential risks to the public from radioactive particles (PRAG 2012). Therefore, there is an environmental and public health interest to characterize various types of Dounreay particles with respect to properties of relevance for ecosystem transfer, weathering and remobilization, as well as potential biological uptake and effects associated with contact doses. The compositional and morphological characteristics should also be of relevance to a broader range of environmental radioactive particles (e.g., other spent fuel particles such as those from Sellafield).

The Dounreay fuel fragments presented in the current study displayed physico-chemical properties that were closely associated with their unique source term and release scenario (Paper I). A review of literature descriptions and reports from the UKAEA and SEPA (Dennis et al. 2007; DPAG 2008; Harrison et al. 2005; PRAG 2012) was needed to reconstruct the series of events that led to the formation and release of these particles and guided the characterization efforts by focusing work on the U-Al distribution in MTR samples and stoichiometric considerations of U and Nb in DFR samples. As Dounreay fuel fragments represent a significant source of external radiation exposure, characterization methods required safety protocols to be in place at the local laboratory in order to perform measurements, making studies at an external facility, such as a synchrotron, challenging. However, the laboratory μ-XRF exhibited sufficient sensitivity and spatial resolution for visualizing the elemental distribution in Dounreay fuel fragments, and the results complemented SEM-XRMA analyses. Heterogeneously distributed U and Al in MTR particles was characteristic of "swarf" created from reprocessing of UAl_x type fuels (DPAG 2008; Hough 1997). In contrast, the spatial symmetry of U and Nb in DFR particles was an intermetallic U-Nb alloy (UNb_2O_7) formed during high temperature (> 1133° C) reprocessing incidents (Henderson 2007). The characterization presented in this work should be seen as a refinement of previously published descriptions (Bremier et al. 2002; Dennis et al. 2007) and a step towards reducing uncertainties related to the origin, formation, and release scenario of historical radioactive particles that escaped from the Dounreay facility.

Most Dounreay fuel fragments spend a significant period of time (e.g., up to decades) in the marine ecosystem before washing up on the local shoreline. The particles are

identified by their gamma emissions and characterized a long time after the initial release. Structural investigations by SEM-XRMA revealed features that suggest environmental weathering processes occurred in the marine environment. In MTR particles, pitted regions of higher U concentration relative to smooth surfaces suggested weathering of exposed U-bearing phases. Corrosion of UAl_x fuels has been shown to contain a UO_2 colloidal phase (Kaminski & Goldberg 2002; Kaminski et al. 2005), conceivable for MTR particles. Therefore, leaching studies that utilize size fractionation of leachates, like the IAEA CRP/EU COMET-RATE protocol (Salbu & Lind 2020), could demonstrate such potential in MTR particles in the future. Smaller particles and colloids may form through mechanical breakdown as well, particularly for DFR particles which were prone to fragmentation. Particle contaminated sites tend to have log normal size distributions (Kashparov et al. 2000; Shevchenko 2004) and increasingly small fragments of DFR (and probably MTR) particles should be expected. The majority of recovered Dounreay fuel fragments are classified by site authorities as *minor* based on radiological risk; meaning gamma spectrometry measurements showing < 10^5 Bq ^{137}Cs (Dennis et al. 2007). However, smaller particles, especially colloids and nanoparticles formed through weathering processes, would be difficult to identify through ^{137}Cs activity, while still posing a risk due to a higher ecological transfer compared to larger particles. Although studies have indicated the probability of encountering a Dounreay fuel fragment is low for biota (Jackson et al. 2007), smaller particles and colloidal species bring uncertainties to such assessments as they are assumed to be more mobile and potentially more bioavailable than larger particles.

4.2 Exposure to Dounreay Fuel Fragments

The physical-chemical properties of particles and nanoparticles are important to assessing the exposure in biota. Upon uptake and retention of a Dounreay fuel fragment, the major risk at the target site is an acute radiological exposure resulting from the high specific activity from a point source. Based on measurements of beta/gamma emissions from the particles in this work, MTR and DFR particles delivered contact doses of 4.9 – 74 mGy $h^{-1}$and 0.22 – 0.82 mGy h^{-1}, respectively, that were roughly proportional to the particle size (Paper I). Modeling studies have shown near complete self-absorption of alpha emissions within the particle matrix for sizes > 20 μm (Caffrey et al. 2017), therefore, the alpha dose was considered negligible for this study. For the largest MTR

particle (MTR1), the threshold for skin ulceration (2 Gy) would be reached within 27 h (NRPB 1997). This was in line with Jaeschke et al. (2015) who demonstrated up to 70 h retention times in blue mussels that led to localized necrosis in the mantle tissues. The potential radiological risks from contacting a Dounreay fuel fragment have been studied previously and a model was put forward that assumed an MTR particle that contained 15 % U, uniformly distributed with a 0.9 $^{90}Sr/^{137}Cs$ ratio (Charles 2009; Harrison et al. 2005; J. Darley et al. 2003). Dounreay Fast Reactor particles were not evaluated separately as they are generally smaller, found less frequently, and have a lower specific activity than MTR particles. Therefore, a model effective for MTR particles was assumed to deliver conservative estimates for DFR particles as well. The dose assessment performed in this work found a $^{90}Sr/^{137}Cs$ ratio of ~ 0.8 for every studied particle (MTR and DFR) and the resulting beta/gamma dose rates were in close agreement with the existing model. Therefore, this work showed the model was effective for the assessment of DFR particles despite their differences in physico-chemical properties. Furthermore, the μ-XRF analysis of the MTR particles showed that U on the surface varied from 25 – 45 % by mass, counter to the 15 % assumption in the model. However, these results did not have a measurable impact on the dose assessment. By validating the model, this work reduced the overall uncertainties by demonstrating its application to well characterized MTR and DFR particles.

4.3 Characterization of Uranium Nanoparticles

Characterization of the UNPs following synthesis indicated that UO_2 was predominant in their pristine condition (Paper II). Further characterization of the particles in suspension and throughout the exposure time was necessary to interpret the subsequent biodistribution and effects in *D. magna*. As discussed previously, UO_2 based NPs were considered relevant test particles as they have been observed in both laboratory and field cases (Kaminski et al. 2005; Neill et al. 2019; Wang et al. 2014). The characterization of the stock suspension for all three exposures showed that the sonication was an effective and highly reproducible method for UNP preparation (Paper II – III). However, a minor variation in the average hydrodynamic diameter, possibly resulting from slight differences between sonication procedures, was observed in the adult daphnia toxicity test (273.3 ± 1.2 nm as opposed to 205.7 ± 8.1 and 185.6 ± 0.6 nm for the neonate toxicity test and imaging sample exposure respectively) indicating aggregation of the UNPs in the

MHRW. All measurements of zeta potential were between -9.01 and -11.8 mV. Collectively, these results indicate that particle repulsive forces were insufficient to completely prevent aggregation, indicating that the stock suspensions were slightly unstable (Handy et al. 2008). Due to the comparatively low concentration of UNPs in the exposures as well as confounding factors from the media (MHRW), DLS measurements were not possible and size fractionation was needed to assess the distribution of U species therein.

Size fractionation measurements after the introduction of the UNPs to the MHRW in all experiments revealed a consistent distribution pattern of U throughout measured concentrations over the course of the 48 h exposure (Papers II – III). Uranium was observed in the colloidal fraction (27 – 71 %, 3 kDa < x < 0.45 μm) as well as the LMM (0 – 53 %, < 3 kDa) and particulate (5 – 28 %, > 0.45 μm) fractions indicating both dissolution of the UNPs and aggregation to particle sizes > 0.45 μm. Dissolution of the UNPs into LMM species was greater than expected, often equal to or larger than the colloidal fraction, and may have occurred immediately following the addition into the MHRW given the t = 0 h distributions. The release of LMM species may have been promoted by oxidation, which was observed in the pristine UNPs measured at microXAS for μ-XANES analysis (Paper II). During the preparation of UNP stock suspensions, the particles could have been oxidized by heat development from the high frequency sonication despite the use of an ice bath during the procedure. The UNPs were synthesized using a method that included photochemical reduction of U(VI) to U(IV) (Pavelkova et al. 2013) and may have been inherently prone to oxidation. Therefore, dissolution would be unavoidable upon suspension in an oxic environment such as the MHRW media used in the present work.

The same fractionation measurements were carried out on the U_{Ref} exposures and yielded a somewhat similar size distribution to the UNP suspensions in all experiments. Uranium species were present in the LMM fraction (10 – 59 %), but also in the colloidal (22 – 61 %) and particulate (3 – 25 %) fractions. These results were surprising as the U_{Ref} exposure was expected to contain predominantly LMM species. The freshwater speciation of U is, however, complex due to the formation of several hydrolysis products and complexes with organic and inorganic ligands (Lofts et al. 2015). Uranium observed in colloidal and particulate phases of the U_{Ref} solution could occur through

polymerization of U in the media or potentially by complexation with organic exudates from *D. magna*. Exposure experiments in this work were conducted at pH 6.8, where the predominant uranyl species was expected to be uranyl-hydroxide-carbonate $(UO_2)_2(OH)_2CO_3^-$, while polymeric species were expected to constitute an important phase at concentrations > 200 µg U L^{-1} (Markich 2002). Additionally, ternary uranyl complexes, such as $Ca_2UO_2(CO_3)_3$ or $Mg_2UO_2(CO_3)_3$, could be present in the exposure, as evidenced by modeling studies (Vercouter et al. 2015). Given the LMM fraction observed in the UNP exposures, it is conceivable that the same processes may have occurred there as well, and the commensurate colloidal fractions may have contained additional U colloids different from the original UNPs.

The size distributions observed in these experiments were comparable with those found in uranyl exposure studies using Atlantic salmon by Song et al. (2012), who conducted similar size fractionation and observed 38 – 74 % in the LMM fraction and 18 – 58 % in the colloidal fraction in lake water of pH 7.1. Additionally, the LMM fraction was highly anionic suggesting the presence of mostly uranyl species (Song et al. 2012). In many ecotoxicology studies with U, it is common practice to filter water samples through a 0.45 µm filter and report the filtered fraction as the "dissolved fraction". However, this description is incomplete and does not capture the contribution of colloidal species. In some cases, when the > 0.45 µm fraction is reported, the distribution appears similar to the U_{Ref} in this work (up to 30 %) (Simon et al. 2019). Therefore, U colloids may be more prevalent in U toxicity studies than are reported and the characterization of colloids and NPs in this work may be a model for future U toxicity studies, providing a framework to better characterize U exposures.

4.4 Uranium Biodistribution in *Daphnia magna* following Exposure to Uranium Nanoparticles

To study the uptake and retention of colloidal species, the U biodistribution in *D. magna* following exposure to UNP (320 µg L^{-1}) and U_{Ref} (159 µg L^{-1}) solutions was visualized using laboratory and synchrotron based µ-XRF analysis (Fig. 11). However, the resolution and superior LOD at the microXAS beamline (SLS) was critical to determining U in target organs and tissues. At the highest concentrations (> 200 µg U L-1), U was visible in the digestive tract of exposed daphnia during *in vivo* measurements using the M4 Tornado laboratory µ-XRF (20 µm step size, 90 ms $pixel^{-1}$). However, the low signal-

to-noise resulted in an unclear map for any area outside of the intestine and subdivisions of the intestine itself were not identifiable due to the 20 µm step size used for live measurements. Chemically drying the daphnia allowed for long measurement times (5 µm step size, 300 ms pixel^{-1}) under vacuum (20 mbar) using the M4 Tornado. Although this technique had the effect of reducing the background noise, it did not result in identification of other regions of U accumulation outside of the digestive tract.

The improvements in the elemental mapping brought by the measurements at microXAS clearly demonstrated the advantages of synchrotron beamline measurements. First, the tunability of the X-ray beam energy means that U can be excited specifically at the absorption energy (17.3 keV) resulting in an improved fluorescent yield. Second, beamlines are paired with detector systems that allow measurements of concentrations down to ppb. As a result, U was identifiable throughout the daphnia following exposure to UNPs with key areas of accumulation including the epipodites, the digestive tract, the heart, the maxillary gland, and the embryos (Paper II).

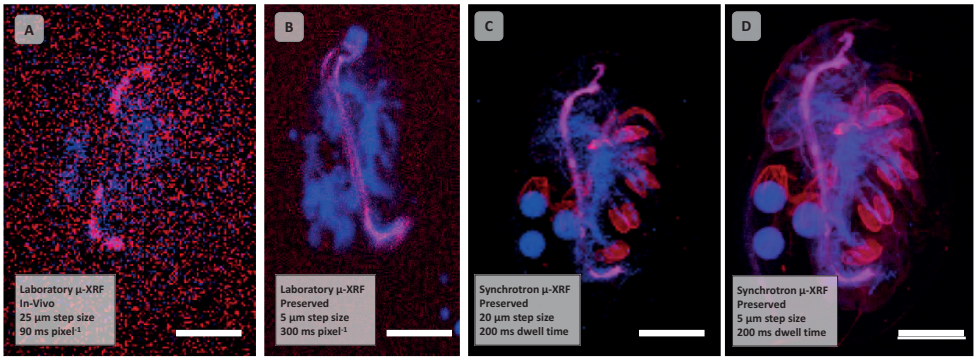

Figure 11: Composite maps showing the U (red) and Fe (blue) biodistributions following various U exposures conducted in this PhD project. *Scalebar = 500 µm*

Uranium was distributed throughout the daphnia in similar areas following both the UNP and the U_{Ref} exposures (Paper II). Because U species were present in all size distributions, it is difficult to attribute specific features to either the UNPs or LMM species by comparing the two samples. Nevertheless, small differences between the exposures may suggest UNP specific effects. The average U body burden in UNP exposed daphnia was ~ 3- to 5-fold greater than that of daphnia exposed to the U_{Ref} solution, potentially reflecting a

significant accumulation of UNPs in the intestine. Analysis of the toxicity test results suggested the increased body burden reflected less toxic U species derived from the UNP exposures (discussed further in section 4.5).

High intensity U hotspots, identified in the μ-SRXRF investigation of the midgut and hepatic ceca, compartments of the digestive tract, may represent aggregates of UNPs (Paper III). Analysis of oxidation state at these hotspots indicated that U was oxidized with a signature "uranyl shoulder" in the XANES spectra. Given that the pristine UNPs also appeared oxidized (Paper II), it was difficult to pinpoint the mechanisms that may have led to oxidation. Contributing factors from the sample preparation or from the photooxidation at the beamline cannot be excluded (Alessi et al. 2013).

Tomographic reconstructions of UNP exposed daphnia revealed large numbers of high-density features, relative to the soft tissues, in the digestive tract (Paper III). Interestingly, such structures were not observed in the U_{Ref} exposed daphnia, despite the large colloidal fractions measured in the exposure media speciation analysis. Another feature unique to the UNP exposed daphnia was the U distribution observed in the embryo and chorion-like structures. However, such differences are related to life stage of the specific daphnid, rather than the exposure. Similar chorion-like structures were observable in CT measurements of replicate daphnia from the U_{Ref} exposure, although U identification is not possible with this method.

Through the results of Paper II and Paper III, several target organs and tissues were identified following exposure to UNPs and the toxicokinetic implications are summarized briefly in the following sections:

Surface Bound Uranium

Uranium was observed on the surfaces of exposed daphnia and was significantly accumulated on the gills, called epipodites (Paper II). X-ray fluorescence tomographic sections indicated that the majority of U was concentrated on the surface compared to uptake into the gill sac. These results were similar to those of De Samber et al (2013) who identified surface bound Zn on the epipodites in histological sections. However, by studying intact daphnia in this work, the epipodites were observed to constitute a significant fraction of the surface bound U, an observation that is difficult to make by studying histological sections. The epipodites are a location of ion exchange (Kikuchi

1983) and haemoglobin synthesis (Goldmann et al. 1999), and represent a potential pathway for systemic uptake of U. The surface bound fraction also has implications for depuration, as the work by Scheibener et al. (2021) demonstrated 60 % U loss via molting (ecdysis). Based on the results in Paper II, it appears that epipodites and foregut ecdysis contribute substantially to U depuration.

Ingested Uranium and Uranium Nanoparticles

The digestive tract was the area of highest U accumulation in daphnia from either exposure (Paper II). The filter feeding behavior, the binding of U in the lumen contents by the peritrophic membrane, and the gut chemistry likely all promoted aggregation of the UNPs as indicated by the high signal intensity relative to soft tissues observed in the synchrotron measurements (μ-SRXRF), the high-density features in the CT renderings, and greater body burden measured by ICP-MS (discussed further in section 4.5). The results presented here were in line with previous distribution studies in daphnia that identified the intestine as an area of significant toxicant accumulation (Caumette et al. 2012; Fouqueray et al. 2012; Jackson et al. 2009). Therefore, histological sections measured by nano-SRXRF provided further detail of the distribution between the various intestinal phases and compartments (e.g., midgut and hepatic ceca). In the ROI measurements of midgut sections, U appeared within the epithelial tissues, indicating a potential uptake pathway. Uranium was identified in the hepatic ceca of daphnia derived from both exposures (UNP and U_{Ref}), and nano-SRXRF of histological sections found small U particulates (< 500 nm) throughout the tissues (Paper III). Additionally, investigations by nano-SRXRF showed the gut contents included ingested algae cells, thus corroborating the notion that organic matter from feed can sequester U (Paper III).

Systemic Uptake and Detoxification through the Maxillary Gland

Systemic U uptake following exposure to either UNPs or the U_{Ref} was observed in various organs including the heart, in the maxillary gland and nephridium, and in the embryos (Paper II). Accumulation in the heart suggested U transport by the haemolymph, further supported by the identification of uptake routes through the epipodites and the midgut epithelial cells. The maxillary gland and the nephridium comprise an excretory system (Smirnov 2017) and U accumulation in these organs would suggest potential removal of U from the haemolymph in what may be a previously undescribed detoxification

pathway. Information on the structure and function of the maxillary gland, which is also called the shell gland, seems relatively scarce (Dejdar 1930; Gicklhorn 1931; Green 1956). Thus, the techniques used in this work represent new possibilities for assessing the relationship between the maxillary gland, the nephridium, and *D. magna* metal detoxification.

Uranium in Embryos

Measurements of U within embryos in the UNP exposed daphnids may suggest maternally transfer (Paper II). However, since the U_{Ref} exposed daphnia had not undergone egg laying at the end of the 48 h exposure and bore embryos only within the ovary and it that did not contain measurable U, maternal transfer either occurred very late in oogenesis or within the brood chamber. Additionally, U-bearing structures were observed around the embryos in the UNP exposed daphnia and may be the remnants of the chorion, the outer protective layer of the egg. Measurements of histological sections of embryo via nano-SRXRF were conducted but did not yield any U signal possibly due to complications from the sample preparation or the 1 μm section thickness leading to issues related to the limit of detection.

4.5 Effects Due to Uranium Nanoparticle Exposure

In Paper II, the acute exposures to UNPs and the U_{Ref} were shown to lead to mortality in *D. magna*. A similar dose-response for survival as a function of measured total U water concentration was observed for both the UNP (LC_{50} = 402 μg L^{-1} [336 - 484], LC_{10} = 183 μg L^{-1} [130 - 238]) and the U_{Ref} (LC_{50} = 268 μg L^{-1} [229 - 315], LC_{10} = 133μg L^{-1} [97.8 - 168]) treatments. The acute toxicity was 4-fold greater in daphnia neonates with considerable overlap in the LC_{10} 95% credible intervals (UNP: 35.7 – 73.4 μg L^{-1} and U_{Ref}: 26.5 – 62.0 μg L^{-1}). Previous studies of U acute toxicity to *D. magna* have identified a range of thresholds (LC_{50}: 0.39 – 6.4 mg U L^{-1}) that are highly dependent on the chemical parameters of the exposure media, particularly lower pH that promotes uranyl ions (Barata et al. 1998; Sheppard et al. 2005; Zeman et al. 2008). The work from Zeman et al. (2008) identified the lowest previous LC_{50} of 390 μg L^{-1} in waterborne U exposures at pH 7 in M4 media which contains phosphates likely to bind uranyl ions. The reduction in LC_{50} observed in this work most likely reflects the changes to MHRW as an exposure media, which was chosen specifically to reduce complexation with phosphates and carbonates as much as feasible. Furthermore, the adjusted pH 6.8 likely promotes a

higher fraction of free uranyl ions which increase exponentially with a reduction in pH (Markich & Brown 2019).

The free ion activity model (FIAM) suggests that cationic LMM species of U, such as UO_2^{2+} or UO_2OH^+, are primarily responsible for the observed toxicity due to their greater bioavailability (Fortin et al. 2004). However, based on the characterization of the adult toxicity test exposures (Paper II), the LMM fractions constitute approximately equal amounts (UNP LMM ~ 33 % / U_{Ref} LMM ~ 35.3 %) indicating the difference in toxicity (LC_{50}) observed in the adult daphnia exposures was due to other factors. To further investigate differences between the exposures, total U body burden measurements were correlated with total U water concentration and revealed an approximately 3-fold greater burden on adult daphnia exposed to the UNPs (8.5 ± 3.3 – 64.6 ± 22.0 ng U daphnid^{-1}) than the U_{Ref} (6.5 ± 0.7 – 20.3 ± 0.4 ng U daphnid^{-1}). This difference was not observed in the neonates and may be related to a more effective NP capturing by the adult daphnia filter feeding apparatus. Plotting the survival of adult daphnia against the total body burden revealed a statistically significant correlation (Paper II). These analyses showed that the U_{Ref} exposures had a higher specific toxicity compared to the UNPs, which required a 3- to 5-fold greater body burden (ng U daphnid^{-1}) to achieve similar toxic effects.

Daphnia magna exposed to concentrations below the LC_{50} for both the UNP and the U_{Ref} survived 24 h following the toxicity test to deliver the first spawning (F1). The neonates were all delayed in reaching reproductive maturity compared with the F0, however, F1 daphnia derived from both the UNP and the U_{Ref} exposures > 50 µg L^{-1} matured 48 h earlier. Given these results, the maternally transferred U observed in the µ-SRXRF analysis did not prevent the F1 generation from developing, nor did the damaged chorion, which may have protected the embryos. Studies of chronic U exposures found reductions in size and fecundity in the F1 generation (Massarin et al. 2010; Zeman et al. 2008). However, the results in this work were more in line with Reis et al., (2018) who found an increased body length in subsequent generations following short term exposure to U mining effluents (Reis et al. 2018). A more robust study of reproduction, using the OECD protocol (OECD 2012), should be useful in the future to assess the impacts of maternally transferred U derived from the UNP exposure.

To study the localized effects of exposure on a tissue and cell level, histological and anatomical analyses (2D and 3D) were compared with micro and nano-focused XRF in *D. magna* following exposure to UNPs (320 μg L^{-1}) and the U_{Ref} (159 μg L^{-1}) (Paper III). On an organ scale, the CT results allowed 3D analysis of the digestive tract that proved critical to the assessment in this work. By comparing CT results with a control organism, the hepatic ceca and midgut of UNP exposed daphnids appeared shrunken and distorted (Fig. 12). Volumetric analysis between the two organisms revealed ~ 4-fold reduction in the organ after exposure. To confirm that the morphological changes were co-localized with the presence of U, ROI scans conducted using μ-SRXRF (2 μm) showed U migrating out of the digestive tract and throughout the hepatic ceca. To investigate these results further, histological sections of hepatic ceca tissues revealed damaged and destroyed epithelial cells, which were normally cuboidal and lined with microvilli as observed in the control organism. Utilizing near-identical sections, nano-SRXRF (75 nm) revealed U prevalent throughout the damaged tissues as well as U particulates (< 500 nm) that were independent of other elemental distributions suggesting UNP aggregates. Interestingly, similar U particulates were observed in the U_{Ref} exposed daphnia as well suggesting the colloidal fraction in these exposures were possibly transported into the organ by similar pathways. Unfortunately, XANES analyses of these particulates were unsuccessful due to low signal-to-noise ratio.

The hepatic ceca are reported to have two functions in the production of digestive fluids (Ebert 2005) and the assimilation of salts (Smirnov 2017). Similar damages to the organ as observed in the present work have been reported following cadmium exposure (Griffiths 1980; Munger et al. 1998), another toxic element often present as bioavailable, divalent cationic species. Similar mechanisms may be present following UNP exposure. Indeed, disruption of digestive fluid production or ion assimilation would have impacts on the overall gut health of *D. magna*, as suggested by chronic U toxicity studies conducted by Massarin et al. (2011). Based on the combined analyses in this work, the hepatic ceca appeared to be a major target of U toxicity (Fig. 12).

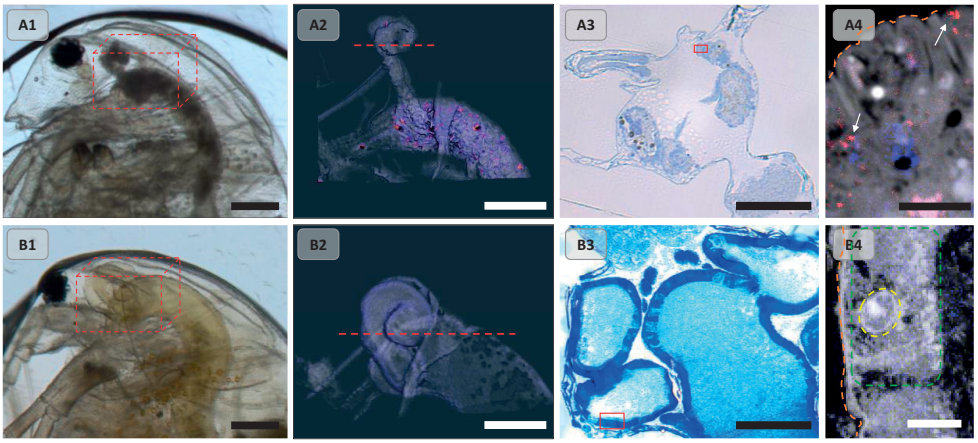

Figure 12: Comparative analysis of UNP exposed *D. magna* (320 µg L^{-1}) in the A series and control *D. magna* in the B series. (A1/B1) Light microscopy of the organisms follow 48 h exposure with the red dotted cube indicating the area investigated by CT. *Scalebar = 500 µm* (A2/B2) Tomographic reconstruction of the hepatic ceca. The red dotted line indicates the approximate area of the histological section. *Scalebar = 200 µm* (A3/B3) Histology showing degradation of the hepatic ceca tissues. The solid red box shows the approximate area investigated by nano-SRXRF. *Scalebar = 100 µm* (A4/B4) Elemental mapping of U (red), Os (grey), and Fe (blue). The step size is 75 nm for A4 and 225 nm for B4. White arrows show independent U hotspots of < 500 nm. The orange dotted line shows the serous coat that sits below the epithelial cells which are damaged in A4. The dotted green box indicates the normal structure of the epithelial cell in B4 with the nucleus circled by the yellow dotted line. *Scalebar = 5 µm*.

Under normal conditions, the hepatic ceca are protected by the peritrophic membrane, a fibrous mesh that extends the length of the midgut and binds the luminal contents (Smirnov 2017). However, the membrane was absent in histological sections of the midgut following exposure to UNPs and the U_{Ref}, indicating that it was damaged or destroyed (Paper III). As reviewed by van der Zande et al., (2020), the peritrophic membrane is a critical barrier whose function is key to understanding NP toxicity as it has a mesh of 130 nm that would prevent most aggregates from escaping the lumen (Hansen & Peters 1998). Similar effects to the peritrophic membrane observed in this work have been documented following CuO NP exposures (Heinlaan et al. 2011). Given the stress observed in the epithelial cells of UNP and U_{Ref} exposed daphnia in this study, a likely explanation is disruption of the cells responsible for secretion of the peritrophic membrane.

The epithelial cells of the midgut appeared stressed and elongated following exposure to UNPs and the U_{Ref}, although the extent of damage was less than those observed in cells of the hepatic ceca (Paper III). A previous study had demonstrated, via TEM analysis, U precipitates inside the intestinal cells of *D. magna* exposed in a chronic U toxicity test (Massarin et al. 2011). Transcellular uptake across the gut epithelia is important in all NP ecotoxicological assessments and nanoscale X-ray techniques applied in this work appeared well suited to establishing this mechanism for UNPs. A detached cell observed in the midgut of a U_{Ref} exposed daphnia did exhibit U and U particulates (< 500 nm) adsorbed to the surface and internalized (Paper III). However, the specific mechanisms surrounding the release of the cell and the uptake of U particulates remain to be confirmed. Unfortunately, U was not detected in the regions of the epithelial wall studied with nano-SRXRF, despite relatively long dwell times at the I14 beamline (up to 800 ms). However, due to time constraints, only a few areas of epithelial cells were investigated, and the section thickness (1 μm) may have led to LOD issues for the method. Nanoscopic elemental mapping of the histological sections of hepatic ceca tissues did identify U particulates in the tissues of both the UNP and the U_{Ref} exposed organisms (Paper III). The co-localization of U particulates and cell damages suggests a possible causal relationship, although further analysis is needed to confirm this notion.

Based on the elemental mapping of whole daphnia (Paper II), the digestive tract appeared to be the location of highest U accumulation following exposure to UNPs as observed by the combination of histological and XRF analyses (Paper III). Furthermore, results provided evidence that failure within the digestive tract was a major contributor to the observed mortality in the toxicological tests. Uranium particulates (< 500 nm) appeared within tissue sections of all measured samples from both exposure groups, indicating that colloidal fractions of U exposure should be considered when assessing the aquatic toxicity of U. The digestive tract was critically affected by UNP exposure, however, the methods used here could be employed to study other organs as well including the epipodites and the maxillary gland to determine if U particulates were also present in those regions. The identification of target organs and tissues represent a major advancement for U and UNP toxicity and exposure characterization that should ultimately contribute to reducing uncertainties in environmental impact and risk assessments.

5 Limitations of The Study and Future Perspective

The current study characterized radioactive particle exposures by using analytical X-ray techniques to assess spatially resolved elemental data on Dounreay fuel fragments and *D. magna* following UNP exposure. However, a few sources of uncertainty must be addressed before drawing conclusions. Limits of detection (LOD) are a constant issue for any analytical technique. The laboratory μ-XRF was suitable for measurements of the Dounreay fuel fragments, however, could not identify the U biodistribution outside of the *D. magna* digestive tract. This was a limitation of the detector instrumentation and the work presented here represent the best achievable results with an M4 Tornado μ-XRF. However, to the benefit of the research objectives, this issue was overcome via measurements at the microXAS beamline with a <trace level LOD. Limit of detection problems were also encountered for the measurements of daphnia sections at the i14 beamline (Diamond). Uranium should have been observable in the epithelial wall cells of the exposed daphnid sections based on the results of the whole organism measurements at microXAS. However, this distribution was not observed in the daphnia sections measured at the I14 beamline, probably due to a combination of contributing factors including the low section thickness (1 μm), the sample preparation, and the beamline instrumentation. In the future, a thicker section (~ 5 μm) should greatly improve the measurement quality.

Sample preparation methods employed in this work all involved the chemical alteration of the original daphnia sample that may affect X-ray measurements. The methods from Laforsch and Tollerian (2000) appear to have preserved the elemental distribution. However, alterations to U oxidation state that would affect the μ-XANES measurements, brought on by the chemical drying, are not known. Similarly, the preparation of daphnia sections for nano-SRXRF was chemically strenuous and the impact on the U speciation was difficult to quantify.

The radiation dosimetry of U exposed *D. magna* utilizes a dose conversion coefficient (mGy h^{-1}/Bq mL^{-1}) by assuming a homogeneous water body of some specific activity based on the radionuclide (natural U in the case of this study) and the mass of the organism (either measured or estimated) (Beaugelin-Seiller et al. 2006). However, based on this work, the distribution of U was predominantly in the digestive tract and other potentially sensitive organs such as the hepatic ceca, epipodites, and embryos. The

results may be useful to establishing estimates of organ dose, thus providing a relevant description of the radiological exposure to *D. magna*. Furthermore, the CT work in this study could provide the basis to construct a computational phantom similar to the work of Caffrey et al., (2017). Using the biodistribution results, micro-dosimetric evaluations would provide tissue and cell-specific doses.

Regarding limitations with respect to the experimental design and environmental relevance, there are certain areas that should be pursued by future investigations. In the characterization of the exposure media (MHRW), both the UNP suspension and the U_{Ref} solution contained LMM, colloidal, and particulate species and the biodistribution images were comparable. As a result, it was difficult to attribute observed effects to NP/colloid exposure. Thus, more emphasis should be put on exposure media characterization when colloidal and NP experiments are performed.

All ecotoxicological studies struggle to balance experimental parameters with environmental relevance. The exposures with *D. magna* conducted in this work relied on acute exposures which are designed to assess retention and adverse effects of lethal toxic levels. Although lower concentration samples were prepared, time constraint prevented robust measurements of those samples. Furthermore, chronic exposures at lower concentrations are more relevant to ecotoxicological studies by leaving organs and tissues operating under more "normal" conditions. Long term (21 d), reproductive tests with *D. magna* and UNPs would provide such information and are thus within the scope for future research.

6 Conclusions

Assessing the impact of radionuclide contamination in the environment should include evaluating the potential exposure to particulate species ranging from nm to mm. Exposure to particle associated radionuclides is dependent on their physico-chemical properties, environmental behavior, and uptake and retention in biota. In this work, spatially resolved analytical X-ray techniques were employed to determine the compositional and morphological characteristics of spent fuel particles (> 0.45 μm) and the U biodistribution in *D. magna* following exposure to UNPs. The characterization data were used to draw conclusions related to overall exposure risk to particle associated radionuclides in the environment.

The analyses of Dounreay fuel fragments revealed compositional and morphological characteristics that were unique to the specific origin, formation, and release scenario of the respective particle type (Paper I). However, the radiation dose assessment performed in this work was consistent with and validated the existing dosimetry model put forward by SEPA. Therefore, the first hypothesis that detailed knowledge on the composition and morphological variations of Dounreay particles would improve existing impact and risk assessments was not supported. Nevertheless, the characterization in this work supports future environmental impact assessment, given the potential for smaller, undetected particles remaining in the marine environment which are expected to be more mobile and bioavailable.

Uptake and retention of UNPs in *D. magna* was resolved using micro and nano-focused synchrotron XRF (Papers II – III). The results showed substantial U accumulation in several critical organs including the gills, the digestive tract, the maxillary gland, and the embryos. Furthermore, U particulates were observed throughout the midgut and into the tissues of the hepatic ceca leading to an uneven distribution of U within the organism. Therefore, these results supported the hypothesis that radioactive nanoparticles can incorporate into organs and tissues resulting in a heterogeneous biodistribution. By demonstrating the distribution of U following exposure, this work provides further insights into the uptake and detoxification pathways of important model organism *D. magna* with potential relevance also to other metals and metal NPs. Through a better understanding of the retention and elimination of UNPs in *D. magna*, the environmental impacts of radionuclide associated colloids and NPs can be better assessed.

Exposure to UNPs after 48 h resulted in morphological effects and mortality in *D. magna* (LC_{50} = 401 µg L^{-1} [336 - 484]). Histological and anatomical analyses (2D and 3D) showed effects on the digestive tract where damages were observed in the hepatic ceca, the midgut, and the peritrophic membrane. Using micro and nano-focused XRF analyses, these damages were co-localized with the presence of U particulates (< 500 nm) especially in the hepatic ceca where cell damage was extensive (Paper III). These results were in line with the hypothesis that radioactive nanoparticles may exert local tissue and organ stress leading to adverse effects in exposed organisms. This work was critical to identifying the hepatic ceca and midgut epithelial cells as target organs following exposure to UNPs.

The main findings of this work were integrated into an Aggregate Exposure Pathway (AEP) framework (Teeguarden et al. 2016), to visualize the complete exposure characterization (Fig. 13 and 14). The main components of an AEP framework are the key exposure states, defined as the state of the stressor at a given point in space and time, at the source and the target site in an organism (Tan et al. 2018). For Dounreay fuel fragments, the characterization in Paper I was incorporated with the work of other studies to show the path from particle formation to external and internal exposure resulting in a contact radiological dose (Fig. 13). As ecotoxicological studies of UNPs have not been previously performed, the findings of Papers II and III were assembled into a separate AEP framework presenting the route from pristine UNPs to organ and tissue specific retention in *D. magna* (Fig. 14). By integrating results using AEP frameworks, knowledge gaps for future studies can be identified and interpretation of biological effects and adverse outcomes due to exposure can be improved.

Collectively, this work provided new information relevant to the exposure characterization of nm to mm sized radioactive particles. For Dounreay fuel fragments, detailed characterization of the physico-chemical properties of MTR and DFR particles improves the understanding of origin, formation, and release scenario. Furthermore, validation of the existing dose assessment model should build confidence for impact and risk assessments. Studies using UNPs were unprecedented and generated novel findings regarding U toxicokinetics. By identifying target organs of exposure and correlating those locations with observed biological effects, this work should improve the overall

understanding of UNP and U ecotoxicology while providing a basis for future studies on the impacts of radionuclide bearing colloid species.

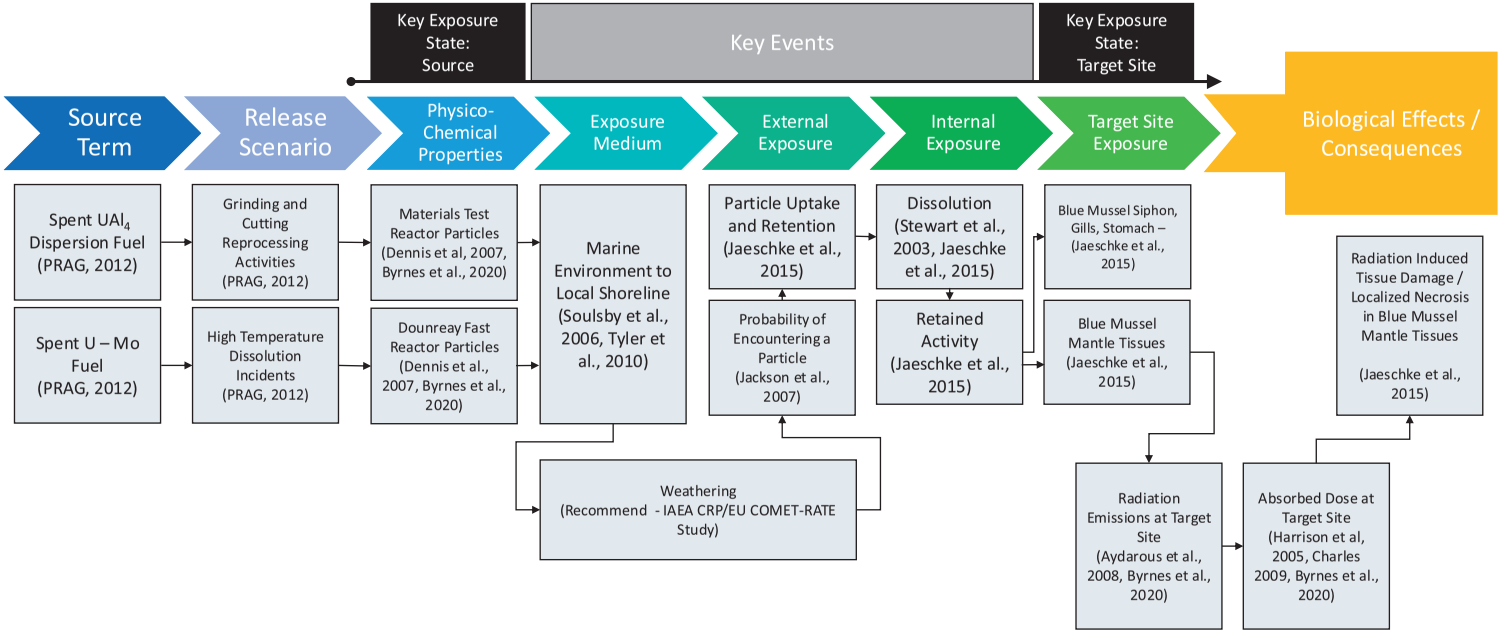

Figure 13: A conceptual AEP model for Dounreay fuel fragments resulting in the uptake and exposure in blue mussels (*Mytilus edulis*). The key exposure state of the particle at the source is characterized in Paper I. These characteristics were linked with the source term and release scenario which have been added to the left side of the AEP. In blue mussels, Dounreay fuel fragments were retained long enough in tissues to induce ulcerations and the characterization and radiation dosimetry in Paper I support description of that exposure. These states are linked by key events that include studies of particle transport in the marine environment, environmental risk assessment of encountering a particle, uptake and retention experiments, and possible dissolution studies. A major remaining gap includes the potential weathering of Dounreay fuel fragments in the marine environment.

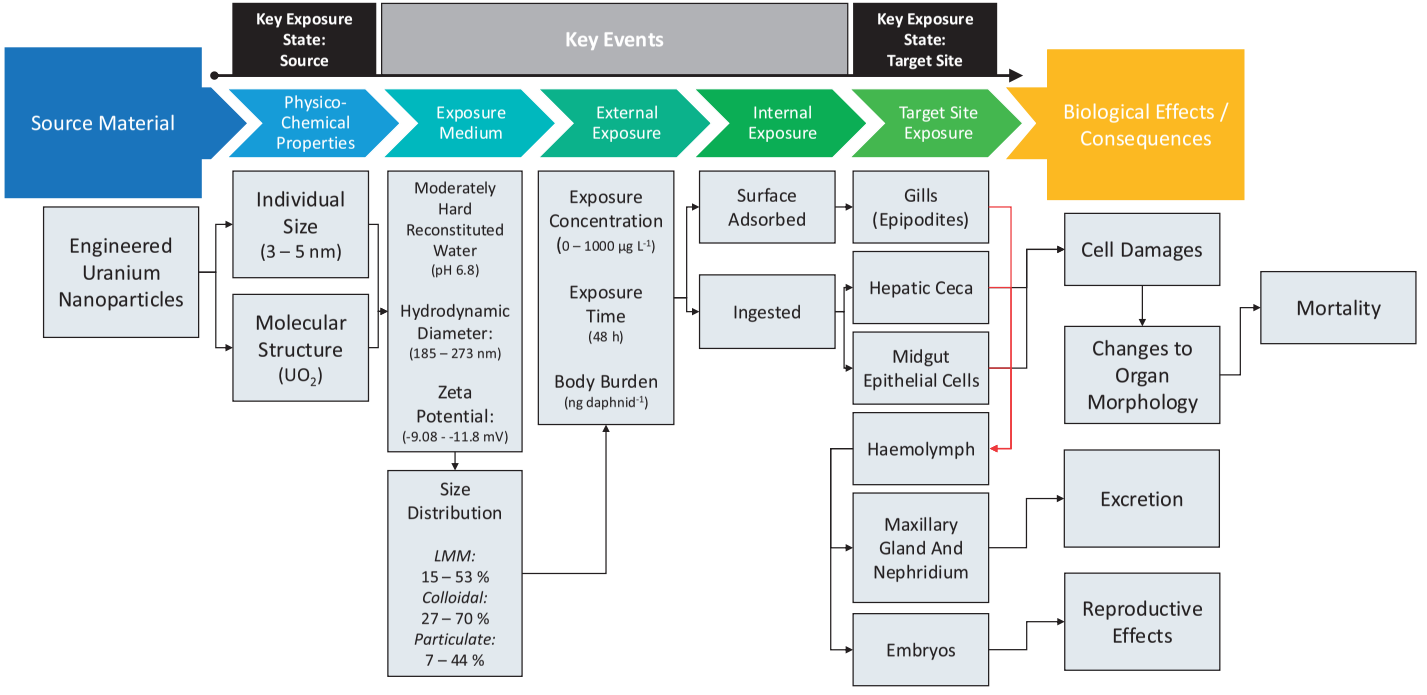

Figure 14: A conceptual AEP model of UNP exposure to freshwater crustacean *D. magna*. The pristine UNPs were 3 – 5 nm and were predominantly UO_2 prior to dispersion in MHRW. Evaluated key events included characterization of the UNPs in MHRW, concentration of exposure over 48 h to *D. magna*, and identified routes of uptake (surface adsorption, gills, and ingestion). The micro and nano-focused X-ray techniques shown in this work allowed for the identification of target sites that included the gills (epipodites), the hepatic ceca, midgut epithelial cells, haemolymph, the maxillary gland, and the embryos. Red lines indicate potential routes of systemic uptake. By integrating these results, this conceptual framework will support further studies of biological effects due to UNP exposure such as molecular initiating events that lead to adverse outcomes in the population.

References

Alessi, D. S., Uster, B., Borca, C. N., Grolimund, D. & Bernier-Latmani, R. (2013). Beam-induced oxidation of monomeric U(IV) species. *Journal of Synchrotron Radiation*, 20 (1): 197-199.

Alfeld, M. & Janssens, K. (2015). Strategies for processing mega-pixel X-ray fluorescence hyperspectral data: a case study on a version of Caravaggio's painting Supper at Emmaus. *Journal of Analytical Atomic Spectrometry*, 30 (3): 777-789.

Anspach, L. J. & Hamby, D. M. (2018). Performance of the VARSKIN 5 (v5.3) Electron Dosimetry Model. *Radiation Protection Dosimetry*, 181 (2): 111-119.

Aragón, A., Espinosa, A., de la Cruz, B. & Fernández, J. A. (2008). Characterization of radioactive particles from the Palomares accident. *Journal of Environmental Radioactivity*, 99 (7): 1061-1067.

Aydarous, A. S., Charles, M. W. & Darley, P. J. (2008). Dose distribution measurements and calculations for Dounreay hot particles. *Radiation Protection Dosimetry*, 128 (2): 146-158.

Barata, C., Baird, D. J. & Markich, S. J. (1998). Influence of genetic and environmental factors on the tolerance of Daphnia magna Straus to essential and non-essential metals. *Aquatic Toxicology*, 42 (2): 115-137.

Beaugelin-Seiller, K., Jasserand, F., Garnier-Laplace, J. & Gariel, J. C. (2006). Modeling radiological dose in non-human species: principles, computerization, and application. *Health Phys*, 90 (5): 485-93.

Bots, P., Morris, K., Hibberd, R., Law, G. T. W., Mosselmans, J. F. W., Brown, A. P., Doutch, J., Smith, A. J. & Shaw, S. (2014). Formation of Stable Uranium(VI) Colloidal Nanoparticles in Conditions Relevant to Radioactive Waste Disposal. *Langmuir*, 30 (48): 14396-14405.

Bremier, S., Potter, P., Ray, I. & Walker, C. (2002). On the Constitution of Dounreay Radioactive Particles, Vol 2 EMPA': UKAEA Dounreay Internal Report.

Caffrey, E. & Higley, K. (2014). The creation of voxel phantoms for the purpose of environmental dosimetry.

Caffrey, E., Johansen, M., Caffrey, J. & Higley, K. J. H. p. (2017). Comparison of Homogeneous and Particulate Lung Dose Rates For Small Mammals. 112 (6): 526-532.

Caffrey, E. A., Johansen, M. P. & Higley, K. A. (2016). Voxel modeling of rabbits for use in radiological dose rate calculations. *Journal of Environmental Radioactivity*, 151: 480-486.

Cagno, S., Lind, O. C., Popic, J. M., Skipperud, L., De Nolf, W., Nuyts, G., Vanmeert, F., Jaroszewicz, J., Janssens, K. & Salbu, B. (2020). Micro-analytical characterization of thorium-rich aggregates from Norwegian NORM sites (Fen Complex, Telemark). *Journal of Environmental Radioactivity*, 219: 106273.

Caumette, G., Koch, I., Moriarty, M. & Reimer, K. J. (2012). Arsenic distribution and speciation in Daphnia pulex. *Science of The Total Environment*, 432: 243-250.

Charles, M. W. (2009, 2009). *Health Effects of Dounreay Hot Particles: A Benchmark for the Evaluation of Doses and Risks*. Dordrecht: Springer Netherlands. 235-248 pp.

Charles, S., Veber, P. & Delignette-Muller, M. L. (2018). MOSAIC: a web-interface for statistical analyses in ecotoxicology. *Environmental Science and Pollution Research*, 25 (12): 11295-11302.

Choppin, G., Liljenzin, J.-O. & Rydberg, J. (2002). *Radiochemistry and nuclear chemistry*: Butterworth-Heinemann.

Christian, P., Von der Kammer, F., Baalousha, M. & Hofmann, T. (2008). Nanoparticles: structure, properties, preparation and behaviour in environmental media. *Ecotoxicology*, 17 (5): 326-343.

Clement, C. H., Strand, P., Beresford, N., Copplestone, D., Godoy, J., Jianguo, L., Saxén, R., Yankovich, T. & Brown, J. (2009). Environmental Protection: Transfer Parameters for Reference Animals and Plants. *Annals of the ICRP*, 39 (6): 1-111.

Cruz, G. A. S. (2016). Microdosimetry: Principles and applications. *Reports of Practical Oncology and Radiotherapy*, 21 (2): 135-139.

Čubová, K. & Čuba, V. (2019). Synthesis of inorganic nanoparticles by ionizing radiation – a review. *Radiation Physics and Chemistry*, 158: 153-164.

De Samber, B., De Schamphelaere, K. A. C., Janssen, C. R., Vekemans, B., De Rycke, R., Martinez-Criado, G., Tucoulou, R., Cloetens, P. & Vincze, L. (2013). Hard X-ray nanoprobe investigations of the subtissue metal distributions within Daphnia magna. *Analytical and Bioanalytical Chemistry*, 405 (18): 6061-6068.

Dejdar, E. (1930). Vitale elektivfärbungen der rudimentären antennendrüse von cladoceren. *Zeitschrift für Morphologie und Ökologie der Tiere*: 768-777.

Delignette-Muller, M., Ruiz, P., Charles, S., Duchemin, W., Lopes, C., Kon-Kam-King, G. & Veber, P. (2016). *Morse: Modelling Tools for Reproduction and Survival Data in Ecotoxicology*. R package version 2.2.0 ed.

Denecke, M. A. (2006). Actinide speciation using X-ray absorption fine structure spectroscopy. *Coordination Chemistry Reviews*, 250 (7-8): 730-754.

Dennis, F., Morgan, G. & Henderson, F. (2007). Dounreay hot particles: the story so far. *Journal of Radiological Protection*, 27 (3A): A3–A11.

DPAG. (2008). Dounreay Particles Advisory Group 4th Report: Scottish Environmental Protection Agency.

Ebert, D. (2005). *Ecology, epidemiology, and evolution of parasitism in Daphnia*: National Library of Medicine.

Eriksson, M., Lindahl, P., Roos, P., Dahlgaard, H. & Holm, E. (2008). U, Pu, and Am Nuclear Signatures of the Thule Hydrogen Bomb Debris. *Environmental Science & Technology*, 42 (13): 4717-4722.

Fortin, C., Dutels, L. & Garnier-Laplace, J. (2004). Uranium complexation and uptake by a green alga in relation to chemical speciation: The importance of the free uranyl ion. *Environmental Toxicology and Chemistry*, 23 (4): 974-981.

Fouqueray, M., Dufils, B., Vollat, B., Chaurand, P., Botta, C., Abacci, K., Labille, J., Rose, J. & Garric, J. (2012). Effects of aged TiO2 nanomaterial from sunscreen on Daphnia magna exposed by dietary route. *Environmental Pollution*, 163: 55-61.

Furuki, G., Imoto, J., Ochiai, A., Yamasaki, S., Nanba, K., Ohnuki, T., Grambow, B., Ewing, R. C. & Utsunomiya, S. (2017). Caesium-rich micro-particles: A window into the meltdown events at the Fukushima Daiichi Nuclear Power Plant. *Scientific Reports*, 7 (1): 42731.

Geckeis, H., Rabung, T. & Schäfer, T. (2011). Actinide-Nanoparticle Interaction: Generation, Stability and Mobility. In Kalmykov, S. N. & Denecke, M. A. (eds) *Actinide Nanoparticle Research*, pp. 1-30. Berlin, Heidelberg: Springer.

Gesell, T., Baum, J., Scott, B., Hopewell, J., Seltzer, S., Lantz, M., and Shore, R. (1999). *Biological Effects and Exposure Limits for "Hot Particles"*. Bethesda, Maryland: National Council on Radiation Protection and Measurements.

Gesell, T. F., Hopewell, J. W., Lantz, M. W., Osborne, J. W., Scott, B. R., Seltzer, S. M., Shore, R. E. & Worgul, B. V. (1999). Biological Effects and Exposure Limits for'Hot Particles,'.

Gicklhorn, J. (1931). Beobachtungen an den lateralen Frontalorganen von Daphnia magna M. nach elektiver Vitalfärbung. *Protoplasma*, 13 (1): 725-739.

Goldmann, T., Becher, B., Wiedorn, K. H., Pirow, R., Deutschbein, M. E., Vollmer, E. & Paul, R. J. (1999). Epipodite and fat cells as sites of hemoglobin synthesis in the branchiopod crustacean Daphnia magna. *Histochem Cell Biol*, 112 (5): 335-9.

Goulet, R. R., Thompson, P. A., Serben, K. C. & Eickhoff, C. V. (2015). Impact of environmentally based chemical hardness on uranium speciation and toxicity in six aquatic species. *Environmental Toxicology and Chemistry*, 34 (3): 562-574.

Green, J. (1956). Variation in the Haemoglobin Content of Daphnia. *Proceedings of the Royal Society of London. Series B, Biological Sciences*, 145 (919): 214-232.

Griffiths, P. R. E. (1980). Morphological and ultrastructural effects of sublethal cadmium poisoning on Daphnia. *Environmental Research*, 22 (2): 277-284.

Handy, R. D., von der Kammer, F., Lead, J. R., Hassellöv, M., Owen, R. & Crane, M. (2008). The ecotoxicology and chemistry of manufactured nanoparticles. *Ecotoxicology*, 17 (4): 287-314.

Hansen, U. & Peters, W. (1998). Structure and permeability of the peritrophic membranes of some small crustaceans. *Zoologischer Anzeiger*, 236 (2-3): 103-108.

Harrison, J., Fell, T., Phipps, A., Smith, T., Ellender, M., Ham, G., Hodgson, A., Wilkins, B., Charles, M. & Darley, P. (2005). Health implications of Dounreay fuel fragments: estimates of doses and risks. *Radiation Protection Division (RPD), Health Protection Agency (HPA). RPD-RE-11-2005*.

Hasan, S. & Ghosh, T. K. (2013). Synthesis of Silica-Coated Uranium Oxide Nanoparticles by Surfactant-Templated Sol-Gel Process for Use as Catalysts. *Nuclear Technology*, 181 (2): 371-379.

Haschke, M. (2014). Laboratory micro-X-ray fluorescence spectroscopy. *Cham: Springer International Publishing*, 10: 978-983.

Heinlaan, M., Kahru, A., Kasemets, K., Arbeille, B., Prensier, G. & Dubourguier, H.-C. (2011). Changes in the Daphnia magna midgut upon ingestion of copper oxide nanoparticles: A transmission electron microscopy study. *Water Research*, 45 (1): 179-190.

Henderson, F., Toole, J., Cartwright, P. (2007). *The Dounreay Particle Technical Resume*. Protection, D. o. E. United Kingdom: UKAEA.

Higley, K., Ruedig, E., Gomez-Fernandez, M., Caffrey, E., Jia, J., Comolli, M. & Hess, C. (2015). Creation and application of voxelised dosimetric models, and a comparison with the current methodology as used for the International Commission on Radiological Protection's Reference Animals and Plants. *Annals of the ICRP*, 44 (1_suppl): 313-330.

Hochella, M. F., Mogk, D. W., Ranville, J., Allen, I. C., Luther, G. W., Marr, L. C., McGrail, B. P., Murayama, M., Qafoku, N. P., Rosso, K. M., et al. (2019). Natural, incidental, and engineered nanomaterials and their impacts on the Earth system. *Science*, 363 (6434): eaau8299.

Hough, N. (1997). Reprocessing of MTR fuel at Dounreay.

International Atomic Energy Agency (IAEA). *Strengthening Control Over Radioactive Sources in Authorized Use and Regaining Control Over Orphan Sources: National Strategies*. (2004) Vienna: International Atomic Energy Agency.

International Atomic Energy Agency Coordinated Research Activities (IAEA-CRP). *Radioactive Particles in the Environment: Sources, Particle Characterization and Analytical Techniques*. (2011). Vienna: International Atomic Energy Agency.

J. Darley, P., W. Charles, M., P. Fell, T. & D. Harrison, J. (2003). Doses and risks from the ingestion of Dounreay fuel fragments. *Radiation Protection Dosimetry*, 105 (1-4): 49-54.

Jackson, B. P., Pace, H. E., Lanzirotti, A., Smith, R. & Ranville, J. F. (2009). Synchrotron X-ray 2D and 3D elemental imaging of CdSe/ZnS quantum dot nanoparticles in Daphnia magna. *Analytical and Bioanalytical Chemistry*, 394 (3): 911-917.

Jackson, D., Stone, D. M., Smith, K., Morgan, G. & Shimmield, T. (2007). Assessing the environmental risk from hot particles in the vicinity of Dounreay—a case for inaction? *Journal of Radiological Protection*, 27 (3A): A111–A118.

Jaeschke, B. C., Lind, O. C., Bradshaw, C. & Salbu, B. (2015). Retention of radioactive particles and associated effects in the filter-feeding marine mollusc Mytilus edulis. *Science of The Total Environment*, 502: 1-7.

Janssens, K., De Nolf, W., Van Der Snickt, G., Vincze, L., Vekemans, B., Terzano, R. & Brenker, F. E. (2010). Recent trends in quantitative aspects of microscopic X-ray fluorescence analysis. *TrAC Trends in Analytical Chemistry*, 29 (6): 464-478.

Johansen, M. P., Child, D. P., Davis, E., Doering, C., Harrison, J. J., Hotchkis, M. A. C., Payne, T. E., Thiruvoth, S., Twining, J. R. & Wood, M. D. (2014). Plutonium in wildlife and soils at the Maralinga legacy site: persistence over decadal time scales. *Journal of Environmental Radioactivity*, 131: 72-80.

Kaminski, M. D. & Goldberg, M. M. (2002). Aqueous corrosion of aluminum-based nuclear fuel. *Journal of Nuclear Materials*, 304 (2): 182-188.

Kaminski, M. D., Dimitrijevic, N. M., Mertz, C. J. & Goldberg, M. M. (2005). Colloids from the aqueous corrosion of uranium nuclear fuel. *Journal of Nuclear Materials*, 347 (1): 77-87.

Kashparov, V. A., Protsak, V. P., Ahamdach, N., Stammose, D., Peres, J. M., Yoschenko, V. I. & Zvarich, S. I. (2000). Dissolution kinetics of particles of irradiated Chernobyl nuclear fuel: influence of pH and oxidation state on the release of radionuclides in the contaminated soil of Chernobyl. *Journal of Nuclear Materials*, 279 (2): 225-233.

Kastner, J. & Heinzl, C. (2018). *X-Ray Tomography*.

Kikuchi, S. (1983). The fine structure of the gill epithelium of a fresh-water flea, Daphnia magna (Crustacea: Phyllopoda) and changes associated with acclimation to various salinities. *Cell and tissue research*, 229 (2): 253-268.

Kim, J.-I. (2006). SIGNIFICANCE OF ACTINIDE CHEMISTRY FOR THE LONG-TERM SAFETY OF WASTE DISPOSAL. *Nuclear Engineering and Technology*, 38 (6): 459-482.

Kim, J. I. (1991). Actinide Colloid Generation in Groundwater. *Radiochimica Acta*, 52-53 (1): 71-82.

Kleiven, M., Rossbach, L. M., Gallego-Urrea, J. A., Brede, D. A., Oughton, D. H. & Coutris, C. (2018). Characterizing the behavior, uptake, and toxicity of NM300K silver nanoparticles inCaenorhabditis elegans. *Environmental Toxicology and Chemistry*, 37 (7): 1799-1810.

Kunze, P., Seher, H., Hauser, W., Panak, P. J., Geckeis, H., Fanghänel, T. & Schäfer, T. (2008). The influence of colloid formation in a granite groundwater bentonite porewater mixing zone on radionuclide speciation. *Journal of Contaminant Hydrology*, 102 (3): 263-272.

Laforsch, C. & Tollrian, R. (2000). A new preparation technique of daphnids for Scanning Electron Microscopy using hexamethyldisilazane. *Archiv für Hydrobiologie*: 587-596.

Lind, O. C., De Nolf, W., Janssens, K. & Salbu, B. (2013). Micro-analytical characterisation of radioactive heterogeneities in samples from Central Asian TENORM sites. *Journal of Environmental Radioactivity*, 123: 63-70.

Lofts, S., Fevrier, L., Horemans, N., Gilbin, R., Bruggeman, C. & Vandenhove, H. (2015). Assessment of co-contaminant effects on uranium and thorium speciation in freshwater using geochemical modelling. *Journal of Environmental Radioactivity*, 149: 99-109.

Markich, S. & Brown, P. (2019). Actinide speciation and bioavailability in fresh and marine surface waters. In William J. Evans, T. P. H. (ed.) *The Heaviest Metals: Science and Technology of the Actinides and Beyond*, pp. 367-400: Wiley.

Markich, S. J. (2002). Uranium Speciation and Bioavailability in Aquatic Systems: An Overview. *The Scientific World Journal* (2): 707-729.

Martinez, N. E., Johnson, T. E. & Pinder, J. E. (2016). Application of computational models to estimate organ radiation dose in rainbow trout from uptake of molybdenum-99 with comparison to iodine-131. *Journal of Environmental Radioactivity*, 151: 468-479.

Massarin, S., Alonzo, F., Garcia-Sanchez, L., Gilbin, R., Garnier-Laplace, J. & Poggiale, J.-C. (2010). Effects of chronic uranium exposure on life history and physiology of Daphnia magna over three successive generations. *Aquatic Toxicology*, 99 (3): 309-319.

Massarin, S., Beaudouin, R., Zeman, F., Floriani, M., Gilbin, R., Alonzo, F. & Pery, A. R. R. (2011). Biology-Based Modeling To Analyze Uranium Toxicity Data on Daphnia magna in a Multigeneration Study. *Environmental Science & Technology*, 45 (9): 4151-4158.

Munger, C., Hare, L., Craig, A. & Charest, P.-M. (1998). Influence of exposure time on the distribution of cadmium within the cladoceran Ceriodaphnia dubia. *Aquatic Toxicology*, 44 (3): 195-200.

NANoREG. (2017). Framework for the safety assessment of nanomaterials, JRC105651.

Neck, V., Altmaier, M. & Fanghänel, T. (2007). Solubility of plutonium hydroxides/hydrous oxides under reducing conditions and in the presence of oxygen. *Comptes Rendus Chimie*, 10 (10): 959-977.

Neill, T. S., Morris, K., Pearce, C. I., Abrahamsen-Mills, L., Kovarik, L., Kellet, S., Rigby, B., Vitova, T., Schacherl, B. & Shaw, S. (2019). Silicate stabilisation of colloidal UO2 produced by uranium metal corrosion. *Journal of Nuclear Materials*, 526.

NRPB. (1997: 3). *Assessment of Skin Doses*. Board, N. R. P. London: NRPB.

OECD. (2004). *Test No. 202: Daphnia sp. Acute Immobilisation Test*.

OECD. (2012). *Test No. 211: Daphnia magna Reproduction Test*.

Pavelkova, T., Cuba, V. & Sebesta, F. (2013). Photo-induced low temperature synthesis of nanocrystalline UO2, ThO2 and mixed UO2-ThO2 oxides. *Journal of Nuclear Materials*, 442 (1-3): 29-32.

Pavelková, T., Čuba, V., De Visser-Týnová, E., Ekberg, C. & Persson, I. (2016). Preparation of UO2, ThO2 and (Th,U)O2 pellets from photochemically-prepared nano-powders. *Journal of Nuclear Materials*, 469: 57-61.

Poston, T. M., Hanf, R. W. & Simmons, M. A. (1984). Toxicity of uranium to Daphnia magna. *Water, Air, and Soil Pollution*, 22 (3): 289-298.

PRAG. (2012). Particles Retrieval Advisory Group: Scottish Environmental Protection Agency.

Quinn, P. D., Alianelli, L., Gomez-Gonzalez, M., Mahoney, D., Cacho-Nerin, F., Peach, A. & Parker, J. E. (2021). The Hard X-ray Nanoprobe beamline at Diamond Light Source. *Journal of Synchrotron Radiation*, 28 (3): 1006-1013.

Reis, P., Pereira, R., Carvalho, F. P., Oliveira, J., Malta, M., Mendo, S. & Lourenco, J. (2018). Life history traits and genotoxic effects on Daphnia magna exposed to waterborne uranium and to a uranium mine effluent - A transgenerational study. *Aquatic Toxicology*, 202: 16-25.

Ritman, E. L. (2011). Current Status of Developments and Applications of Micro-CT. In Yarmush, M. L., Duncan, J. S. & Gray, M. L. (eds) Annual Review of Biomedical Engineering, vol. 13 *Annual Review of Biomedical Engineering, Vol 13*, pp. 531-552. Palo Alto: Annual Reviews.

Rossbach, L. M., Oughton, D. H., Maremonti, E., Coutris, C. & Brede, D. A. (2020). In vivo assessment of silver nanoparticle induced reactive oxygen species reveals tissue specific effects on cellular redox status in the nematode Caenorhabditis elegans. *Science of the Total Environment*, 721.

Salbu, B., Krekling, T., Lind, O. C., Oughton, D. H., Drakopoulos, M., Simionovici, A., Snigireva, I., Snigirev, A., Weitkamp, T., Adams, F., et al. (2001). High energy X-ray microscopy for characterisation of fuel particles. *Nuclear Instruments and Methods in Physics Research Section A: Accelerators, Spectrometers, Detectors and Associated Equipment*, 467-468: 1249-1252.

Salbu, B., Lind, O., Borretzen, P., Oughton, D., Brechignac, F. & Howard, B. (2001). Advanced speciation techniques for radionuclides associated with colloids and particles. *Radioactive Pollutants: Impact on the Environment*.

Salbu, B., Lind, O. C. & Skipperud, L. (2004). Radionuclide speciation and its relevance in environmental impact assessments. *Journal of Environmental Radioactivity*, 74 (1): 233-242.

Salbu, B., Janssens, K., Lind, O. C., Proost, K., Gijsels, L. & Danesi, P. R. (2005). Oxidation states of uranium in depleted uranium particles from Kuwait. *Journal of Environmental Radioactivity*, 78 (2): 125-135.

Salbu, B. (2009). Fractionation of radionuclide species in the environment. *Journal of Environmental Radioactivity*, 100 (4): 283-289.

Salbu, B., Skipperud, L. & Lind, O. C. (2015). Sources Contributing to Radionuclides in the Environment: With Focus on Radioactive Particles. In Walther, C. & Gupta, D. K. (eds) *Radionuclides in the Environment: Influence of chemical speciation and plant uptake on radionuclide migration*, pp. 1-36. Cham: Springer International Publishing.

Salbu, B., Kashparov, V., Lind, O. C., Garcia-Tenorio, R., Johansen, M. P., Child, D. P., Roos, P. & Sancho, C. (2018). Challenges associated with the behaviour of radioactive particles in the environment. *Journal of Environmental Radioactivity*, 186: 101-115.

Salbu, B., Teien, H. C., Lind, O. C. & Tollefsen, K. E. (2019). Why is the multiple stressor concept of relevance to radioecology? *International Journal of Radiation Biology*, 95 (7): 1015-1024.

Salbu, B. & Lind, O. C. (2020). Analytical techniques for charactering radioactive particles deposited in the environment. *Journal of Environmental Radioactivity*, 211: 106078.

Scheibener, S., Song, Y., Tollefsen, K. E., Salbu, B. & Teien, H.-C. (2021). Uranium accumulation and toxicokinetics in the crustacean Daphnia magna provide perspective to toxicodynamic responses. *Aquatic Toxicology*: 105836.

Schindelin, J., Rueden, C. T., Hiner, M. C. & Eliceiri, K. W. (2015). The ImageJ ecosystem: An open platform for biomedical image analysis. *Molecular Reproduction and Development*, 82 (7-8): 518-529.

Schindler, M., Lussier, A. J., Bellrose, J., Rouvimov, S., Burns, P. C. & Kyser, T. K. (2017). Mobilization and agglomeration of uraninite nanoparticles: A nano-mineralogical study of samples from the Matoush Uranium ore deposit. *American Mineralogist*, 102 (9): 1776-1787.

Sheppard, S. C., Sheppard, M. I., Gallerand, M.-O. & Sanipelli, B. (2005). Derivation of ecotoxicity thresholds for uranium. *Journal of Environmental Radioactivity*, 79 (1): 55-83.

Shevchenko, S. V. (2004). On the uncertainty in activity measurements for samples containing "hot particles". *Applied Radiation and Isotopes*, 61 (6): 1303-1306.

Shoesmith, D. W. (2000). Fuel corrosion processes under waste disposal conditions. *Journal of Nuclear Materials*, 282 (1): 1-31.

Silva, L. F. O., Santosh, M., Schindler, M., Gasparotto, J., Dotto, G. L., Oliveira, M. L. S. & Hochella Jr, M. F. (2021). Nanoparticles in fossil and mineral fuel sectors and their impact on environment and human health: A review and perspective. *Gondwana Research*, 92: 184-201.

Simon, O., Gagnaire, B., Sommard, V., Pierrisnard, S., Camilleri, V., Carasco, L., Gilbin, R. & Frelon, S. (2019). Uranium transfer and accumulation in organs of Danio rerio after waterborne exposure alone or combined with diet-borne exposure. *Environmental Toxicology and Chemistry*, 38 (1): 90-98.

Skipperud, L. & Salbu, B. (2015). Sequential extraction as a tool for mobility studies of radionuclides and metals in soils and sediments. *Radiochimica Acta*, 103 (3): 187-197.

Smirnov, N. N. (2017). *Physiology of the Cladocera*: Academic Press.

Solé, V. A., Papillon, E., Cotte, M., Walter, P. & Susini, J. (2007). A multiplatform code for the analysis of energy-dispersive X-ray fluorescence spectra. *Spectrochimica Acta Part B: Atomic Spectroscopy*, 62 (1): 63-68.

Song, Y., Salbu, B., Heier, L. S., Teien, H.-C., Lind, O.-C., Oughton, D., Petersen, K., Rosseland, B. O., Skipperud, L. & Tollefsen, K. E. (2012). Early stress responses in Atlantic salmon (Salmo salar) exposed to environmentally relevant concentrations of uranium. *Aquatic Toxicology*, 112-113: 62-71.

Stollewerk, A. (2010). The water flea Daphnia - a 'new' model system for ecology and evolution? *Journal of Biology*, 9 (2): 21.

Tan, L.-Y., Huang, B., Xu, S., Wei, Z.-B., Yang, L.-Y. & Miao, A.-J. (2016). TiO 2 Nanoparticle Uptake by the Water Flea Daphnia magna via Different Routes is Calcium-Dependent. 50 (14): 7799-7807.

Tan, Y.-M., Leonard, J. A., Edwards, S., Teeguarden, J., Paini, A. & Egeghy, P. (2018). Aggregate exposure pathways in support of risk assessment. *Current Opinion in Toxicology*, 9: 8-13.

Teeguarden, J. G., Tan, Y.-M., Edwards, S. W., Leonard, J. A., Anderson, K. A., Corley, R. A., Kile, M. L., Simonich, S. M., Stone, D., Tanguay, R. L., et al. (2016). Completing the Link between Exposure Science and Toxicology for Improved Environmental Health Decision Making: The Aggregate Exposure Pathway Framework. *Environmental Science & Technology*, 50 (9): 4579-4586.

United States Environmental Protection Agency (USEPA). (2002). *Methods for measuring the acute toxicity of effluents and receiving waters to freshwater and marine organisms*.

Vercouter, T., Reiller, P. E., Ansoborlo, E., Février, L., Gilbin, R., Lomenech, C. & Philippini, V. (2015). A modelling exercise on the importance of ternary alkaline earth carbonate species of uranium(VI) in the inorganic speciation of natural waters. *Applied Geochemistry*, 55: 192-198.

Wang, Q., Li, G.-D., Xu, S., Li, J.-X. & Chen, J.-S. (2008). Synthesis of uranium oxide nanoparticles and their catalytic performance for benzyl alcohol conversion to benzaldehyde. *Journal of Materials Chemistry*, 18 (10): 1146-1152.

Wang, W.-X. (2021). Bioimaging of metals in environmental toxicological studies: Linking localization and functionality. *Critical Reviews in Environmental Science and Technology*: 1-31.

Wang, Y., Frutschi, M., Suvorova, E., Phrommavanh, V., Descostes, M., Osman, A. A., Geipel, G. & Bernier-Latmani, R. J. N. c. (2013). Mobile uranium (IV)-bearing colloids in a mining-impacted wetland. 4 (1): 1-9.

Wang, Y., Bagnoud, A., Suvorova, E., McGivney, E., Chesaux, L., Phrommavanh, V., Descostes, M. & Bernier-Latmani, R. (2014). Geochemical Control on Uranium(IV) Mobility in a Mining-Impacted Wetland. *Environmental Science & Technology*, 48 (17): 10062-10070.

Willmott, P. (2019). *An introduction to synchrotron radiation: techniques and applications*: John Wiley & Sons.

WHO (2001). Depleted uranium: sources, exposure and health effects: World Health Organization.

Zeman, F. A., Gilbin, R., Alonzo, F., Lecomte-Pradines, C., Garnier-Laplace, J. & Aliaume, C. (2008). Effects of waterborne uranium on survival, growth, reproduction and physiological processes of the freshwater cladoceran Daphnia magna. *Aquatic Toxicology*, 86 (3): 370-378.

Paper I

Science of the Total Environment 727 (2020) 138488

Contents lists available at ScienceDirect

Science of the Total Environment

journal homepage: www.elsevier.com/locate/scitotenv

Characterization of radioactive particles from the Dounreay nuclear reprocessing facility

Ian Byrnes [a,*], Ole Christian Lind [a], Elisabeth Lindbo Hansen [a,b], Koen Janssens [c], Brit Salbu [a]

[a] Center for Environmental Radioactivity (CERAD CoE), Faculty of Environmental Sciences and Natural Resource Management, Norwegian University of Life Sciences (NMBU), P.O. Box 5003, 1433 Ås, Norway
[b] Norwegian Radiation and Nuclear Safety Authority (DSA), P.O. Box 329, Skøyen, NO-0213 Oslo, Norway
[c] AXES, Department of Physics, University of Antwerp, Groenenborgerlaan 171, B-2020 Antwerp, Belgium

HIGHLIGHTS

- Multi-technique characterization of radioactive Dounreay (MTR and DFR) particles
- Particle characteristics reflect nuclear fuel designs and accidental release scenarios.
- Highly enriched ($^{235}U/^{238}U$ range of 2.2–4.0), tetravalent U in both particle types
- Particles from MTR (Al, Nd ~ 1–2 atom %) can be differed from DFR (Nb, Mo ~ 0.5–1 atom %).
- Beta emission derived dose rates for Dounreay particles support existing models.

GRAPHICAL ABSTRACT

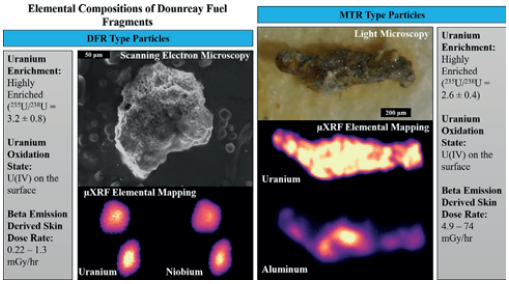

ARTICLE INFO

Article history:
Received 22 December 2019
Received in revised form 2 April 2020
Accepted 4 April 2020
Available online 7 April 2020

Editor: Kevin V. Thomas

Keywords:
Uranium particles
Electron microscopy
Micro-XRF
Micro-XANES
Contact dosimetry
Dounreay

ABSTRACT

Radioactive particles originating from nuclear fuel reprocessing at the United Kingdom Atomic Energy Authority's Dounreay Facility were inadvertently released to the environment in the late 1950s to 1970s and have subsequently been found on site grounds and local beaches. Previous assessments of risk associated with encountering a particle have been based on conservative assumptions related to particle composition and speciation. To reduce uncertainties associated with environmental impact assessments from Dounreay particles, further characterization is relevant.

Results of particles available for this study showed variation between Dounreay Fast Reactor (DFR) and Materials Test Reactor (MTR) particles, reflecting differences in fuel design, release scenarios, and subsequent environmental influence. Analyses of DFR particles showed they are small (100–300 μm) and contain spatially correlated U and Nb. Molybdenum, part of the DFR fuel, was identified at atomic concentrations below 1%. Based on SR-based micrometer-scale X-ray Absorption Near Edge Structure spectroscopy (μ-XANES), U may be present as U(IV), and, based on a measured Nb/U atom ratio of ~2, stoichiometric considerations are commensurable with the presence of UNb_2O_7. The MTR particles were larger (740–2000 μm) and contained U and Al inhomogeneously distributed. Neodymium (Nd) was identified in atomic concentrations of around 1–2%, suggesting it was part of the fuel design. The presence of U(IV) in MTR particles, as indicated by μ-XANES analysis, may be related to oxidation of particle surfaces, as could be expected due to corrosion of UAl_x fuel particles in air. High $^{235}U/^{238}U$ atom ratios in individual DFR (3.2 ± 0.8) and MTR (2.6 ± 0.4) particles reflected the presence of highly enriched

* Corresponding author at: Norwegian University of Life Sciences, Center of Excellence for Environmental Radioactivity (CERAD), Faculty of Environmental Sciences and Natural Resource Management, P.O. Box 5003, 1433 Ås, Norway.
E-mail address: ian.byrnes@nmbu.no (I. Byrnes).

https://doi.org/10.1016/j.scitotenv.2020.138488

uranium. The DFR particles featured lower ^{137}Cs activity levels (2.00–9.58 kBq/particle) than the MTR (43.2–641 kBq ^{137}Cs/particle) particles. The activities of the dose contributing radionuclides ^{90}Sr/^{90}Y were proportional to ^{137}Cs (^{90}Sr/^{137}Cs activity ratio ≈ 0.8) and particle activities were roughly proportional to the size. Based on direct beta measurements, gamma spectrometry, and the VARSKIN6 model, contact dose rates were calculated to be approximately 74 mGy/h for the highest activity MTR particle, in agreement with previously published estimates.

1. Introduction

In nuclear fuel reprocessing, uranium (U) and plutonium (Pu) from spent nuclear fuel are recovered for civil or military uses. Essential to reprocessing is the dissolution of the spent fuel, a procedure that increases the potential for contaminant release in liquid waste discharges (Choppin et al., 2013). Reports on radioactive particles found in the vicinity of reprocessing sites indicate that the dissolution of fuel may be incomplete and that residual fuel fragments and particles in the discharges can give rise to radioactive particle contamination in the environment such as in the case of Krasnoyarsk-26, Sellafield, and Dounreay reprocessing facilities (Bolsunovsky et al., 2017; Dennis et al., 2007; Geckeis et al., 2019; Lind, 2006). Failure to recognize the presence of radioactive particles, defined by the International Atomic Energy Agency (IAEA) as "a localized aggregation of radioactive atoms that give rise to an inhomogeneous distribution of radionuclides significantly different from that of the matrix background", may have a number of serious consequences (IAEA, 2011). The presence of insoluble particles in bulk samples may cause incomplete dissolution, which may give rise to analytical inconsistencies, irreproducible results, and erratic conclusions (Cooper et al., 1994; Danesi et al., 2002; Oughton et al., 1993; Simon et al., 1995). Furthermore, there will be unacceptably large uncertainties associated with model predictions for dispersion and ecosystem transport as well as dose assessment (Bunzl, 1997; Darley et al., 2003). To characterize particle properties of relevance for impact assessments, however, a combination of advanced technologies are needed (Salbu et al., 1994; Salbu and Lind, 2020).

Particles have been identified as part of the radioactive contamination of many sites in addition to nuclear reprocessing facilities, such as from nuclear weapon tests, conventional detonation of nuclear weapons, fallout from nuclear reactor explosions or fires, and use of depleted uranium (DU) for ammunitions (Salbu et al., 2011). Research has demonstrated that the particle composition will depend on the source, while the release scenario will influence particle properties of relevance for environmental transfer. (Salbu and Lind, 2020). Particle structure and morphology, elemental composition, and oxidation state of U or Pu have been shown to be key parameters in determining potential subsequent weathering and remobilization in the ecosystem (Salbu, 2016).

Radioactive particles were identified at the Dounreay facility foreshore in November 1983 and have since been recovered at a rate of approximately eight particles per month from foreshore sediments at the United Kingdom Atomic Energy Authority's (UKAEA) former reactor research establishment at Dounreay (Fig. 1), Caithness, Scotland, and from the nearby Sandside (2.5 km west of site) and Dunnet (25 km east of site) public beaches (Tyler et al., 2010). These highly radioactive (MBq) particles and fragments are small pieces (typically 0.2–2 mm) of fuel material, formed and accidentally released to the marine environment during historical nuclear fuel reprocessing operations involving irradiated spent fuel, which took place during the late 1950s, 1960s, and 1970s (Henderson et al., 2007; Potter et al., 2003). Opened in 1955, the UKAEA Dounreay facility included three nuclear reactors, the Dounreay Fast Reactor (DFR), the Prototype Fast Reactor (PFR), and the Material Testing Reactor (MTR) along with fuel fabrication and reprocessing capabilities. A total activity of about 10 PBq was

Fig. 1. The location of Dounreay Site Restoration Ltd. with nearby public beaches shown.

discharged to the marine environment from the facility until decommissioning in 1994 (CEG, 1990). Studies of the extent of particle contamination were commissioned by Scottish Environmental Protection Agency (SEPA) in 1997 and coincided with the implementation of a fishing exclusion zone of 2 km around the facility as a result of foreshore particle finds (Dennis et al., 2007). Routine monitoring programs of facility grounds and local public beaches (Sandside, Murkle, and Dunnet) remain in place today (DSRL, 2019a; DSRL, 2019b; DSRL, 2019c).

As they are relatively small in size, these particles escaped the main filtration systems of the facility and were released via the low activity liquid effluent systems (the Low Activity Drain (LAD), Old Diffusion Chamber (ODC), and the Sea Tanks) into the surrounding marine environment (PRAG(D), 2012). This system, which was withdrawn from use in 1992, was connected to a discharge point on the seabed by sixteen 23 m long boreholes. The integrity of these boreholes failed some time prior to identification in 1981, creating a release pathway to the marine environment. This has been described in previous reports to be the primary pathway for particle releases, and efforts have been made to seal and prevent future releases (Henderson et al., 2007; PRAG(D), 2012). Other potential release pathways are minor, but include a fire in 1967 and an incident associated with a work shaft that was repurposed for solid waste storage (Dennis et al., 2007). The work shaft was originally built to support work on the active waste effluent system; it was modified and used for solid waste storage from 1958 to 1977. An explosion due to hydrogen build up occurred on May 10, 1977 (Henderson et al., 2007). Particle release via the shaft explosion may have occurred; however, groundwater pumping from the work shaft to the low activity liquid effluent system also occurred, as required for use as waste storage, making the specific source difficult to identify.

Released particles can be assumed to have spent years to decades in the marine environment. Modeling work has been performed to estimate the transport and numbers of particles released. Initial modeling predicted that the majority of particles would move northeast of the old diffuser (Henderson et al., 2007; Soulsby et al., 2006). More recent efforts compared the modeling work with seabed particle finds and confirmed that the discharge location around the ODC and LAD are the point of exit and that the particles have, generally, formed a plume traveling northeast and parallel to the shore (PRAG(D), 2012). Continued work with the model has shown that wave action drives the particles from the seabed to the Dounreay foreshore where the bulk of particles are found. Reviews of potential new or ongoing sources of particles have been conducted and do not find evidence of either case, leading to the conclusion that all particles found are from past releases (Dennis et al., 2007). The majority of the particles from Dounreay are attributed to the reprocessing of fuel from either the MTR or the DFR. However, a few particles with other characteristics have been identified, including ^{60}Co containing particles and ^{90}Sr enriched particles with activities of ^{90}Sr significantly greater than for ^{137}Cs (PRAG(D), 2012).

Estimates suggest there are several hundred thousand Dounreay particles in the surrounding environment although the risk to members of the public remains very low (Dale et al., 2008; Henderson et al., 2007; Tyler et al., 2010). In conjunction with Dounreay Site Restoration Ltd. (DSRL), routine monitoring of affected areas using vehicle mounted detectors was established and the number of particle finds increased to an average of eight per month (PRAG(D), 2012). The detection limit and efficiency of doing so would depend not only on the detector, but also on the speed of the vehicle. Complete inventories of particle finds are available to the public through DSRL (DSRL, 2019a; DSRL, 2019b; DSRL, 2019c). The radioactivity of particles largely depends on the size and typically varies from 10^2 to 10^7 Bq, MTR particles having significantly higher activities than the ones originating from DFR operations. To develop a categorization of the particles based on activity, and thereby health risk, SEPA organizes recovered particles by ^{137}Cs activity, which is easy for recovery teams to measure by gamma spectrometry (PRAG (D), 2012). The ^{137}Cs activity particles with the highest activities, i.e., above 10^6 Bq, are termed *significant*. *Relevant* particles contain $>10^5$ Bq ^{137}Cs, while any particle with ^{137}Cs activity below 10^5 Bq is classified as *minor*. The majority of particles identified fall into the *minor* classification. As the size distribution of radioactive particles found at other contaminated sites would, to a certain extent, follow a log-normal distribution (Kashparov et al., 2000; Shevchenko, 2004), the potential exists that a significant number of undetected, low activity particles would be situated in the marine ecosystem and the beaches around the Dounreay facility, and that the *minor* classification category could be defined too broadly.

Radioactive particles, like Dounreay fuel fragments, can carry a substantial amount of radioactivity and act as point sources of potential long-term significance for human health as well as for biota (Salbu et al., 2018). There is a risk from inhalation, dermal absorption, skin exposure, and ingestion. For filter-feeders (e.g., mollusks) and soil-dwelling animals (e.g. gastropods), particles can be retained by the organism and eventually be ingested by humans (Jaeschke et al., 2015; Salbu et al., 2018). Upon prolonged contact, radioactive particles can give rise to skin ulceration (Charles, 1991; Darley et al., 2003; Gesell et al., 1999) and damage epithelial tissues of biota (Jaeschke et al., 2015). Furthermore, particle weathering can increase the mobility and potential for the transfer of particle associated radionuclides into the biosphere. As a result of particle weathering, radionuclides originally associated with large particles or fragments may also occur as submicron and even nanoscale particles with biological uptake properties potentially very different from those of ions (Salbu et al., 2018). Thus, uncertainties in environmental impact assessments of particle contaminated areas may be unacceptably large if heterogeneous distributions are not taken into account. At Dounreay, uncertainties are magnified by the potential existence of small, non-detected particles in the marine environment. Previous risk assessments related to Dounreay particles have primarily focused on human health. However, environmental biota are not necessarily adequately protected from ionizing radiation even if humans are sufficiently protected (Strand et al., 2009).

The purpose of the present work is to fill identified knowledge gaps associated with Dounreay fuel fragment characteristics by linking data on morphology, elemental and isotopic composition, as well as oxidation state to the release scenario and potential health risks. To achieve these goals, the present work presents (1) new information on Dounreay fuel fragment characteristics based on analysis using laboratory based X-ray fluorescence (μ-XRF), scanning electron microscopy (SEM-XRMA), and inductively coupled plasma mass spectroscopy (ICP-MS), (2) results from synchrotron radiation based micro X-ray Absorption Near Edge Spectroscopy (μ-XANES), and (3) an estimation of the potential contact dose from encountering a particle by direct beta measurements using a Si semiconductor detector (Canberra PIPS) and skin dose calculator software VARSKIN6.

2. Materials and methods

2.1. Particle handling and gamma spectrometry

Archived particles (3 of the DFR type and 3 of the MTR type) were supplied from SEPA for analysis. The original particle details are shown in Table S1. Some of the particles were utilized in connection with previous blue mussel exposure experiments in which physical deterioration and loss of activity from particles were observed in some cases (Jaeschke et al., 2015).

Individual particles were re-examined by gamma spectrometry using a liquid nitrogen cooled Low Energy Germanium (LEGe) detector (Canberra Instruments, relative efficiency 25%, resolution 1.8 keV) with particles being counted at 10 cm distance from the surface of the detector. SEM-XRMA and μ-XANES measurements were completed prior to exposure experiments with blue mussels (Jaeschke et al., 2015). All μ-XRF and dosimetry measurements were completed after the blue mussel studies.

2.2. ICP-MS

Small fragments of DFR3 and MTR2 were sacrificed for ICP-MS analysis in order to determine the isotope ratio $^{235}U/^{238}U$ as well as niobium (Nb), molybdenum (Mo), neodymium (Nd), and zirconium (Zr) concentrations. The samples were isolated from the main particle and dissolved by microwave digestion (Milestone, Ultraclave III, Italy) at 260 °C for 40 min in a 1 mL mixture of HNO_3, H_2PO_4, and HBF_4 (1:2:1 ratio). An acid mixture selection was made to ensure proper dissolution of Nd along with other metals. The isotope ratios and element concentration were determined by inductively coupled plasma mass spectrometry (Agilent 8800 ICP-MS QQQ, Japan). Isotopic ratio results were mass bias corrected against a 6 μg/L solution of NBL CRM 129-A isotopic standard.

2.3. SEM-XRMA

Individual radioactive particles or sub-samples from these (~10–50 μm grains extracted with tweezers) were attached to carbon double-faced sticky tape and mounted onto Al stubs for analysis of surface structures and elemental composition of the particles by means of scanning electron microscopy (SEM) using a JEOL JSM 840 instrument interfaced with an ISIS 300 X-ray micro-analysis (XRMA) system, Oxford Instruments. Surface structures were viewed using secondary electron imaging (SEI) mode, while backscatter electron imaging (BEI) mode highlighted high density (high atomic number elements) areas as bright structures on the image. XRMA provided semi-quantitative identification of elements. The distribution of elements were shown by x-ray mapping helping to identify locations containing U and other elements of interest (Salbu and Lind, 2020).

2.4. Laboratory based μ-XRF

Each of the particles, or fragments of the original particle, were subjected to laboratory based micro X-ray fluorescence (μ-XRF) to determine the elemental distribution on the particle surface and isotope ratios using a M4 Tornado (Bruker, Germany) (Janssens et al., 2010). Particles were remounted from the SEM stub to a mylar foil stretched over an x-cell (31 mm Double Open-Ended X-CELL®). A rhodium (Rh) target, running at 50 kV and 600 μA, and polycapillary optics provided the beam with a spot size of 25 μm. Fluorescent x-rays were counted by two XFlash® silicon drift detectors (50 keV, 600 μA, 25 μm spot size). The detectors are at a 45° angle to the beam and each feature an active area of 30 mm^2. Two-dimensional elemental mapping was performed under vacuum (20 mbar) and repeated a number of times to ensure good statistics. Collected XRF spectra were analyzed by the ESPIRIT software (Bruker).

2.5. Synchrotron based μ-XANES

After SEM-XRMA analysis, sub-samples from particles DFR2 and MTR3, mounted on carbon double-faced sticky tape, were examined by synchrotron based micro X-ray absorption near edge spectrometry (μ-XANES) analysis using the x-ray microscopic facility at beamline L, HASYLAB, Hamburg (Lind et al., 2007; Lind et al., 2009; Salbu et al., 2003). By tuning the monochromatic, focused x-ray beam (20 μm beam via polycarpellary lens) over the U L_{III} absorption edge (17.163 keV), information related to the oxidation state of U present in the particles can be found (Conradson et al., 2004; Salbu et al., 2001; Schulze and Bertsch, 1995; Silva and Nitsche, 2001). The beam flux at the sample spot was approximately 10^9 photons per second at 17.1 keV. The beam intensity was measured by ionization chambers and the U L_{III} fluorescence intensity was measured by a well collimated, high purity germanium (HPGe) detector (area of 30 mm^2) mounted at a 90° angle to the primary beam and 30 mm from the sample. The μ-XANES spectra were collected over 300 eV in 1 eV increments. Well defined U oxidation standards (UO_2, Institute of Energy Technology, Kjeller; U_3O_8, Institute of Energy Technology, Kjeller; UO_2Ac_2 x $2H_2O$ p.a., Riedel-De Haën AG, Seelze-Hannover; $UO_2(NO_3)_2$ x $6H_2O$ p.a., Merck, Darmstadt) were used to collect standard μ-XANES spectra for comparison with sample spectra.

2.6. Contact dosimetry

Beta ray emissions from individual radioactive particles were determined using a SPAB15 alpha/beta probe connected to a Radiagem 2000 Portable Dose Rate and Survey Meter (Canberra). The particles were counted for 30 s at 1 cm increments to a minimum of 20 cm. The observed count rates were corrected for detector efficiency: 37% for $^{90}Sr/^{90}Y$ (Menanteau, 2009). The beta activity for each particle was calculated using the relationship between the corrected count rate and the particle activity (Bq) in Eq. (1) (Choppin et al., 2013).

$$\text{Corrected Count Rate cps} = \psi_{sample}\psi_{abs}\psi_{geom} \times \text{Particle Activity Bq} \quad (1)$$

here, ψ_{sample} represents the self-absorption of beta rays within the particle. Because the particles are small (<2 mm), ψ_{sample} is taken to be 1. Air attenuation is accounted for by ψ_{abs} and the geometric correction is denoted by ψ_{geom}.

VARSKIN6, a skin dosimetry calculator developed by the United States Nuclear Regulatory Agency (USNRC), was used to compare skin dose estimates provided by Harrison et al., 2005. (Gesell et al., 1999). Combined β-γ skin dose estimates were made for contact doses of a 1 cm^2 area to the epithelial layer of skin (70 μm below the surface) with no mediating shield (Anspach and Hamby, 2018).

3. Results and discussion

The DFR particles examined in this study are classified as *minor* particles by SEPA, while the MTR particles belong to the *relevant* category. DFR particles were below 300 μm in size and appear non-metallic, brittle, and prone to mechanical breakdown, which is important with respect to particle weathering as the surface area of the original particle increases after breaking. Estimates of the specific gravity of DFR particles suggest a broad range of 4.7–7.4 g/cm^3 (Dennis et al., 2007). The MTR particles studied here were larger (<2 mm in size), mostly of metallic appearance and sturdier (Table 1). According to SEPA, the MTR particles in general range from 0.4 mm to 3 mm in size and have a density of 3.1 ± 0.4 g/cm^3 (PRAG(D), 2012).

3.1. Characteristics of DFR particles

Scanning electron microscope imaging of the DFR type particles detail surfaces that are pitted and cracked, giving credence to the assumption that DFR particles lack structural stability (Fig. 2), in line with previous descriptions (Henderson et al., 2007; Potter et al., 2003). Of note, the surface morphology of DFR2 varies across the particle with predominately pitted, porous material along with a few crystallized, smoother regions, indicating a variation in the formation of the original particle or its subsequent weathering. X-ray microanalysis at various locations on the particle surface show the dominant elements to be U and Nb with some inclusions of iron (Fe).

According to the PRAG(D) report (PRAG(D), 2012), DFR particles are expected to contain approximately 40% Nb, 20% U, and 15% Fe. X-ray point analysis on the pitted, porous regions also found titanium (Ti), sodium (Na), aluminum (Al) and Zr to be present. In a nuclear context, Zr is typically related to the cladding material of fuel elements, although Zr can also occur naturally in soils and sediments. In addition, a wide range of elements indicative of soils or sediments adhering to the particle surfaces were identified, such as chlorine (Cl), sulfur (S), and phosphorus (P).

Table 1
Characteristics of particles analyzed in this work (reference date: October 2018).

Particle	Approximate particle dimensions (μm)	$^{235}U/^{238}U$ isotope ratio	Major elements	Elemental ratios mean ± σ (range)	Number of point measurements	^{137}Cs activity (Bq ± σ)
DFR1	100 × 90	N.A.	U, Nb, Mo, Fe, Cr, Al, Ni, Si, Zn	Nb/U = 2.4 ± 0.3 (2.1–2.9) Mo/U = 0.02 ± 0.02 (0–0.1)	8	(2.0 ± 0.1) × 10^3
DFR2	200 × 160	N.A.	U, Nb, Mo, Fe, Cr, Al, Si, Zn	Nb/U = 2.5 ± 0.3 (1.9–3.0) Mo/U = 0.02 ± 0.01 (0–0.03)	10	(6.9 ± 0.2) × 10^3
DFR3P1	300 × 160	3.2 ± 0.8	U, Nb, Mo, Fe, Ca, Cl	Nb/U = 2.1 ± 0.1 (1.9–2.2) Mo/U = 0.1 ± 0.02 (0.03–0.1)	4	(6.6 ± 0.2) × 10^3
DFR3P2	300 × 160	3.2 ± 0.8	U, Nb, Fe, Zn	Nb/U = 2.1 ± 0.1 (1.9–2.2) Mo/U = 0.1 ± 0.02 (0.03–0.1)	4	(9.6 ± 0.3) × 10^3
MTR1	2000 × 1000	N.A.	U, Al, Nd, Fe, Zn, Si	Al/U = 19.8 ± 5.7 (9.5–33.6) Nd/U = 0.02 ± 0.003 (0.01–0.03)	100	(6.4 ± 0.1) × 10^5
MTR2	1400 × 300	2.6 ± 0.4	U, Al, Nd, Zn, Mg, Fe	Al/U = 14.6 ± 8.0 (4.2–56.6) Nd/U = 0.1 ± 0.03 (0.03–0.3)	100	(4.3 ± 0.1) × 10^4
MTR3	50 × 30	N.A:	U, Al, Si, Fe, Ca, Ni, Cr	Al/U = 378 ± 242 (35.5–551) Nd/U = 0.5 ± 0.2 (0.3–0.7)	3	(3.7 ± 0.3) × 10^2

N.A. = not analyzed.

Both SEM-XRMA and μ-XRF analyses show a correlation between U and Nb (Fig. 2, Fig. 3, Fig. 4) and the elemental ratio between Nb/U was approximately 2 for all DFR particles (Table 1). Elemental mapping by μ-XRF also shows a spatial correlation between Nb and U. To further test the Nb-U correlation, a sub-sample of DFR3 was analyzed via ICP-MS and found a Nb/U ratio of 1.7 ± 0.2, in good agreement with the μ-XRF results.

The same ICP-MS results yielded a $^{235}U/^{238}U$ ratio of 3.2 ± 0.8 for DFR3, showing that the U present in the particle was highly enriched (HEU) according to the IAEA classification (IAEA, 2005). The fuel elements used in the DFR were highly enriched U-Mo slugs, clad in a Nb casing (Cartwright, 1997). Investigations by SEPA indicate that the DFR particles were formed by high temperature (1668 °C) dissolver accidents during fuel element dissolution (Henderson et al., 2007). Such high temperatures would exceed the temperature threshold to form a U and Nb alloy such as UNb_2O_7 (Busch and Gruehn, 1994). The formation of such an alloy was supported by x-ray analysis of the DFR particles. The U-L_{III} edge μ-XANES spectra in a subsample of particle DFR2 coincide with the spectrum for UO_2 (Fig. 5) and strongly indicates that U is tetravalent, i.e., present as UO_2 or as an intermetallic compound. The latter interpretation is arguably supported by SEM-XRMA analyses, which showed U and Nb

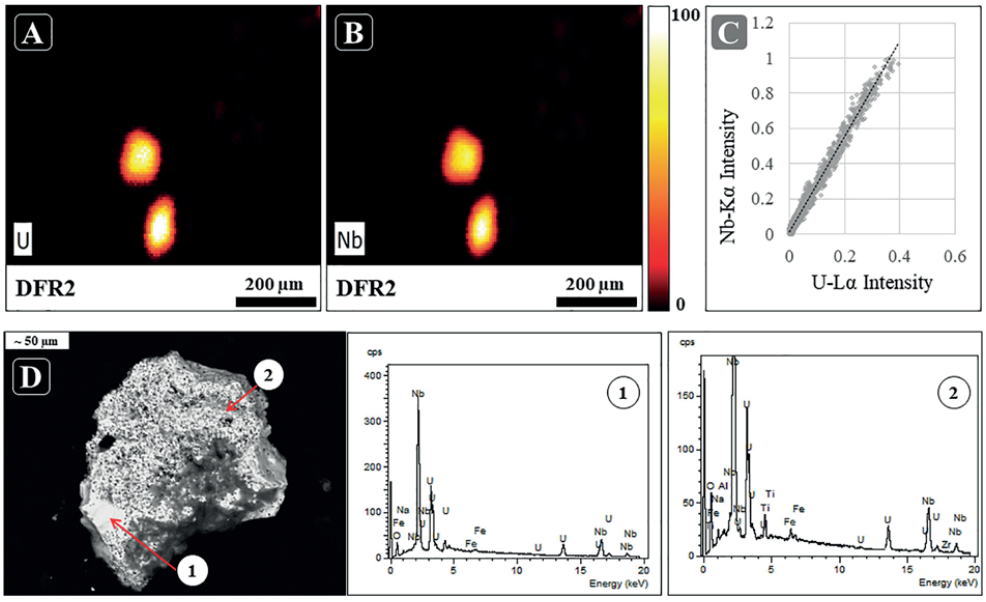

Fig. 2. Elemental mapping by μ-XRF of DFR2 showing (A) the U and (B) the Nb distributions (intensity scale on the right). C) Correlation plot of normalized U Lα and Nb Kα intensities from the XRF elemental mapping. D) SEM BEI image with XRMA spot analysis at a flat smooth region at location (1) and at a porous, pitted region at location (2).

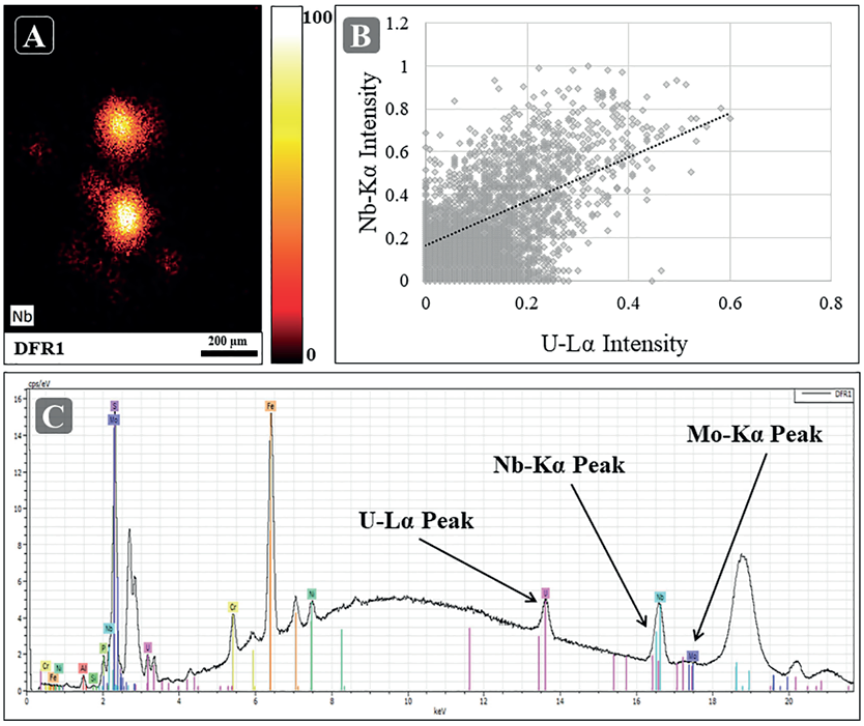

Fig. 3. (A) Nb map of DFR1 obtained by micro-XRF. (B) Correlation plot between normalized U Lα and Nb Kα intensities obtained in (A). (C) XRF spectrum collected from DFR1, showing the U, Nb, and Mo peaks.

co-existing at the micron scale resolution throughout the particle matrices and by Nb/U atom ratios of ~2 observed in μ-XRF analyses. These stoichiometric considerations are commensurable with the presence of UNb_2O_7 in the particles.

Leaching experiments have previously been conducted to investigate the potential bioavailability of DFR particles using simulated human stomach juices (2 h) and two types of intestinal fluids (2 × 4 h), sequentially (Stewart et al., 2003). Results show that, on

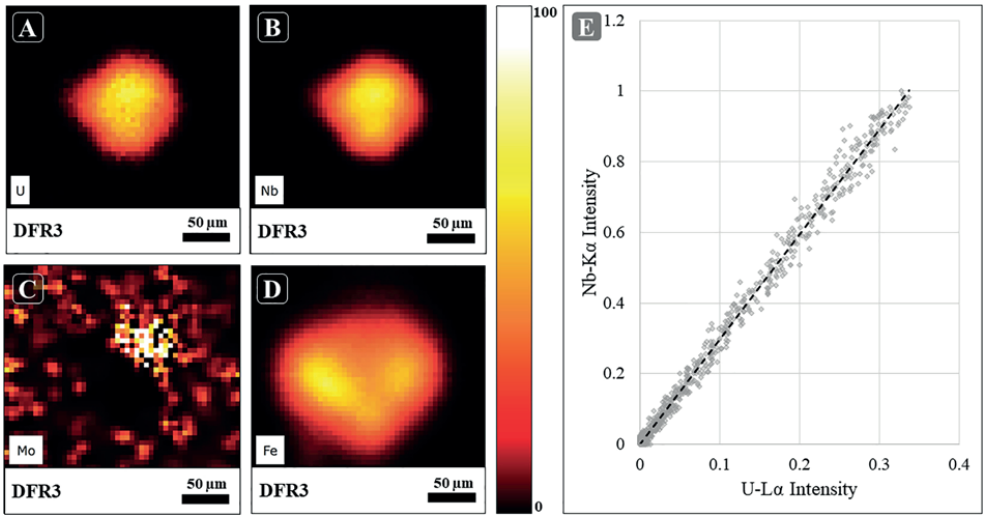

Fig. 4. Micro-XRF elemental maps of DFR3:(A) U, (B) Nb, (C) Mo, and (D) Fe distributions. (E) Correlation plot of normalized intensity signals of U-L_α and Nb-K_α obtained in (A) and (B).

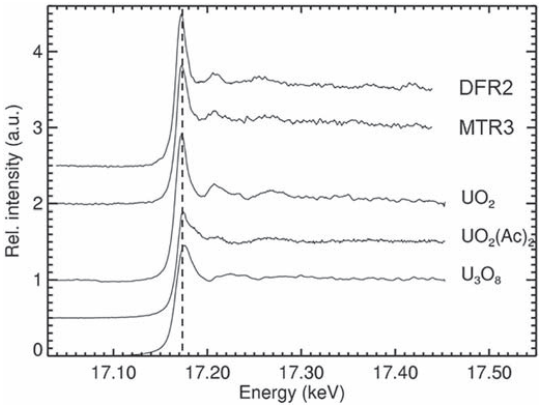

Fig. 5. Fluorescent U μ-XANES profiles obtained from fragments of Dounreay particles DFR2 and MTR3 in comparison to UO_2, $UO_2(Ac)_2$ and U_3O_8 reference compounds. Vertical line indicates position of white line of UO_2.

average, 47% of ^{137}Cs and 85% of ^{241}Am were removed from DFR particles. These results can provide insight into the general mobility and bioavailability of radionuclides associated with these particles and suggest a significant mobilization potential. However, a study of retention of DFR particles in rats found only 1% retention in most cases for the major radionuclides of interest, giving credence to the assumptions that DFR particles do not readily dissolve in the body prior to excretion (Harrison et al., 2005). This conclusion is supported by the fact that the DFR particles have resided approximately 40–50 years in the marine environment, yet, have retained significant concentrations of U and fission products. Given the range of results from these studies, leaching experiments could provide a fertile ground for future work with these particles.

In addition to U and Nb, trace amounts of Mo were detected in each DFR particle (Table 1). Molybdenum was correlated with U, commensurate with the fact that the DFR nuclear fuel contained Mo, which was used to improve thermal stability during irradiation of the fuel element (Cartwright, 1997; Meyer et al., 2014; Rest et al., 2006). In DFR3, the elemental mapping of Mo was possible and showed spatial correlation with U and Nb (Fig. 4). Although it is claimed that DFR fuel contained an approximate atomic concentration of 15% Mo (Meyer et al., 2014), our μ-XRF analyses suggest that Mo is only present in atomic concentrations of ~1%. The Mo loss can possibly be attributed to oxidation and removal of Mo from the fuel as MoO_3 during the high temperature formation of the particles. Material testing of U-Mo type fuels have shown that the significant porosity in fuel elements was similar to the porous, pitted surfaces observed in the present DFR particles, and this could be attributed to the formation of so-called high burnup structures (Jadernas et al., 2018; Leenaers et al., 2016).

3.2. Characteristics of MTR particles

The examination of MTR type particles displayed the rigid crystalline and metallic appearance described in previous reporting, as illustrated in Fig. 6 for particle MTR3. Scanning electron microscopy in BEI mode combined with spot XRMA analysis of the three studied MTR samples show that the particle surfaces contain a matrix of Al and U distributed inhomogeneously. Particle surface elements also included Na, Ca, Si, P, S, and, most significantly, Fe. These elements are common amongst

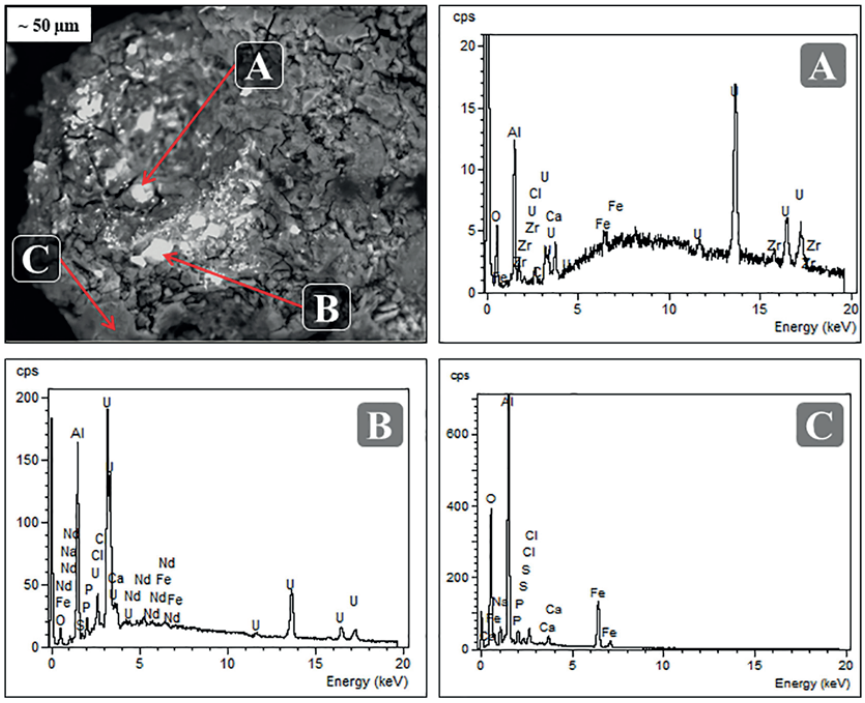

Fig. 6. SEM-XRMA of MTR3. High density regions appear as bright locations on the surface of the particle. SEM-XRMA spectra from three MTR3 locations (A), (B), and (C). High density locations (A) and (B) contain U, while darker location (C) appears to mostly contain Al.

marine sediments and it is plausible that they fill cracks and pores on the particle surfaces due to environmental processes (Potter et al., 2003)

Notably, Nd is present throughout U containing phases of the particle reaching 1–2% by mass, suggesting Nd was included in the original fuel design (Potter et al., 2003), rather than present due to decay of fission products as suggested elsewhere. The X-ray microanalysis of MTR3 also yielded signals of Nd on the surface of the particle that generally were spatially correlated with the U distribution (Fig. 6B). Using μ-XRF elemental mapping, the MTR particles show an inhomogeneous distribution of elements throughout, as seen in Figs. 7 and 8, making each one somewhat unique.

The MTR was fueled by a U dispersion fuel that comprised of small grains, a few microns in size, of uranium-aluminum (UAl_4) embedded in an Al substrate and housed in an Al casing (Gibson, 1997; Tamborini, 2004). Together, the components formed a flat, panel shaped fuel element approximately 2 mm in thickness that includes both the UAl_4 core and the Al casing (Henderson et al., 2007). The fuel elements contained approximately 20% U by weight and had an average enrichment of 70% ^{235}U, with some assemblies containing as high as 90% enrichment (Henderson et al., 2007; Potter et al., 2003). Grinding and cutting operations on the MTR fuel plates were conducted as part of the fuel reprocessing, designed to remove excess Al, but occasionally cut too close to the U containing core and generated swarf that included fuel fragments (DPAG, 2008). In the particles studied, Al was inhomogeneously distributed across each particle with noted enriched areas. Multiple spot μ-XRF analyses on the surface of particle MTR1 revealed a wide variation in Al/U ratios (Fig. 7). Smooth, shiny locations with a metallic luster on the surface exhibited an Al/U atomic ratio of ~16, while the corresponding ratio measured at a dark pit on the surface was significantly lower (~10). The inhomogeneous distribution of Al is likely representative of both the design of the MTR fuel matrix as well as potential mechanical fragmentation from exposure to the environment, as evidenced by the dark pits on the surface of the particle. Analyses made here would indicate that the local U concentration is, on average, 25–45% by weight depending on the location within the particle. Thus, assumptions about the average density of MTR type particles may be affected with large uncertainties.

Secondary ion mass spectrometry (SIMS) of a MTR particle has previously showed the distribution of micron scale inclusions of enriched U within the Al matrix (Tamborini, 2004). An overall Al/U atomic ratio of 6.9 was determined by SIMS and ICP-MS for the examined particles. The resolution of the SIMS instrument (~1 μm) allowed for measurement on the UAl_4 grains themselves while the μ-XRF in this study had a beam size of 20 μm and would collect signal from the surrounding Al material. The isotopic composition (83% ^{235}U, 8% ^{236}U, 8% ^{238}U by atomic concentration, $^{235}U/^{238}U = 10$, $^{239}Pu/^{240}Pu = 6.0$) of the MTR particle in that study was consistent with a calculated composition of HEU fuel with an enrichment of >90% that had been irradiated in an MTR reactor to a burnup of 25–30% (Tamborini, 2004). Results from the present ICP-MS analysis of a fragment from MTR2 showed a slightly lower, but still HEU, $^{235}U/^{238}U$ isotope ratio of 2.6 ± 0.4. However, this variation can be attributed to the original fuel assembly the particle was derived from, as not all fuel assemblies had the same enrichments or burn-ups.

Given that the original MTR fuel was an alloy of Al and the intermetallic compound UAl_4, the U containing phases in MTR particles may remain UAl_4, especially as the assumed formation and release pathway of the particles involved grinding and cutting, but not high heat dissolution (Potter et al., 2001). Examinations of UAl_4 have found that it is well formed with few defects in the structure of the U sublattice, suggesting that the compound is quite sturdy and that fission products are well bound to the structure, important to the potential leaching (Potter et al., 2001; Tougait and Noel, 2004). However, there remains the potential for oxidation of the surface of the particle. Research into the corrosion of uranium aluminide fuels, when placed in long term storage under aqueous conditions, identified oxidation on the surface of the fuel elements that included a UO_2 phase (Kaminski, 2003; Kaminski and Goldberg, 2002). The occurrence of UO_2 in those fuel assemblies was part of a process that resulted in the formation of schoepite on U containing surfaces. The μ-XANES analysis (Fig. 5) of a subsample of MTR3 most closely related to those of the UO_2 standard, indicating the U could be present as U(IV). Although qualitative, U in

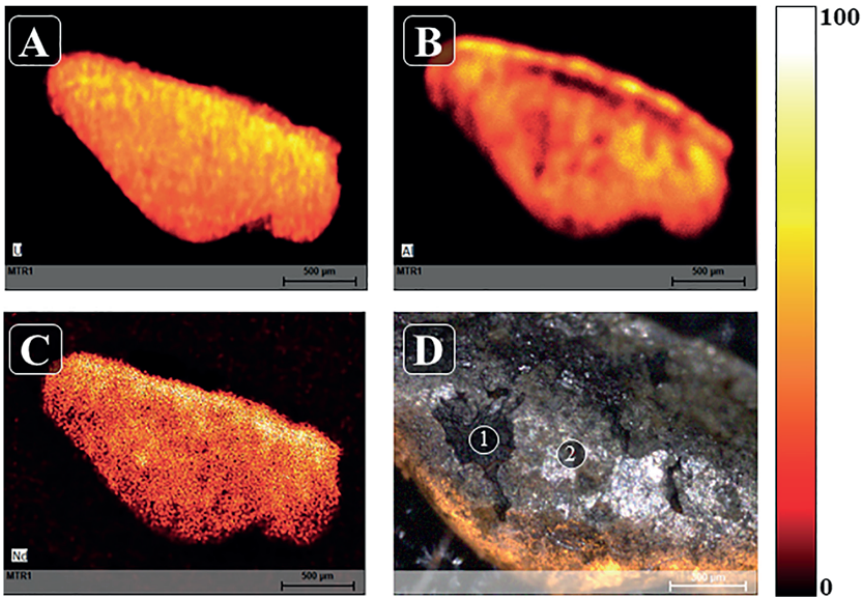

Fig. 7. Elemental maps obtained by μ-XRF: (A) U, (B) Al and (C) Nd distributions within particle MTR1. (D) Light micrographs of the surface of MTR1 show the locations of point measurements (1) and (2), featuring a change in Al/U ratio: 9.6 at (1) and 15.8 at (2).

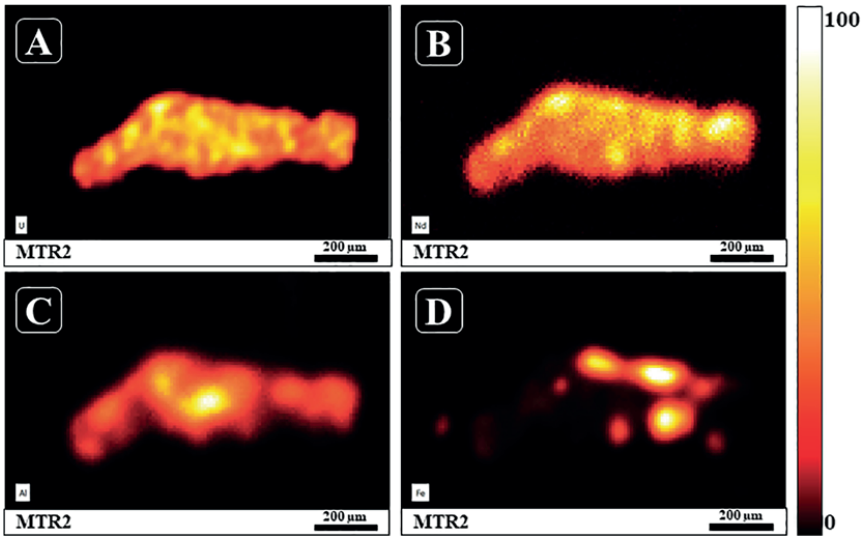

Fig. 8. Micro-XRF elemental maps of (A) U, (B) Nd, (C) Al and (D) Fe in MTR2, showing the inhomogeneous distribution of elements. The intensity scale bar indicates atomic concentration (in %) of the element shown.

the U(IV) state suggest that the exposed U containing phases on the surface of the MTR particle are oxidized. In addition, Kaminski et al. have shown U colloid formations from the corrosion of the fuels to be significant (Kaminski et al., 2005). These studies show that UO_2 is plausible as an intermediate phase in the corrosion of UAl_x type fuels that the MTR particles are derived from and that the potential exists for the formation of U containing colloids during weathering of the particles. The weathering of particles has been shown to decrease the overall particle size distribution giving rise to a colloidal phase and similar responses could be expected for MTR particles (Salbu et al., 2018). However, the analysis via μ-XANES in this study is only qualitative and represents a small subsample of only one particle and further investigation of U in MTR particles is required to confirm these results, such as Extended X-ray Absorption Fine Structure (EXAFS) analysis.

Stewart and coworkers conducted leaching experiments with MTR particles in the same way as for DFR particles (Stewart et al., 2003). The study showed similarly high leaching rates of particle associated radionuclides (60% ^{137}Cs, 51% ^{241}Am) as for DFR particles, suggesting a rather high remobilization of these radionuclides from the fuel matrix. This leaching behavior, along with the potential for colloid formation such as reported by Kaminski et al. (2005), indicates that these particles may be prone to rapid weathering. Thus, the use of the IAEA CRP/EU COMET-RATE protocol for abiotic leaching, including size fractionation of leachates (Salbu and Lind, 2020), should be scope for further studies on Dounreay particles.

3.3. Contact dosimetry from Dounreay particles

An assessment of the activity and contact dose rates of the six particles was made and compared with published, generalized estimates (Harrison et al., 2005). Based on gamma spectrometry, ^{137}Cs activities ranged from 2.0×10^3–9.6×10^3 Bq/particle for DFR particles and 4.3×10^4–6.5×10^5 Bq/particle for MTR particles (Table 2). Due to the high concentration of ^{90}Sr in Dounreay fuel fragments, beta doses from contact with a particle pose a significant risk. Based on the SPAB15 probe measurements, beta activities ranged from 1.6×10^3–7.3×10^3 Bq/particle for DFR particles and 3.5×10^4–5.3×10^5 Bq/particle for MTR samples (Table 2). As expected, beta activities were slightly lower than ^{137}Cs activities and the calculated beta/^{137}Cs ratio was approximately 0.8 for all the studied particles except DFR3P1 which showed a ratio of 0.9. The measured beta activities were lower on average than the estimates made by SEPA, which relies on a ^{90}Sr/^{137}Cs ratio of 0.9, shown in Fig. 9 (Aydarous et al., 2008; Aydarous et al., 2001; Harrison et al., 2005).

SEPA estimates the ^{90}Sr activity in a MTR type particle to be 0.9 of the ^{137}Cs activity, based on isotopic composition analyses (Darley et al., 2003; Harrison et al., 2005; Wilkins et al., 1998). Because they are found in higher abundance, have higher activity, and are of sturdier nature than DFR particles, only MTR particles were assessed by SEPA. As a result, the evaluation states that it will overestimate doses for DFR particles. The results shown here indicate that the 0.9 ratio only slightly

Table 2
Activity and dosimetry results for DFR and MTR particles examined in this paper.

	^{137}Cs activity via HPGe (Bq)	Beta activity via SPAB 15 measurements (Bq)	Beta activity/^{137}Cs activity	VARSKIN6 skin dose rate (mGy/h)	Time to 500 mGy threshold[a] (hrs)
DFR1	$(2.00 \pm 0.09) \times 10^3$	$(1.61 \pm 0.08) \times 10^3$	0.81	0.22	2273
DFR2	$(6.94 \pm 0.19) \times 10^3$	$(5.75 \pm 0.29) \times 10^3$	0.83	0.79	633
DFR3P1	$(6.55 \pm 0.20) \times 10^3$	$(5.91 \pm 0.30) \times 10^3$	0.90	0.82	610
DFR3P2	$(9.58 \pm 0.27) \times 10^3$	$(7.95 \pm 0.40) \times 10^3$	0.83	1.3	385
MTR1	$(6.41 \pm 0.10) \times 10^5$	$(5.30 \pm 0.27) \times 10^5$	0.83	74	7
MTR2	$(4.32 \pm 0.09) \times 10^4$	$(3.53 \pm 0.18) \times 10^4$	0.82	4.9	102
MTR3	$(3.73 \pm 0.30) \times 10^2$	$(3.02 \pm 0.15) \times 10^2$	0.81	0.04	12,500

[a] NCRP 130

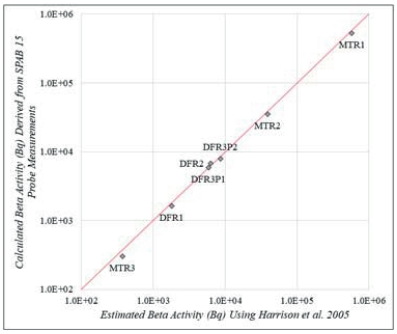

Fig. 9. Correlation between the beta activity (in Bq) determined by the SPAB 15 probe measurements (vertical) and the beta activity estimated according to the method by Harrison et al. (2005) (horizontal). The red diagonal indicates a 1:1 comparison of estimated beta activity based on gamma spectrometry versus calculated beta activity based on direct beta measurements. Particles above the red line have larger estimated activity values, based on gamma activities; particles below the red line have larger estimated activity values based on direct beta measurements.

(i.e., maximum 10%) overestimates the beta activity for all studied particles except for the fragment of DFR3P1.

VARSKIN6, a computer code from the USNRC (Anspach and Hamby, 2018), was used to perform contact dose rate calculations based on the activity determined by gamma spectrometry and from the SPAB15 measurements. VARSKIN6 estimates doses and dose rates based on an assumed infinitely small point source on the surface of the skin. In contrast, the estimate made in Aydarous et al., 2008 was employing Monte Carlo calculations based on radiochromic dye film exposures of MTR type particles. The Monte Carlo estimations were made assuming a homogeneous MTR particle of 15% U composition, an average density of 3.1 g/cm^3, and accounting for variation in particle shape and self-absorption. For particles with a ^{137}Cs activity of 10^4 or 10^5 Bq, the assessment by SEPA outlines expected contact skin dose rates of 30 or 300 mGy/h, respectively. For direct comparison, the MTR1 and MTR2 particles would fit to the same assessments, and the VARSKIN6 calculated dose rates were 74 and 4.9 mGy/h, respectively (Table 2). Although these estimates will suffer from uncertainties, the VARSKIN6 code does not provide for uncertainties on the calculated results. The National Council on Radiation Protection and Measurements (NCRP) outlines an occupational health threshold for radioactive particle skin dose of 0.5 Gy (Gesell et al., 1999). The particles assessed in this study would require contact times of several hundred hours to reach this threshold, with the exception of the large MTR particles, particularly MTR1, which would deposit 0.5 Gy in 7 h (Table 2).

Risk assessments associated with Dounreay particles have been based on assumed low probabilities of man and organisms encountering highly radioactive (*significant*) particles in the environment (Jackson et al., 2007; Pellet, 2004; Smith and Bedwell, 2005). However, both field observations (on gastropods) and laboratory experiments (on filter feeders) have shown that ingestion and retention of particles does occur and that retained particles may induce acute effects (Jaeschke et al., 2015). The dose assessment in this report is lower than the TLD based assessment made in Jaeschke et al. and the difference should be attributed to the dose assessment method used. Given that the retention times for particles retained in blue mussels were high (70 h), the threshold to skin ulceration, 2 Gy (NRPB, 1997) would be reached using both assessment methodologies.

Radioactive particles, including those originating from Dounreay, will be subject to weathering, transforming larger fragments to small, bioavailable species, of relevance for biological uptake, retention, and subsequent dose impact, as well as risk assessments for particle contaminated sites (Shevchenko, 2004). The bioavailability and uptake of particle-bound radionuclides compared with those existing as ions or simple molecules has so far largely been ignored when impact and risks are assessed (Salbu, 2016). As a result, there is a high degree of scientific uncertainty about the long term ecological consequences and risk to human health from radioactive particles present in the environment (IAEA, 2011). Finally, these factors contribute to the overall challenge related to conceptual or structural uncertainties in environmental impact and risk assessments associated with radioactive particle contaminated areas (Salbu, 2016). Important aspects of the contamination are often ignored, such as source term and particle characteristics with implications for transport, deposition, and ecosystem transfer. In addition, particle specific weathering and dynamics can change uptake pathways and retention in organisms resulting in particle specific dose estimates that are unevenly distributed. These structural challenges are present in dose assessments for Dounreay particles, but the results presented in this work should contribute to reduce the uncertainties.

4. Conclusions

Two types of Dounreay U fuel particles, DFR and MTR, were characterized with respect to particle structure and morphology, elemental and U isotopic composition, as well as oxidation states of U via techniques not previously employed (μ-XRF and μ-XANES). The results provide clues about the speciation of U in the particles and can be linked to source term and release scenarios. The studied DFR particles appeared to contain UNb_2O_7 formed during fuel dissolution, while the MTR particles appeared to contain UAl_4 + Al, as stated in the fuel design. The μ-XANES data suggest that particle weathering and oxidation of particles surfaces have to a certain extent occurred.

Previously unreported elements, Mo (<1%) in DFR particles and Nd (1–2%) in MTR particles, were identified. As previous characterization of Dounreay particles only considered an average MTR particle of uniform composition, the structural and elemental analysis presented here should prove useful for developing a representative DFR particle model as well as refining the MTR model. While early conservative assessments are important for initial safety assessments, they can lead to unrepresentative environmental assessments and issues with public perceptions of radiation risk. However, based on the present dose assessments, the elemental composition of the two types of particles, which influences the particle density and self-absorption, does not seem to contribute significantly to the dose estimates. Based on these results, further environmental impact assessment may be relevant given that 1) there is a high probability of smaller, undetected particles remaining in the marine environment and 2) risk to biota exists where long term to permanent retention of particles is possible, particularly for filter feeders such as blue mussels.

CRediT authorship contribution statement

Ian Byrnes: Conceptualization, Methodology, Formal analysis, Investigation, Data curation, Writing - original draft, Writing - review & editing, Visualization.**Ole Christian Lind:**Conceptualization, Methodology, Formal analysis, Investigation, Resources, Data curation, Writing - original draft, Writing - review & editing, Visualization, Supervision, Project administration.**Elisabeth Lindbo Hansen:**Methodology, Formal analysis, Resources, Data curation, Writing - review & editing.**Koen Janssens:**Methodology, Investigation, Formal analysis, Resources, Data curation, Writing - review & editing.**Brit Salbu:**Conceptualization, Methodology, Resources, Writing - review & editing, Supervision, Project administration, Funding acquisition.

Declaration of competing interest

The authors declare that they have no known competing financial interests or personal relationships that could have appeared to influence the work reported in this paper.

Acknowledgements

This study has been funded by the Research Council of Norway through its Centre of Excellence (CoE) funding scheme (Project No. 223268/F50). The authors are grateful to the Scottish Environmental Protection Agency for providing the samples examined in this study and Deutsches Elektronen-Synchrotron (DESY) for granting beamtime at HASYLAB BL. The authors would like to thank Prof. D.H. Oughton for fruitful discussions on dosimetry, Dr. K. Proost for assistance with micro-XANES measurements, Dr. T. Gävfert for assistance with calibration of the Canberra SPAB15 instrument, and Dr. E. Reinoso-Maset for support on the Bruker M4 Tornado μ-XRF. The authors also thank Karl Andreas Jensen for guidance and support on ICP-MS. Finally, the authors express gratitude to Dr. D. Hamby and the RAMP organization for providing access to the VARSKIN6 code.

Appendix A. Supplementary data

Supplementary data to this article can be found online at https://doi.org/10.1016/j.scitotenv.2020.138488.

References

Anspach, L.J., Hamby, D.M., 2018. Performance of the VARSKIN 5 (v5.3) Electron Dosimetry Model. p. 111.
Aydarous, A.S., Darley, P., Charles, M., 2001. A wide dynamic range, high-spatial-resolution scanning system for radiochromic dye films. Phys. Med. Biol. 46, 1379.
Aydarous, A.S., Charles, M.W., Darley, P.J., 2008. Dose distribution measurements and calculations for Dounreay hot particles. Radiat. Prot. Dosim. 128, 146.
Bolsunovsky, A., Melgunov, M., Chuguevskii, A., Lind, O.C., Salbu, B., 2017. Unique diversity of radioactive particles found in the Yenisei River floodplain. Sci. Rep. 7, 11132.
Bunzl, K., 1997. Probability for detecting hot particles in environmental samples by sample splitting. Analyst 122, 653–656.
Busch, J., Gruehn, R., 1994. Chemischer Transport und Struktur von UNb2O7–einem neuen MM′ 2O7-Typ. Z. Anorg. Allg. Chem. 620, 1066–1072.
Cartwright, P., 1997. Reprocessing of Research Reactor Fuel the Dounreay Option.
CEG, 1990. Comprehensive dismantlement of the Lepse technical floating base. In: Kashka, M. (Ed.), The Contact Expert Group for Nuclear Legacy Initiatives in the Russian Federation (CEG). IAEA, IAEA.
Charles, M.W., 1991. The hot particle problem. Radiat. Prot. Dosim. 39, 39–47.
Choppin, G., Liljenzin, J.-O., Rydberg, J., Ekberg, C., 2013. Radiochemistry and Nuclear Chemistry. Elsevier Science.
Conradson, S.D., Manara, D., Wastin, F., Clark, D.L., Lander, G.H., Morales, L.A., et al., 2004. Local structure and charge distribution in the UO2-U4O9 system. Inorg. Chem. 43, 6922–6935.
Cooper, M.B., Burns, P.A., Tracy, B.L., Wilks, M.J., Williams, G.A., 1994. Characterization of plutonium contamination at the former nuclear-weapons testing range at Maralinga in South-Australia. J. Radioanal. Nucl. Chem. 177, 161–184.
Dale, P., Robertson, I., Toner, M., 2008. Radioactive particles in dose assessments. J. Environ. Radioact. 99, 1589–1595.
Danesi, P.R., Moreno, J., Makarewicz, M., Radecki, Z., 2002. Residual radioactivity in the terrestrial environment of the Mururoa and Fangataufa Atolls nuclear weapon test sites. J. Radioanal. Nucl. Chem. 253, 53–65.
Darley, P.J., Charles, M.W., Fell, T.P., Harrison, J.D., 2003. Doses and risks from the ingestion of Dounreay fuel fragments. Radiat. Prot. Dosim. 105, 49.
Dennis, F., Morgan, G., Henderson, F., 2007. Dounreay hot particles: the story so far. J. Radiol. Prot. 27, A3.
Dounreay Site Restoration Ltd. (DSRL), 2019a. Foreshore Particle Finds.
Dounreay Site Restoration Ltd. (DSRL), 2019b. Murkle Beach Particle Finds.
Dounreay Site Restoration Ltd. (DSRL), 2019c. Sandside Particle Finds.
DPAG, 2008. Dounreay Particles Advisory Group (DPAG) 4th Report. Scottish Environmental Protection AGency (SEPA).
Geckeis, H., Zavarin, M., Salbu, B., Lind, O.C., Skipperud, L., 2019. Environmental chemistry of plutonium. In: Clark, D.L., Geeson, D.A., Hanrahan, R.J. (Eds.), Plutonium Handbook. 4. American Nuclear Society, pp. 1979–2118.
Gesell, T., Baum, J., Scott, B., Hopewell, J., Seltzer, S., Lantz, M., Shore, R., 1999. Biological Effects and Exposure Limits for "Hot Particles". National Council on Radiation Protection and Measurements, Bethesda, Maryland.
Gibson, J., 1997. The Manufacture of MTR Fuel Elements and Mo 99 Production Targets at Dounreay.
Harrison, J., Fell, T., Phipps, A., Smith, T., Ellender, M., Ham, G., Hodgson, A., Wilkins, B., Charles, M., Darley, P., Aydarous, A., 2005. In: Divison, R.P. (Ed.), Health Implications of Dounreay Fuel Fragments: Estimates of Doses and Risks. Health Protection Agency, Oxfordshire, UK.
Henderson, F., Toole, J., Cartwright, P., 2007. The Dounreay Particles Technical Resume. Department of Environmental Protection, United Kingdom Atomic Energy Agency, United Kingdom.
IAEA CRP, 2011. Radioactive Particles in the Environment: Sources, Particle Characterization and Analytical Techniques. International Atomic Energy Agency (IAEA), Vienna, Austria.
International Atomic Energy Agency (IAEA), 2005. Management of High Enriched Uranium for Peaceful Purposes: Status and Trends. IAEA, Vienna.
Jackson, D., Stone, D., Smith, K., Morgan, G., Shimmield, T., 2007. Assessing the environmental risk from hot particles in the vicinity of Dounreay—a case for inaction? J. Radiol. Prot. 27, A111.
Jadernas, D., Gan, J., Keiser, D., Madden, J., Bachhav, M., Jue, J.-F., et al., 2018. Microstructural characterization of as-fabricated and irradiated U-Mo fuel using SEM/EBSD. J. Nucl. Mater. 509, 1–8.
Jaeschke, B.C., Lind, O.C., Bradshaw, C., Salbu, B., 2015. Retention of radioactive particles and associated effects in the filter-feeding marine mollusc Mytilus edulis. Sci. Total Environ. 502, 1–7.
Janssens, K., De Nolf, W., Van Der Snickt, G., Vincze, L., Vekemans, B., Terzano, R., et al., 2010. Recent trends in quantitative aspects of microscopic X-ray fluorescence analysis. Trends Anal. Chem. 29, 464–478.
Kaminski, M.D., 2003. In: USDo, Energy (Ed.), Aqueous Corrosion of Aluminum-Based Nuclear Fuels. Argonne National Laboratory, Argonne, IL.
Kaminski, M.D., Goldberg, M.M., 2002. Aqueous corrosion of aluminum-based nuclear fuel. J. Nucl. Mater. 304, 182–188.
Kaminski, M.D., Dimitrijevic, N.M., Mertz, C.J., Goldberg, M.M., 2005. Colloids from the aqueous corrosion of uranium nuclear fuel. J. Nucl. Mater. 347, 77–87.
Kashparov, V., Yoshchenko, V., Levchuk, S., Tschiersch, J., Wagenpfeil, F., 2000. Application of the method of repeated mixing to non-uniformly contaminated bulky samples. An International Journal Dealing with All Aspects and Applications of Nuclear Chemistry 246, 165–172.
Leenaers, A., Van Renterghem, W., Van Den Berghe, S., 2016. High burn-up structure of U (Mo) dispersion fuel. J. Nucl. Mater. 476, 218–230.
Lind, O.C., 2006. Characterisation of Radioactive Particles in the Environment Using Advanced Techniques. PhD thesis. Norwegian University of Life Sciences, Ås.
Lind, O.C., Salbu, B., Janssens, K., Proost, K., García-León, M., García-Tenorio, R., 2007. Characterization of U/Pu particles originating from the nuclear weapon accidents at Palomares, Spain, 1966 and Thule, Greenland, 1968. Sci. Total Environ. 376, 294–305.
Lind, O.C., Salbu, B., Skipperud, L., Janssens, K., Jaroszewicz, J., De Nolf, W., 2009. Solid state speciation and potential bioavailability of depleted uranium particles from Kosovo and Kuwait. J. Environ. Radioact. 100, 301–307.
Menanteau, F., 2009. SPAB 15 Alpha/Beta Calibration Report. CANBERRA.
Meyer, M.K., Gan, J., Jue, J.F., Keiser, D.D., Perez, E., Robinson, A., et al., 2014. Irradiation performance of U-Mo monolithic fuel. Nucl. Eng. Technol. 46.
National Radiation Protection Board (NRPB), 1997. Assessment of Skin Doses. NRPB, London.
Oughton, D.H., Salbu, B., Brand, T.L., Day, J.P., Aarkrog, A., 1993. Under-determination of SR-90 in soils containing particles of irradiated uranium oxide fuel. Analyst 118, 1101–1105.
Pellet, C., 2004. Estimation of the Contact Frequencies of Critical Groups with Radioactive Particles from the Dounreay Site. RMC Ref. R04-018 (A).
Potter, P., Ray, I., Thiele, H., Wiss, T., 2001. On the Constitution of Dounreay Radioactive Particles, Vol 1 SEM'. United Kingdom Atomic Energy Authorities (UKAEA) Dounreay Internal Report.
Potter, P., Ray, I., Tamborini, G., Theile, H., Wiss, T., 2003. On the Constitution of Dounreay Radioactive Particles Vol 2a'. UKAEA Dounreay Internal Report.
PRAG(D), 2012. Particles Retrieval Advisory Group (Dounreay). Scottish Environmental Protection Agency (SEPA), United Kingdom.
Rest, J., Kim, Y.S., Hofman, G.L., Meyer, M.K., Hayes, S.L., 2006. U-Mo Fuels Handbook. Version 1.0. Argonne National Lab.(ANL), Argonne, IL (United States).
Salbu, B., 2016. Environmental impact and risk assessments and key factors contributing to the overall uncertainties. J. Environ. Radioact. 151 (Pt 2), 352–360.
Salbu, B., Lind, O.C., 2020. Analytical techniques for charactering radioactive particles deposited in the environment. J. Environ. Radioact. 211, 9.
Salbu, B., Krekling, T., Oughton, D.H., Ostby, G., Kashparov, V.A., Brand, T.L., et al., 1994. Hot particles in accidental releases from chernobyl and windscale nuclear installations. Analyst 119, 125–130.
Salbu, B., Krekling, T., Lind, O.C., Oughton, D.H., Drakopoulos, M., Simionovici, A., et al., 2001. High energy X-ray microscopy for characterisation of fuel particles. Nucl. Inst. Methods Phys. Res. A 467, 1249–1252.
Salbu, B., Janssens, K., Lind, O.C., Proost, K., Danesi, P.R., 2003. Oxidation states of uranium in DU particles from Kosovo. J. Environ. Radioact. 64, 167–173.
Salbu, B., Lind, O.C., Kalmykov, S.N., Denecke, M.A., 2011. Radioactive Particles Released into the Environment from Nuclear Events. Springer, Berlin, Heidelberg.
Salbu, B., Kashparov, V., Lind, O.C., Garcia-Tenorio, R., Johansen, M.P., Child, D.P., et al., 2018. Challenges associated with the behaviour of radioactive particles in the environment. J. Environ. Radioact. 186, 101–115.
Schulze, D.G., Bertsch, P.M., 1995. Synchrotron X-ray techniques in soil, plant, and environmental research. In: Sparks, D.L. (Ed.), Advances in Agronomy, Vol 55. 55. Elsevier Academic Press Inc, San Diego, pp. 1–66.
Shevchenko, S.V., 2004. On the uncertainty in activity measurements for samples containing "hot particles". Appl. Radiat. Isot. 61, 1303–1306.
Silva, R.J., Nitsche, H., 2001. Environmental actinide science. MRS Bull. 26, 707–713.

Simon, S.L., Jenner, T., Graham, J.C., Borchert, A., 1995. A comparison of macroscopic and microscopic measurements of plutonium in contaminated soil from the Republic of the Marshall Islands. J. Radioanal. Nucl. Chem. 194, 197–205.

Smith, K., Bedwell, P., 2005. Public Health Implications of Fragments of Irradiated Fuel. Module 3: The Likelihood of Encountering a Fuel Fragment on Sandside Beach. Radiation Protection Division (RPD), Health Protection Agency (HPA) RPD-EA-9-2005.

Soulsby, R.L., Mead, C.T., Wild, B.R., 2006. A Model for Simulating the Dispersal Tracks of Sand-sized Particles in Coastal Areas–"SandTrack". UKAEA, Wallingford, Oxfordshire, UK.

Stewart, A., Cook, G.T., Mackenzie, A.B., 2003. Simulation of Human Stomach and Intenstine Leaching of Dounreay Hot Particles. Scottish Universities Research and Reactor Centre, Scottish Environmental Protection Agency (SEPA).

Strand, P., Beresford, N., Copplestone, D., Godoy, J., Jianguo, L., Saxén, R., et al., 2009. Environmental protection: transfer parameters for reference animals and plants. Ann. ICRP 39, 1–111.

Tamborini, G., 2004. SIMS analysis of uranium and actinides in microparticles of different origin. Micro Trance Anal. 145, 237–242.

Tougait, O., Noel, H., 2004. Stoichiometry of UAl4. Intermetallics 12, 219–223.

Tyler, A.N., Scott, E.M., Dale, P., Elliott, A.T., Wilkins, B.T., Boddy, K., et al., 2010. Reconstructing the abundance of Dounreay hot particles on an adjacent public beach in Northern Scotland. Sci. Total Environ. 408, 4495–4503.

Wilkins, B., Fry, F., Burgess, P., Fayers, C., Haywood, S., Bexon, A., et al., 1998. Radiological Implications of the Presence of Fragments of Irradiated Fuel in the Sub-tidal Zone at Dounreay. NRPB-M1005.

Supplementary Material

Table S1: List of archived particles investigated in the present study. Uncertainties are presented as counting error (Ref date - March, 2002).

Name	*Number*	*Approximate Particle Dimensions (μm)*	*Location*	*^{137}Cs Activity (Bq±σ)*
DFR1	LSN983853	100 x 90	Seabed	(1.90±0.02) x 10^4
DFR2	LSN990090	200 x 160	Seabed	(2.07±0.03) x 10^4
DFR3	LSN984042	300 x 160	Seabed	1.25 x 10^5
MTR1	LSN950056	2000 x 1000	Foreshore	(5.70±0.19) x 10^5
MTR2	LSN983796	1400 x 300	Seabed	(9.53±0.12) x 10^4
MTR3	LSN990091	740 x 500	Seabed	(1.01±0.01) x 10^5

Paper II

Synchrotron based X-ray Fluorescence Imaging Provides New Insights on Uranium Toxicokinetics in *Daphnia magna* following Exposure to Uranium Nanoparticles

Ian Byrnes[1], Lisa Magdalena Rossbach[1], Dag Anders Brede[1], Daniel Grolimund[3], Dario Ferreira Sanchez[3], Gert Nuyts[4], Vaclav Cuba[2], Estela Reinoso-Maset[1], Brit Salbu[1], Koen Janssens[4], Deborah Oughton[1], Shane Scheibener[1], Hans-Christian Teien[1], Ole Christian Lind[1]

[1] Norwegian University of Life Sciences, Centre for Environmental Radioactivity (CERAD), Faculty of Environmental Sciences and Natural Resource Management, P.O. Box 5003, 1433 Ås, Norway

[2] Czech Technical University in Prague, Faculty of Nuclear Sciences and Physical Engineering, Brehova 7, Prague 1, Czech Republic

[3] Swiss Light Source, Paul Scherrer Institute (PSI), 5232 Villigen, Switzerland

[4] University of Antwerp, Department of Chemistry, Groenenborgerlaan 171, 2020 Antwerp, Belgium

*Corresponding Author

Phone: +47-93820876 Fax: +47-64948359

Email Address: ian.byrnes@nmbu.no

Address: Norwegian University of Life Sciences, Centre for Environmental Radioactivity (CERAD), Faculty of Environmental Sciences and Natural Resource Management, P.O. Box 5003, 1433 Ås, Norway

Abstract

A combination of synchrotron based elemental analysis and acute toxicity tests were used to investigate the biodistribution and adverse effects in *Daphnia magna* exposed to uranium nanoparticles (UNPs, 3 – 5 nm) or a uranium (U) reference (U_{Ref}) solution. Toxicity test results showed comparable acute effects (UNP: 402 µg L-1 [336 - 484], U_{Ref}: 268 µg L-1 [229 - 315]) and speciation analysis revealed similar size distributions between exposures. However, the U body burden was 3- to 5-fold greater in UNP exposed daphnia. Furthermore, analysis of survival as a function of body burden revealed a ~ 5-fold higher specific toxicity from the U_{Ref} exposure. High resolution (2 µm) XRF elemental maps of intact, whole daphnia derived from sublethal, acute exposures revealed similar biodistributions between treatments, with high U accumulation onto the gills (epipodites) as well as within the hepatic ceca and the intestinal lumen. Uranium uptake into the haemolymph circulatory system was visible in organs such as the heart and the maxillary gland, a part of the daphnia excretory system. The substantial uptake in the maxillary gland and nephridium suggest that these organs play a role in U removal from the haemolymph and subsequent excretion. Maternal transfer was demonstrated by U signals observed in the embryos and remnants of the chorion. The reported whole organism biodistribution links the exposure to toxic effects in *D. magna* and provides novel insights that should improve the understanding of the uptake and elimination pathways of U in cladocerans.

Keywords

Uranium nanoparticles, Uranium Toxicokinetics, X-ray Fluorescence, *Daphnia magna*

Introduction

Uranium (U) is present in the environment due to releases from naturally occuring minerals or from antropogenic sources such as releases from the nuclear weapon and fuel cycles (Salbu, Skipperud, and Lind 2015) including global weapons fallout, U mining (Strømman et al. 2013; Wang et al. 2014) and nuclear accidents (e.g. the Chernobyl exclusion zone) (Kashparov 2003), as well as many non-nuclear related sources (e.g. the catalyst industry) (Hasan and Ghosh 2011). Historically, assessments of U contamination in the environment have assumed a homogenous distribution of ionic uranyl species of low molecular mass (LMM, < 3 kDa) and have not accounted for the contribution of particles (> 0.45 μm) and colloids (1 nm – 0.45 μm) (Salbu et al. 2018). Through weathering of larger particles or by direct precipitation as a result of biogeochemical processes, the prevalence of increasingly smaller particles gives rise to a log-normal size distribution that should be taken into account in environmental impact and risk assessments (Kashparov et al. 2004; Suzuki et al. 2002; Bargar et al. 2008). Nanoparticles (NPs) have unique properties, such as a high surface-to-volume ratio, chemical reactivity, and high mobility, which may influence organism uptake and result in heterogeneous accumulation in tissues (Guarnieri et al. 2014). As a result, there is a high degree of uncertainty about the long-term ecological consequences and risk posed by uranium NPs (UNPs) in the environment.

Aquatic freshwater invertebrates, such as *Daphnia magna*, have a key function in nutrient cycling and constitute an essential part of the food web (Ebert 2005; Stollewerk 2010). In ecotoxicological assessments, *D. magna* is an important sentinel test organism with high sensitivity to metals, including U (Poston, Hanf, and Simmons 1984; Barata, Baird, and Markich 1998; Sheppard et al. 2005; Scheibener et al. 2021), but to date no toxicity studies have been carried out on UNP exposure. Traditional toxicity assessments have relied on measurements of total water concentration and whole body burden to provide overall uptake and depuration rates in *D. magna*. However, total water concentrations do not account for metal speciation in exposure media while whole body burden measurements do not differentiate internal uptake from surface bound or intestinally confined elements. Therefore, the customary methods of toxic assessment should be complemented with analyses that assess whole organism biodistribution and tissue-specific localization to better interpret subsequent effects (Wang 2021).

X-ray spectroscopic methods, including X-ray fluorescence (XRF) mapping, are powerful tools for investigating metals and metal NP distribution in biological samples (Pushie et al. 2014). Despite the large body of toxicology research devoted to *D. magna*, specific metal uptake pathways and distributions remain largely unknown with most work focusing on metallothionein expression studies or XRF imaging of the intestine (Jackson et al. 2009; Caumette et al. 2012; Fouqueray et al. 2012; Acharya and Blindauer 2016; Hao et al. 2016). Furthermore, U biodistribution in daphnia remains largely unexplored, as research have been primariliy focused on cell level histological analyses (Massarin et al. 2011). Recent advances in synchrotron beamline technology enable assessment of tissue specific trace metal distributions that is highly useful for examining potential uptake and detoxification pathways in daphnia (Van Malderen et al. 2017; De Samber et al. 2008). Applying such techniques to ecotoxicological studies could provide valuable insights into the overall toxic assessment and fill knowledge gaps with respect to toxicokinetics and toxic mode of action, required for Aggregate Exposure Pathway (AEP) framework development (Teeguarden et al. 2016, Tan et al., 2018).

Therefore, this study investigated the accumulation and distribution of U in *D. magna* following acute exposure to UNPs or aqueous U reference solutions (U_{Ref}) by utilizing highly sensitive, micro-focused XRF elemental mapping and XRF tomography to determine the tissue level localization in preserved intact organisms. This approach provided unprecedented detail of U uptake, target organs, and detoxification pathways, thereby providing important information that links biodistribution to toxic effects.

Experimental Methods

Uranium Nanoparticle Synthesis and Characterization

Engineered UNPs were produced from uranyl nitrate ($UO_2(NO_3)_2$) at the Czech Technical University. The synthesis procedure is described in detail in the supplemental material S1. The UNPs were stored as dry powders in Eppendorf tubes inside a desiccator at room temperature (20°C) until use (Pavelkova, Cuba, and Sebesta 2013; Pavelková et al. 2016). Dry powders were characterized by laboratory based X-ray diffraction (XRD) and synchrotron based micro X-ray absorption near edge structure analysis (μ-XANES; details in synchrotron analyses section). For exposure experiments, UNP stock suspensions were prepared in ultrapure water (supplemental material, S2). Average hydrodynamic

diameter and zeta potential of stock suspensions (1.0 g U L^{-1}) were characterized using dynamic light scattering (DLS) (supplemental material, S2). Individual particle size was determined by transmission electron microscopy (TEM) (supplemental material, S2). Fractionation experiments were conducted on selected concentrations from the UNP and U_{Ref} exposures to determine the U species size distribution (supplemental material, S2).

Daphnia magna Exposure and Sample Preparation

Laboratory *D. magna* cultures (DHI Water & Environment, Hørsholm, Denmark) were used in exposures according to a standard acute (48 h) toxic elemental test protocol (OECD 2004) (supplemental material, S3). All daphnia exposures were conducted using a range of UNP concentrations from 0 – 781 ± 84.6 µg U L^{-1} in moderatly hard reconstituded water (MHRW, pH 6.8) (USEPA 2002). The UNP exposures were compared with a similar range (0 – 790 ± 41.5 µg L^{-1} U) of the U_{Ref} solution which was prepared from a U standard (1.0 g L^{-1} in 2 % HNO_3; CRM 129-A, U.S. Department of Energy, Argonne, Illinois, USA). Acute toxicity concentrations, 48 h LC_{50} and LC_{10} (lethal concentration in 50 % of the population), were determined with the MOSAIC tool for ecotoxicology assessments (Charles et al., 2018). MOSAIC employs a bayesian model in the R package 'morse', which uses observed survival at each exposure concentration in this study as inputs (Delignette-Muller et al. 2016). One-way ANOVA was applied to assess for simple group comparison when residuals were normally distributed, using MinitabVR 18 (Minitab Inc. 2010). Where data were non-parametric, the Kruskal-Wallis test was used.

Following the acute exposure, daphnia (F0) from sublethal concentrations were moved to clean MHRW and maintained with feed for 24 h to observe reproduction. In the following generation (F1), timing of first spawning and clutch size were documented (supplementary material, S3). Additionally, an acute toxicity test was conducted using *D. magna* neonates (< 18 h) to better compare with literature LC_{50} values. All reported concentrations and LC_{50} values refer to measured concentrations in the exposure media.

After determining the LC_{50} for both exposures, adult daphnia (< 7 d) were exposed to sublethal concentrations (320 ± 30.6 µg L^{-1} UNP, 159 ± 13.7 µg L^{-1} U_{Ref}, and a control) for 48 h in MHRW (pH 6.8, 5 mL per daphnid). Micro-focused, XRF and XAS measurements were conducted on whole, intact organisms that were preserved by chemical drying. In brief, daphnia were rinsed once with MHRW and twice with deionized water and then fixed in 5 % methanol for 10 min (Tan et al. 2016). Subsequently, samples were

dehydrated following a stepwise protocol of graded acetone (i.e., once with 70, 80, and 90 % for 10 min each, and twice with 98 and 100 % for 10 min each). Lastly, samples were immersed in 2 mL hexamethyldisilazane (HMDS) for 1 h (Laforsch and Tollrian 2000). After removal of approximately 90 % HMDS, samples were dried overnight in a desiccator with an applied vacuum of 200 mbar. Dried samples were gently moved into new Eppendorf tubes avoiding external contamination and kept at room temperature until measurement.

Synchrotron-based X-ray Analyses

Elemental distribution mapping of whole *D. magna* was conducted at the microXAS beamline (X05LA) at the Swiss Light Source (Paul Scherrer Institute, SLS, Switzerland). Daphnia samples were mounted on Kapton tape or glued to the fine tip of a wooden toothpick (Fig. S1). A 17.2 keV incident beam was micro-focused using a Kirkpatrick-Baez (KB) mirror system to a size of 1 μm^2 and samples were raster-scanned in projection mode with a step size of 5 µm for whole organism scans and 2 µm for region of interest (ROI) maps. Based on the resulting 2D projection map, XRF tomographic sections were collected by situating the beamline in computed tomography mode and rotating the sample 180° in equal increments along the horizontal axis. All XRF spectra were collected using four silicon drift detectors (SDD; Ketek GmbH, Germany) positioned around the sample at 50° to the incoming beam with a 200 ms dwell time. Tomographic sinograms were reconstructed using the ASTRA Toolbox (FBP and SIRT) (van Aarle et al. 2016; van Aarle et al. 2015), whereas the XRF sum spectra were fitted using PyMCA and the resulting elemental maps were compiled and colored with ImageJ (Solé et al. 2007; Schindelin et al. 2015).

Additionally, U L_{III}-edge (17.163 keV) XANES spectra of the UNP and a uranyl nitrate salt (uranyl nitrate hexahydrate, Sigma Aldrich, St. Louis, USA), prepared as dry powder thinly spread on kapton tape, were collected in fluorescence and transmission mode using 1 eV steps from ~100 eV below to ~300 eV above the absorption edge. To improve the signal-to-noise ratio, 9 spectra were taken at each point and processed for background subtraction and normalization using the ATHENA software (Ravel and Newville 2005). The resulting µ-XANES spectra were qualitatively compared with those of the uranyl nitrate salt as well as reference UO_2 and U_3O_8 spectra (UO_2, U_3O_8, Institute

of Energy Technology, Kjeller, Norway) that were measured at HASYLAB, beamline L (unpublished data).

Results and Discussion

Uranium Nanoparticle and Exposure Media Characterization

The engineered, dry UNPs consisted predominantly of UO_2 as indicated by the XRD analysis (Fig. S2), although the μ-XANES indicated that oxidation of the UNPs (i.e., from U(IV) to U(VI)) had occurred since the time of synthesis (Fig. S3). According to TEM analysis of the stock suspension, individual NPs featured physical diameters of 3 – 5 nm (Fig. S4). The average hydrodynamic diameter of the UNP stock suspension was 273.3 ± 1.2 nm (Table S1). The zeta potential of the stock was -11.8 mV indicating an unstable suspension, where repulsive forces were not sufficient to prevent further aggregation during the exposure (Handy et al., 2008). Elemental composition of the UNP stock suspension, measured by inductively coupled plasma mass spectrometry (ICP-MS), showed the presence of several trace elements (i.e., B, Ti, Mo, V, Ag, and Sn) in addition to U (Table S2). All trace metals remained below reported toxic effect levels for *D. magna*.

Size fractionation analyses of the exposure media showed similar LMM, colloidal, and particulate size distributions for both the UNP and U_{Ref} exposures in MHRW (Fig. S5). In general, the colloidal and particulate fractions (> 3 kDa) comprised between ~ 50 to 80 % of total U. However, the ~ 20 to 50 % LMM fraction signified substantial particle dissolution. Since μ-XANES of dry powders indicated oxidation of the UNPs, dissolution and concomitant formation of LMM species in the MHRW (pH 6.8) solution is plausible. The aqueous speciation of U is complex due to the great variety of hydrolysis products and the formation of complexes with inorganic and organic ligands (Lofts et al. 2015), which in exposures of > 200 μg U L^{-1} at pH 6.8 in MHRW-comparable media would include $(UO_2)_2(OH)_2CO_3^-$, UO_2CO_3, $UO_2(OH)_2$, and UO_2OH^+, as well as dimeric and polymeric U species (Markich 2002; Goulet, Fortin, and Spry 2011), factors potentially influencing both uptake and toxicity of both UNPs and U_{Ref} materials.

Determination of Toxic Effects

The acute toxicity tests in the current study were designed to remain within the tolerable pH range for *D. magna* (Ebert 2005), while maximizing the bioavailable U fraction. Therefore, MHRW (USEPA 2002) adjusted to pH 6.8, was chosen as an exposure media to

minimize the presence of uranyl complexing ligands as much as feasible. Standard acute toxicity tests were conducted with both neonates (< 18 h) and adults (< 7 d) to assess mortality and total body burden. In line with the speciation analysis (Fig. S5), the results revealed a similar dose response relationship for mortality as a function of measured total U water concentration from both UNP and U_{Ref} exposures (Fig. S6). Furthermore, significant effects (ANOVA $p < 0.05$) were observed from ≥ 388 ± 10.2 μg L^{-1} and ≥ 260 ± 12.5 μg L^{-1}, for UNP or U_{Ref} respectively. The calculated LC_{50} and LC_{10} values (Table S3) revealed minor differences between the exposures to U_{Ref} (LC_{50} of 268 μg L^{-1} [229 - 315]) and UNPs (402 μg L^{-1} [336 - 484]). This notion was further supported by the LC_{10} 95 % credible limits of 130 – 238 μg L^{-1} and 97.8 – 168 μg L^{-1}, for UNP and U_{Ref} exposures respectively. The neonates were approximately 4-fold more susceptible than the adults with LC_{50} values of 127 μg L^{-1} [102 - 163] and 112 μg L^{-1} [89.5 - 136] for UNP and U_{Ref}, respectively. Furthermore, the predicted LC_{10} 95 % credible intervals were calculated to 35.7 – 73.4 μg L^{-1} and 26.5 – 62.0 μg L^{-1} for UNP and U_{Ref}, respectively. Acute toxicity of U is dependent on several chemical parameters of the exposure media and is closely connected to speciation, indicated by the large LC_{50} concentration range for U in *D. magna* in previous studies (0.39 – 6.4 mg U L^{-1}) (Barata, Baird, and Markich 1998; Sheppard et al. 2005; Zeman et al. 2008). The observed LC_{50} values in the current study were slightly lower than previous reports at similar pH levels (Sheppard et al. 2005; Zeman et al. 2008), which could be related to the U speciation in the media composition, where bioavailability is closely linked to the pH dependent abundance of uranyl ions, such as UO_2^{2+} and UO_2OH^+(Fortin, Dutels, and Garnier-Laplace 2004).

The total body burden following exposure to the UNPs and U_{Ref} exposures were investigated to evaluate potential relationships between U speciation and survival. The results revealed that the U body burden (ng U $daphnid^{-1}$) correlated to the total water concentration for both treatments (Fig. S8). The U body burden in neonates showed similar concentrations for UNPs (0.7 ± 0.5 – 3.2 ± 0.2 ng $daphnid^{-1}$) and the U_{Ref} (0.8 ± 0.5 – 5.6 ± 1.9 ng $daphnid^{-1}$). However, total body burden for adults exposed to UNPs (8.5 ± 3.3 – 64.6 ± 22.0 ng U $daphnid^{-1}$) was approximately 3-fold higher than those exposed to the U_{Ref} (6.5 ± 0.7 – 20.3 ± 0.4 ng U $daphnid^{-1}$). These results suggest that, although the size distributions were similar between the exposures, functional differences related to uptake and bioavailability lead to the higher body burden of UNPs compared to the U_{Ref}.

This difference may be related to the UNPs, and aggregates thereof, captured more effectively by the filter feeding apparatus of adult daphnia. Therefore, survival was plotted as a function of body burden to evaluate potential differences in specific toxicity (Fig. S9). Regression analysis showed a statistically significant correlation (R^2 = 0.53 for U_{Ref}, and 0.63 for UNP, $p < 0.05$) between body burden and survival of adult daphnia. Furthermore, the slope of the regression curve was 6-fold steeper for U_{Ref} compared to UNP (Fig. S8). The observed narrow range from no effect at < 10 ng daphnid^{-1}, to 90% mortality from 20 ng daphnid^{-1}, implied the presence of U species with high specific toxicity in the U_{Ref} exposure. Conversely, UNP body burden were 3- to 5-fold higher, thus suggesting a high proportion of less toxic species in the UNP exposures. However, uptake and excretory pathways of U in daphnia remained unclear. Therefore, synchrotron X-ray analyses were used to assess the U biodistribution in organisms exposed to sublethal concentrations of UNPs and the U_{Ref}.

Uranium Biodistribution

Intact *D. magna* individuals were imaged by means of synchrotron based XRF elemental mapping at 5 and 2 µm resolution to obtain whole body biodistributions of U and essential elements such as Fe, Zn, and Ca at unprecedented detail for this organism (Fig. 1). The U biodistributions were similar for daphnia from the UNP and the U_{Ref} exposures. Areas of significant U accumulation included the gills (epipodites), inside the digestive tract, and the maxillary gland (Fig. 1). However, U was also present on the carapace surface, within soft tissues including the heart, and within the brood chamber and embryos, albeit at lower intensities. Notably, despite the use of a single, synchronized daphnia cohort (< 18 h) in the exposures, the studied U_{Ref} specimen had not yet undergone oviposition at the time of sampling, thus no embryos could be observed in the brood chamber.

The above results are in line with previous assessments of U toxicity in *D. magna* that indirectly reported accumulation in the intestine via histological observations (Massarin et al. 2011) and on the carapace, as well as maternal transfer (Scheibener et al. 2021). However, the biodistribution in the current study provides detailed information on the whole-body uptake and distributions. The following sections describe the identified key areas of U accumulation of importance to toxicokinetic and toxicodynamic assessments.

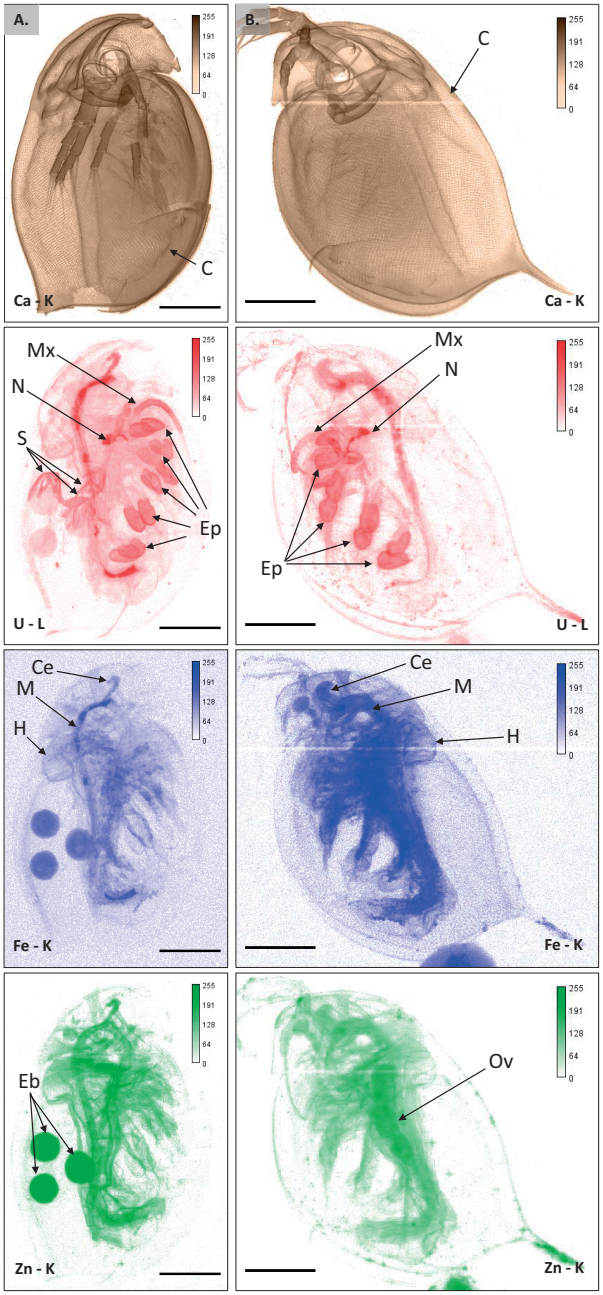

Figure 1: Whole body elemental maps (Ca, U, Fe, Zn) of *D. magna* exposed to either 320 µg L^{-1} UNP (**A**) or 159 µg L^{-1} U_{Ref} (**B**). Both scans were conducted with a 5 µm step size and 200 ms dwell time. All scale bars represent 500 µm and all signal intensities are scaled logarithmically from 0 to 255. *Abbreviations:* carapace (C), maxillary gland (Mx), nephridium (N), epipodites (Ep), chorion structures (S), hepatic ceca (Ce), midgut (M), heart (H), embryo (Eb), and ovary (Ov).

Surface Bound Uranium

Based on whole body XRF scans (Fig. 1), surface bound U was shown by a low signal coinciding with the Ca-rich carapace and a high accumulation on the gills, called epipodites, which are located on the end of each thoracic appendage. Daphnia were preserved using a low impact chemical drying procedure and a separate analysis of the sample preparation chemicals indicated < 10 % U loss, presumably related to leaching of surface bound U (Fig. S9). The observation of the U surface distribution has important implications for understanding uptake and depuration pathways for *D. magna.* Accumulation on the epipodites may be a potential uptake pathway via ion exchange with the outside media (Smirnov 2017). On the other hand, removal of excess U from the carapace and epipodites via molting represents a significant depuration pathway for the daphnia (Kikuchi 1983, Scheibener et al., 2021).

High-resolution (2 μm) ROI scans of the epipodites provided an unprecedented view of U accumulation in these ~ 100 μm sized organs (Fig. 2). The elemental maps showed U concentrated on the surface of the epipodites and internalized within Fe and Zn rich tissues (Fig. 2A, 2C). Moreover, the XRF tomographic section showed U accumulation surrounding the epipodite, suggesting that U was primarily adsorbed or bound to the surface tissue layer (Fig. 2B). This observation is similar to those observed in XRF mapping of histological sections of Zn exposed *D. magna* (De Samber et al. 2013). High resolution maps of the epipodites also showed the Fe-rich vesicle extending through the appendage, further supporting previous assertions that such tissues are responsible for haemoglobin synthesis and connected to the circulatory system (Goldmann et al. 1999; De Samber et al. 2013).

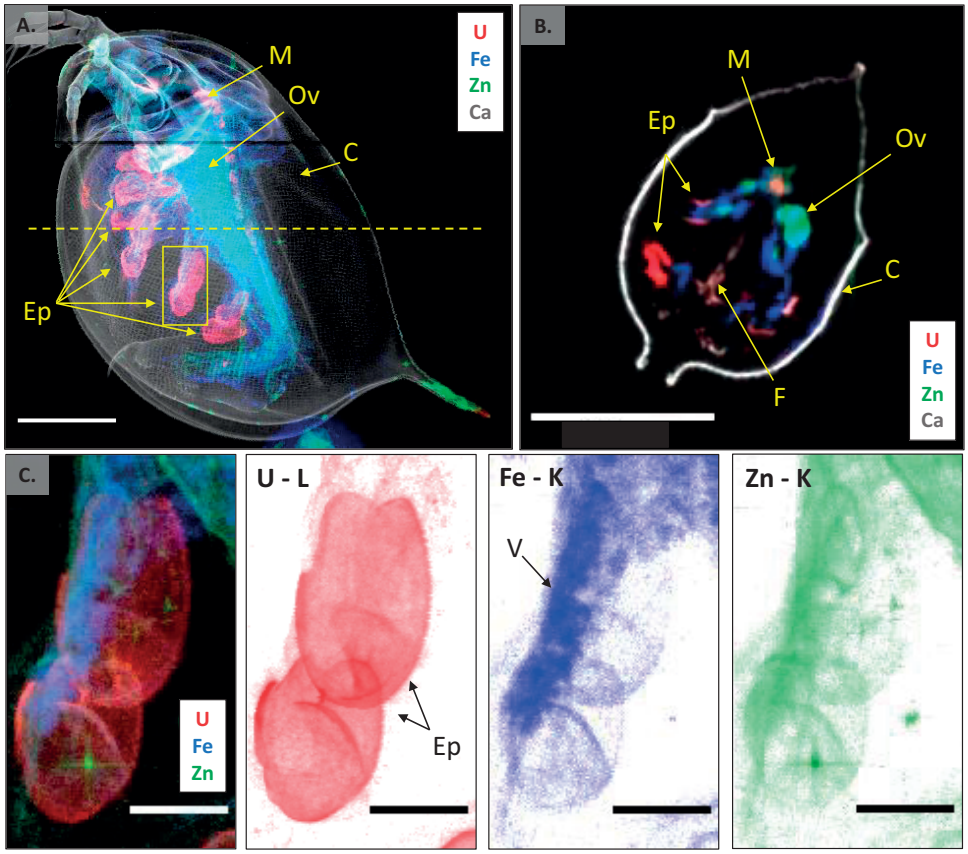

Figure 2: (**A**) Composite elemental map (U, Fe, Zn, Ca) of *D. magna* exposed to the U_{Ref} (159 µg U L^{-1}), indicating the U accumulated onto epipodites, the area chosen for 2 µm high resolution mapping (yellow box) and the location of the tomographic section (yellow dotted line). (**B**) Tomographic section showing the dorsal distributions of U, Fe, Zn, and Ca. (**C**) High resolution U, Fe, and Zn maps of the epipodites (composite and individual maps). Scale bars represent 500 µm (A), 50 µm (B) or 100 µm (C), and all signal intensities are scaled logarithmically from 0 to 255. *Abbreviations:* epipodite (Ep), carapace (C), midgut (M), vesicle (V), ovary (Ov), and food groove (F). Hotspots on the Zn elemental map were due to dust contamination on the surface of the sample.

Uranium toxicokinetic assessment showed that molting (ecdysis) is an important depuration pathway for *D. magna* exposed to U (Scheibener et al. 2021). The biodistribution mapping in the current study provided further insights and detail to specific areas where U is lost via molting. For *D. magna*, molting is not limited to the general carapace but also includes the cuticle surrounding the epipodites and the intestinal foregut and hindgut (Kikuchi 1983; Duneau and Ebert 2012). Therefore, findings from the current study suggest that in addition to the surface bound U, a major contribution to depuration via molting may be attributed to shedding of epipodites and the fore- and hindgut, rather than the surface.

Ingestion

Daphnia magna from both exposures exhibited significant amounts of U particulates in the midgut region, important for digestion and nutrient uptake (Fig. 3). Previous studies suggest that the midgut function is vulnerable to U exposure, and failure to properly assimilate nutrients may constitute a major toxic effect (Massarin et al. 2011; Zeman et al. 2008). In the current study, U-containing materials in the digestive tract were predominantly associated with algal material, despite the removal of the daphnia from feed 24 h prior to the exposure (Byrnes et al., unpublished). This observation is consistent with previous findings showing that, green algae species have the capacity to effectively bind U (Fortin, Dutels, and Garnier-Laplace 2004). The detailed mapping showed small (< 2 µm), very high U intensity hotspots corresponding to NP aggregates in the midgut of UNP exposed daphnia intestines (Fig. 3A). The UNP aggregates may have been ingested or formed through induced aggregation by the daphnia gut chemistry, as seen for other types of NPs (van der Zande et al. 2020). The filter feeding behavior of daphnia may promote ingestion of particle aggregates, which would also explain the high body burden in the UNP treatment observed in the current study (Fig. S7). Importantly, U was found in the soft tissue structures of the midgut of all exposed organisms, which is a strong indication that the intestine constitutes an important uptake pathway (Fig. 3A - B).

Systemic Uptake

The results of this study identified two critical U uptake pathways into the haemolymph circulatory system, i.e., via the epipodite gill tissues, and translocation across the intestinal barrier. The methods used in the current study involved the dehydration and

drying of sample organisms, which precludes assessment of the haemolymph. Therefore, evidence of systemic uptake was interrogated by assessing U in muscle tissues and internal organs (Fig. 3). The fact that U was detected in the heart, albeit at low relative intensity compared to other organs and tissues, is uneqvivocal evidence of systemic uptake into the circulatory system.

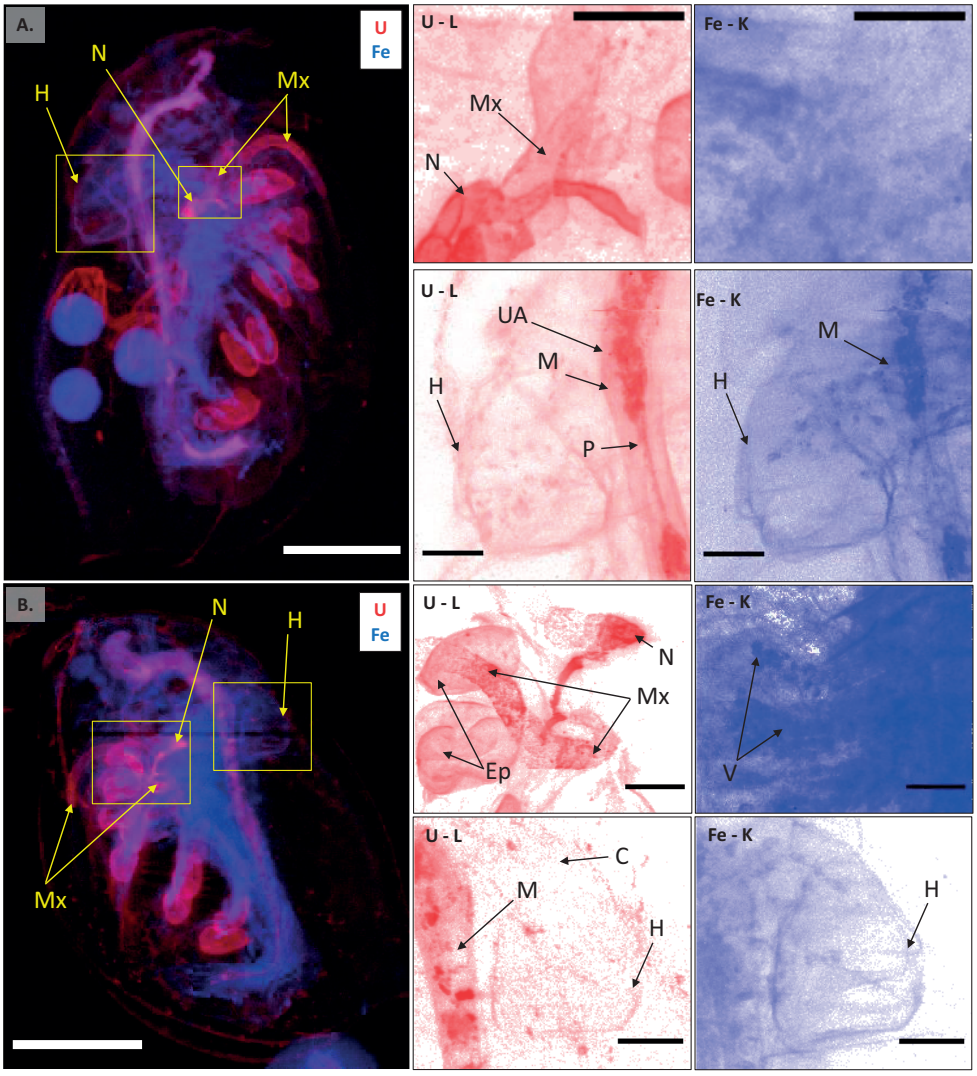

Figure 3: Composite map of U (red) and Fe (blue) of (A) UNP exposed D. magna (320 µg L-1) and (B) U_{Ref} exposed organism (159 µg L^{-1}). High resolution (2 µm) ROI maps (right) showing the maxillary gland and nephridium, and the heart. Scale bars represent 500 µm on the whole daphnia maps and 100 µm on the ROI maps. All signal intensities are scaled logarithmically from 0 to 255. *Abbreviations:* mandible (Ma), vesicle (V), maxillary gland (Mx), UNP aggregates (UA), midgut (M), heart (H), carapace (C), and muscle tissue (Mu).

Furthermore, high U intensities observed in the maxillary gland and nephridium (Fig. 3), corroborated systemic uptake. The maxilliary gland and nephridium represent a kidney-like organ system proposed to participate in osmoregulation and excretion of metabolic byproducts (Smirnov 2017). These observations are consistent with the nephrotoxic mode of action of uranium (Vicente-Vicente et al., 2010, Goulet, Fortin, and Spry 2011). The elevated U presence in the maxillary gland and nephridium thus implies the removal of U from the haemolymph via this organ system that may represent a hitherto unidentified metal detoxification pathway in *D. magna*. Unfortunately, the maxillary gland and nephridium were not clearly visible in other elemental maps or in the unexposed control organism (Fig. S10), probably due to the structure and composition primarily consisting of elements that were either below detection limits or not detectable by XRF, such as carbon. Additionally, this region of the organism also contains large soft tissue structures associated with the appendages, which may be denser and obscure the signal of essential elements, such as Zn, in 2D projection mapping. Since the maxillary gland is involved in excretion of ferrous breakdown products (Smirnov 2017), it is thus conceivable that U may follow a pathway from uptake via the epipodites, and/or the intesine into the circulatory system, and excretion via the nephridium and maxillary gland. Previously published depuration rates for U in *D. magna* found a 75% loss after 24 h, out of which 50 % was bound to the carapace and shed by molting (Scheibener et al. 2021). Therefore, the remaining 25 % might present a combination of egestion of intestinal content and excretion through the maxillary gland. The latter may serve as an important function for U removal from the haemolymph and thus prevent toxicity to internal cells, tissues, and organs.

Maternally Transferred Uranium

Based on elemental mapping of the brood chamber of UNP exposed daphnia, maternal transfer of U was confirmed (Fig. 4). Uranium was detected inside embryos and in chorion structures inside the chamber (Fig. 4A). Such findings may have implications for the potential development of offspring and the long-term stability of a population. Previous studies have shown that maternal transfer to embryos comprised approximately 1 – 7 % of total body U (Scheibener et al. 2021; Plaire et al. 2013). Studies of multigenerational U exposure also indicated long term population effects (Massarin et al. 2010; Massarin et al. 2011). Interestingly, in the current study, no U signal was

detected in three embryos present in the ovary of the U_{Ref} exposed animal, which had not yet undergone oviposition (Fig. 4D). It has been shown that haemoglobin is produced by fat cells located in the epipodites (Goldmann et al. 1999) and transferred via lipid droplets into developing oocytes inside the ovary in the final stages prior to oviposition (Lee et al. 2019). Recently, maternal transfer of Ag^{+} and AgNP was document via these lipid droplets (Yan et al., 2020). It is conceivable that the observed maternal transfer of U is facilitaded by a similar process, however, further work is needed to verify these mechanisms.

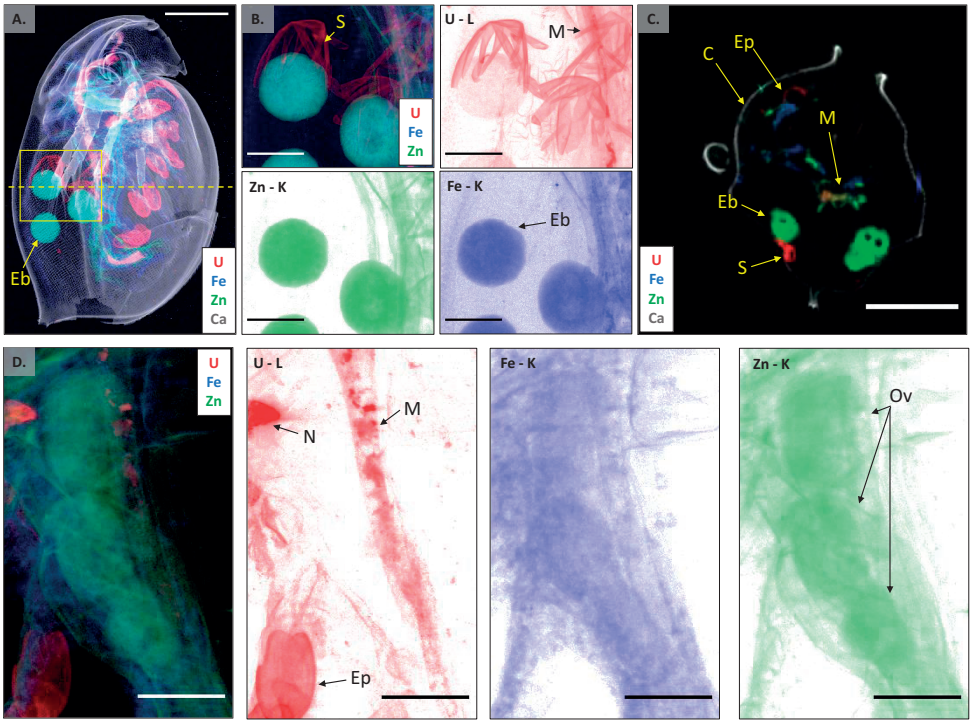

Figure 4: (**A**) Overview, combined elemental map (5 µm step size) of a UNP (320 µg L^{-1}) exposed *D. magna* for U, Ca, Fe, and Zn distributions, indicating the ROI area chosen for 2 µm high resolution mapping (yellow box) and the location of the tomographic section (yellow dotted line). (**B**) Elemental distribution (combined and individual maps) on the ROI showing the U-bearing, chorion structures in the brood chamber, and embryos. (**C**) XAS tomographic section showing the distributions of U, Fe, Zn, and Ca in the brood chamber, including the U-bearing structures and embryos. (**D**) High resolution elemental distribution maps (combined and individual) for U, Fe and Zn of a ROI on the ovary of a U_{Ref} exposed *D. magna* (159 µg L^{-1}), where U is not observed in the developing embryo. All signal intensities are scaled logarithmically from 0 to 255 and scale bars represent 500 µm (A) 200 µm (B, D) or 500 µm (C). *Abbreviations:* embryo (Eb), chorion structures (S), midgut (M), epipodite (Ep), carapace (C), nephridium (N), and ovary (Ov).

Alternatively, the brood chamber of *D. magna* remains open to the outside environment (Aladin and Potts 1995), and the interior fluids must be regulated by the parent to some extent, evidenced by an increase in Na^+ and Ca^{2+} to support embryo development (Charmantier and Charmantier-Daures 2015; Morris and O'Donnell 2019). Therefore, LMM U species could enter the embryo by similar pathways. However, to protect the developing embryo from any hostile environmental conditions, *D. magna* eggs develop a double layered envelope with chorion immediately after oviposition (Mittmann et al. 2014; Lee et al. 2019). Within the brood chamber and around the embryos, the UNP exposed organism exhibited U-containing structures that appeared to be the remains of a protective outer layer of the embryo (Fig. 4A - C). These structures did not appear in other elemental maps indicating constituents were < LOD or not detectable by XRF, such as carbon. Additionally, XRF mapping of the control organisms did not show these structures indicating that the fractured chorion was a result of the U exposures (Fig. S9). The chorion has been shown to accumulate hazardous materials including Ag^+, Ag NPs, and polystyrene beads (Yan et al. 2020; Brun et al. 2017), and it is probable that U is transferred in a similar fashion.

To assess potential effects of U exposure on the subsequent generation of daphnia (F1), survivors from the adult (F0) exposure experiment were maintained until the first reproduction. Only daphnia from exposures below the LC_{50} survived to first spawning. However, all surviving daphnia reproduced and the clutch sizes did not differ from the control organism (Table S4, Fig. S11). All of the F0 daphnia spawned within 18 h of each other resulting in 18 h synchronized broods (F1). This subsequent F1 generation was raised under normal culture conditions as previously described and observed daily for development and first reproduction. However, offspring born from exposures > 50 µg L^{-1} of either UNP or U_{Ref} treatments achieved reproduction up to 48 h earlier than the controls and the < 10 µg L^{-1} concentration exposures. Furthermore, the F1 generation exhibited larger clutch sizes overall compared witht the F0 (Fig. S11). Studies of chronic U toxicity (21 d) in *D. magna* suggest effects on reproduction (reduced fecundity in first brood) starting at concentrations of 25 µg U L^{-1} (pH 7) (Zeman et al. 2008). Chronic exposure to U has also been shown to induce a reduction of body size and fecundity in subsequent generations of daphnia (Massarin et al. 2010). In that study, growth retardation in F1 caused a delay in the deposition of the first brood, which was not observed in this study. In contrast, another study exposing *D. magna* to U mining effluent

or dissolved U for 48 h observed that the offspring of short-term exposed parents were larger than control organisms (Reis et al. 2018). In line with the observations of the current study, the authors suggest a compensatory mechanism, noting that similar results have been observed with *Rana perezi* larvae (Iberian frogs) and zebrafish (*Danio rerio*) embryos (both exposed to similar mining effluent) (Lourenço et al. 2017; Marques, Gonçalves, and Pereira 2008). Regardless, the results in this study provide visual evidence of maternal transfer into *D. magna*, demonstrating that the egg envelope was unable to prevent U from entering embryos, leading to potential long term effects onto subsequent generations.

Conclusions

The current study employed state-of-the-art integrated methods to link the U biodistribution to toxic effects in *D. magna*. Whole body XRF elemental mapping combined with detailed exposure characterization and toxic effects analysis provided novel insights into U toxicokinetics. The results contribute to an improved understanding with respect to routes of U uptake, tissue and organ accumulation, as well as organism detoxification. This study demonstrates the power of synchrotron based X-ray techniques in identifying target organs of exposure, critical for construction of an AEP framework to guide toxicokinetic research. Furthermore, the identification of high U accumulation in target organs and tissues is scope for future investigation, such as the impacts on intestinal function and the surrounding soft tissues as well as the role of the epipodites and maxillary gland on the uptake and excretion of U and other toxic metals.

Acknowledgements

This study has been funded by the Research Council of Norway through its Centre of Excellence (CoE) funding scheme (Project No. 223268/F50). We acknowledge the Paul Scherrer Institut, Villigen, Switzerland for provision of synchrotron radiation beamtime at beamline microXAS (X05LA) of the SLS. We are thankful to Knut Erik Tollefsen and You Song at the Norwegian Institute of Water Research (NIVA) for providing the *Daphnia magna culture* and to Karl Andreas Jensen and Yetneberk Kassaye at NMBU/MINA for support with the ICP-MS analyses. The Research Council of Norway is acknowledged for support to the NORTEM national infrastructure (project number 197405).

References

Radioactive Particles in the Environment: Sources, Particle Characterization and Analytical Techniques. International Atomic Energy Agency, Vienna, 2011.

Acharya C, Blindauer CA. Unexpected Interactions of the Cyanobacterial Metallothionein SmtA with Uranium. Inorganic Chemistry 2016; 55: 1505-1515.

Aladin N, Potts W. Osmoregulatory capacity of the Cladocera. Journal of Comparative Physiology B 1995; 164: 671-683.

Barata C, Baird DJ, Markich SJ. Influence of genetic and environmental factors on the tolerance of Daphnia magna Straus to essential and non-essential metals. Aquatic Toxicology 1998; 42: 115-137.

Bargar JR, Bernier-Latmani R, Giammar DE, Tebo BM. Biogenic Uraninite Nanoparticles and Their Importance for Uranium Remediation. Elements 2008; 4: 407-412.

Brun NR, Beenakker MMT, Hunting ER, Ebert D, Vijver MG. Brood pouch-mediated polystyrene nanoparticle uptake during Daphnia magna embryogenesis. Nanotoxicology 2017; 11: 1059-1069.

Byrnes, I., Rossbach, L.M., Jaroszewicz, J., Grolimund, D., Sanchez, D.F., Gomez-Gonzalez, M., Nuyts, G., Reinoso-Maset, E., Janssens, K., Salbu, B., Brede, D.A., Lind, O.C. Combined Structural and Nanoscopic Elemental Imaging Identifies Damage to Digestive Tract of Daphnia magna associated with Uranium Nanoparticle Acute Toxicity (unpublished)

Caumette G, Koch I, Moriarty M, Reimer KJ. Arsenic distribution and speciation in Daphnia pulex. Science of The Total Environment 2012; 432: 243-250.

Charles S, Veber P, Delignette-Muller ML. MOSAIC: a web-interface for statistical analyses in ecotoxicology. Environmental Science and Pollution Research 2018; 25: 11295-11302.

Charmantier G, Charmantier-Daures M. Ontogeny of Osmoregulation in Crustaceans: The Embryonic Phase1. American Zoologist 2015; 41: 1078-1089.

De Samber B, De Schamphelaere KAC, Janssen CR, Vekemans B, De Rycke R, Martinez-Criado G, et al. Hard X-ray nanoprobe investigations of the subtissue metal distributions within Daphnia magna. Analytical and Bioanalytical Chemistry 2013; 405: 6061-6068.

De Samber B, Silversmit G, Evens R, De Schamphelaere K, Janssen C, Masschaele B, et al. Three-dimensional elemental imaging by means of synchrotron radiation micro-XRF: developments and applications in environmental chemistry. Analytical and Bioanalytical Chemistry 2008; 390: 267-271.

Delignette-Muller M, Ruiz P, Charles S, Duchemin W, Lopes C, Kon-Kam-King G, et al. Morse: Modelling Tools for Reproduction and Survival Data in Ecotoxicology, 2016.

Duneau D, Ebert D. The role of moulting in parasite defence. Proceedings of the Royal Society B: Biological Sciences 2012; 279: 3049-3054.

Ebert D. Ecology, epidemiology, and evolution of parasitism in Daphnia: National Library of Medicine, 2005.

Fortin C, Dutels L, Garnier-Laplace J. Uranium complexation and uptake by a green alga in relation to chemical speciation: The importance of the free uranyl ion. Environmental Toxicology and Chemistry 2004; 23: 974-981.

Fouqueray M, Dufils B, Vollat B, Chaurand P, Botta C, Abacci K, et al. Effects of aged TiO2 nanomaterial from sunscreen on Daphnia magna exposed by dietary route. Environmental Pollution 2012; 163: 55-61.

Goldmann T, Becher B, Wiedorn KH, Pirow R, Deutschbein ME, Vollmer E, et al. Epipodite and fat cells as sites of hemoglobin synthesis in the branchiopod crustacean Daphnia magna. Histochem Cell Biol 1999; 112: 335-9.

Goulet RR, Fortin C, Spry DJ. 8 - Uranium. In: Wood CM, Farrell AP, Brauner CJ, editors. Fish Physiology. 31. Academic Press, 2011, pp. 391-428.

Guarnieri D, Sabella S, Muscetti O, Belli V, Malvindi MA, Fusco S, et al. Transport across the cell-membrane dictates nanoparticle fate and toxicity: a new paradigm in nanotoxicology. Nanoscale 2014; 6: 10264-10273.

Handy RD, von der Kammer F, Lead JR, Hassellöv M, Owen R, Crane M. The ecotoxicology and chemistry of manufactured nanoparticles. Ecotoxicology 2008; 17: 287-314.

Hao Y, Huang J, Liu C, Li H, Liu J, Zeng Y, et al. Differential protein expression in metallothionein protection from depleted uranium-induced nephrotoxicity. Scientific Reports 2016; 6: 38942.

Hasan S, Ghosh TK. Synthesis of Uranium Oxide Nanoparticles in Aqueous Solutions. Nuclear Technology 2011; 173: 310-317.

Jackson BP, Pace HE, Lanzirotti A, Smith R, Ranville JF. Synchrotron X-ray 2D and 3D elemental imaging of CdSe/ZnS quantum dot nanoparticles in Daphnia magna. Analytical and Bioanalytical Chemistry 2009; 394: 911-917.

Kashparov VA. Hot particles at Chernobyl. Environmental Science and Pollution Research 2003: 21-30.

Kashparov VA, Ahamdach N, Zvarich SI, Yoschenko VI, Maloshtan IM, Dewiere L. Kinetics of dissolution of Chernobyl fuel particles in soil in natural conditions. Journal of Environmental Radioactivity 2004; 72: 335-353.

Kikuchi S. The fine structure of the gill epithelium of a fresh-water flea, Daphnia magna (Crustacea: Phyllopoda) and changes associated with acclimation to various salinities. Cell and tissue research 1983; 229: 253-268.

Laforsch C, Tollrian R. A new preparation technique of daphnids for Scanning Electron Microscopy using hexamethyldisilazane. Archiv für Hydrobiologie 2000: 587-596.

Lee D, Nah JS, Yoon J, Kim W, Rhee K. Live observation of the oviposition process in Daphnia magna. PLOS ONE 2019; 14: e0224388.

Lofts S, Fevrier L, Horemans N, Gilbin R, Bruggeman C, Vandenhove H. Assessment of co-contaminant effects on uranium and thorium speciation in freshwater using geochemical modelling. Journal of Environmental Radioactivity 2015; 149: 99-109.

Lourenço J, Marques S, Carvalho FP, Oliveira J, Malta M, Santos M, et al. Uranium mining wastes: The use of the Fish Embryo Acute Toxicity Test (FET) test to evaluate toxicity and risk of environmental discharge. Science of The Total Environment 2017; 605-606: 391-404.

Markich S, Brown P. Actinide speciation and bioavailability in fresh and marine surface waters. In: William J. Evans TPH, editor. The Heaviest Metals: Science and Technology of the Actinides and Beyond. Wiley, 2019, pp. 367-400.

Markich SJ. Uranium Speciation and Bioavailability in Aquatic Systems: An Overview. The Scientific World Journal 2002: 707-729.

Marques SM, Gonçalves F, Pereira R. Effects of a uranium mine effluent in the early-life stages of Rana perezi Seoane. Science of The Total Environment 2008; 402: 29-35.

Massarin S, Alonzo F, Garcia-Sanchez L, Gilbin R, Garnier-Laplace J, Poggiale J-C. Effects of chronic uranium exposure on life history and physiology of Daphnia magna over three successive generations. Aquatic Toxicology 2010; 99: 309-320.

Massarin S, Beaudouin R, Zeman F, Floriani M, Gilbin R, Alonzo F, et al. Biology-Based Modeling To Analyze Uranium Toxicity Data on Daphnia magna in a Multigeneration Study. Environmental Science & Technology 2011; 45: 4151-4158.

Mittmann B, Ungerer P, Klann M, Stollewerk A, Wolff C. Development and staging of the water flea Daphnia magna (Straus, 1820; Cladocera, Daphniidae) based on morphological landmarks. EvoDevo 2014; 5: 12.

Morris C, O'Donnell M. Multiple functions of ion transport by the nuchal organ in embryos and neonates of the freshwater branchiopod crustacean Daphnia magna. The Journal of Experimental Biology 2019; 222: jeb211128.

OECD. Test No. 202: Daphnia sp. Acute Immobilisation Test, 2004.

Pavelková T, Čuba V, De Visser-Týnová E, Ekberg C, Persson I. Preparation of UO2, ThO2 and (Th,U)O2 pellets from photochemically-prepared nano-powders. Journal of Nuclear Materials 2016; 469: 57-61.

Pavelkova T, Cuba V, Sebesta F. Photo-induced low temperature synthesis of nanocrystalline UO2, ThO2 and mixed UO2-ThO2 oxides. Journal of Nuclear Materials 2013; 442: 29-32.

Plaire D, Bourdineaud J-P, Alonzo A, Camilleri V, Garcia-Sanchez L, Adam-Guillermin C, et al. Transmission of DNA damage and increasing reprotoxic effects over two generations of Daphnia magna exposed to uranium. Comparative Biochemistry and Physiology Part C: Toxicology & Pharmacology 2013; 158: 231-243.

Poston TM, Hanf RW, Simmons MA. Toxicity of uranium to Daphnia magna. Water, Air, and Soil Pollution 1984; 22: 289-298.

Pushie MJ, Pickering IJ, Korbas M, Hackett MJ, George GN. Elemental and Chemically Specific X-ray Fluorescence Imaging of Biological Systems. Chemical Reviews 2014; 114: 8499-8541.

Ravel B, Newville M. ATHENA, ARTEMIS, HEPHAESTUS: data analysis for X-ray absorption spectroscopy using IFEFFIT. Journal of synchrotron radiation 2005; 12: 537-541.

Reis P, Pereira R, Carvalho FP, Oliveira J, Malta M, Mendo S, et al. Life history traits and genotoxic effects on Daphnia magna exposed to waterborne uranium and to a uranium mine effluent - A transgenerational study. Aquatic Toxicology 2018; 202: 16-25.

Salbu B, Kashparov V, Lind OC, Garcia-Tenorio R, Johansen MP, Child DP, et al. Challenges associated with the behaviour of radioactive particles in the environment. Journal of Environmental Radioactivity 2018; 186: 101-115.

Salbu B, Skipperud L, Lind OC. Sources Contributing to Radionuclides in the Environment: With Focus on Radioactive Particles. In: Walther C, Gupta DK, editors. Radionuclides in the Environment: Influence of chemical speciation and plant uptake on radionuclide migration. Springer International Publishing, Cham, 2015, pp. 1-36.

Scheibener S, Song Y, Tollefsen KE, Salbu B, Teien H-C. Uranium accumulation and toxicokinetics in the crustacean Daphnia magna provide perspective to toxicodynamic responses. Aquatic Toxicology 2021: 105836.

Schindelin J, Rueden CT, Hiner MC, Eliceiri KW. The ImageJ ecosystem: An open platform for biomedical image analysis. Molecular Reproduction and Development 2015; 82: 518-529.

Sheppard SC, Sheppard MI, Gallerand M-O, Sanipelli B. Derivation of ecotoxicity thresholds for uranium. Journal of Environmental Radioactivity 2005; 79: 55-83.

Smirnov NN. Physiology of the Cladocera: Academic Press, 2017.

Solé VA, Papillon E, Cotte M, Walter P, Susini J. A multiplatform code for the analysis of energy-dispersive X-ray fluorescence spectra. Spectrochimica Acta Part B: Atomic Spectroscopy 2007; 62: 63-68.

Stollewerk A. The water flea Daphnia - a 'new' model system for ecology and evolution? Journal of Biology 2010; 9: 21.

Strømman G, Rosseland BO, Skipperud L, Burkitbaev LM, Uralbekov B, Heier LS, et al. Uranium activity ratio in water and fish from pit lakes in Kurday, Kazakhstan and Taboshar, Tajikistan. Journal of Environmental Radioactivity 2013; 123: 71-81.

Suzuki Y, Kelly SD, Kemner KM, Banfield JF. Nanometre-size products of uranium bioreduction. Nature 2002; 419: 134-134.

Tan L-Y, Huang B, Xu S, Wei Z-B, Yang L-Y, Miao A-J. TiO2 Nanoparticle Uptake by the Water Flea Daphnia magna via Different Routes is Calcium-Dependent. Environmental Science & Technology 2016; 50: 7799-7807.

Tan YM, Leonard JA, Edwards S, Teeguarden J, Egeghy P. Refining the aggregate exposure pathway. Environmental Science-Processes & Impacts 2018; 20: 428-436.

Teeguarden JG, Tan Y-M, Edwards SW, Leonard JA, Anderson KA, Corley RA, et al. Completing the Link between Exposure Science and Toxicology for Improved Environmental Health Decision Making: The Aggregate Exposure Pathway Framework. Environmental Science & Technology 2016; 50: 4579-4586.

United States Environmental Protection Agency. Methods for measuring the acute toxicity of effluents and receiving waters to freshwater and marine organisms. EPA-821-R-02-012, 2002.

van Aarle W, Palenstijn WJ, Cant J, Janssens E, Bleichrodt F, Dabravolski A, et al. Fast and flexible X-ray tomography using the ASTRA toolbox. Optics Express 2016; 24: 25129-25147.

van Aarle W, Palenstijn WJ, De Beenhouwer J, Altantzis T, Bals S, Batenburg KJ, et al. The ASTRA Toolbox: A platform for advanced algorithm development in electron tomography. Ultramicroscopy 2015; 157: 35-47.

van der Zande M, Kokalj AJ, Spurgeon DJ, Loureiro S, Silva PV, Khodaparast Z, et al. The gut barrier and the fate of engineered nanomaterials: a view from comparative physiology. Environmental Science-Nano 2020; 7: 1874-1898.

van Malderen SJM, Laforce B, Van Acker T, Nys C, De Rijcke M, de Rycke R, et al. Three-Dimensional Reconstruction of the Tissue-Specific Multielemental Distribution within Ceriodaphnia dubia via Multimodal Registration Using Laser Ablation ICP-Mass Spectrometry and X-ray Spectroscopic Techniques. Analytical Chemistry 2017; 89: 4161-4168.

Vicente-Vicente L, Quiros Y, Pérez-Barriocanal F, López-Novoa JM, López-Hernández FJ, Morales AI. Nephrotoxicity of Uranium: Pathophysiological, Diagnostic and Therapeutic Perspectives. Toxicological Sciences 2010; 118: 324-347.

Wang W-X. Bioimaging of metals in environmental toxicological studies: Linking localization and functionality. Critical Reviews in Environmental Science and Technology 2021: 1-31.

Wang Y, Bagnoud A, Suvorova E, McGivney E, Chesaux L, Phrommavanh V, et al. Geochemical Control on Uranium(IV) Mobility in a Mining-Impacted Wetland. Environmental Science & Technology 2014; 48: 10062-10070.

Yan N, Tsim SMJ, He X, Tang BZ, Wang W-X. Direct Visualization and Quantification of Maternal Transfer of Silver Nanoparticles in Zooplankton. Environmental Science & Technology 2020; 54: 10763-10771.

Zeman FA, Gilbin R, Alonzo F, Lecomte-Pradines C, Garnier-Laplace J, Aliaume C. Effects of waterborne uranium on survival, growth, reproduction and physiological processes of the freshwater cladoceran Daphnia magna. Aquatic Toxicology 2008; 86: 370-378.

Supplemental Material

Synchrotron based X-ray Fluorescence Imaging Provides New Insights on Uranium Toxicokinetics in *Daphnia magna* following Exposure to Uranium Nanoparticles

Ian Byrnes[1], Lisa Magdalena Rossbach[1], Dag Anders Brede[1], Daniel Grolimund[3], Dario Ferreira Sanchez[3], Gert Nuyts[4], Vaclav Cuba[2], Estela Reinoso-Maset[1], Brit Salbu[1], Koen Janssens[4], Deborah Oughton[1], Shane Scheibener[1], Hans-Christian Teien[1], Ole Christian Lind[1]

[1] Norwegian University of Life Sciences, Centre for Environmental Radioactivity (CERAD), Faculty of Environmental Sciences and Natural Resource Management, P.O. Box 5003, 1433 Ås, Norway

[2] Czech Technical University in Prague, Faculty of Nuclear Sciences and Physical Engineering, Brehova 7, Prague 1, Czech Republic

[3] Swiss Light Source, Paul Scherrer Institute (PSI), 5232 Villigen, Switzerland

[4] University of Antwerp, Department of Chemistry, Groenenborgerlaan 171, 2020 Antwerp, Belgium

*Corresponding Author

Phone: +47-93820876 Fax: +47-64948359

Email Address: ian.byrnes@nmbu.no

Address: Norwegian University of Life Sciences, Centre for Environmental Radioactivity (CERAD), Faculty of Environmental Sciences and Natural Resource Management, P.O. Box 5003, 1433 Ås, Norway

Summary

The following supplementary materials include description of experimental method and additional results.

Experimental Method

S1. Uranium Nanoparticle Synthesis and Characterization

S2. Uranium Nanoparticle Stock Suspension Characterization

S3. Daphnia magna Culturing and Acute Toxicity Tests

Results

Experimental Method

S1. Uranium Nanoparticle Synthesis and Characterization

All chemicals, such as propan-2-ol and nitric acid, were of analytical grade (Merck, Czech Republic). Deionized water was used for the preparation of aqueous solutions. Uranyl nitrate (Lachema, CSSR) was annealed at 1200 °C for 2 h. The purity of U_3O_8 was evaluated by X-ray powder diffraction (XRD).

A reaction mixture was prepared by dissolution of U_3O_8 (5.614 g, 6.7 mmol) in 4 mL of concentrated nitric acid (65 %), which corresponds to 10% excess of nitric acid. The dissolution is accompanied with release of nitric fumes. Following the complete dissolution of U_3O_8, the resulting solution was diluted by deionized water, to prevent precipitation after addition of propan-2-ol. Finally, 200 mL of propan-2-ol ($10\%_{vol}$) was added and the solution was again diluted with deionized water to a total volume of 2 L. The resulting concentration of UO_2^{2+} was 10 mM. This solution was stirred with a magnetic stirrer and irradiated for 150 min in a photochemical reactor with immersed quartz-protected low-pressure mercury lamps (variable power input: 400 W (nominal value), wavelength 254 nm; Philips TUV 25WP SE) and cooled by air-ventilators. The formed dark grey product was separated from solution by centrifugation, washed in ethanol in order to get rid of any residues, and subsequently air dried at 40 °C.

The final material was also characterized by XRD using a Rigaku MiniFlex 600 (Ni-filtered Cu-Kα1,2 radiation) equipped with a NaI:Tl scintillation detector. XRD patterns were compared to the relevant records in the ICDD PDF-2 database (version 2013). The angular range was 10° – 80°, with a step of 0.02° and a scanning speed of 2°/min.

S2. Uranium Nanoparticle Suspension and Stock Characterization

Stocks were prepared (1.0 g L^{-1}) by weighing UNPs into 20 mL glass vials, applying a dispersion agent, polyoxyethelene glycerol triolate (1% v/v), and then dispersing them in 10 mL N_2-purged ddH_2O (15 MΩ cm). A 400-W Branson Sonifier S-450D (Branson Ultrasonics) equipped with a standard 13 mm disruptor tip (model 101-147-037) was used to sonify the UNP stocks for 13 min at a 15 % amplitude.

Dynamic Light Scattering Measurements

Zeta-average hydrodynamic diameters and zeta-potentials of the UNP stock suspensions were determined by dynamic light scattering (DLS) using a Malvern Zetasizer ZS (Malvern Instruments Ltd., Worcestershire, United Kingdom) equipped with a 633 nm laser. Zeta-average hydrodynamic diameter measurements were conducted in triplicate, 5 runs each, with autocorrection function of 10 s. Electrophoretic mobility (zeta potential) was determined by Smoluchowski approximations.

Electron Microscopy

Particle crystalline structure and individual sizes were confirmed by high resolution (HR) transmission electron microscopy (TEM), while scanning transmission electron microscopy (STEM) with energy dispersive X-ray spectroscopy (EDS) was used for elemental composition. Immediately following sonication, 10 µL of UNP stock suspension was added to a 400 mesh formvar-carbon film (Agar Scientific Ltd., Essex, United Kingdom) and allowed to air dry. Samples were measured at 200 kV accelerating voltage on a JEOL JEM-2100F equipped with a Gatan Porius 200D CCD camera (JOEL Ltd., Tokyo, Japan). Fluorescent X-rays were collected by an Oxford X-Max-80 SDD EDS detector at a 0.23 srad collection angle.

Uranium Reference Solution Preparation

To compare with the UNP exposure, a U reference (U_{Ref}) solution was prepared from a 1.0 g L^{-1} uranium oxide (U_3O_8) assay and isotopic standard (CRM 129-A, U.S. Department of Energy, Argonne, Illinois, USA). A stock solution of 100 mg U L^{-1} was prepared in ddH_2O and aliqouts of this stock were added directly to empty 50 mL plastic exposure cups (Graduated Polypropylene, VWR, Radnor, PA) to result in a given exposure U concentration. The solutions were evaporated to dryness and, 24 h prior to the start of the daphnia exposure, re-dissolved with 25 mL of exposure media (i.e., MHRW at pH 6.8).

Exposure Media Size Fractionation

Size fractionation was used to determine the U size distribution at 0, 24, and 48 h in the UNP and U_{Ref} exposures. The size fractions were *particulate* (> 0.45 µm), *colloidal* (3 kDa < x < 0.45 µm), and *low molecular mass* (LMM, < 3 kDa). In sampled exposures, 1 mL of media was passed through a pre-conditioned (1 mL) 0.45 µm syringe filter (VWR, Radnor,

Pennsylvania, United States) and 100 µL was sampled from the filtrate. Next, 400 µL was sampled from the < 0.45 µm solution into a pre-conditioned (300 µL) 3 kDa Amicon cellulose membrane filter (Amicon Millipore, Billerica, MA) and centrifuged at 14,000 g for 30 min. From the filtrate, 100 µL was sampled for ICP-MS measurement.

Inductively Coupled Plasma Mass Spectrometry

Elemental analysis of exposure solutions and size fractionation samples was conducted by triple quadrupole inductively coupled plasma mass spectrometry (QQQ-ICP-MS, Agilent 8900, Mississauga, California). Aliquots were diluted in 5% HNO_3 (V/V) 48 h prior to measurement of U.

S3. *Daphnia magna* Culturing and Toxicity Tests

Laboratory cultured *Daphnia magna*, DHI strain (DHI Water & Environment, Hørsholm, Denmark), were reared in M7 media (OECD 2004). Cultures were maintained at 20°C (±1°C) with a day-night cycle of 16 h light:8 h darkness while the media was renewed 3 times weekly with neonates removed at those times. Daphnia were fed a diet of concentrated green algae (*Raphidocelis subcapitata*) at a rate of 2.10 x 10^7 cells day^{-1} $daphnid^{-1}$. Synchronized neonates (< 18 h) derived from the second clutch or later were used for exposure experiments.

Acute toxicity tests, using < 18 h *D. magna* neonates and < 7 d adults, were conducted in US EPA moderately hard reconstituted water (MHRW, pH 6.8, 350 µS cm^{-1}, 20°C) and 48 h LC_{50} values for UNPs and the U_{Ref} were determined according to OECD *Test No. 202* (OECD 2004). The measured exposure concentrations are found in Table S1. Uranium concentrations were measured by QQQ-ICP-MS after 48 h of exposure. Live daphnia were washed three times (MHRW, MHRW, Deionized water) and moved to sample preparation. Three individuals were collected for U body burden measurements via QQQ-ICP-MS where they were digested in 500 µL ultrapure HNO_3 for at least 48 h. In the adult exposure, F0 individuals (n = 3) per sublethal UNP and the U reference exposure groups were placed into clean MHRW with algae feed and allowed to spawn. Neonates from each individual (F1) were counted and placed into fresh M7 media (pH 8) with algae feed and cultured as described previously. The age of the daphnia (F1) at the first spawning and the clutch size was then recorded.

Results

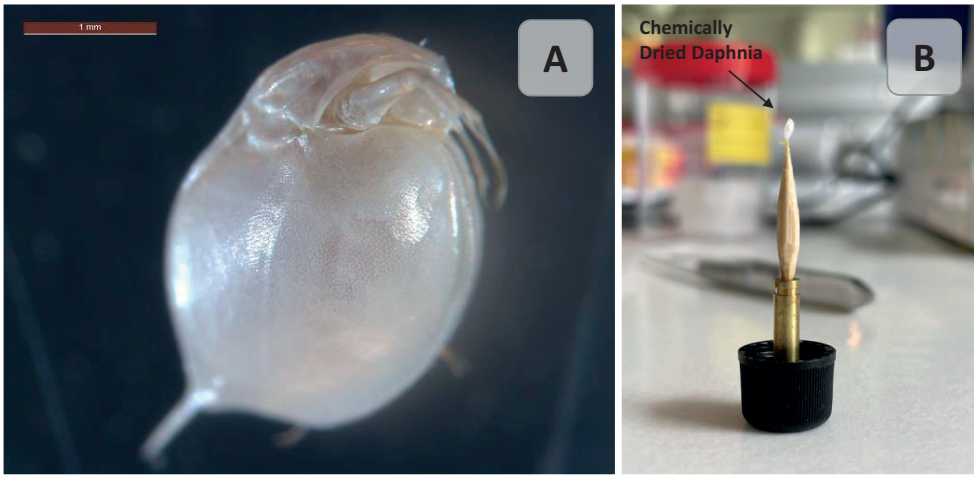

Figure S1: (**A**) Chemically dried *D. magna* and (**B**) sample mounted to the end of a wooden toothpick.

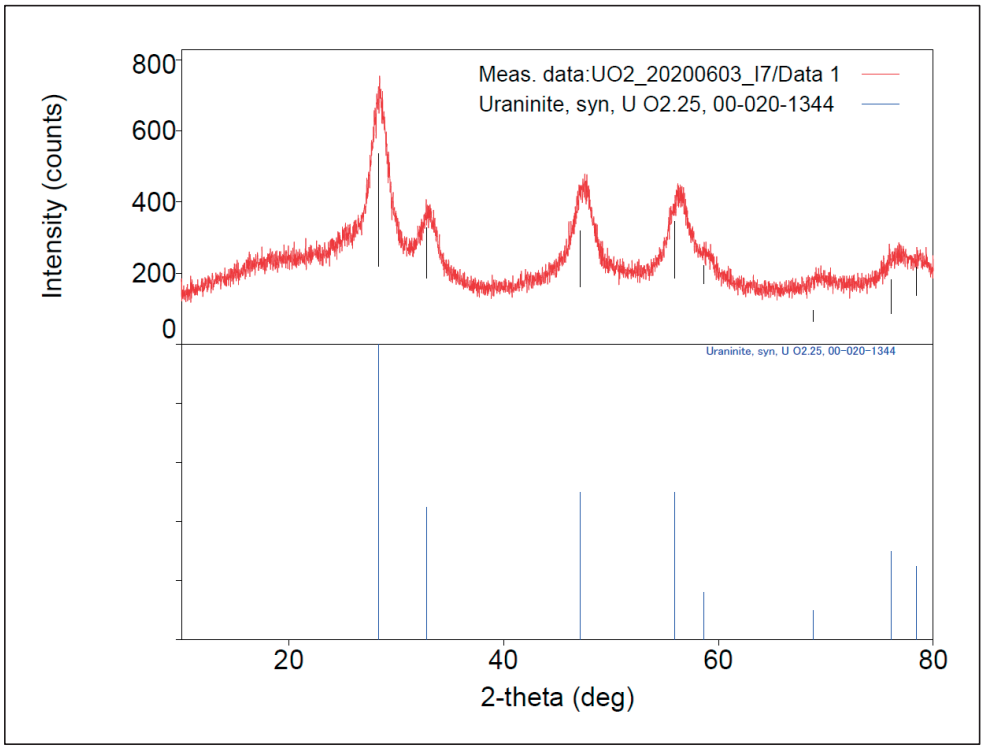

Figure S2: X-ray diffraction patterns of the synthesized UNP Powders and reference compound (synthetic uraninite).

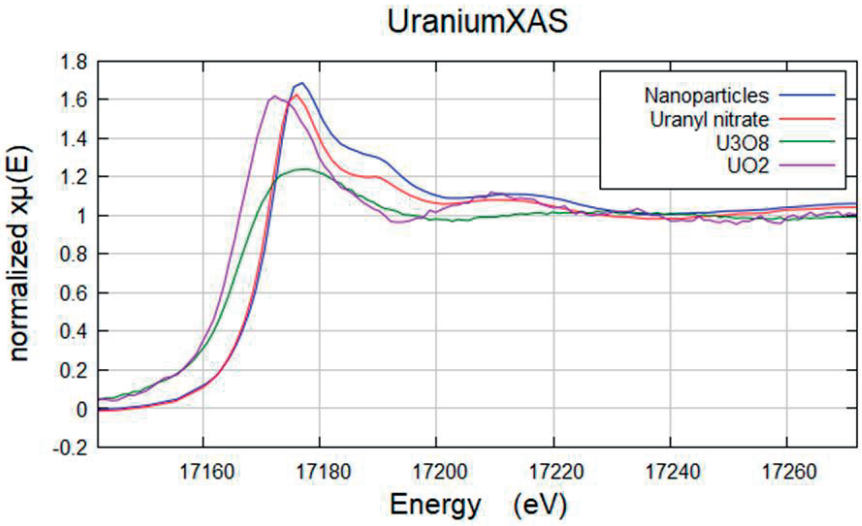

Figure S3: Micro-X-ray absorption near edge structure (μ-XANES) analysis of UNP dry powders and a uranyl nitrate salt for comparison with reference spectra of UO_2 and U_3O_8.

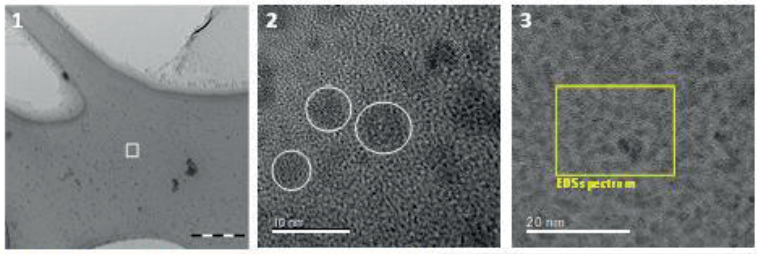

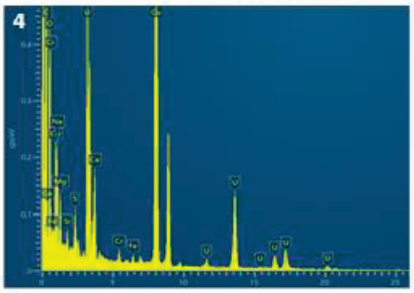

5

Element	Weight %	Atomic %
U	52.67	8.63
O	26.70	65.06
Ca	6.23	6.06
S	2.85	3.46
Mg	3.09	4.96
Na	5.04	8.55
Cr	1.31	0.98
Fe	0.89	0.62
Si	1.21	1.68

Figure S4: Transmission electron microscopy analysis of the UNPs in ddH2O (1 and 2), or MHRW (3, 4 and 5). Bright field TEM image (1) of the U NPs reveals individual particles with some larger aggregates. HR-TEM image (2) of the area within the white square in 1 shows a clear lattice fringes of individual particles (white circles) (~5 nm diameter). EDS analysis of the area within the yellow square (3) with the resulting spectrum (4) and associated elemental quantification (5).

Table S1: Uranium nanoparticle suspension details and *D. magna* exposure parameters.

Experiment	Z-average diameter 0 h (nm)	Zeta potential at 0 h (mV)	UNP Measured Exposure Concentrations 48 h ($\mu g\ U\ L^{-1}$)	U_{Ref} Measured Exposure Concentrations 48 h ($\mu g\ U\ L^{-1}$)
Neonates (< 18 h)	205.7 ± 8.07	-9.01	6.51 ± 1.12	8.98 ± 0.79
			28.1 ± 1.83	34.2 ± 2.52
				93.3 ± 20.7
			64.8 ± 4.30	111 ± 4.27
				188 ± 17.3
			80.3 ± 5.77	258 ± 10.1
				522 ± 41.4
			148 ± 6.14	691 ± 9.41
			427 ± 22.5	1250 ± 141
Adults (< 7 d)	273.3 ± 1.2	-11.8	8.8 ± 1.9	10.8 ± 1.6
			82.5 ± 12.7	91.4 ± 12.9
			112 ± 3.8	139 ± 14.9
			161 ± 11.9	203 ± 6.53
			195 ± 13.3	260 ± 12.5
			388 ± 10.2	510 ± 47.6
			591 ± 36.8	689 ± 29.1
			781 ± 84.6	790 ± 41.5

Table S2: Concentration of the different elements identified in the UNP exposure suspensions used in the neonate and adult daphnia experiments.

	Li (µg L^{-1})	B (µg L^{-1})	Ti (µg L^{-1})	V (µg L^{-1})	Mo (µg L^{-1})	Ag (µg L^{-1})	Sn (µg L^{-1})	Lu (µg L^{-1})	U (mg L^{-1})
Neonate Experiment	47.9 ± 2.12	3213 ± 106.6	1480 ± 618.2	41.4 ± 7.12	0.79 ± 0.07	19.5 ± 0.42	3.60 ± 0.03	2.19 ± 0.08	665 ± 16.3
Adult Experiment	50.27 ± 0.58	2257 ± 9.430	373.7 ± 25.42	21.1 ± 1.84	1.32 ± 0.08	17.2 ± 0.98	3.14 ± 0.80	1.80 ± 0.22	708 ± 19.6

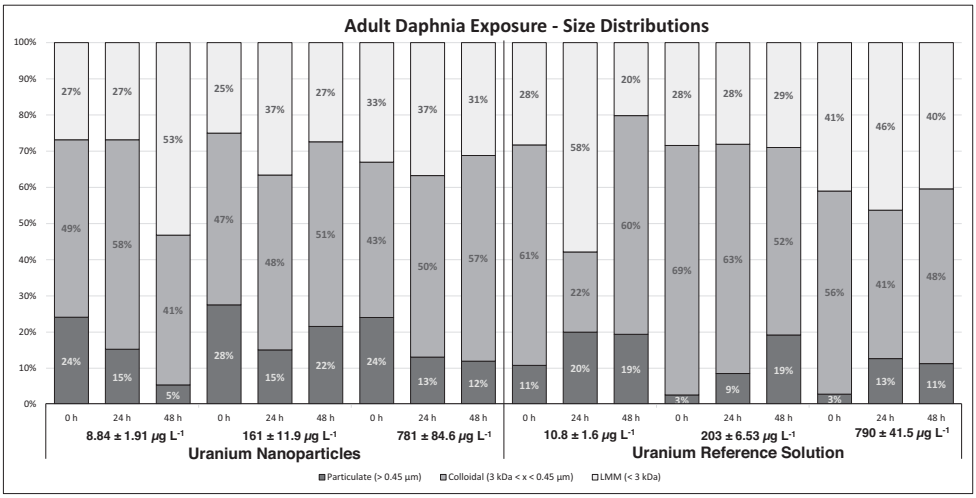

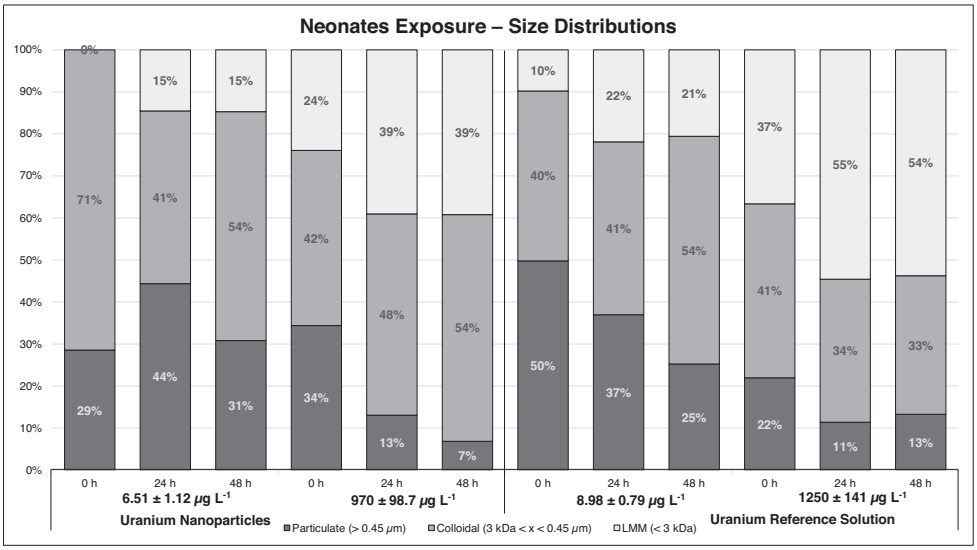

Figure S5: Size distribution of U species in the UNP (*left*) and U_{Ref} (*right*) exposure media solutions.

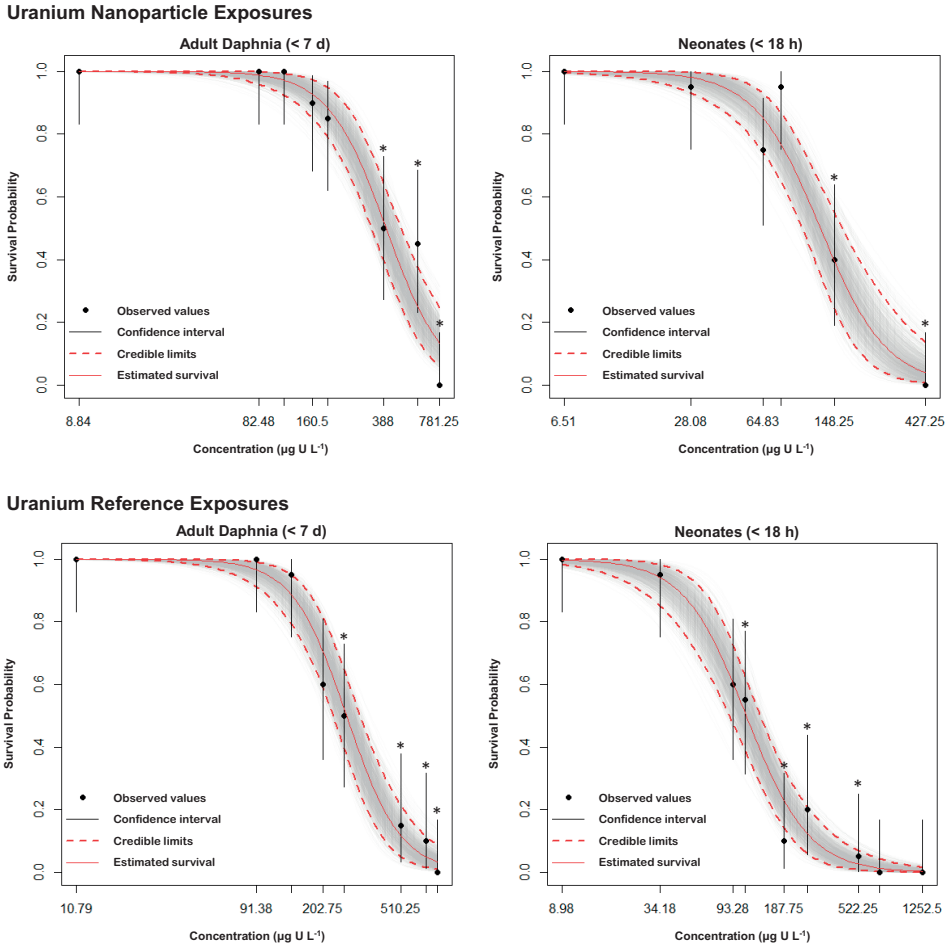

Figure S6: Survival curves for the UNP (*above*) and U_{Ref} (*below*) exposures with the modeled survival probability in terms of average measured exposure concentration (µg U L^{-1}). Survival in the adult (< 7 d) (*left*) and neonate (*right*) exposure are presented for each treatment. Input (observed) values are marked by black points with 95 % confidence bars. Fitted survival probability is indicated by the red line while the grey bands indicate the 95 % credible limits of the model. The confidence interval of all observations was within the model 95 % credible limit. For each exposure, the 48 h LC_{50} and LC_{10} are provided including the 95 % credible limits. Asterisks (*) indicate statistically significant differences (ANOVA and non-parametric Kruskal-Wallis (U_{Ref} neonates) test $p < 0.05$) compared to control.

Table S3: 48 h LC_{50} and LC_{10} Determinations

	Adult Daphnia (< 7 d)	Neonates (< 18 h)
Uranium Nanoparticles		
LC_{50}	402 µg L^{-1} [336 - 484]	127 µg L^{-1} [102 - 163]
LC_{10}	183 µg L^{-1} [130 - 238]	54.7 µg L^{-1} [35.7 - 73.4]
Uranium Reference		
LC_{50}	268 µg L^{-1} [229 - 315]	112 µg L^{-1} [89.5 - 136]
LC_{10}	133 µg L^{-1} [97.8 - 168]	44.0 µg L^{-1} [26.5 - 62.0]

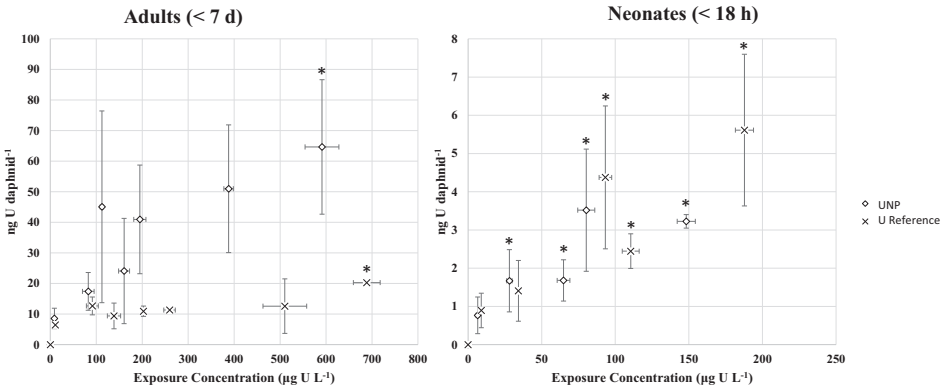

Figure S7: Total U body burden (n = 3) after 48 h acute exposures for neonates (left) and adult daphnia (right). Asterisks (*) indicate statistically significant differences (ANOVA $p < 0.05$) compared to control.

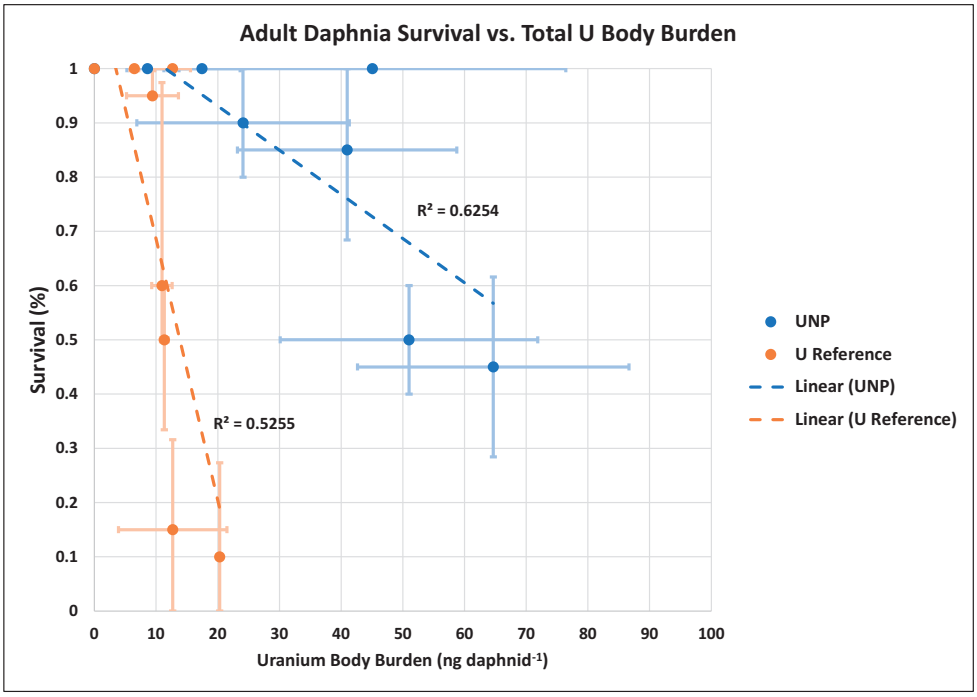

Figure S8: Adult *D. magna* survival as a function of U body burden (ng daphnid^{-1}). Regression analysis found $p < 0.05$ for both the UNP and the U_{Ref} exposures.

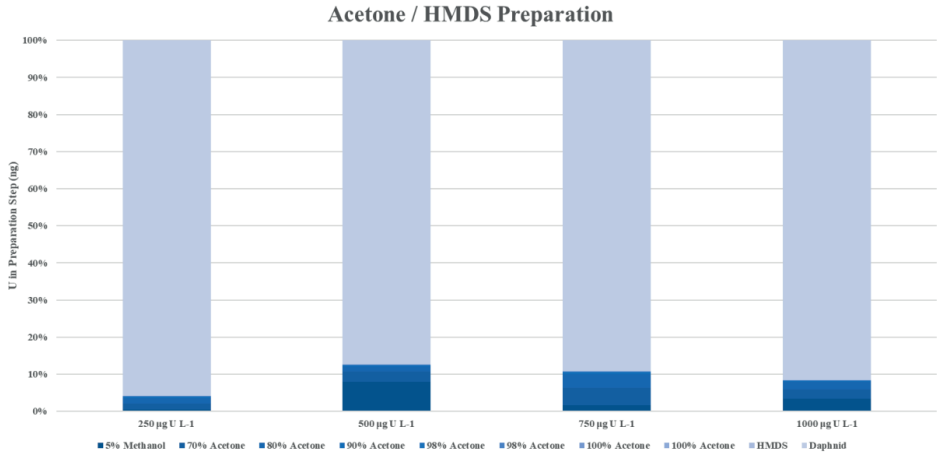

Figure S9: Determination of U loss following chemical drying using acetone and HMDS. The amount of U (in ng) was determined in each step of the method for the exposure media containing different U concentrations.

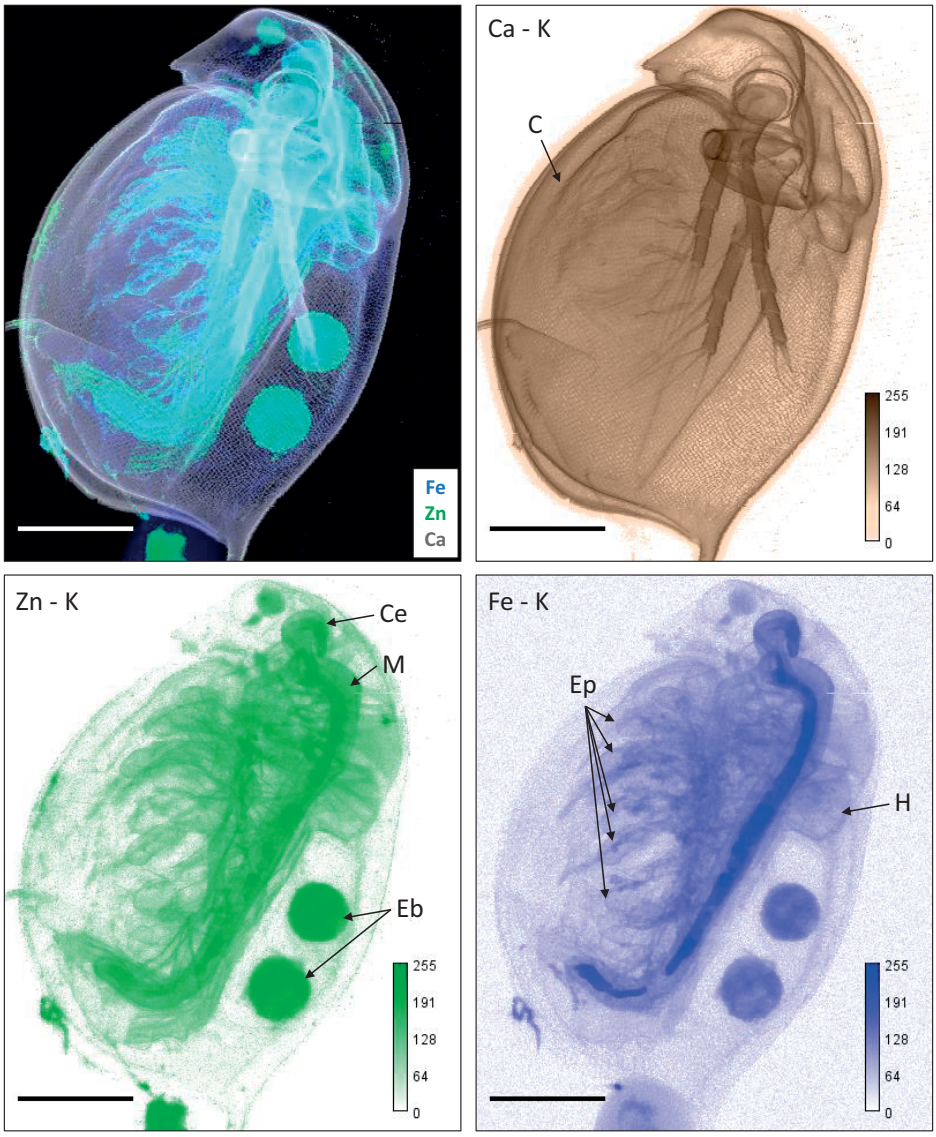

Figure S10: XRF elemental mapping (Ca, Fe, Zn) of a control organism (5 µm step size, 200 ms dwell time), combined (*top left*) and individual maps. All scale bars represent 500µm and all signal intensities are scaled logarithmically from 0 to 255. *Abbreviations:* mandible (Ma), carapace (C), hepatic ceca (Ce), midgut (M), vesicle (V), epithelial wall (Ew), lumen bound by peritrophic membrane (P), epipodites (Ep), muscle tissue (Mu), heart (H), and embryos (Eb).

Table S4: Reproduction test results for UNP and U_{Ref} exposure experiments.

Uranium Nanoparticles			**Uranium Reference Solution Exposures**		
Parent Exposure Concentration (ug L^{-1} UNP)	Parent Clutch Size	Age of Neonates at First Spawning (Day)	Parent Exposure Concentration (ug L^{-1} U)	Parent Clutch Size	Age of Neonates at First Spawning (Day)
8.8 ± 1.9	2	14	0 (A)	2	17
8.8 ± 1.9	1	15	0 (B)	4	15
8.8 ± 1.9	3	14	0 (C)	3	12
82.5 ± 12.7	2	16	10.8 ± 1.6	4	14
82.5 ± 12.7	3	12	10.8 ± 1.6	5	14
112 ± 3.8	3	11	10.8 ± 1.6	2	14
112 ± 3.8	3	11	91.4 ± 12.9	3	12
112 ± 3.8	2	12	91.4 ± 12.9	4	14
161 ± 11.9	2	11	91.4 ± 12.9	1	11
161 ± 11.9	5	13	139 ± 14.9	5	11
161 ± 11.9	4	11	139 ± 14.9	3	11
195 ± 13.3	2	11	139 ± 14.9	3	11
195 ± 13.3	3	11	203 ± 6.53	1	11
388 ± 10.2	1	11			

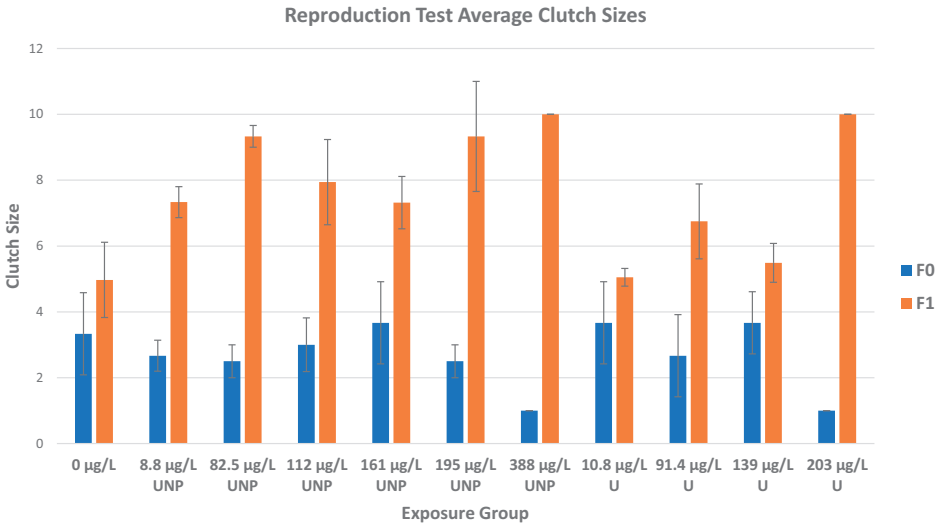

Figure S11: Average clutch size (n </= 3) of the F0 and F1 generations.

Paper III

Combined Structural and Nanoscopic Elemental Imaging Identifies Damage to Digestive Tract of *Daphnia magna* associated with Uranium Nanoparticle Acute Toxicity

Ian Byrnes[1], Lisa Magdalena Rossbach[1], Jakub Jaroszewicz[2], Daniel Grolimund[3], Dario Ferreira Sanchez[3], Miguel Gomez-Gonzalez[4], Gert Nuyts[5], Estela Reinoso-Maset[1], Koen Janssens[5], Brit Salbu[1], Dag Anders Brede[1], Ole Christian Lind[1]

[1] Norwegian University of Life Sciences, Center for Environmental Radioactivity (CERAD), Faculty of Environmental Sciences and Natural Resource Management, P.O. Box 5003, 1433 Ås, Norway

[2] Warsaw University of Technology, Faculty of Materials Science and Engineering, Woloska St. 141, 02-507 Warsaw, Poland

[3] Swiss Light Source, Paul Scherrer Institute (PSI), 5232 Villigen, Switzerland

[4] Diamond Light Source Ltd., Harwell Science and Innovation Campus, Didcot, Oxfordshire OX11 0DE, United Kingdom

[5] University of Antwerp, Department of Chemistry, Groenenborgerlaan 171, 2020 Antwerp, Belgium

*Corresponding Author

Phone: +47-93820876 Fax: +47-64948359

Email Address: ian.byrnes@nmbu.no

Address: Norwegian University of Life Sciences, Center for Environmental Radioactivity (CERAD), Faculty of Environmental Sciences and Natural Resource Management, P.O. Box 5003, 1433 Ås, Norway

Abstract

Micro and nanoscopic X-ray techniques were used to investigate the relationship between uranium (U) tissue distributions and adverse effects to the digestive tract of aquatic model organism *Daphnia magna* following uranium nanoparticle (UNP) exposure. Whole body X-ray absorption computed tomography (CT) measurements (2 µm voxel size) of daphnia exposed to sublethal concentrations of UNPs or a U reference solution (U_{Ref}) showed adverse morphological changes to the midgut and the hepatic ceca. Histological analyses of exposed organisms revealed a high proportion of abnormal and irregularly shaped intestinal epithelial cells. Disruption of the hepatic ceca and midgut epithelial tissues implied both digestive functions and intestinal barriers were compromised. Two-dimensional µ-SRXRF elemental imaging (2 µm resolution) identified U co-localized with morphological changes, with substantial accumulation of U in the lumen as well as in the epithelial tissues. Capitalizing on the high resolution nano-SRXRF elemental maps (75 nm resolution), 400 - 1000 nm sized U particulates could be identified throughout the midgut and within hepatic ceca cells, coinciding with tissue damages. Furthermore, nano-SRXRF showed U bound to luminal content, including ingested algae (*Raphidocelis subcapitata*), that appeared to contribute to the sequestration of U within the digestive tract. The presented results highlight disruption of intestinal function as an important mode of action of acute U toxicity in *D. magna,* and that midgut epithelial cells as well as the hepatic ceca are key target organs.

Keywords

Uranium Nanoparticles, X-ray Fluorescence, X-ray Absorption Computed Tomography, Histology, *Daphnia magna*

Introduction

Uranium (U) is released to the environment from a series of naturally occurring U rich minerals and bedrocks such as alum shale and granite. Uranium is also associated with the release from anthropogenic sources, particularly those stemming from the nuclear weapon and fuel cycles (2005), such as uranium mining and milling industries, nuclear reactor accidents, nuclear weapon detonations, nuclear waste storage, nuclear fuel reprocessing, civilian and military use of depleted uranium, and, potentially, from the catalyst industry (Bots et al., 2014; Hasan and Ghosh, 2013; Lind et al., 2020; Novikov et al., 2009; Reynolds et al., 2018; Tamborini, 2004; Wang et al., 2014).

In the environment, U can be present in different physico-chemical forms varying in size and charge properties. The speciation (e.g., low molecular mass (LMM) species, colloids, and particles) is known to influence the mobility and potential transfer of U in the environment, where LMM species (<1 nm) are assumed to be mobile and bioavailable, colloidal forms (1 nm - 0.45 µm) including nanoparticles can be relatively mobile, while particles (> 0.45 µm) are considered inert (Dublet et al., 2019; Lind et al., 2020; Salbu et al., 2004; Wang et al., 2014). Molecular growth processes or weathering of minerals and nuclear fuel material may give rise to nanoscale uranium particles with properties that may be different from those of ions and larger particles with respect to mobility, biological transfer, and toxicity (Bargar et al., 2008; Kaminski et al., 2005; Suzuki et al., 2002).

Uranium concentrations in aquatic systems vary widely depending on the surrounding minerals and sedimentary rock formations as well as anthropogenic activities, with maximum values reaching several mg L^{-1} in surface waters (Salbu et al., 2013; Strømman et al., 2013), which exceeds the World Health Organization (WHO) guideline value (< 30 µg L^{-1}) for drinking water by two orders of magnitude (WHO, 2011). Uranium contamination is especially problematic for aquatic ecosystems where U is known to be taken up into the food web, and its chemotoxicity can drive acute effects (Markich, 2002; Scheibener et al., 2021; Sheppard et al., 2005). The freshwater invertebrate *Daphnia magna* is a preferred model for aquatic toxicological studies due to their role as primary consumers of various algae and bacterial species as well as their functional role in nutrient cycling (Ebert 2005; Stollewerk 2010). *Daphnia magna* are highly sensitive to waterborne U where chronic effects have been shown at concentrations > 10 µg L^{-1}

(Massarin et al., 2010), while the 48 h LC_{50} occurs at concentrations > 390 µg L^{-1} (Zeman et al., 2008), depending on water conditions such as pH or U binding ligands (Goulet et al., 2015). Traditionally, aquatic toxicology studies have relied on total water concentrations and body burden measurements that lack detailed information to identify underlying toxicokinetic mechanisms. The biodistribution of internalized U remains unexplored with indirect evidence pointing towards nutrient uptake related to disruption of intestinal processes as a potential toxic mode of action (Massarin et al., 2011; Zeman et al., 2008). Upon ingestion of metal species such as metal NPs, the intestine presents a highly exposed organ as well as the primary barrier for uptake (van der Zande et al., 2020). Furthermore, colloids such as NPs inherit distinct properties from LMM species including the ability to cross biological membranes and accumulate in tissues resulting in heterogeneous biodistributions (Guarnieri et al., 2014). Therefore, spatial distribution and characterization of U species within the digestive tract can provide insights into the toxicokinetic mechanisms underpinning acute effects from the exposure, especially when paired with histological analyses of tissues with cell damages.

Micro and nano-focused X-ray spectroscopic methods, including X-ray fluorescence (XRF) mapping, are powerful tools for investigating the spatial distributions of metal NPs down to the organ, tissue, and cell level (Pushie et al., 2014). In *D. magna*, elemental distribution studies have identified metal accumulation in the intestine, but have so far not differentiated between various compartments or phases, such as luminal contents versus epithelial cells (Caumette et al., 2012; Jackson et al., 2009; Tan and Wang, 2014). However, recent synchrotron beamline advances have allowed improved resolution and detection limits such that the distribution of metals associated with tissues and cells may be identified (De Samber et al., 2013,Cagno et al., 2017).

The objectives of the current study were to characterize uptake and biodistribution in *Daphnia magna* exposed to engineered UNPs or a U reference solution (U_{Ref}) aiming to identify target organs related to adverse effects observed in the digestive tract. To this end, micro and nano-focused, sycnchrotron based XRF elemental mapping was employed to assess U localization with organ, tissue, and cell damages visualized using X-ray absorption computed tomography (CT) and histology.

Experimental Methods

Uranium Nanoparticles

Uranium nanoparticles were synthesized using a natural uranium source (Pavelková et al., 2016; Pavelkova et al., 2013). Particles were stored as lyophilized, dry powder aliquots in a N_2 purged bottle inside a desiccator at room temperature. Suspensions (1.0 g U L^{-1}) of UNPs were prepared immediately prior to exposure (supplementary material, S1). All UNP stock solutions were characterized for individual particle size, aggregation state, and surface charge using transmission electron microscopy (TEM) and dynamic light scattering (DLS), which is described in further detail in the supplementary material (S1).

Daphnia magna Exposure Experiment

Laboratory cultured, adult (< 7 d) *D. magna*, DHI strain (DHI Water & Environment, Hørsholm, Denmark), were exposed in moderately hard reconstituted water (MHRW, pH 6.8) for 48 h at sublethal concentrations, 320 ± 30.6 µg L^{-1} UNP and 159 ± 13.7 µg L^{-1} U_{Ref}, based on LC_{50} values determined in a previous study (Byrnes et al., unpublished). The U_{Ref} solution was prepared from a uranium oxide standard (1.0 g L^{-1} in 2 % HNO_3; CRM 129-A, US Department of Energy, Argonne, Illinois, USA). All exposed daphnia were removed from normal culturing conditions, including feed, 24 h prior to the start of the experiment to clear their digestive tract as much as feasible. Size fractionation measurements were conducted to assess the LMM (< 3 kDa), colloidal (3 kDa < x < 0.45 µm), and particulate (> 0.45 µm) fractions (supplementary material, S1). After 48 h, daphnia (n = 3) were prepared for whole body burden (ng U $daphnid^{-1}$) measurements using inductively coupled plasma mass spectrometry (ICP-MS, Agilent 8900, Mississauga, California).

X-ray Absorption Computed Tomography and Microscale X-ray Fluorescence Imaging

Daphnia magna specimens for CT scanning were suspended in ethanol. Individuals were placed in a fixative solution of 2.5 % glutaraldehyde and 3 % paraformaldehyde in a 0.1 M Na cacodylate buffer at 4°C overnight. Next, the samples were washed in fresh 0.1 M Na cacodylate buffer and dehydrated through a graded ethanol series (30, 50, 70, 90, 95 % 1 x 60 min, and 100 % 2 x 30 min). Dehydrated, suspended samples were stored at

4°C until measurement by CT using an XRadia MicroXCT-400 (Carl Zeiss AG, Oberkochen, Germany). Daphnia samples, secured inside an Eppendorf tube, were rotated along their central axis and 1,000 tomographic projections were collected per sample. Volumetric rendering of the results was completed using Bruker visualization software solutions (CTVOX, CTVOL, CTAN, Bruker Nano GmbH, Berlin, Germany).

Preserved, whole organisms were prepared for synchrotron based micro-XRF (μ-SRXRF) by fixation in 5 % methanol for 10 min (Tan et al., 2016) followed by dehydration by graded acetone series (70, 80, 90 % 1x 10 min, 98, and 100% 2x 10 min) and submersion in 2 mL of hexamethyldisilazane (HMDS) for 1 h (Laforsch and Tollrian, 2000). Subsequently, 1.8 mL HMDS was carefully removed, and samples were dried overnight in a desiccator with an applied vacuum of 200 mbar. These preserved samples were stored in closed planchets or Eppendorf tubes and kept at room temperature until measurement.

High sensitivity μ-SRXRF scanning of preserved specimens was conducted at the microXAS beamline (X05LA) at the Swiss Light Source (Paul Scherrer Institute, SLS, Switzerland). Organisms were secured on the sample holder by either Kapton tape or by gluing to the end of a wooden toothpick. Whole body scans were collected using 20 μm step size and 200 ms dwell time followed by high resolution scanning (2 μm step size, 200 ms dwell time) of a selected region of interest (ROI) of the *D. magna* digestive tract. A 17.2 keV incident beam was focused using a Kirkpatrick-Baez (KB) mirror system to a size of 1 μm^2 and the sample was raster-scanned in projection mode. X-ray fluorescence spectra were collected using four silicon drift detectors (SDD; Ketek GmbH, Germany) positioned around the sample at 50° to the incoming beam. Sum spectra results were fitted using PyMCA and resulting maps were compiled and colored with ImageJ (Solé et al. 2007; Schindelin et al. 2015).

Moreover, U L_{III}-edge micro-X-ray absorption near edge structure (μ-XANES) spectra were collected on points within the ROI of the daphnia in fluorescence and transmission mode. Multiple spectra (n = 9) were collected in 1 eV increments from ~100 eV below the U L_{III}-edge (17.163 keV) to ~300 eV above. Processing of the μ-XANES spectra was conducted using the ATHENA software (Ravel and Newville, 2005) and qualitatively compared with μ-XANES spectra of UNP dry powders and reference compounds (Byrnes et al., unpublished).

Combined Histological Analysis and Synchrotron based Nanoscale X-ray Fluorescence Imaging

Thin sections of *D. magna* samples were prepared for histological analysis and synchrotron based nano-XRF (nano-SRXRF). In brief, whole organisms were subjected to overnight fixation (2.5 % glutaraldehyde and 3 % paraformaldehyde in a 0.1 M Na-cacodylate buffer, pH 7.2) at 4°C. The following day, samples were washed in fresh buffer and decalcified in 10 % HCl for 30 min followed by a 1% osmium (Os) tetroxide buffer stabilization for 1 h in the dark at constant shaking. Next, samples were washed in fresh buffer again and dehydrated in a graded ethanol series (30, 50, 70, 90 % 1 x 1 h, and 100% 3 x 1 h) before embedding in EPON resin (Agar Scientific Ltd., Essex, United Kingdom).

Sections of 1 – 5 µm (histology) and 1 µm (nano-SRXRF) were cut using a ultramicrotome equipped with a diamond knife (Diatome Ltd., Nidau, Switzerland). Histological sections were dried on a glass slide and stained with Stevenell Blue dye. Sections were imaged at 10x, 20x, 40x, and 100x magnifications on a Leica DM6B light microscope using the LAS X analysis software (Leica Microsystems, Wetzlar, Germany).

Sections for nano-SRXRF were mounted on 5 x 5 mm SiN_3 membranes (Silson Ltd., Warwickshire, UK). X-ray fluorescence scanning was carried out at the I14 Hard X-Ray Nanoprobe beamline of the Diamond Light Source (UK) (Quinn et al., 2021) using an incident beam energy of 17.3 keV and a 4-element silicon drift detector (SGX-RaySpec, UK). Coarse maps were obtained using a 225 nm step size and a 200 ms dwell time, while 75 nm step size and 400 ms dwell time were used for fine resolution maps. The PyMCA suite was used for batch fitting and primary analysis of maps (Solé et al. 2007). Further image processing was done using the ImageJ software (Schindelin et al. 2012).

Additional analyses of daphnia midgut tissues were conducted using scanning transmission electron microscopy (STEM) with energy dispersive X-ray spectroscopy (EDS) (described in detail in the supplementary material, S3).

Results and Discussion

Nanoparticle and Exposure Media Characterization

Dry UNPs were characterized in a parallel study using TEM, X-ray diffraction analysis, and μ-XANES showing that the NPs were between 3 – 5 nm in diameter and most closely resembled UO_2 after synthesis but appeared to have been oxidized by the time of synchrotron measurements (Byrnes et al., unpublished). The mean size of UNP aggregates in the UNP stock suspension was 185.6 ± 0.6 nm, while the zeta potential was -9.48 mV (Table S1). These results are consistent with (Byrnes et al., unpublished), and indicate a propensity of the UNPs to aggregate in aqueous suspensions (Handy et al., 2008). This notion was corroborated by size fractionation measurements of the UNP and the U_{Ref} exposure media (MHRW, pH 6.8) (USEPA, 2002) (Fig. S1). In fact, colloidal and particulate fractions (> 3 kDa) were large in both the UNP (62 %) and the U_{Ref} (64 %) after 48 h. Furthermore, the LMM fractions were also comparable after 48 h (39 % UNP, 36 % U_{Ref}) leading to similar U species size distributions between both treatments.

X-ray Absorption Computed Tomography Identified Morphological Effects from Uranium Exposure

Using CT, changes to the morphological structure of the digestive tract, compared with the control organism, were observed. The hepatic ceca and midgut, regions critical to digestion and nutrient absorption, were isolated and rendered independently of the rest of the organism (Fig. 1). Despite removing the daphnia from feed conditions for 24 h, the midgut of all studied organisms contained some food (algae). In the UNP exposed organisms, the luminal contents had a significantly higher density relative to the soft tissues (Fig. 1D), suggesting the presence of aggregated UNPs potentially promoted by the daphnia gut chemistry (van der Zande et al., 2020). Consistent with a parallel study (Byrnes et al., unpublished), these organisms also exhibited a greater total U body burden on average compared with the U_{Ref} exposed daphnia (Fig. S2), further indicating elevated concentrations of U within the digestive tract mainly constituted UNP aggregates. Tomographic renderings revealed that the hepatic ceca of exposed daphnia appeared severely shrunken and straightened (Fig. 1C - D), comparable to observations made following Cd exposure (Munger et al., 1998). Based on CT, the volumes of the hepatic ceca were reduced by a factor of ~2 (U_{Ref}) and ~4.6 (UNP) compared to the control. In the UNP

exposed organism, high density structures, suggesting aggregates, appeared far into the ceca, signifying impaired gut barrier functions that would normally isolate contents within the lumen.

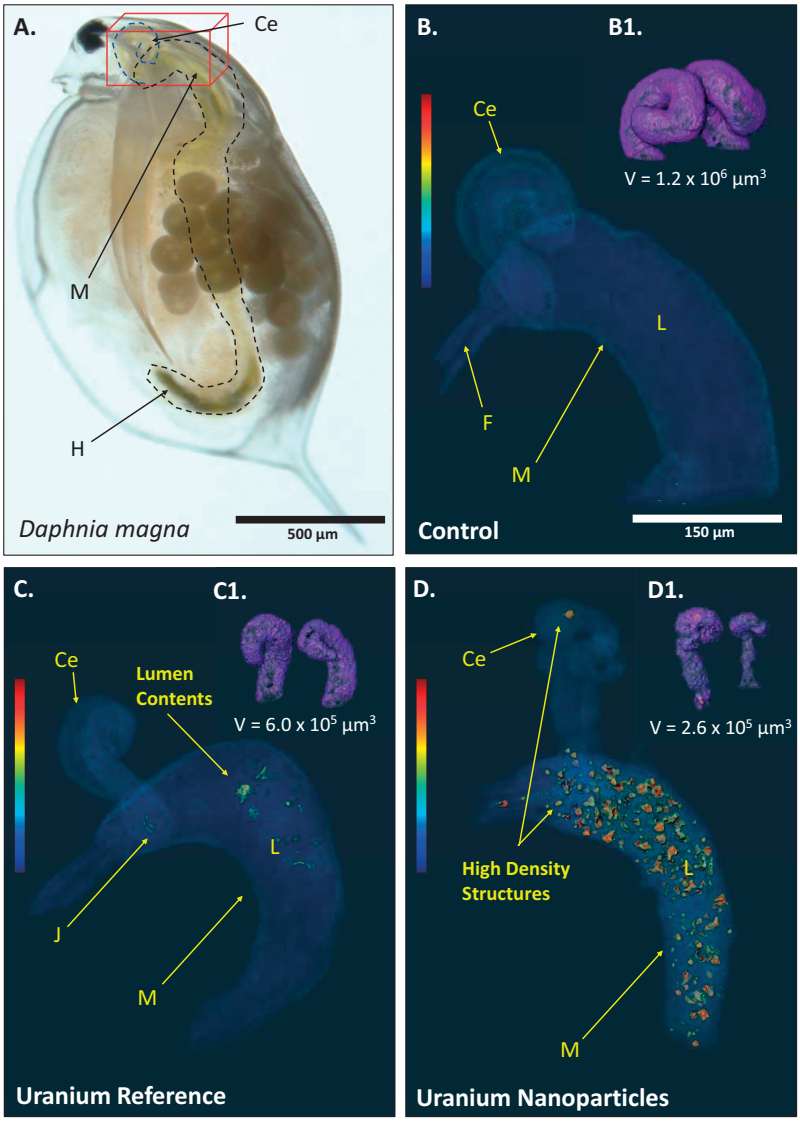

Figure 1: (**A**) Light microscopy image of a *D. magna* showing the midgut, hepatic ceca, and the hindgut, and the region of interest where the hepatic ceca connect to the midgut (red box). Tomographic renderings (voxel size = 2 µm) of this region are shown for the (**B**) control, (**C**) U_{Ref} solution (159 µg L^{-1}), and (**D**) UNP (320 µg L^{-1}) exposed organisms. Tomographic analyses provided the volume of the hepatic ceca for the (**B1**) control, (**C1**) U_{Ref}, and (**D1**) UNP exposed daphnia. Color scale indicates relative density per tomographic reconstruction. *Abbreviations:* hepatic ceca (Ce), midgut (M), hindgut (H), lumen (L), hepatic ceca – midgut junction (J).

Microscale XRF Investigations Confirm Extensive Intestinal Damage are Associated with U Accumulation

Low resolution μ-SRXRF scans of the whole daphnia showed U signals throughout the digestive tract including the hepatic ceca and midgut (Fig. 2A). Distributions of Fe and Zn constituted the major elements of the soft tissues, while Ca was indicative of the carapace. Within the digestive tract, a high U signal was also observed within the hindgut. This region is protected by a 1 – 2 μm cuticle and is associated only with the movement of food and gut material and not with nutrient uptake or digestion (Quaglia et al., 1976), therefore, it is not necessarily critically affected by U retention. High resolution mapping of the ROI around the junction of the hepatic ceca and midgut allowed distinguishing between the lumen contents and the epithelial tissues of the organs (Fig. 2B). In all imaged daphnia, elevated levels of U were detected at this junction, where the ceca are excreting digestive enzymes into the midgut and the peritrophic membrane is secreted around the food bolus (Ebert, 2005; Hansen and Peters, 1998). Uranium was clearly visible translocated from the lumen cavity into the hepatic ceca, implying failure of intestinal barrier functions. Cellular uptake of U in epithelial tissues was weakly visible due to a low relative intensity compared with the high signals observed in the lumen, where U was strongly associated with gut materials not cleared by the daphnia prior to the exposure (shown in more detail in Fig. 5). Finally, U was not observed in the foregut, a region which also bears a 1 - 2 μm cuticle (Smirnov, 2017), indicating that the retention of U was negligible prior to entry into the midgut.

The μ-XANES spectra on locations of high U intensity in the hepatic ceca and midgut shared the same characteristics as those collected as part of dry UNP characterization work (Byrnes et al., unpublished), suggesting the UNPs retained in daphnia are also oxidized (Fig. S3). However, contributing factors from the sample preparation or potential photooxidation incurred on the beamline could not be excluded and further analysis is required to confirm the results from this work (Alessi et al., 2013).

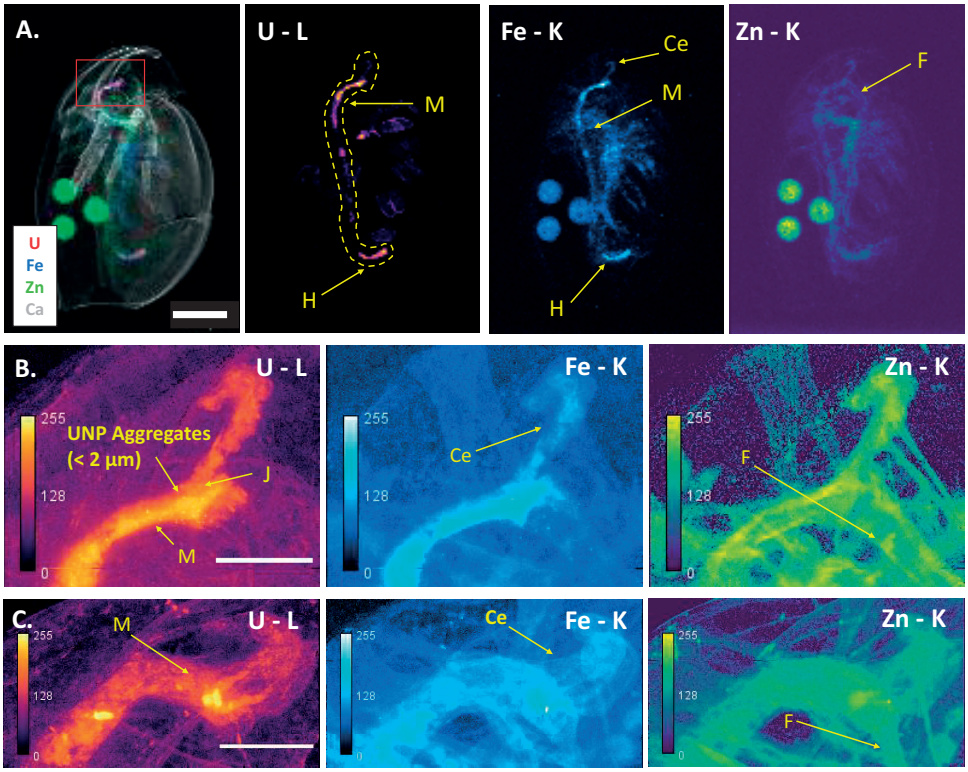

Figure 2: (**A**) Composite and individual elemental µ-SRXRF mapping (20 µm step size, 200 ms dwell time) of *D. magna* exposed to UNPs (320 µg L^{-1}) showing the whole-body distribution of U (red), Ca (grey), Fe (blue), and Zn (green), and the ROI for high resolution investigation (red box). (**B**) Two-dimensional mapping of the ROI from the same UNP exposed daphnia via µ-SRXRF (2 µm step size, 200 ms dwell time) and (**C**) the same region studied on a daphnia exposed to the U_{Ref} solution (159 µg L^{-1}). Scale bars represent 500 µm (**A**) or 100 µm (**B, C**), and all signal intensities are scaled logarithmically from 0 to 255. *Abbreviations:* hepatic ceca (Ce), midgut (M), hindgut (H), foregut (F), and the hepatic ceca – midgut junction (J).

Combined Histological and nano-SRXRF Analyses of the Hepatic Ceca

Histological analysis of the hepatic ceca showed the epithelial cells were largely destroyed, with remnants entering the luminal space (Fig. 3). In contrast, the control organism exhibited healthy, cuboidal cells that were lined with microvilli. The tissues of the U_{Ref} exposed organism retained some normal structure (Fig. 3B) with reduced microvilli present, while such cell features were absent in the UNP exposed daphnia (Fig.

3C). The cell and tissue damage in the hepatic ceca observed in the exposed daphnia were commensurate with the observed reduced organ size and straightening in the CT renderings, indicating that cell damage could be a leading cause of the morphological changes.

By using the Os distribution to align the elemental maps with the histology section, nano-SRXRF scans (Fig. 3B - C) showed the presence of U-containing materials throughout the damaged hepatic ceca tissues, further confirming translocation into the organ from the midgut. Both exposures resulted in small (< 500 nm) U hotspots distributed throughout the investigated section of hepatic ceca. In UNP exposed samples, these hotspots were likely small aggregates of UNPs, while, in the U_{Ref} derived organism, these particulates probably originated from the particulate (> 0.45 µm) fraction and/or due to aggregation of colloids (Fig. S1). Nanoparticles and colloids have the potential to act as diffuse sources of long-term release of ions when embedded in tissues as observed here in the hepatic ceca potentially leading to localized stress to cells (Handy et al., 2008). Given the damage to the cell structures and the presence of U throughout the tissues, it is conceivable that hepatic ceca dysfunction is a key event leading to acute mortality (Byrnes et al., unpublished).

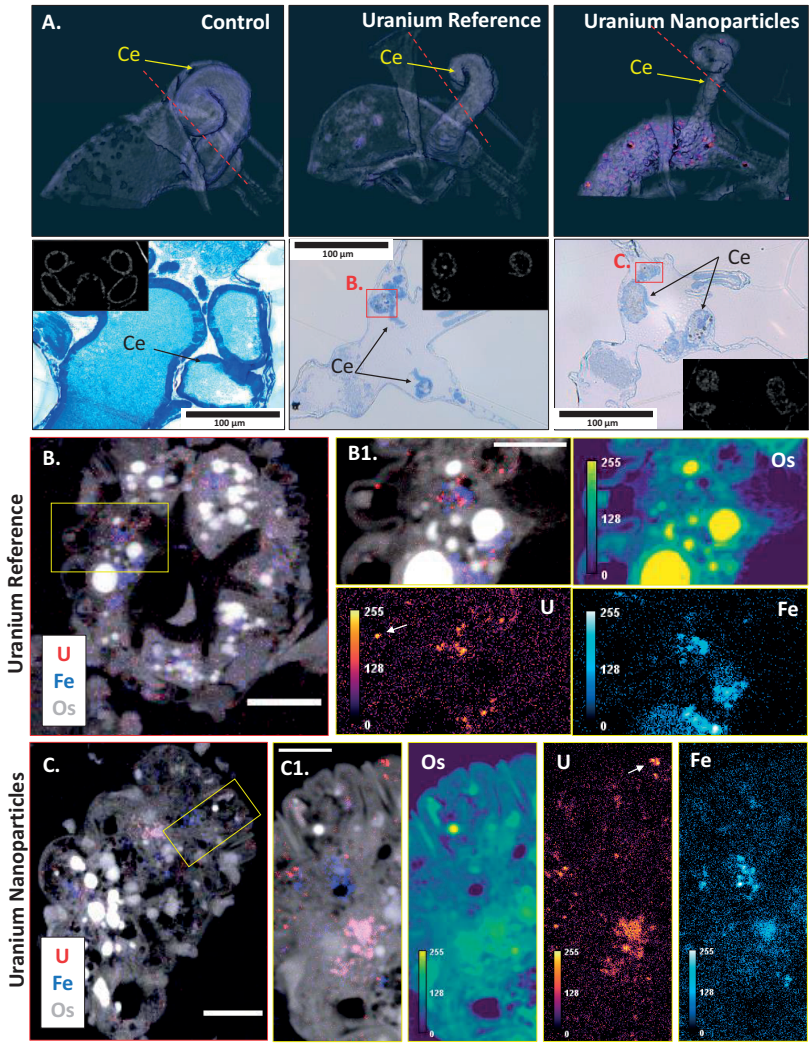

Figure 3: (**A**) Tomographic reconstruction (*top images*) of the *D. magna* hepatic ceca in an unexposed individual (*left*) and in individuals exposed to 159 µg L^{-1} U_{Ref} (*center*) and 320 µg U L^{-1} UNP (*right*), indicating the location of the histology sections (bottom images) by red dotted lines and the areas of hepatic ceca tissues investigated by nano-SRXRF (225 nm step size, 400 ms dwell time) by red boxes. Representative CT tomograms are located in the corner of histology images for comparison. (**B, C**) Combined U, Fe and Os nano-SRXRF maps of U_{Ref} and UNP exposed daphnia, indicating the ROI investigated further (yellow boxes). (**B1, C1**) Combined and individual high-resolution nano-SRXRF maps (75 nm step size, 400 ms dwell time) of the ceca tissue region. The white arrows in the U maps indicate one (**B1**) and two (**C2**) U particulates of ca. 560 and 450 nm in size, respectively. Scale bars represent 100 µm (**A**) and 5 µm (**B, C**) and all intensities are scaled logarithmically from 0 to 255. *Abbreviations:* hepatic ceca (Ce).

Combined Histological and nano-SRXRF Analyses of the Midgut

Histological sections of both UNP and the U_{Ref} exposed *D. magna* revealed intestinal damage and cell distortion in gut epithelia (Fig. 4). In UNP exposed organisms, epithelial cells appeared irregular and protruded into the gut lumen with dilatation of the intercellular spaces, and microvilli were damaged. Similar effects, although less pronounced, were observed in the U_{Ref} exposed daphnia that featured lower body burden than the UNP exposed organisms, indicating that intestinal cell damage could be U concentration dependent. These observations are consistent with a previous study of U toxicity to *D. magna* that reported similar damages to intestinal cells (Massarin et al., 2011). The peritrophic membrane, a chitinous mesh that confines the lumen contents (Quaglia et al., 1976), appeared disintegrated in the exposed daphnia with very little ectoperitrophic space remaining between the gut materials and the microvilli (Fig. 4). A normally functioning peritrophic membrane was expected to prevent the majority of the UNPs from reaching areas around the epithelial cells as hydrodynamic diameter measurements indicated average UNP aggregate sizes > 130 nm, i.e., larger than the approximate mesh size of the membrane (Hansen and Peters, 1998). Using STEM-EDS to examine the midgut of UNP exposed organisms, U aggregates were observed around the intestinal epithelia and between the microvilli further indicating that the peritrophic membrane was not functioning (Fig. S4). These results are similar to those of Heinlaan et al. (2011), who observed the absence of the peritrophic membrane after a 48 h exposure to CuO NPs with aggregates spread into the brush border of the epithelial cells. The specific mechanisms that lead to peritrophic membrane failure remain unknown, although the stress observed in gut epithelial cells of this study (protrusion and elongation) may also occur in the epithelial cells that secrete the peritrophic membrane, thus potentially inhibiting the process.

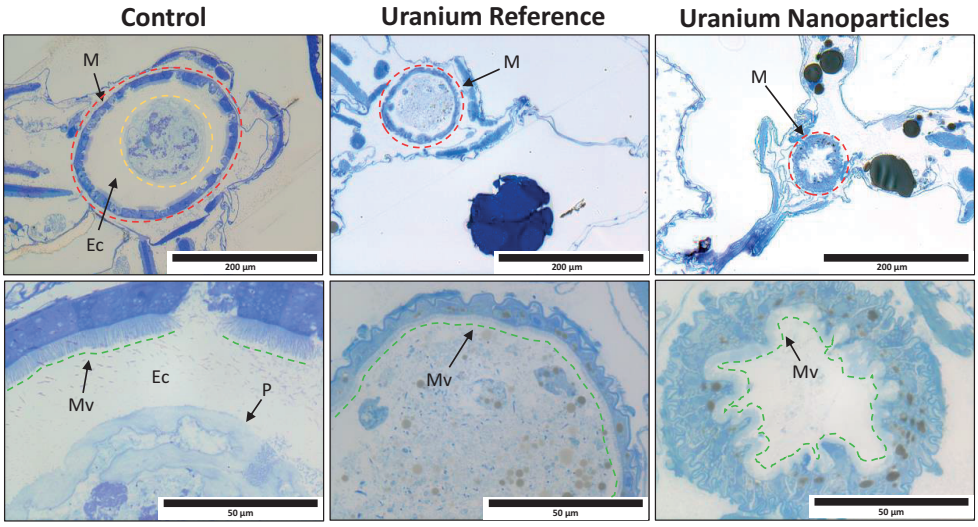

Figure 4: (*Top*) Histological sections of *D. magna* midgut and surrounding area in a control organism (*left*), a U_{Ref} exposed organism (159 µg L^{-1}, center), and a UNP exposed organism (320 µg L^{-1}, right). The midgut is represented by dashed red lines and, only in the control organism, the well bound lumen contents are outlined with yellow dashes. (*Bottom*) High magnification (100x) images of the epithelial cell wall (green dashed lines) in a control organism (*left*), a U_{Ref} exposed organism, and a UNP exposed organism. *Abbreviations:* midgut (M), ectoperitrophic space (Ec), peritrophic membrane (P), microvilli (Mv).

High resolution nano-SRXRF mapping of a dorsal midgut section of U_{Ref} exposed daphnia was used to show the localization of U between the lumen and the epithelial cells (Fig. 5). A large area of the lumen and epithelial wall was selected for study and overlaid with the histological section using the Os map to align the images. Within the lumen, U particulates (< 500 nm) were prevalent, while U was also associated with a detached epithelial cell and partially digested algae content. The small, particulates of U observed in the lumen (Fig. 5B – C) were similar to those within the hepatic ceca (Fig. 3B). The µ-SRXRF results (Fig. 2B) indicated uptake into the intestinal epithelia. However, any U present in the epithelial cells or the microvilli of the section measured by nano-SRXRF remained below the detection limit. Uranium bearing precipitates have previously been observed in histological sections of chronically exposed *D. magna* (Massarin et al., 2011), but these phenomena were not identified in the region of epithelial cells as presented here. However, the detached epithelial cell contained substantial U signals in the membrane, cytosol and nucleus. It is tempting to speculate that the U content may have induced

stress that eventually caused shedding of the cell. Shedding is normally part of tissue maintenance (Williams et al., 2015), but may be enhanced by stress (Nogueira et al., 2006).

The greatest U signal in the midgut of the U_{Ref} exposed daphnia was observed in a 10 µm, partially digested algae cell (Fig. 5C), *Raphidocelis subcapitata*, which are known to effectively bind bioavailable U species (Fortin et al., 2004; Krienitz et al., 2011). Although the test organisms were removed from feed prior to exposure, complete evacuation of the intestine was not possible and the presence of the U bearing algal cell demonstrated the relationship between U uptake and binding to gut contents. This observation highlights inherent constraints of whole body burden measurements that are not able to differentiate between tissue uptake and intestinally confined U.

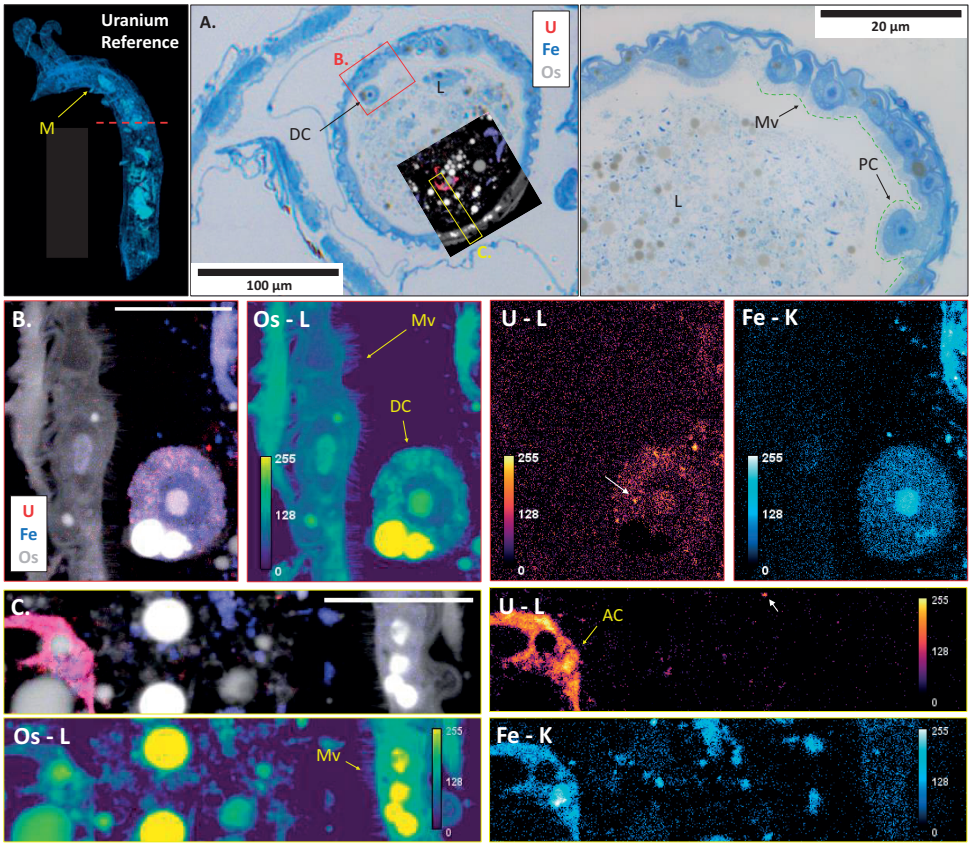

Figure 5: Elemental analysis of histological section from *D. magna* (U_{Ref}, 159 µg L^{-1}) showing the U (red) and Fe (blue) distributions using the Os (grey / green) to orient the features. (**A**) Histological sections of exposed organism midgut with cell features and areas of nano-SRXRF analysis (area B indicated by a red box and area C indicated by a yellow box). The tomographic rendering (left) shows the approximate location of the section (red dashed line). (**B**) Detached epithelial cells with small (< 500 nm) particulates indicated by the white arrow (~ 530 nm). (**C**) Lumen contents including a green algae cell and small (< 500 nm) U particulates indicated by the white arrow (~ 380 nm). Scale bars = 10 µm. All intensities are scaled logarithmically from 0 to 255. *Abbreviations:* midgut (M), detached epithelial cell (DC), lumen (L), microvilli (Mv), protruded epithelial Cell (PC), algae cell (AC).

Conclusions

The combined XRF and histological analyses confirmed the presence of U in damaged tissues of the digestive tract of *D. magna*. The application of nanoscopic XRF enabled the visualization of U internalized in hepatic ceca tissues and intestinal cells. Both the UNPs and the U_{Ref} exposures compromised key functions of the intestine. Breakdown of the midgut epithelia, peritrophic membrane disintegration, and deterioration of the hepatic ceca, were identified and likely contributed to the U induced acute toxicity. Collectively, these results demonstrate the power of synchrotron based XRF methodology to investigate tissue and cell biodistribution of metals and a wide range of toxicants at nanoscale resolution thus providing an improved basis for environmental impact and risk assessments.

Acknowledgements

This study has been funded by the Research Council of Norway through its Centre of Excellence (CoE) funding scheme (Project No. 223268/F50). We acknowledge the Paul Scherrer Institut, Villigen, Switzerland for provision of synchrotron radiation beamtime at beamline microXAS (X05LA) of the SLS. We gratefully acknowledge the Diamond Light Source for granting beamtime at I14 under proposal MG27615. We are very thankful to Knut Erik Tollefsen and You Song at the Norwegian Institute of Water Research (NIVA) for providing *Daphnia magna* and to Shane Scheibener (MINA/NMBU) for supporting the culture. We would like to thank Vaclav Cuba and the Czech Technical University for providing the uranium nanoparticles, and Karl Andreas Jensen and Yetneberk Kassaye (MINA/NMBU) for support during ICP-MS analyses. We would also like to thank Deborah H. Oughton at MINA/NMBU for helpful discussions on U and UNP toxicity, The Research Council of Norway is acknowledged for support to the NORTEM national infrastructure (project number 197405). The authors are very grateful to the staff of the imaging center at NMBU, YeonKyeong Lee, Hilde Kolstad, and Lene Hermansen, for guidance on fixation and microtomy techniques.

References

Developments in Uranium Resources, Production, Demand and the Environment. Vienna: International Atomic Energy Agency, 2005.

Alessi DS, Uster B, Borca CN, Grolimund D, Bernier-Latmani R. Beam-induced oxidation of monomeric U(IV) species. Journal of Synchrotron Radiation 2013; 20: 197-199.

Bargar JR, Bernier-Latmani R, Giammar DE, Tebo BM. Biogenic Uraninite Nanoparticles and Their Importance for Uranium Remediation. Elements 2008; 4: 407-412.

Bots P, Morris K, Hibberd R, Law GTW, Mosselmans JFW, Brown AP, et al. Formation of Stable Uranium(VI) Colloidal Nanoparticles in Conditions Relevant to Radioactive Waste Disposal. Langmuir 2014; 30: 14396-14405.

Byrnes, I., Rossbach, L.M., Brede, D.A., Grolimund, D., Sanchez, D.F., Nuyts, G., Cuba, V., Reinoso-Maset, E., Salbu, B., Janssens, K., Oughton, D., Scheibener, S., Teien, H.C., Lind, O.C. Synchrotron-based X-ray Fluorescence Imaging Provides New Insights on Uranium Toxicokinetics in Daphnia magna following Exposure to Uranium Nanoparticles (unpublished)

Cagno S, Brede DA, Nuyts G, Vanmeert F, Pacureanu A, Tucoulou R, et al. Combined

Computed Nanotomography and Nanoscopic X-ray Fluorescence Imaging of Cobalt

Nanoparticles in Caenorhabditis elegans. Analytical Chemistry 2017; 89: 11435-11442.

Caumette G, Koch I, Moriarty M, Reimer KJ. Arsenic distribution and speciation in Daphnia pulex. Science of The Total Environment 2012; 432: 243-250.

De Samber B, De Schamphelaere KAC, Janssen CR, Vekemans B, De Rycke R, Martinez-Criado G, et al. Hard X-ray nanoprobe investigations of the subtissue metal distributions within Daphnia magna. Analytical and Bioanalytical Chemistry 2013; 405: 6061-6068.

Dublet G, Worms I, Frutschi M, Brown A, Zünd GC, Bartova B, et al. Colloidal Size and Redox State of Uranium Species in the Porewater of a Pristine Mountain Wetland. Environmental Science & Technology 2019; 53: 9361-9369.

Ebert D. Ecology, epidemiology, and evolution of parasitism in Daphnia: National Library of Medicine, 2005.

Fortin C, Dutels L, Garnier-Laplace J. Uranium complexation and uptake by a green alga in relation to chemical speciation: The importance of the free uranyl ion. Environmental Toxicology and Chemistry 2004; 23: 974-981.

Goulet RR, Thompson PA, Serben KC, Eickhoff CV. Impact of environmentally based chemical hardness on uranium speciation and toxicity in six aquatic species. Environmental Toxicology and Chemistry 2015; 34: 562-574.

Guarnieri D, Sabella S, Muscetti O, Belli V, Malvindi MA, Fusco S, et al. Transport across the cell-membrane dictates nanoparticle fate and toxicity: a new paradigm in nanotoxicology. Nanoscale 2014; 6: 10264-10273.

Handy RD, Owen R, Valsami-Jones E. The ecotoxicology of nanoparticles and nanomaterials: current status, knowledge gaps, challenges, and future needs. Ecotoxicology 2008; 17: 315-325.

Handy RD, von der Kammer F, Lead JR, Hassellöv M, Owen R, Crane M. The ecotoxicology and chemistry of manufactured nanoparticles. Ecotoxicology 2008; 17: 287-314.

Hansen U, Peters W. Structure and permeability of the peritrophic membranes of some small crustaceans. Zoologischer Anzeiger 1998; 236: 103-108.

Hasan S, Ghosh TK. Synthesis of Silica-Coated Uranium Oxide Nanoparticles by Surfactant-Templated Sol-Gel Process for Use as Catalysts. Nuclear Technology 2013; 181: 371-379.

Heinlaan M, Kahru A, Kasemets K, Arbeille B, Prensier G, Dubourguier H-C. Changes in the Daphnia magna midgut upon ingestion of copper oxide nanoparticles: A transmission electron microscopy study. Water Research 2011; 45: 179-190.

Jackson BP, Pace HE, Lanzirotti A, Smith R, Ranville JF. Synchrotron X-ray 2D and 3D elemental imaging of CdSe/ZnS quantum dot nanoparticles in Daphnia magna. Analytical and Bioanalytical Chemistry 2009; 394: 911-917.

Kaminski MD, Dimitrijevic NM, Mertz CJ, Goldberg MM. Colloids from the aqueous corrosion of uranium nuclear fuel. Journal of Nuclear Materials 2005; 347: 77-87.

Krienitz L, Bock C, Nozaki H, Wolf M. SSU rRNA Gene Phylogeny of Morphospecies Affiliated to the Bioassay Alga "Selenastrum Capricornutum" Recovered the Polyphyletic Origin of Crescent-Shaped Chlorophyta1. Journal of Phycology 2011; 47: 880-893.

Laforsch C, Tollrian R. A new preparation technique of daphnids for Scanning Electron Microscopy using hexamethyldisilazane. Archiv für Hydrobiologie 2000: 587-596.

Lind OC, Tschiersch J, Salbu B. Nanometer-micrometer sized depleted uranium (DU) particles in the environment. Journal of Environmental Radioactivity 2020; 211: 106077.

Markich SJ. Uranium Speciation and Bioavailability in Aquatic Systems: An Overview. The Scientific World Journal 2002: 707-729.

Massarin S, Alonzo F, Garcia-Sanchez L, Gilbin R, Garnier-Laplace J, Poggiale J-C. Effects of chronic uranium exposure on life history and physiology of Daphnia magna over three successive generations. Aquatic Toxicology 2010; 99: 309-319.

Massarin S, Beaudouin R, Zeman F, Floriani M, Gilbin R, Alonzo F, et al. Biology-Based Modeling To Analyze Uranium Toxicity Data on Daphnia magna in a Multigeneration Study. Environmental Science & Technology 2011; 45: 4151-4158.

Munger C, Hare L, Craig A, Charest P-M. Influence of exposure time on the distribution of cadmium within the cladoceran Ceriodaphnia dubia. Aquatic Toxicology 1998; 44: 195-200.

Novikov A, Kalmykov S, Kuzovkina E, Myasoedov B, Fujiwara K, Fujiwara A. Evolution of actinide partitioning with colloidal matter collected at PA "Mayak" site as studied by sequential extraction. Journal of Radioanalytical and Nuclear Chemistry 2009; 280: 629-634.

Nogueira ICG, Lobo-Da-Cunha A, Vasconcelos VM. Effects of Cylindrospermopsis raciborskii and Aphanizomenon ovalisporum (cyanobacteria) ingestion on Daphnia magna midgut and associated diverticula epithelium. Aquatic Toxicology 2006; 80: 194-203.

Pavelková T, Čuba V, De Visser-Týnová E, Ekberg C, Persson I. Preparation of UO2, ThO2 and (Th,U)O2 pellets from photochemically-prepared nano-powders. Journal of Nuclear Materials 2016; 469: 57-61.

Pavelkova T, Cuba V, Sebesta F. Photo-induced low temperature synthesis of nanocrystalline UO2, ThO2 and mixed UO2-ThO2 oxides. Journal of Nuclear Materials 2013; 442: 29-32.

Pushie MJ, Pickering IJ, Korbas M, Hackett MJ, George GN. Elemental and Chemically Specific X-ray Fluorescence Imaging of Biological Systems. Chemical Reviews 2014; 114: 8499-8541.

Quaglia A, Sabelli B, Villani L. Studies on Intestine of Daphnidae (Crustacea, Cladocera) Ultrastructure of Midgut of Daphnia-Magna and Daphnia-Obtusa. Journal of Morphology 1976; 150: 711-725.

Quinn PD, Alianelli L, Gomez-Gonzalez M, Mahoney D, Cacho-Nerin F, Peach A, et al. The Hard X-ray Nanoprobe beamline at Diamond Light Source. Journal of Synchrotron Radiation 2021; 28: 1006-1013.

Ravel B, Newville M. ATHENA, ARTEMIS, HEPHAESTUS: data analysis for X-ray absorption spectroscopy using IFEFFIT. Journal of synchrotron radiation 2005; 12: 537-541.

Reynolds JG, Cooke GA, Page JS, Warrant RW. Uranium-bearing phases in Hanford nuclear waste. Journal of Radioanalytical and Nuclear Chemistry 2018; 316: 289-299.

Salbu B, Burkitbaev M, Strømman G, Shishkov I, Kayukov P, Uralbekov B, et al. Environmental impact assessment of radionuclides and trace elements at the Kurday U mining site, Kazakhstan. Journal of Environmental Radioactivity 2013; 123: 14-27.

Salbu B, Kashparov V, Lind OC, Garcia-Tenorio R, Johansen MP, Child DP, et al. Challenges associated with the behaviour of radioactive particles in the environment. Journal of Environmental Radioactivity 2018; 186: 101-115.

Salbu B, Lind OC, Skipperud L. Radionuclide speciation and its relevance in environmental impact assessments. Journal of Environmental Radioactivity 2004; 74: 233-242.

Scheibener S, Song Y, Tollefsen KE, Salbu B, Teien H-C. Uranium accumulation and toxicokinetics in the crustacean Daphnia magna provide perspective to toxicodynamic responses. Aquatic Toxicology 2021: 105836.

Sheppard SC, Sheppard MI, Gallerand M-O, Sanipelli B. Derivation of ecotoxicity thresholds for uranium. Journal of Environmental Radioactivity 2005; 79: 55-83.

Smirnov NN. Physiology of the Cladocera: Academic Press, 2017.

Strømman G, Rosseland BO, Skipperud L, Burkitbaev LM, Uralbekov B, Heier LS, et al. Uranium activity ratio in water and fish from pit lakes in Kurday, Kazakhstan and Taboshar, Tajikistan. Journal of Environmental Radioactivity 2013; 123: 71-81.

Suzuki Y, Kelly SD, Kemner KM, Banfield JF. Nanometre-size products of uranium bioreduction. Nature 2002; 419: 134-134.

Tamborini G. SIMS Analysis of Uranium and Actinides in Microparticles of Different Origin. Microchimica Acta 2004; 145: 237-242.

Tan C, Wang W-X. Modification of metal bioaccumulation and toxicity in Daphnia magna by titanium dioxide nanoparticles. Environmental Pollution 2014; 186: 36-42.

Tan L-Y, Huang B, Xu S, Wei Z-B, Yang L-Y, Miao A-J. TiO2 Nanoparticle Uptake by the Water Flea Daphnia magna via Different Routes is Calcium-Dependent. Environmental Science & Technology 2016; 50: 7799-7807.

United States Environmental Protection Agency (USEPA). Methods for measuring the acute toxicity of effluents and receiving waters to freshwater and marine organisms. EPA-821-R-02-012, 2002.

van der Zande M, Kokalj AJ, Spurgeon DJ, Loureiro S, Silva PV, Khodaparast Z, et al. The gut barrier and the fate of engineered nanomaterials: a view from comparative physiology. Environmental Science-Nano 2020; 7: 1874-1898.

Wang Y, Bagnoud A, Suvorova E, McGivney E, Chesaux L, Phrommavanh V, et al. Geochemical Control on Uranium(IV) Mobility in a Mining-Impacted Wetland. Environmental Science & Technology 2014; 48: 10062-10070.

WHO G. Guidelines for drinking-water quality. World Health Organization 2011; 216: 303-304.

Williams JM, Duckworth CA, Burkitt MD, Watson AJM, Campbell BJ, Pritchard DM. Epithelial Cell Shedding and Barrier Function. Veterinary Pathology 2015; 52: 445-455.

Zeman FA, Gilbin R, Alonzo F, Lecomte-Pradines C, Garnier-Laplace J, Aliaume C. Effects of waterborne uranium on survival, growth, reproduction and physiological processes of the freshwater cladoceran Daphnia magna. Aquatic Toxicology 2008; 86: 370-378.

Supplemental Material:

Combined Structural and Nanoscopic Elemental Imaging Identifies Damage to Digestive Tract of *Daphnia magna* associated with Uranium Nanoparticle Acute Toxicity

Ian Byrnes[1], Lisa Magdalena Rossbach[1], Jakub Jaroszewicz[2], Daniel Grolimund[3], Dario Ferreira Sanchez[3], Miguel Gomez-Gonzalez[4], Gert Nuyts[5], Estela Reinoso-Maset[1], Koen Janssens[5], Brit Salbu[1], Dag Anders Brede[1], Ole Christian Lind[1]

[1] Norwegian University of Life Sciences, Center for Environmental Radioactivity (CERAD), Faculty of Environmental Sciences and Natural Resource Management, P.O. Box 5003, 1433 Ås, Norway

[2] Warsaw University of Technology, Faculty of Materials Science and Engineering, Woloska St. 141, 02-507 Warsaw, Poland

[3] Swiss Light Source, Paul Scherrer Institute (PSI), 5232 Villigen, Switzerland

[4] Diamond Light Source Ltd., Harwell Science and Innovation Campus, Didcot, Oxfordshire OX11 0DE, United Kingdom

[5] University of Antwerp, Department of Chemistry, Groenenborgerlaan 171, 2020 Antwerp, Belgium

*Corresponding Author

Phone: +47-93820876 Fax: +47-64948359

Email Address: ian.byrnes@nmbu.no

Address: Norwegian University of Life Sciences, Center for Environmental Radioactivity (CERAD), Faculty of Environmental Sciences and Natural Resource Management, P.O. Box 5003, 1433 Ås, Norway

Summary

This document includes the supplementary material supporting the methods (further description) and results (2 tables and 4 figures).

Experimental Method

Results

Experimental Methods:

S1. Uranium Nanoparticle Suspension and Characterization

Stock suspensions (1.0 g U L^{-1}) were prepared by weighing UNPs in a non-static environment on a microbalance and placed in an empty 20 mL glass vial. A dispersion agent, 1% polyoxyethelene glycerol triolate, was applied directly to the dry particles before the addition of 10 mL N_2 purged (4 h) ddH_2O (15 MΩ cm). Immediately afterwards, the UNP suspension was sonicated for 13 min at a 15 % amplitude using a 400-W Branson Sonifier S-450D (Branson Ultrasonics) equipped with a standard 13 mm disruptor tip (model 101-147-037). All prepared stocks were used immediately following sonication.

Dynamic Light Scattering

Zeta-average hydrodynamic diameter of the UNPs in the stock suspension were determined by dynamic light scattering (DLS) measurements using a Malvern Zetasizer ZS (Malvern Instruments Ltd., Worcestershire, United Kingdom) equipped with a 633 nm laser. Measurements were conducted in triplicate, 5 runs each, with autocorrection functions of 10 s. Electrophoretic mobility was measured and zeta-potentials for the stock suspensions were determined by Smoluchowski approximations.

Transmission Electron Microscopy

High resolution transmission electron microscopy (TEM) with energy dispersive X-ray spectroscopy (EDS) was used to image the UNPs from the stock suspension and to measure the diameter of individual particles. Immediately following sonication, 10 µL of stock suspension was added to a 400-mesh Cu-coated formvar-carbon film (Agar Scientific Ltd., Essex, United Kingdom) and allowed to air dry. Samples were measured at 200 kV accelerating voltage on a JEOL JEM-2100F equipped with a Gatan Porius 200D CCD camera (JEOL Ltd., Tokyo, Japan). Uranium fluorescent X-rays were collected by an Oxford X-Max-80 SDD EDS detector at a 0.23 srad collection angle.

QQQ-ICP-MS

Uranium concentrations in both the stock suspensions and exposure media were determined by triple quadrupole inductively coupled plasma mass spectrometry (QQQ-ICP-MS; Agilent 8900, Mississauga, CA). All measurements were completed in triplicate

and each sample (100 µL) was mixed with 400 µL of ultrapure HNO_3 and the samples were digested for 48 h before dilution with ddH_2O (15 MΩ cm) to final volume of 10 mL.

Size Fractionation

To determine the particulate (> 0.45 µm), colloidal (0.45 µm < x > 3 kDa), and LMM (< 3 kDa) fractions, QQQ-ICP-MS analysis of size fractionated exposure media was performed. In each exposure group, 1 mL of media was passed through a pre-conditioned 0.45 µm syringe filter (VWR, Radnor, Pennsylvania, United States) and 100 µL was sampled from the filtrate. Next, 400 µL of the < 0.45 µm filtrate was sampled into a pre-conditioned 3 kDa Amicon cellulose membrane filter (Amicon Millipore, Billerica, MA) and centrifuged at 14,000 g for 30 min. From the < 3 kDa filtrate solution, 100 µL was sampled for QQQ-ICP-MS measurement to determine the LMM fraction.

S2. *Daphnia magna* Culture and Exposure Experiments

Laboratory cultured *D. magna*, DHI strain (DHI Water & Environment, Hørsholm, Denmark), were reared at 20°C (± 1°C) with a day-night cycle of 16 h light:8 h darkness in M7 media (OECD 2004). The culture media was renewed three times weekly at which point neonates were removed. Daphnia were fed a diet of concentrated algae (*Raphidocelis subcapitata*) at a rate of 5.25 x 10^{-6} cells day^{-1} $daphnid^{-1}$ for neonates and 2.10 x 10^{-7} cells day^{-1} $daphnid^{-1}$ for adults. Synchronized neonates (< 18 h) derived from the second clutch or later were used for exposure experiments.

Uranium nanoparticle and the U_{Ref} exposures were conducted in US EPA moderately hard reconstituted water (MHRW, pH 6.8, 350 µS cm^{-1}, 20°C), which was prepared a week prior to the exposures (USEPA 2002). Daphnia were exposed at a concentration of 5 mL per individual. The concentration chosen was reflective of sublethal acute effects determined by acute toxicity tests reported previously (Byrnes et al., unpublished). For UNP exposures, 25 mL of MHRW was added to a 50 mL plastic cup and UNP stock additions were added just prior to the start of exposure. Dissolved U_{Ref} solutions were prepared by pipetting 50 µL from a 100 mg U L^{-1} dilution of U_{Ref} solution (CRM 129-A, Spectrapure Standards AS, Oslo, Norway) into empty 50 mL plastic exposure cups. The U_{Ref} solutions were evaporated to dryness in order to resolve issue related to the low pH originating from the nitric acid. The dry residuals were redissolved in 25 mL of MHRW exposure

solution 24 h prior to exposure start. The pH of the U_{Ref} and UNP exposures were confirmed (6.8 ± 0.1) at the start of the experiment.

S3. Additional Imaging Measurements

Laboratory X-ray Absorption Computed Tomography

The reconstructed output from X-ray absorption tomography contained a stack of tomograms (virtual slices), visualized using DataViewer (Bruker Nano GmbH, Berlin, Germany), that reveal the inner morphology of measured organisms in a greyscale that is correlated to the X-ray attenuation. Volumetric rendering of the results was completed using Bruker visualization software solutions (CTVOX, CTVOL, CTAN, Bruker Nano GmbH, Berlin, Germany). In brief, CTVOX and CTVOL handle the rendering of tomographic data and sample coloring and transparency while CTAN provides density examination, size and structure measurements, and region-of-interest analyses.

Analytical Transmission Electron Microscopy

High magnification, subcellular resolution analyses of daphnia sections was conducted using scanning transmission electron microscopy (STEM) with energy dispersive X-ray spectroscopy (EDS) (JOEL JEM-2100F), with particular focus on the intestine and microvilli of LRwhite embedded organisms. Ultrathin sections (<100 nm) were prepared using the same ultramicrotome described previously. Sections were mounted on copper slot grids with a formvar carbon film (EM Resolutions Ldt, Sheffield, UK). Samples were analyzed under the same specifications as previously described for individual particle imaging.

Results:

Table S1: Uranium Nanoparticle Suspension Details and *D. magna* Exposure Parameters

Experiment	Average Hydrodynamic diameter (nm)	Zeta potential (mV)	Measured UNP Test Concentration 48 h ($\mu g\ U\ L^{-1}$)	Measured U_{Ref} Test Concentrations 48 h ($\mu g\ U\ L^{-1}$)
D. magna Adults (< 7 d)	185.6 ± 0.6	-9.48	320 ± 30.6	159 ± 13.7

Table S2: Major Constituents of UNP Stock Suspension

UNP Stock	Li (µg L^{-1})	B (µg L^{-1})	Ti (µg L^{-1})	V (µg L^{-1})	Mo (µg L^{-1})	Ag (µg L^{-1})	Sn (µg L^{-1})	Lu (µg L^{-1})	U (mg L^{-1})
Suspension	64.4 ± 7.04	3613 ± 70.40	800 ± 29.1	79.1 ± 1.80	1.54 ± 0.07	28.4 ± 1.47	103 ± 139	1.75 ± 0.02	639 ± 21.9

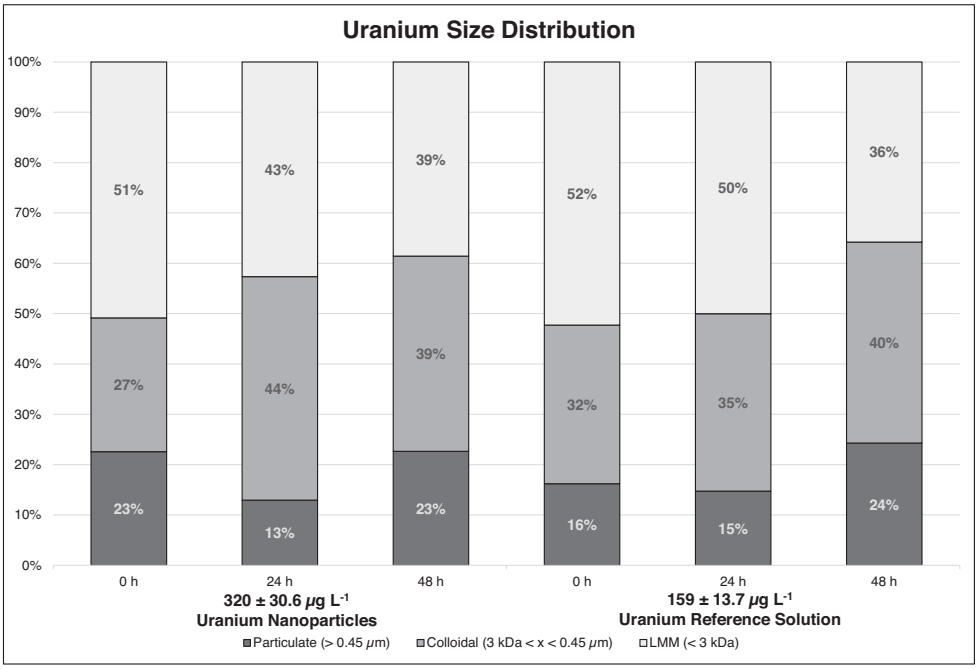

Figure S1: Size distributions of U species in the exposure media showed the complex chemical processes in action during the experiment. (Left) UNP exposures (Right) U_{Ref} solution exposures.

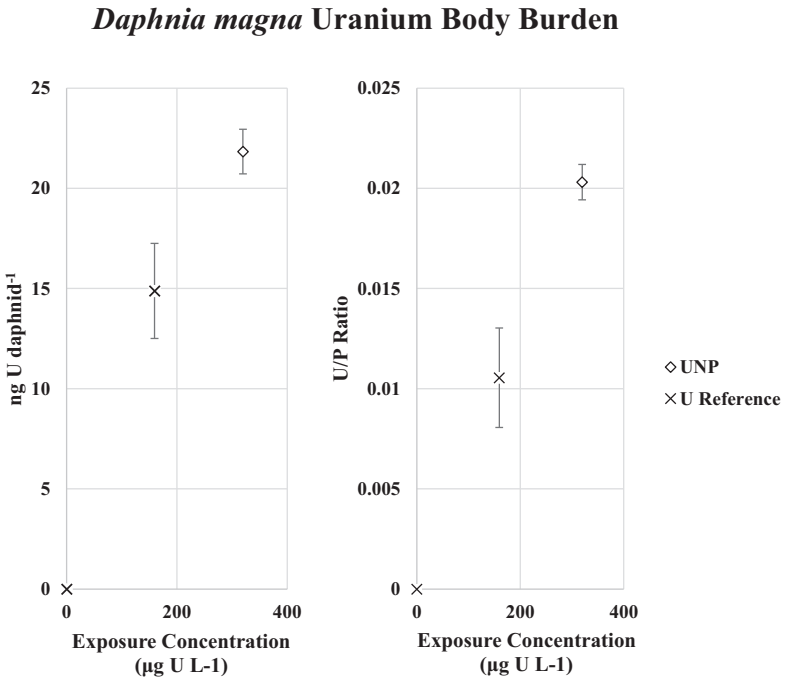

Figure S2: Whole daphnia, U body burden measurements for both the UNP and the U_{Ref} solution exposures.

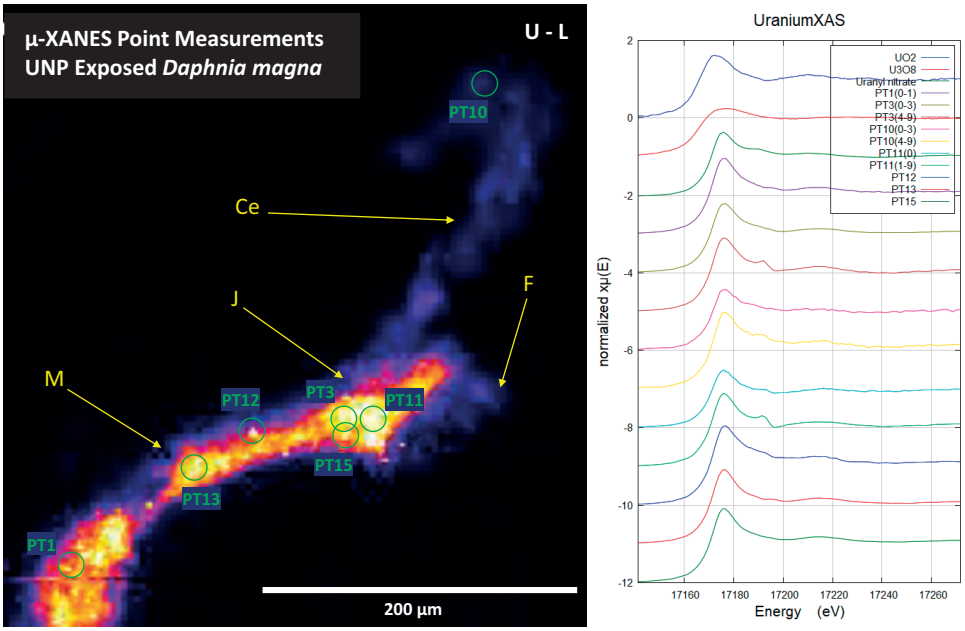

Figure S3: Point µ-XANES measurements in *D. magna* following exposure to UNPs (320 µg L^{-1}). Locations 1, 12, and 13 are located away from the junction of the midgut and hepatic ceca, while locations 3, 11, and 15 are taken at that junction immediately following the foregut. Location 10 was taken towards the anterior of the hepatic ceca. *Abbreviations:* hepatic ceca (Ce), foregut (F), junction (J), midgut (M)

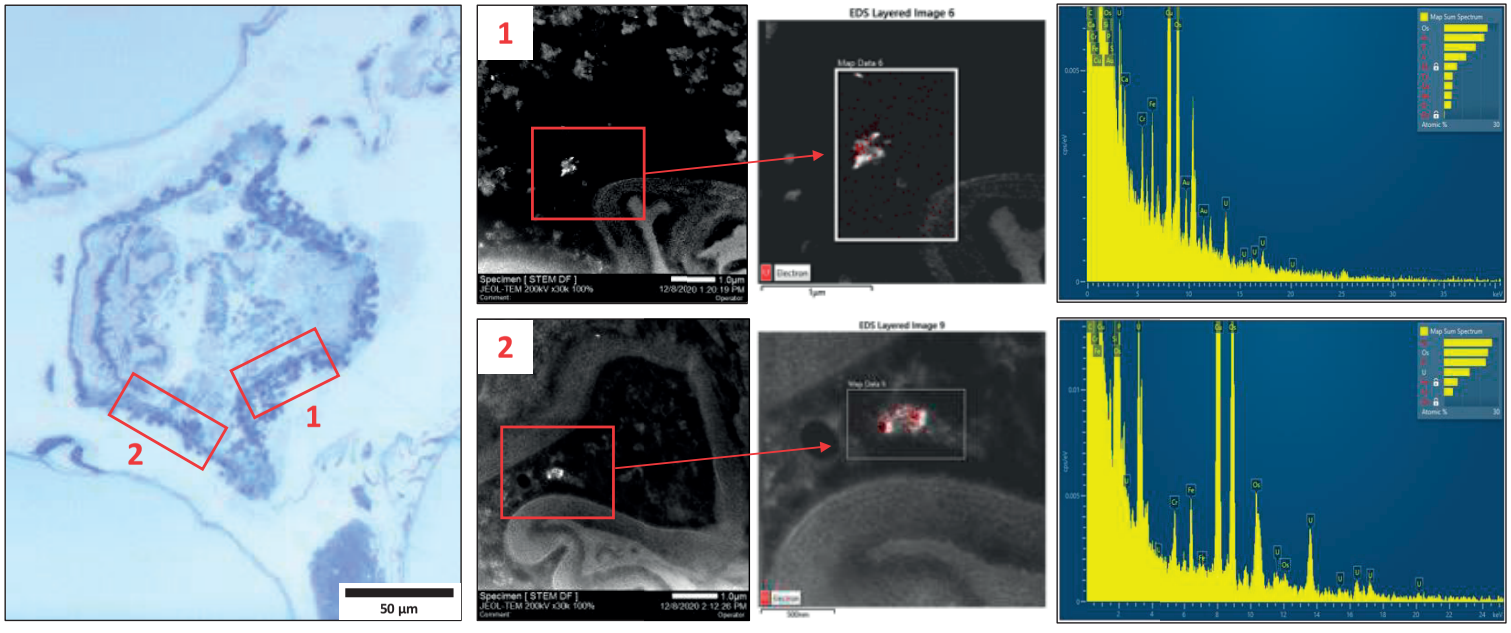

Figure S4: Transmission Electron Microscopy examinations of midgut sections from UNP exposed *D. magna* (320 µg L^{-1}). Two investigation sites are noted where small (< 250 nm) high density aggregates were found along the brush border of the epithelial cells. X-ray analysis shows the particles contain U indicating that UNP aggregates are present at least along the epithelial cells.

ISBN: 978-82-575-1872-1
ISSN: 1894-6402

Norwegian University
of Life Sciences

Postboks 5003
NO-1432 Ås, Norway
+47 67 23 00 00
www.nmbu.no

112257 / ANDVORDGRAFISK.NO